INVESTIGATIONS OF WATER AND TRACER MOVEMENT IN COVERED AND UNCOVERED UNSATURATED WASTE ROCK

by

JOSEPH R. MARCOLINE

B.A., Hamilton College, 1994

M.Sc., New Mexico Institute of Mining and Technology, 1997

A THESIS SUBMITTED IN PARTIAL FULFILLMENT OF

THE REQUIREMENTS FOR THE DEGREE OF

DOCTOR OF PHILOSOPHY

in

THE FACULTY OF GRADUATE STUDIES

(Geological Sciences)

UNIVERSITY OF BRITISH COLUMBIA

(Vancouver)

July 2008

ABSTRACT

A better understanding of the hydrogeology of mine waste rock and cover systems is essential for the quantification, prediction and reduction of metals loading to the receiving environment. A series of experiments were conducted on an instrumented intermediate-scale waste rock pile at the Cluff Lake Mine in Saskatchewan to investigate the changes in flow and solute transport within coarse waste rock under three different surface conditions. Following these studies, the waste rock pile was deconstructed, structures were mapped, and samples were collected for physical characterization and pore water extraction. The internal structure of the waste rock pile was more important than the texture and topography under the free-dumped and ripped/leveled surface, while the surface condition was found to be the dominant control on spatial and temporal variability of outflow from the waste rock with the covered surface. Data from a deuterium tracer test, lysimeter outflow, and from TDR probes were used to derive estimates of the maximum and an average pore water velocity through the uncovered and the covered waste rock. An average pore water velocity through the matrix materials of the uncovered waste rock was approximately 1.5 m/yr and maximum preferential flow velocities were as high as 5 m/day. The post-cover pressure wave velocity of 0.1 to 1 m/day is inferred from outflow and TDR data, and average pore water velocities (0.39 m/y and 0.73 m/y) are calculated by the water flux and tracer

methods, respectively. The distribution of the tracers in pore water and the internal structure were mapped during a detailed deconstruction of the waste rock pile and attempts were made to link the data to the spatial and temporal patterns of lysimeter outflow. The pore water chloride concentrations and the deuterium values did not provide conclusive data necessary to link the spatial and temporal patterns observed in the lysimeter hydrographs to internal structure; however, it provided insight into the internal flow mechanisms and water residence times.

TABLE OF CONTENTS

LIST OF TABLES

LIST OF FIGURES

ACKNOWLEDGMENTS

I acknowledge the generous support and funding from Areva Resources, the Cameco Corporation and grants from the Natural Sciences and Engineering Research Council of Canada (NSERC).

I owe a great deal of thanks to numerous people who provided support, assistance and friendship throughout the duration of this project. I am especially thankful to Craig Nichol for his generous time and assistance throughout the early phases of the research. I am thankful for the support and field assistance provided by the staff at the Cluff Lake Mine Site. The laborious deconstruction could not have been completed without the hard work of both Craig Thompson and Karin Wagner. Doreen Hacker provided months of laboratory work with exceptional QA/QC practices. I am grateful to Frank Marcoline who without any compensation developed a commercial grade software package for this research project. The software effectively and efficiently managed the huge quantity of site data with data parsing, instrument calibration, error detection and data management routines. I am thankful for the many discussions with Fernando Junqueira, Justin Stockwell, Mike O'Kane and Matthew Neuner. The numerous editorial reviews and endless support provided by Malisa Niemeyer are greatly appreciated and will be remembered, thank you.

I would like to express my sincere gratitude to Leslie Smith, Roger Beckie and Ward Wilson who each provided unparalleled support, encouragement and guidance from the first to the last day of this project. It has been an honor and a privilege to have worked under the guidance of each of you. Thank you.

CHAPTER 1: INTRODUCTION

Products from the hard-rock mining industry are essential for the maintenance of the modern global society and are a major part of the worldwide economic foundation. While mining is essential to maintain our modern society, it is estimated that mining and mining-related activities are the leading sources of metal releases to the environment (USEPA, 1999). From exploration through post-closure phase of hard-rock mining, the potential exists for negative environmental impacts to both surface water and ground water. The Mine Waste Technology Program reports that the United States (US) hard-rock mining industry (excluding coal) released 3.5 billion pounds of toxic pollution in 1998, greater than half of all pollution released that year in the US (USEPA, 1999). Acid mine drainage, which includes acidic water and elevated metal concentrations is considered by the USEPA to be the primary 'toxic pollutant' contributed by hard-rock mines.

Waste rock piles, stockpiles and leach ore piles comprise only a subset of the many facilities found within the mining industry. Waste rock piles, stockpiles and leach ore piles occupy a footprint greater than 90,000 hectares in the US alone and are a significant source of the reported metal release. While the US is used as an example, metal release is a global problem with significant volumes of waste rock existing in other countries such as Australia, Canada, Chile, and Mexico to name a few.

To minimize future effects from mining and to ensure the sustainability of the industry, additional knowledge of the systematics causing metal releases is required. Such information is used for prediction, planning and design of closure and mitigation strategies.

This thesis describes work conducted as part of the University of British Columbia (UBC) waste rock research program designed to provide data to better understand water flow and solute transport processes occurring within unsaturated waste rock piles. Specifically, this research focuses on the link between infiltration into a waste rock pile, the surface condition, its internal structure, and the spatial and temporal distribution of flow at the base of the pile.

1.1. RESEARCH OBJECTIVES

It is believed that a better understanding of the hydrogeology of waste rock piles is essential for quantification, prediction and prevention of acid rock drainage and metal loadings to the environment (Smith et al, 1995). For example, variable surface infiltration rates and material heterogeneities are believed to result in the preferential flow of water; and cyclical and seasonal evaporation of the pore water in the upper portions of the waste rock piles are believed to result in the consequent precipitation of metal-rich salts, and subsequent dissolution of salts by precipitation after extended dry periods. The flow of water and transport of metals through unsaturated waste rock is complicated by the heterogeneous material properties, dynamic climatic stresses and the configuration of the piles and/or covers. To improve our understanding, an intermediate-scale constructed waste rock pile experiment (CPE) was constructed and monitored for five years at a mine site in northern Saskatchewan. The CPE was used to investigate the flow of water and the transport of solutes through heterogeneous waste rock. The objectives of the experiments examined in this thesis are:

- To develop a comprehensive liquid and vapor flux balance for an uncovered waste rock pile and compare it to the water balance for the same pile after placement of a compacted surface cover.
- To investigate the relationship between the volume and timing of basal outflow relative to the surface texture and topography of the waste rock pile.
- To characterize the degree of spatial variability of infiltration into the covered waste rock and to estimate the magnitude and rate of flow within the covered waste rock.
- To identify the physical properties most important for understanding how water flows through coarse waste rock and to determine the mechanisms controlling the flow of water in covered waste rock.
- To characterize the in-situ waste rock structure and the distribution of tracers in pore water at the time of pile deconstruction.
- To understand the relationship between the structure of the pile, the in-situ tracer concentrations and the hydrographs observed in the basal lysimeters.
- To identify practices that might improve existing closure practices for waste rock and/or stockpiles.

Often predictions of the quantity and duration of metal leaching from waste rock are performed with little data about the hydrologic processes occurring within waste rock. The general hypothesis examined in this thesis is that the reliable prediction of mass loading from a waste rock pile demands a detailed understanding and characterization of the fluid flow and solute transport pathways, even in the case where a low-infiltration cover has been placed on the waste rock pile.

1.2. WASTE ROCK HYDROGEOLOGY

The mine waste rock hydrogeology project consisted of faculty and student researchers from UBC and the University of Saskatchewan (U of S) and was funded jointly by AREVA Resources Canada (formally Cogema Resources), Cameco Corporation and Natural Science and Engineering Research Council of Canada (NSERC). This research completes the flow and transport portion of the project conducted on an experimental waste rock pile at the Cluff Lake Mine. This section introduces the site and experimental design of the research experiment as a background for the following chapters.

1.2.1. Cluff Lake Mine

Cluff Lake is owned by AREVA Resources Canada. The mine operated between 1980 and 2002, producing approximately 30,000 metric tons of uranium. Cluff Lake is located in northern Saskatchewan, approximately 15 km from the Alberta border (Figure 1.1).

1.2.2. Climate

Cluff Lake is located in a semi-arid climate, in the northwestern Saskatchewan boreal forest region. Temperature, rainfall, snow depth, wind velocity and evaporation have been recorded since the start of mining at Cluff Lake. Average daily temperature during the summer months ranges from 14.0 ^{o}C to 17.0 ^{o}C and the range of average monthly temperatures in the winters months is -17.5 ^{o}C to -20.3 ^{o}C. AREVA estimates that the average frost-free period is approximately 90 days per year. Precipitation amounts for the region are highest during the summer months, typically during the months of June through to September. The greatest amount of snowfall usually occurs between January and April. Average annual precipitation from 1981 to 1998 was 459 mm and the average yearly pan evaporation measured at Cluff Lake is 704.5 mm (Cluff Lake Project, 2001).

1.2.3. Geology and the DJ-X Waste Rock

Cluff Lake is situated on the southern side of the Carswell Structure within the Athabascan basin. The Carswell Structure consists of three concentric rings of dolomite, sandstone and Precambrian gneiss, from the outer ring to the center respectively. The structure is surrounded by the younger, undisturbed Athabasca Formation (Harper, 1982). The structure is thought to be the result of a meteorite impact.

Airborne exploration began in 1958. Open pit mining at Cluff Lake began in 1980 and was followed by underground mining until May of 2002. Three waste rock piles were constructed, the Claude pile, D-Pit pile, and the DJN pile. The Claude waste rock pile was constructed between 1982 and 1989 and contains approximately 7.23 million tonnes of waste rock from the Claude pit. The pile is approximately 30 meters high and covers an area of 26.4 hectares. The D-Pit waste rock pile is small (2.3 ha) and contains less than 150,000 m^3. The DJN pile was constructed between 1989 and 1991. The pile is 16 meters high and covers an area of 15.3 hectares and contains approximately 1.62 million tonnes of waste rock. The DJN pile was constructed by end-dumping and contained well developed traffic surfaces between the lifts of dumped material. The D-JX waste rock was excavated from the D-JX open pit between 1994 and 1997 and placed in the DJN open pit. A small portion of the D-JX waste rock was used to construct the CPE. The D-JX material consisted of brecciated Precambrian gneiss, hosting both a uraninite-selenide-sulfide assemblage, containing molybdenite, and a uraninite-dravite-lead-copper-zinc sulphide assemblage (Baudemont et al, 1996). The highest grade uraninite sulphides were removed during mining. Other minerals present in the waste include epidote, coffinite (the main uranium-bearing mineral), magnesium chlorites, illite, and rare fluorite and dravite. The D-JX material has a total sulphur content of 0.2 to 0.5% and contains iron, copper, lead, zinc, uranium, aluminum and molybdenum as the major metals. Even though the site is located in a semi-arid, cool climate and the total sulfur content is low, low pH and metals are observed in the drainage from the CPE.

1.2.4. Experimental Design

An intermediate-scale waste rock pile was constructed and fully instrumented at the Cluff Lake Mine (Nichol, Smith and Beckie, 2000). The CPE was built in 1998 and was 32 m by 32 m-wide, with an 8 meter by 8 meter-wide by 5 meter-high central core (Figure 1.2). The waste rock pile was composed of run-of-mine waste rock, randomly dumped on a contiguous grid of 16 lysimeters, each 2 m by 2 m (Figure 1.3). The details of the lysimeter construction are outlined in Figure 1.4 and described by Nichol (2003). The outer walls of the lysimeter grid extended to the top surface of the CPE. Outflow from each lysimeter was piped to an instrument hut where the volume and rate were measured and recorded continuously. In addition, water samples were collected manually from nine soil water solution samplers, and nine tensiometers buried in the waste rock. The waste rock pile was instrumented with automatic temperature, soil moisture (TDR) and matrix suction sensors (tensiometer and thermal dissipation sensors). Detailed results from the three years of experiments on the uncovered CPE are described in Nichol (2003), Smith and Beckie (2003), and Nichol et al, (2000, 2003, and 2005) and are reviewed below.

1.3. RESEARCH METHODS

The studies described above produced significant results regarding water flow processes occurring in an uncovered, coarse unsaturated waste rock. The research not only advanced the understanding of flow mechanisms in waste rock, but also identified areas where further research was needed and provided insight into how to obtain needed data using existing instrumentation.

To meet the specific objectives of this dissertation, data were obtained during and following both natural and artificial rainfall events on the uncovered and the covered CPE. Methods included the application of an isotopic tracer, construction of a surface cover, and a detailed deconstruction of the CPE. Data included field observations of the waste rock structure and characteristics, measurements of lysimeter outflow, internal water content and temperature, climatic variables and tracer concentrations of pore water.

1.4. PREVIOUS RESULTS AND BACKGROUND

This section contains a summary of the previous results from experiments conducted with the CPE and background information about measuring soil water characteristic curves and estimating actual and potential evaporation from coarse waste rock. The information provided serves as general background to support the following four chapters.

1.4.1. CPE - Previous Results

The construction of the CPE was completed in September of 1998. The initial wetting-up of the waste rock required greater than a year, and the CPE first reached a state of dynamic equilibrium in late fall of 1999. Nichol (2003) analyzed lysimeter outflow between the summer of 1999 and the summer of 2001 following both natural and artificial rainfall events on the CPE. The average yearly net-percolation, into the uncovered CPE, measured as direct outflow relative to cumulative rainfall, varied from 55 to 59 percent. Hydrographs from the 16 basal lysimeters show that at a 2 m by 2 m scale, surface infiltration on the uncovered waste rock pile led to a large range of wetting front arrival times (Nichol et al, 2000, 2002, Nichol, 2003). The outflow response observed from each individual lysimeter was consistent in form from rainfall event to event. Furthermore, the magnitude of the spatial variability in flow was observed to increase with an increase in intensity of precipitation. Each individual wetting front arrival was believed to represent at least one spatially distinct flow path. The high variability in magnitude of flow observed in the hydrographs was proposed to be a result of the the irregular surface topography of the CPE and to a lesser degree related to internal structure of the waste rock (Nichol, 2003).

A chloride tracer was applied to the surface of the pile during an artificial rainfall event in the fall of 1999 and high frequency samples of the outflow were collected during rainfall events for tracer analysis. From the tracer data, Nichol (2003) was able to confirm that the outflow hydrographs represent a contribution of water from multiple flow paths. The chloride breakthrough curves and the hydrographs allowed for insights into the relationship between distinct flow paths, chemistry, and residence time. Nichol concluded that between 5 and 9 percent of the outflow during larger rainfall events was event water, and approximately 91 to 95 percent was pre-event water. In addition, he estimated a mean water residence time of 3.0 to 3.9 years for the 5-meter high pile at the average annual rainfall rate.

Wagner (2005) conducted a comprehensive study of the minerals that contribute to the weathering processes in the CPE. Wagner identified the primary minerals responsible for the cations measured in the outflow water as chlorite and muscovite, and determined that kaolinite, smectite and amphibole were secondary suppliers. Secondary minerals observed during the deconstruction of the CPE were gypsum, jarosite, ferryhydrite, goethite, annabergite and hydrated aluminum and magnesium sulfates. Based on data from 2001 to 2002, Wagner observed an initial, rapid and short-lived spike in the solute concentrations (up to 10,000 mg/L sulfate) following large natural and artificial rainfall events. Following the spike in solute concentrations, a general inverse relationship between outflow concentrations and rate of outflow was observed. The negative correlation between outflow and concentrations became apparent with the lowest concentrations during elevated flow rates and increasing concentrations as the flow rate gradually decreased to pre-rainfall levels. Wagner estimated sulfur release rates between 0.1 and 19 mg SO_4/(kg*week), yielding an approximate total of 150 kg of sulfur released from the CPE between 2000 and 2003.

1.4.2. Water Content and Matric Suction

The soil water characteristic curve (SWCC) is a relationship between the saturation of a porous material and matric suction. The shape of the curve is a function of the pore size distribution. Based on a SWCC, the relationship between either the water content or matric suction and the unsaturated hydraulic conductivity for a particular soil can be estimated using the Brooks and Corey (1964), the van Genuchten (1980) or the Fredlund et al (1994a) methods.

The SWCC can be measured from laboratory tests on small samples, estimated numerically using a model such as SoilVision (SoilVision Systems, 1997) or the MK model (Aubertin et al, 2003), or measured directly from in-situ matric suction and water content data over time. There are challenges associated with each method, and the best method often depends on material properties, as well as the moisture conditions.

The SWCC's of coarse waste rock determined in the laboratory are rarely representative of field conditions because of the small representative sample volume and because the testing process disrupts the waste rock structure. The disruption occurs during the sampling, sieving and packing of the waste rock into the testing apparatus. For situations where in-situ measurements cannot be made, laboratory SWCC's can be useful for understanding general waste rock properties of the finer grained size fraction, and are a necessary check on numerically predicted SWCC's. Laboratory SWCC's are also important in dual-continuum approaches, where the matrix and the coarse fraction are treated distinctly.

Field SWCC's can be obtained for materials where a wide range of water content and matric suction values are collected along an uninterrupted wetting or drying cycle. Near-surface soils are better candidates for the measurement of field curves where evaporation can result in high matric suctions that correspond to water contents below the value at residual saturation. In contrast, waste rock located below the effect of evaporation will have a smaller range of matric suction values making the measurement of a complete curve difficult.

Few examples of field based SWCC's exist from both in-situ instrumentation and from direct measurements of water content and matric suction from waste rock samples. Stockwell (2002), Stockwell et al (2006) and Nichol et al (2002) were unable to obtain meaningful field SWCC's from coincident field measurements of moisture content and matric suction. The majority of their field data plot within the portion of the SWCC most affected by hysteresis and they were unable to conclusively determine if the waste rock was wetting or drying at the time of measurement. In the laboratory, samples are subjected to uninterrupted periods of drying, starting from saturation and periods of wetting starting from a dry state. During the wetting and drying cycles, the matric suction and water content properties are measured and a wetting and a drying curve is determined. In the field, the waste rock is subjected to natural rainfall making it difficult to determine if the waste rock is on a wetting curve, drying curve or on a scanning curve. Since the matric suction/water content relationship in the field is typically along a scanning curve with a small range in suction, the end members of the field SWCC (ie. residual saturation and near- saturated portions of the SWCC) are not represented.

Shurniak (2003) has shown that reliable field derived SWCC's can be produced from a matric suction sensor and a TDR probe in the same location in near-surface waste rock and cover systems. Unlike the CPE, the material studied by Shurniak was fine grained and experienced uninterrupted cycles of wetting and drying. Fine grained material located at the soil/atmosphere interface can experience matric suctions far in excess of those produced in a standard Tempe Cell apparatus. As a result, a larger range in suction, including the end members, was represented.

The CPE was in an extended state of drain down since cover placement and was still draining at the time of deconstruction. The field conditions at the time of deconstruction, and the matric suction measurement techniques allowed for sampling of a larger range of the matric suction/water content relationship of the in-situ waste rock. The technique is discussed in Chapter 2.

1.4.3. Potential and Actual Evaporation

Evaporation from a waste rock surface is difficult to directly measure and is an important parameter of concern. Instrumentation to directly measure the surface energy flux were not available on the waste rock pile and the actual and potential evaporation were both estimated using the modified Penman approach, and calculated as a residual based on the water balance equation (1) in Chapter 2. The potential evaporation (PE) of water from a free-water surface requires a continuous supply of energy for the latent heat of vaporization and requires that a vapor pressure gradient exists away from the surface. For evaporation to proceed, a continuous supply of water must be available at the evaporating surface. In waste rock, the water supply is controlled by the moisture content and the particle size characteristics of the waste rock. Under saturated conditions, the evaporation rate from a soil should be nearly equal to the evaporation rate from a free-water surface (Holmes, 1961, Wilson et al, 1997). As the degree of saturation decreases, the evaporation rate becomes transport limited and is more dependent on the ability of the soil to deliver water to the evaporation surface. As the soil dries, the actual evaporation rate significantly decreases compared to the potential evaporation rate.

Potential evaporation is typically measured using evaporation pans or calculated from meteorological data using the Penman equation (Penman, 1948). The direct measurement of AE from a soil surface is difficult. Methods used to measure or estimate the AE are the energy balance method (Bowen 1926), the eddy covariance method (Baldocchi et al, 1988, Carey et al, 2005) and the modified Penman equation (Wilson, 1990 and 1994). Wilson (1994) modified the Penman (1948) equation for PE to estimate AE from a soil. The modified equation replaces the term describing the vapor pressure of the water at the surface by a term that describes the vapor pressure of the water held in capillarity within the soil. The modified Penman approach to calculate the vapor pressure is embedded in the numerical evaporative flux model used in this research. Model inputs for the calculation of the soil water vapor pressure include soil parameters derived from the SWCC and meteorological parameters such as temperature and relative humidity of the air.

1.4. STRUCTURE OF DISSERTATION

This dissertation consists of an introductory chapter (1), four independent research papers in Chapters 2 through 5, and one summary chapter (6).

Chapter 2 presents a pre-cover and post-cover water balance for the CPE and a discussion of the major water balance components. Chapter 2 also includes a discussion of techniques for characterization of the physical properties of coarse waste rock that are essential for evaporative flux modeling. The use of a model based on Richards' equation for simulating flux in and out of covered waste rock is discussed.

Chapter 3 presents the results of experiments that investigate the spatial and temporal distribution of outflow as measured in the basal lysimeters in response to rainfall events following two successive surface modifications. Surface modifications include the ripping and leveling of the surface followed by the installation of a compacted waste rock cover surface. Chapter 3 also presents observational data that links the waste rock heterogeneity and variable infiltration to the character and rate of water flow within covered waste rock.

Chapter 4 provides a discussion of a stable isotope tracer study conducted on the covered surface of the waste rock pile in the final year of the field study. The isotopic tracer is used to investigate the flow patterns within the covered waste rock, and to constrain estimates of the residence time of water in the covered waste rock pile.

Chapter 5 presents the results and a discussion of multiple investigations conducted during and following the deconstruction of the waste rock pile. The investigations attempt to link data obtained during deconstruction to earlier experimental results including the relationship between waste rock structure and lysimeter outflow, a dye tracer and a chloride tracer experiment.

Chapter 6 provides an overall summary and conclusions for the thesis and suggestions for future studies.

1.5. REFERENCES

Aubertin, M., Mbonimpa, M., Chapuis, R.P., 2003. A model to predict the water retention curve from basic geotechnical properties. Canadian Geotechnical Journal. v.40. pp. 1104-1122.

Baldocchi, D.D., Hicks, B.B. and Meyers, T.P., 1988. Measuring biosphere-atmosphere exchanges of biologically related gases with micrometeorological methods. Ecology. v. 69. n. 5. pp. 1331-1340.

Baudemont, D. and Fedorowich, J., 1996. Structural control of uranium mineralization at the Dominique Peter deposit, Saskatchewan, Canada. Economic Geology. v. 91. pp. 855-874.

Bowen, G.J. and Wilkinson, B, 2002. Spatial distribution of $D^{18}O$ in meteoric precipitation. Geology. v. 30. no. 4. pp. 315-318.

Carey, S.K., Barbour, S.L. and Hendry, M.J., 2005. Evaporation from a waste-rock surface, Key Lake, Saskatchewan, Canadian Geotechnical Journal. v. 42. pp. 1189-1199.

Cluff Lake Project, 2001. Comprehensive Study Report and Appendices, Submitted to the Canadian Nuclear Safety Commission on January 19, 2001. v. 1-2.

Harper, C.T., 1982. Geology of the Carswell structure, central part. Saskatchewan Geological Survey, Report 214. 6 p.

Holmes, R. M., 1961. Estimation of soil moisture content using evaporation data.

In: Evaporation, Proceedings of Hydrological Symposium 2, Toronto. Queen's Printer, Ottawa. pp. 184-196.

Marcoline, J.R., Smith, L, Beckie, R.D., 2006, Water Migration in Covered Waste Rock, Investigations Using. Deuterium as a Tracer. Proceedings of the 7th International Conference on Acid Rock Drainage, R.I. Barnhisel (ed.). The American Society of Mining and Reclamation, pp. 1142-1156.

Nichol, C.F., 2003. Transient flow and transport in unsaturated heterogeneous media: Field experiments in mine waste rock. Ph.D. dissertation, University of British Columbia, Canada.

Nichol, C.F., Smith, L. and Beckie, R., 2000. Hydrogeologic behavior of unsaturated mine waste rock: An experimental study. In Proceedings of the 5th International Conference on Acid Rock Drainage. Society for Mining, Metallurgy, and Exploration Inc. pp. 215-224.

Nichol, C.F., Smith, L. and Beckie, R., 2002. Evaluation of uncoated and coated time domain reflectometry probes for high electrical conductivity systems. Soil Sci. Soc. Am. Journal. v. 66. pp. 1454-1465.

Nichol, C.F., Smith, L. and Beckie, R., 2003. Water flow in uncovered waste rock - A multi-year large lysimeter study. Sixth International Conference Acid Rock Drainage.

Nichol, C.F., Smith, L. and Beckie, R., 2005. Field scale experiments of unsaturated flow and solute transport in a heterogeneous porous medium. Water Resources Research. v. 41.

Penman, H.L., 1948. Natural evapotranspiration from open water, bare soil, and grass. Proceedings of the Royal Society of London Series A. v. 193. pp. 120-145.

Shurniak, R.E., 2003, Predictive modeling of moisture movement within soil cover systems for saline/sodic overburden piles, MS Thesis, University of Saskatchewan, Canada. pp. 1-129.

Smith, L., Lopez, D., Beckie, R.D., Morin, K., Dawson, R. and Price, W., 1995. Hydrogeology of waste rock dumps. Report prepared for CANMET and BC Ministry of Energy, Mines and Petroleum Resources. pp. 1-130.

Smith, L. and Beckie, R., 2003. Hydrological and geochemical transport processes in mine waste rock, Ch 3 in Environmental Aspects of Mine Wastes, Mineral. Assoc. Canada, Short Course Series. v. 31. pp. 51-72.

SoilVision Systems Ltd., 1997. User's guide for a knowledge-based database program for estimating soil properties of unsaturated soils for use in geotechnical engineering. SoilVision Systems Ltd., Saskatchewan, Canada.

Stockwell, J.E., 2002. Investigation of hydrological and geochemical properties and spatial relationships of an unsaturated waste rock pile, Key Lake, Saskatchewan, Masters Thesis, University of British Columbia.

U.S. EPA, 1999. Mine waste technology program, 1999 annual report. Prepared for the U.S. EPA and the U.S. DOE. Inter agency agreement management committee: IAG ID NO. DW89938513-01-0.

Wagner, K., 2005. Geochemical characterization of mine waste rock, Cluff Lake, Saskatchewan. Masters Thesis, University of British Columbia.

Wilson, G.W., 1990. Soil Evaporative Fluxes for Geotechnical Engineering Problems. Ph.D. Thesis, University of Saskatchewan, Saskatoon, Saskatchewan, Canada.

Wilson, G.W., Fredlund, D.G. and Barbour, S.L., 1994. Coupled soil-atmosphere modeling for soil evaporation. Canadian Geotechnical Journal. v. 31. no.2. pp. 151-161.

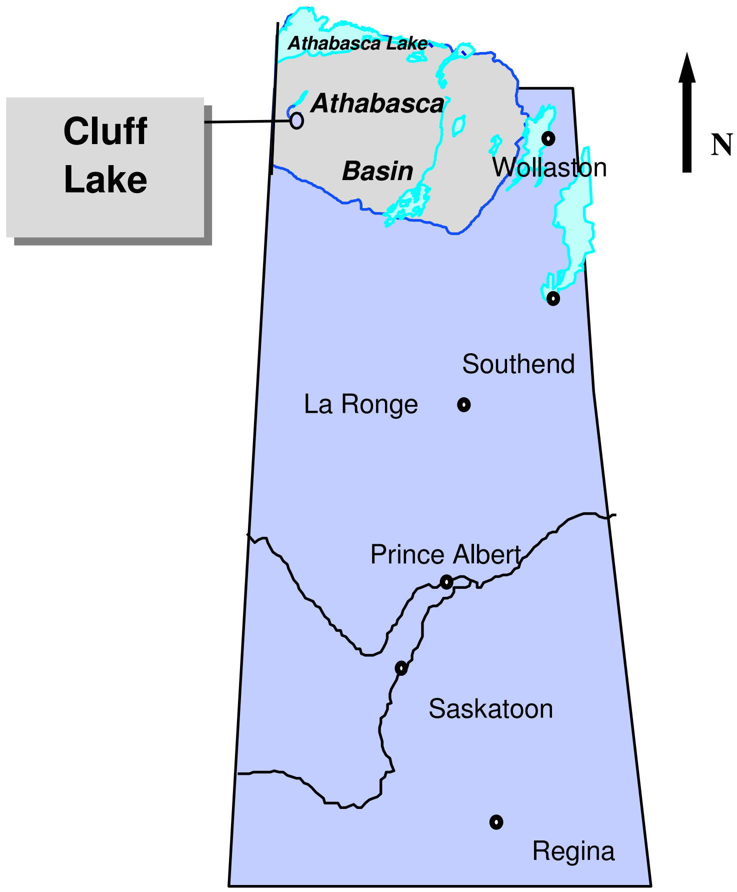

Figure 1.1. Map of Saskatchewan with the location of the Cluff Lake Mine and the constructed waste rock pile experiment.

Figure 1.2. Photograph of the CPE on top of the DJN waste rock pile. Photograph taken in the summer of 2003.

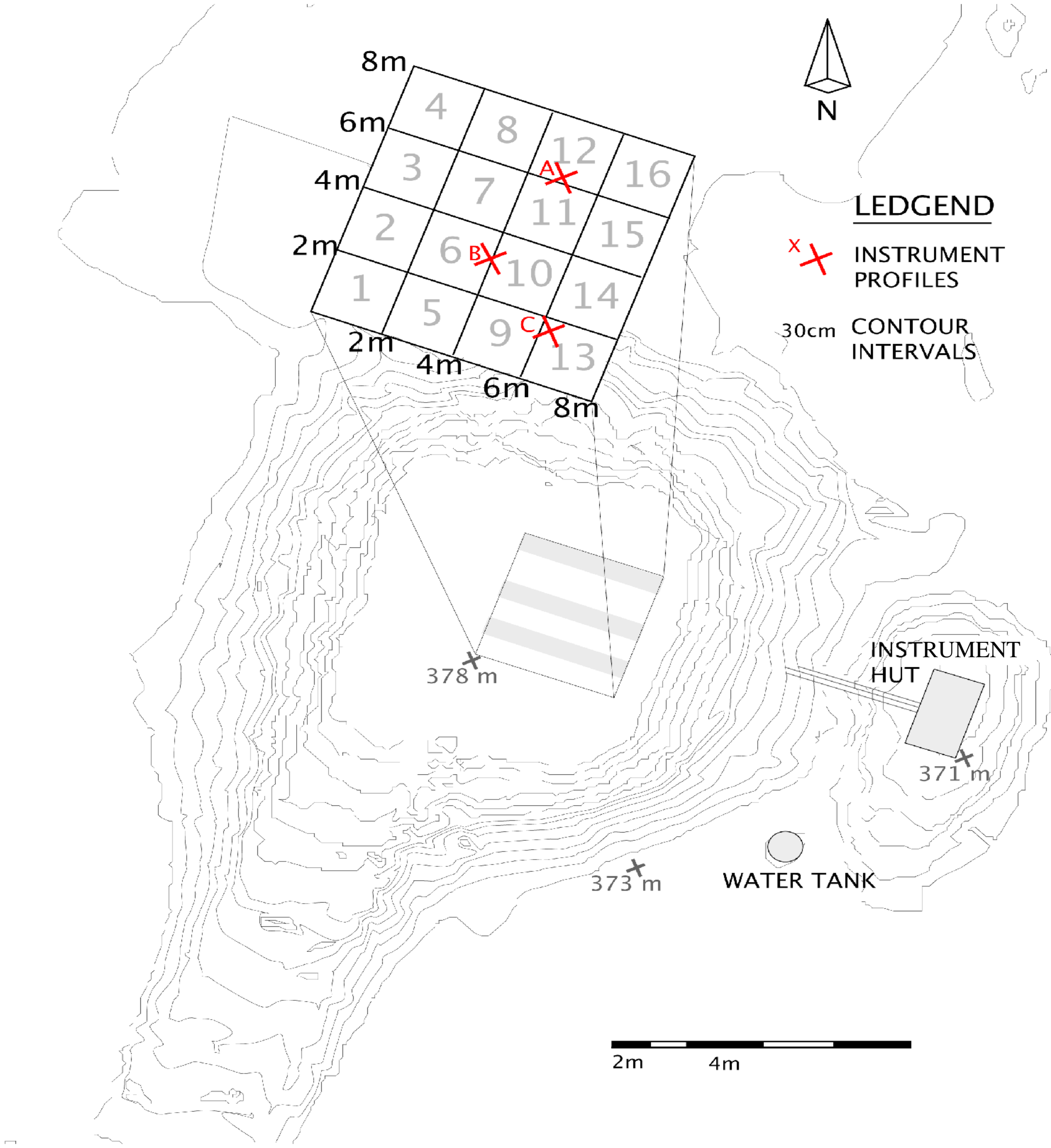

Figure 1.3. Schematic view of the top of the waste rock pile. The grid of sixteen lysimeters is shown in relation to the overlying waste rock. The origin of the grid is on the lower left (south west) side of lysimeter 1. The lysimeter grid is to scale and is superimposed on topographic contours of the constructed waste rock pile. The three instrument profiles are labeled with an X, and contour intervals are 30 cm.

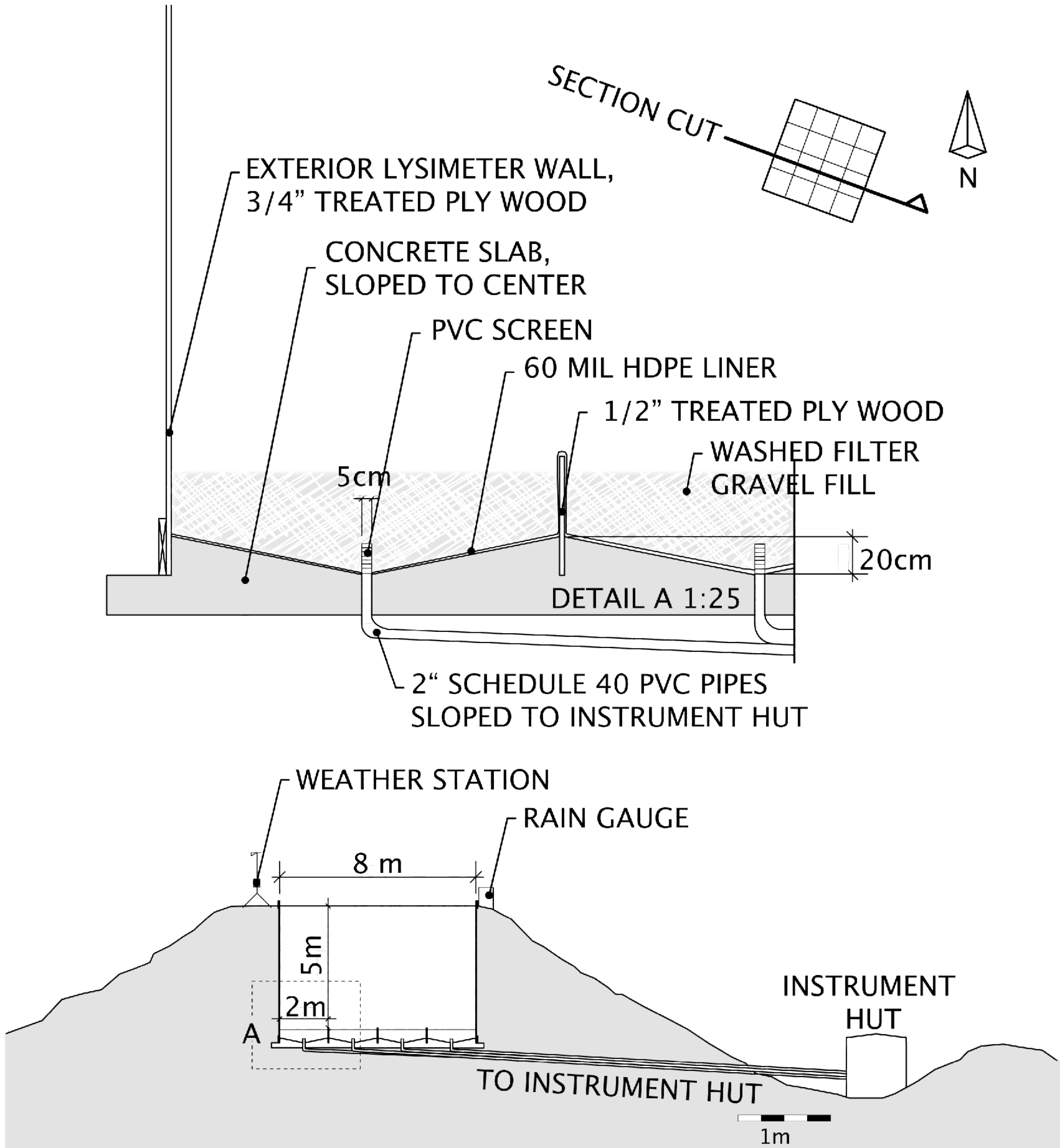

Figure 1.4. Cross-section of the constructed waste rock pile and a detail of the basal lysimeter design.

CHAPTER 2: WATER BALANCE OF THE CONSTRUCTED WASTE ROCK PILE: PRE AND POST-COVER.

2.1. INTRODUCTION

Water is the principal medium by which contaminants are transported from sources in mine waste rock to the receiving environment, and a low permeability cover can be expected to reduce net infiltration and delay metal loadings. As a result, the need to quantify the water balance components for covered and uncovered waste rock stockpiles is common at both operational and closed mines. Water balance components such as net percolation or basal outflow are important input parameters for surface and groundwater modeling (Lopez et al, 1997, Swanson et al, 1998, USEPA, 1999, Kempton and Atkins, 2000). The infiltration, storage and runoff components are important for determining slope and erosional stability of waste rock (Torres et al, 1998, Nicolau, 2003) and for carrying out geochemical modeling (Alpers and Nordstrom, 1999, Bain et al, 2001, Frostad et al, 2005). The relative proportions of runoff, infiltration and evaporation are critical for evaluating cover performance (Khire et al, 1997, O'Kane et al, 2000, Durham, 2002, Noel and Rykaart, 2003), and for evaluating vegetative success (Grigg et al, 2003). Water balance components are also important for estimating when waste rock is no longer

---

A version of this chapter will be submitted for publication. Marcoline, J.R., Water balance of the constructed waste rock pile: pre and post-cover.

accumulating water following initial material placement, and has reached a state of dynamic equilibrium.

Direct measurement of the water balance components in waste rock is often difficult, even with abundant in-situ instrumentation and monitoring devices. Waste rock piles may be hectares in size and consist of highly heterogeneous material with significant variations in particle size and composition. Often data are collected from a few locations across these large piles, and each measurement may only be representative of the material within a few centimeters to a meter of the instrument.

The research presented in this paper is from a controlled, intermediate-scale experimental waste rock pile from which detailed hydrologic and climatological data were collected. The research attempts to quantify the water balance of an experimental waste rock pile and examine how the alteration of the surface condition, by the placement of a low permeability cover, affects the water balance.

The primary objective of this research was to establish the water balance for an unsaturated waste rock pile over the time period from 2000 to 2004. The four years include a three year period when the pile was uncovered, and a one year period after a compacted cover was placed on the pile. Of particular interest is the change in water balance components following the placement of a lower permeability cover that resembled a traffic, or haul surface.

2.2. BACKGROUND AND EXPERIMENTAL DESIGN

2.2.1. Field Location and Climate

Cluff Lake Mine is a hard-rock uranium mine located in northern Saskatchewan, approximately 15 km from the Alberta border. The mine site is located in a semi-arid climate, in the northwestern boreal forest region. The average annual temperature at Cluff Lake is -0.3 °C, with three frost-free months per year. Average daily temperatures are above freezing for approximately 5 months (May to October). The average site rainfall, excluding snow, for the 18 year period between 1981 and 1998 was 310 mm, with a minimum of 231 mm in 1986 and a maximum of 433 mm in 1996 (Cogema Resources, 2001). Monthly precipitation data for the top surface of the waste rock pile are summarized in Table 2.1. Based on the daily Class "A" Evaporation Pan data and rainfall from 1981 to 1998 (Cogema Resources, 2001), potential evaporation at Cluff Lake is approximately twice the precipitation, with an average potential evaporation of 704 mm per year.

2.2.2. Experimental Design

The constructed waste rock pile experiment (CPE) was located on top of the D-JX waste rock pile. The CPE was built in 1998 and was 32 m by 32 m-wide, with an 8 m by 8 m-wide by 5 m-high central core (Nichol, Smith and Beckie, 2000). The waste rock pile was composed of run-of-mine waste rock, dumped on a contiguous grid of 16 lysimeters, each 2 m by 2 m (Figure 2.1). Details of the lysimeter construction are outlined in Figure 2.2. The outer walls of the lysimeter grid extended to the top surface of the CPE. The volume and rate of lysimeter outflow, internal moisture content, temperature, and climatic conditions were measured and recorded continuously. Moisture content was measured by time domain reflectrometry (TDR) by a total of 21 probes placed in 3 vertical profiles and later by 4 additional probes placed in the compacted cover (described below). The pre-covered waste rock pile experiment at Cluff Lake is described in detail by Nichol et al (2000), Nichol (2003), Marcoline et al (2003 and 2006) and Nichol et al (2005); therefore, this paper only provides a summary of the previous work and focuses on the cover experiment.

2.2.3. Compacted Waste Rock Cover on CPE

In September of 2002, a compacted layer was constructed with D-JX waste rock located from within the CPE but outside of the lysimeter grid. Four additional Zegelin-type TDR probes (Zegelin, 1989) with a high resistance coating on the center rod (Nichol et al, 2003) and two temperature probes were installed on the surface just prior to placing the compacted cover. Minus 0.1 m screened waste rock was used for the compacted cover. Moisture was added to approximate the optimal water content of 7% as determined by laboratory Standard Proctor testing (ASTM, 1991a), and the surface was compacted with a jumping-jack compactor delivering approximately 3100 pounds/blow over a 0.34 m by 0.36 m pad. The compacted layer was constructed with an overall slope of 1% towards the north edge of the waste rock pile to allow for surface runoff during higher intensity storms. The cover had a runoff collection drain on the north side, described below. The final surface resembled a mine traffic surface, had a depth of compaction of approximately 0.15 m and an average density of 2280 kg/m^3.

2.3. METHODS

The water balance is determined for the CPE based on data from the four year period between 2000 and 2004. The water balance for the CPE consists of four measured quantities and one calculated quantity. The direct measurements are the water falling on the pile from precipitation (P), the net-percolation (NP) which is equivalent to the water leaving the pile through lysimeter outflow, change in storage (ΔS), and surface runoff (R_S). Evaporation (E) is the calculated quantity. Measurements of P and NP were collected and recorded for the duration of the experiment. R_S was not observed prior to cover placement and was only collected and recorded for the post cover period. Change in storage (ΔS) was evaluated using records of moisture content and outflow. Direct measurements of evaporation for the CPE do not exist and a water balance approach was used to develop an estimate of the evaporation across the top surface of the pile. Evaporation was estimated using the following equation:

$$E = P - R_S - NP - \Delta S \quad (1)$$

A coupled unsaturated flow and evaporative flux model was used as a check on the estimated evaporative component of the water balance for the covered pile.

The water balance data from 2000 to 2004 are presented on an annual basis from April 1st to March 31st. The use of annual estimates simplifies the water balance calculation since the annual net change in internal storage was approximately zero (discussed below). The 1st of April was identified as the beginning of the annual cycle based on the observations that the surface of the waste rock pile thawed between mid-April to early May, and that the lowest outflow volumes were recorded in early April of each year as shown in Figure 2.3. Figure 2.3 shows the hydrograph measured as combined outflow from the 16 lysimeters at the base of the CPE between January of 2000 and May of 2004. The methodology used to acquire data for each component of the water balance is presented below.

2.3.1. Precipitation (P)

Precipitation measured on the CPE consisted of both natural and artificial rainfall events. Natural rainfall was measured by two independent, continuously logging, tipping bucket rain gauges located directly on the top of the waste rock pile. The rainfall record is complete without data gaps. An Environment Canada tipping bucket rain gauge located one kilometer northeast, a manual rain gauge located four kilometers south at the mill site, and a tipping bucket gauge located approximately five kilometers south-southeast at the tailings facility were used as a quality check on the data. Data from the Environment Canada rain gauge and the manual gauge at the mill site were plus or minus 10% of the natural rainfall component recorded in two tipping bucket rain gauges on the top surface of the CPE, however, the rain gauge at the tailings facility recorded a significantly lower amount of precipitation. The quantity and uniformity of artificial rainfall on the CPE was measured using 32 cups placed on the surface of the waste rock pile, two centered above each of the 16 lysimeters. The uniformity of each of the combined sets of 16 cups was greater than 95 using the Christensen Uniformity Coefficient (Christensen, 1942). The coefficient of uniformity approaches 100 as the rainfall approaches complete uniformity (Nichol, 2003). As a result of the even rainfall coverage, the average value from the rainfall cups was used and rainfall was assumed to be evenly distributed across the surface.

2.3.2. Net Percolation (NP)

The 64 m^2 area of the central core of the waste rock pile was located on top of 16 lysimeters, each four square meters in area. Net-percolation was measured as direct outflow from the waste rock pile using 16 tipping bucket rainfall gauges plumbed to the basal lysimeters. The time of each tip for each lysimeter was recorded. Calibrations specific to each tipping bucket were used to convert the tip time difference arrays into precise flow rates. Cumulative volumes from each basal lysimeter were then calculated from the calibrated flow rate data and the tip time arrays.

The term net-percolation is synonymous to net-infiltration and is used to make a clear distinction between net-infiltration and surface infiltration. Net-percolation refers to water that infiltrates into the waste rock pile to a depth beyond which evaporative effects are significant and reports to the base of the CPE. Surface infiltration includes water that percolates into the waste rock and is later removed by evaporation.

2.3.3. Surface Runoff (R_S)

Runoff from the surface of the CPE only occurred after placement of the compacted waste rock cover in the fall of 2002. Prior to cover construction, the perimeter of the waste rock pile was isolated from the surrounding waste rock by the lysimeter perimeter walls, which extended several centimeters above the surface. The design prevented overland flow from entering the 8 m by 8 m surface of the CPE. Localized ponding on the surface of the CPE was observed once during the highest intensity artificial rainfall event. Even during this high intensity event overland flow was not observed. All water that was applied to the surface of the pile prior to covering either infiltrated into the waste rock or was removed by evaporation.

During the placement of the compacted waste rock cover, a runoff gutter was embedded into the surface along the base of the lowest side of the cover. Following placement of the lower permeability cover, runoff occurred in response to large rainfall events. Water collected in the runoff drain was stored in four 200 l drums and measured using two independent tipping bucket rainfall gauges at the base of the pile.

2.3.4. Change in Storage (ΔS)

The water content of the pile increases rapidly during a few rainfall events, and the duration of drain down of the water content is typically on a seasonal scale. The seasonal drain down to a pre-spring water content occurs over a period of approximately 3 months (Figure 2.3). To account for the seasonal pattern of water content within the CPE, the change in storage is defined on a yearly basis. The net-annual percent change in storage was computed based on the difference in the volumetric water content in the CPE in March of each year. The change in the volume of water in storage within the CPE was estimated using water content data measured by 21 TDR probes located and along three vertical profiles at depths of 0.15 m, 0.2 m, 0.3 m, 0.4 m, 0.7 m, 1.2 m, 1.95 m, 3.2 m, and 4.7 m within the waste rock pile and five TDR probes from locations within the cover. Unlike the lysimeters, which sample all water leaving the base of the CPE, the TDR probes provide only limited point data from within the heterogeneous waste rock which must be scaled up to provide estimates of whole-pile water storage. The estimate of the whole-pile water storage was based on the sum of the volume of water calculated to be the cover (0 m to 0.3 m), in the upper half of the waste rock pile (0.3 m to 2.5 m) and in the lower half of the waste rock pile (2.5 m to 5 m).

2.3.5. Evaporation (E)

Direct measurements of evaporation from the surface of the CPE do not exist. As a result, annual evaporation was calculated as a residual based on equation (1) and therefore includes the cumulative errors associated with each of the other four components of measured water balance. While the cumulative errors are not quantified, the most likely sources of error are associated with the change in storage and the net-percolation terms. Transpiration is not included since vegetation was not established on the surface of the CPE during the four year period. Estimated AE, simulated AE and simulated PE rates are compared to Bowen ratio energy balance data collected from the Cluff Lake Mine site in 1996 (Ayres, 1998) and to PE data measured at the mill site.

2.3.5.1 Evaporative Flux Modeling

To assess the reasonableness of the evaporation rate calculated from the measured water balance components, evaporation rates were also calculated using an unsaturated flow model containing an evaporative flux module.

There are many possible models that can be used to estimate evaporation. The HELP model (U.S Army Corps of Engineers, 1994) is one of the most widely used models for water balance evaluations because of its ease of use and minimal data requirements; however, this model is not based on Richards equation and has been shown to provide poor estimates of water balance components (Benson and Pliska 1996, Albright et al, 2002). Increasingly, one and two-dimensional variably-saturated porous media models based on Richards equation such as UNSAT-H (Fayer and Jones 1990), SoilCover (SoilCover, 1997) or VadoseW (Geo-Slope, 2004) are applied for water balance studies in waste rock. These models are physically based, readily available, but do not account for non-Darcy flow such as macropore flow. HYDRUS-2D (Simunek et al, 1996) accounts for preferential flow, but does not take into account heat transfer or vapour flow in evaluating evaporative fluxes at the soil surface.

While several models are available that incorporate evaporative flux modeling, SoilCover Version 4.1 (SoilCover, 1997) was deemed most appropriate for the evaluation of fluxes from the covered waste rock. SoilCover is a transient, one-dimensional finite element, heat and mass transfer model for saturated and unsaturated soils. The unique feature of SoilCover is that it describes moisture flow using the Richards equation and vapor flow using Fick's law, and the water and vapour flow processes are coupled using both heat flow and the modified Penman equation (Wilson, 1990 and Wilson et al, 1994). As a result, SoilCover enables the accurate prediction of actual evaporation and is commonly used (Kowalewski, 1999, Rykaart et al, 2001, Wels, 2001). The model describes heat, water and vapor flow within the soils based on meteorological conditions and soil properties.

SoilCover uses a Richards equation approach to model variably saturated water flow. Therefore, SoilCover may not provide a valid physical representation of flow within the uncovered CPE where a significant macropore flow component was observed (Nichol, 2003, Marcoline et al, 2003, Nichol et al, 2005). If the flow through the lower permeability cover results in water bypassing the coarser regions through which the macropore flow occurred, and the physical parameters measured in the field and laboratory are measured from the finer portions of the waste rock, then it is likely that a capillary-based, porous media model can be used to evaluate the water balance components of the pile following cover placement.

For the measured waste rock properties, and the imposed climate and thermal boundary conditions, SoilCover is used to predict surface flux and basal flux conditions. The flux conditions predicted from the CPE include actual evaporation, potential evaporation, surface runoff and net-percolation. SoilCover input files include daily meteorological data for two years and solver settings (Appendix A).

2.3.5.2. Evaporative Flux Modeling Using SoilCover

SoilCover modeling proceeded in the following steps:

1) Two base case scenarios were developed: one using a soil water characteristic curve (SWCC) and porosity value developed in the laboratory, the other a SWCC and porosity value developed from field measurements in the CPE.

2) Each base case model was run for the April 2002 to April 2003 water year (uncovered) and the April 2003 to April 2004 water year (covered).

3) The initial condition was established by completing a transient simulation with no recharge representative of the final month of the winter drain-down. The moisture content was adjusted at the top boundary, basal boundary, and at one internal boundary to match the in-situ water content profiles measured from TDR probes in the field and the basal lysimeter outflow, representing a quasi-steady state. The initial condition determined was in an equilibrium state and water entering or

leaving storage during each water year can be attributed solely to the imposed change in the upper boundary condition.

4) A small amount of water was artificially introduced into the model in the days prior to large rainfall events to promote numerical convergence of the algorithm.

5) A sensitivity analysis of the model calculations to hydraulic conductivity and porosity was conducted for each of the base case simulations. The sensitivity of the model calculations to the thickness of the cover layer was evaluated for the covered simulations. To ensure the model was conserving mass, the total volume of water entering the CPE as rainfall and the total volume leaving the pile through outflow and evaporation were compared to see if they balanced daily and yearly for each model run.

2.3.5.3. Base Case Simulations

Two base case simulations of liquid and vapor flux through the CPE were conducted. One simulation used a SWCC measured in the laboratory by Dr. Lee Barbour at the University of Saskatchewan, while the other simulation used a SWCC measured in the field. The SWCC's are discussed in detail below. Simulations of the uncovered CPE were conducted for the 2002 water year (April 2002 through April 2003), and data from the 2003 water year (April 2003 through April 2004) were used for the covered simulations.

SoilCover uses a layer system to define the model profile, with boundary condition values assigned at the top and the bottom of each layer. The lower boundary condition was specified as a transient temperature, constant matric potential boundary (0 kPa). Basal flux was evaluated at an observation point located 5 m below the surface. Basal temperature was specified by daily temperatures measured at the base of the CPE. The upper boundary condition was a transient flux boundary, specified by measured daily precipitation, minimum and maximum air temperature, minimum and maximum relative humidity, solar radiation and average wind speed.

The uncovered waste rock profile was modeled as a system of two material layers. The entire profile was discretized into 98 nodes across the profile. SoilCover has a maximum limit of 100 nodes. Nodal spacing decreased near the material layer boundaries. The grid was auto-generated within the model based on a specified minimum and maximum size for each material layer. The first layer was 0 m to 4.85 m deep and the second material layer was 4.85 m to 6.0 m in depth. The node spacing ranged from 0.1 cm at the waste rock surface and outflow boundary to a maximum of 10.0 cm within profile. While the material properties for the two layers were identical, the addition of the bottom layer allowed for a finer discretization resulting in a better fit to initial moisture conditions during model calibration. The 1 m depth added to the lower boundary was arbitrary and did not influence the results.

The covered waste rock was modeled as a three-layer system that included a

0.40 m thick surface layer above the two waste rock layers described above. The three layer models had a total of 98 nodes across the profile with node spacing ranging from 0.5 cm to 1 cm in the cover and lowest layer and from 2 cm to 12.5 cm within the middle waste rock layer. The grids for both the covered and uncovered models were similar, however, the additional surface layer with a fine discretization resulted in a slightly lower discretization throughout the waste rock layer and near the outflow boundary in the covered model.

2.3.5.4. Initial Conditions

Initial water content and matric suction values at each boundary layer strongly affect the model results. If the specified initial moisture conditions were too low the model added water to storage and the annual net-percolation estimates were lower than observed. If the initial moisture conditions were higher than actual, the predicted net-percolation was significantly higher than observed because of a rapid release of water from storage.

Transient simulations were conducted to better constrain the initial antecedent moisture profile for the base case scenarios where TDR data were not available. SoilCover requires that either a water content or matric suction value is specified at the boundary of each layer. The initial "guesses" of the moisture conditions were based on TDR probes located at depths closest to the layer boundary depths. Volumetric water content from April 2002 were obtained from TDR probes located at 0.2 m, 3.0 m, and 4.5 m beneath the waste rock surface, and for April 2003 from

TDR probes located at 0.15 m, 0.4 m, and 4.70 m beneath the cover surface. These water content values were converted to matric suctions using the appropriate SWCC and the data used as initial conditions in the transient simulations for the uncovered and covered scenarios, respectively. Initial matric suction values specified at each layer boundary were then adjusted by trial-and-error until the model outflow matched the observed field data. The final moisture versus depth profiles predicted at the end of the simulations were compared to the initial TDR data points, and the matric suction profiles were used as the initial profiles in each of the base case simulations. The procedures were similar to those used by Swanson et al (2003) and ensured that water was not being accumulated or depleted, except in response to the boundary condition changes specified as part of the transient base case simulations.

The simulations used to determine initial conditions used measured weather conditions and laboratory determined hydraulic conductivity as input parameters. The initial value of porosity corresponded to the volumetric water content on the SWCC at 0 kPa for each base case. The sensitivity to the soil property input parameters (porosity and hydraulic conductivity) and the sensitivity to the cover thickness were evaluated using the base case simulations as described below.

2.4. DETERMINATION OF PHYSICAL PARAMETERS

The physical properties of the waste rock within the CPE and of the compacted cover were used in the model for the determination of a comprehensive water balance. The methodology for the determination of hydraulic conductivity, water content, matric suction, and the SWCC is described below.

2.4.1. Hydraulic Conductivity

Saturated hydraulic conductivity of both the waste rock and the compacted surface cover were estimated using double ring infiltration tests (modified ASTM Standard D3385) in the field. Leakage from the outer ring of the infiltrometer was observed during infiltration measurements on the covered CPE and results were not reliable.

In addition to field testing, hydraulic conductivity was obtained from laboratory constant head tests (ASTM D 2434-68). The waste rock was sampled, shipped to the laboratory and sieved into a 0.15 m permeameter. In-situ density measurements of the non-compacted waste rock were not available at that time of hydraulic conductivity testing. Four sieved waste rock samples were packed to an approximate density of 1800 kg/m^3, higher than the 1100 kg/m^3 to 1750 kg/m^3 range measured one year later on the CPE.

Two laboratory hydraulic conductivity tests were conducted on compacted waste rock material. The permeameters were packed with minus 0.1 m waste rock and compacted to approximately 2100 kg/m^3, resulting in a similar particle size and density as measured in the field.

2.4.2. Water Content and Matric Suction

The soil water characteristic curve can either be measured from laboratory tests on small samples, estimated empirically using a model such as that developed by van Genuchten (1980), Fredlund and Xing (1994), Fredlund and Wilson (1997), Aubertin et al (2003), or measured directly from in-situ matric suction and water content data collected over time. There are challenges associated with each method, and the best method often depends on material properties, as well as moisture conditions.

A single composite field soil water characteristic curve from the waste rock pile was determined using data obtained at the time of deconstruction. Matric suction values derived from the filter paper method were combined with volumetric water content data of waste rock from the same location. Guan (1996) discussed flaws in earlier filter paper methodologies and summarizes the evolution of the filter paper method since the early 1960's. Schleicher & Schuell No. 589-WH filter paper was used to calculate matric suction following ASTM procedure D5298-92 using the matric suction equation derived by Fredlund and Xing (1994) and the procedures recommended by Guan (1996) and Leong et al (2002).

Samples of waste rock were collected during deconstruction from different locations along a 5 m deep profile, including dry waste rock near the surface and nearly saturated waste rock immediately above the basal lysimeters. Each of the 35 samples were carefully placed in a 500 mL glass jar with minimal disruption of the waste rock. Three pieces of filter paper were placed in contact with the waste rock and the jars sealed with minimal head space. The jars were left in a controlled temperature box at 18°C and allowed to come to equilibrium for one week. Theoretically, after equilibrium was achieved, the matric suction of the paper and of the waste rock were equal. The water content of the filter paper was determined and converted to suction values using the calibration matric suction versus water content curve derived in the laboratory for the Schleicher & Schuell No. 589-WH filter paper. The combined measurement pairs of matric suction and volumetric water content from each sample were used to estimate the composite field SWCC (Figure 2.4). The composite SWCC is representative of the finer grained portions of the waste rock that fit within the 500 mL jars. Plotting a single SWCC based on a set of different samples assumes that all of the material sampled was homogeneous. While the assumption may be poor, the curve yields an approximation of the matric suction/volumetric water content relationship similar to that of other waste rock materials published in the literature (Cogema Resources, 2001, Wels et al, 2001, Kabwe et al, 2005).

A distinct drying laboratory SWCC was measured at the University of Saskatchewan by Dr. Lee Barbour from a minus 0.1 m size fraction of D-JX waste rock. The sample tested was a composite of 60, five liter samples collected during the construction of the CPE in 1998 (Nichol, 2003).

A SWCC for the cover material was determined numerically based on the Fredlund & Xing (1994) equation using the program SoilVision (SoilVision Systems Ltd., 1997). SoilVision inputs included particle size distribution data averaged from the eight samples collected from the cover during the deconstruction, and three volume-mass properties (in-situ field density, specific gravity, and porosity).

The hydraulic conductivity curves that correspond to each of the field SWCC, the laboratory SWCC, and the cover SWCC were generated using the Fredlund et al (1994a) equation, which allows for the estimation of the permeability function from the SWCC without knowledge of the residual saturation. Other methods such as Brooks and Corey (1964) and van Genuchten (1980) are available, but require measuring the permeability at various suction levels, or require knowledge of the residual saturation.

2.5. RESULTS AND DISCUSSION

2.5.1. Measured and Calculated Water Balance

The outflow record from the CPE for May to December of 1999 was reported by Nichol (2003), and Nichol et al (2005). Data from the 1999 water year were excluded from this water balance analysis because the CPE did not reach a dynamic equilibrium until October of 1999. The continuous outflow record for the CPE from April 2000 to April 2004 is plotted in liters per day, and shows the seasonal variation in outflow (Figure 2.3). The measured water balance components for the period between January of 2000 and May of 2004 are shown as cumulative plots in Figure 2.6. The cumulative precipitation pattern for each of the four years is similar in both form and magnitude. The precipitation was recorded on the waste rock pile between May and October of each year and does not include the equivalent water from snowfall. Large drifts of snow were observed around the base of the constructed pile and surrounding the instrument hut, however, little to no snow was observed on the top surface. The top surface of the experimental pile was nearly the highest point on the mine site and experienced frequent high winds off Cluff Lake that removed any snow that accumulated on top of the pile. Between November and April of each year, surface infiltration was negligible and the depth of freezing progressively increased to greater than one meter.

The cumulative outflow curve (Figure 2.6) shows a response that is delayed yet similar in shape to the cumulative precipitation plot. A significant reduction of outflow, as well as the first appearance of surface runoff, is evident in the cumulative outflow curve in 2003 to 2004 following the placement of the compacted waste rock cover. Each year during the winter months, basal outflow continued and the volumetric water content would drop to its lowest annual value, typically observed in March and April. For the three years prior to cover placement, the annual cumulative outflow plots (Figure 2.7) show a lower magnitude response to the first few spring rainfall events and higher magnitude response to similar size events later in the year. The lower magnitude responses in the spring are associated with the re-wetting of the waste rock following winter drain down.

A summary of the annual water balance components is provided in Table 2.2. To account for the slow transit times of water within the CPE, water balance calculations were made on a yearly basis. For water years 2000, 2001, and 2002, 44%, 51% and 55% of rainfall was measured as lysimeter outflow. Annual water balance estimates assume that the net change in storage within the pile was zero. The assumption of a zero change in storage is based on similar internal volumetric water content data, and on a stable outflow rate of less than one liter per day (~2.7 $\times 10^{-10}$ m/s) observed in the early spring of each year (Figure 2.3). This suggests at least for the uncovered CPE, that dynamic equilibrium was achieved. Outflow rates decreased following the onset of freezing air temperatures and asymptotically approached a near-steady outflow by March of each year. Calculating evaporation as a residual in the water balance, 56%, 49% and 45% of precipitation was removed by evaporation from the waste rock pile for 2000, 2001 and 2002 years, respectively.

The differences in the annual evaporation are related to different weather patterns, the different number of large magnitude rainfall events in each of the three years, and to a lesser degree, related to an evolving surface texture of the waste rock pile. The physical characteristics or the textural differences of the near-surface waste rock will influence both the upward transport of water to the surface and the amount of actual evaporation.

Fast flow of water to the basal lysimeters and/or to depths below the influence of evaporative forces was observed following larger rainfall events. Fast flow of water results in an event-based net-percolation rate that is greater than the annual average, and an AE that is lower than the annual average AE. Consistent with the observations of Ayres (1998), it appears that the evaporation in the uncovered pile was transport limited, based on the smaller AE/PE ratio in the dry periods between rainfall events. A simple explanation is that the lower magnitude or more frequent rainfall events result in higher near-surface water contents and a more continuous supply of water available at the evaporating surface. The effects of the transport limited system are also observed in the numerical modeling.

The cumulative water balance plots for the water year 2003 are shown in Figure 2.8. Following construction of the compacted cover, the lysimeter outflow was reduced to less than 10% of precipitation, runoff increased from zero to approximately 30% of precipitation, and at least 60% of the precipitation was removed by evaporation (Table 2.2). A higher percentage of precipitation was lost to evaporation than in the two previous years and may be attributed to a higher water holding capacity of the cover material and the underlying compacted coarse waste rock. The water content in the cover remained between 18 and 20% between summer rainfall events as shown by TDR probes in the cover (Figure 2.9), approximately 10% higher than the water content of the pre-cover waste rock between rainfall events. The higher percentage of evaporation may also be attributed to the reduction in macropore and fast preferential flow following the construction of the compacted cover. Reduction of the amount of preferential flow would result in additional water held closer to the evaporation surface and allow for a higher annual evaporation.

To further constrain the evaporation estimates, and to better understand the water balance components, the SoilCover model was used for the 2002 pre-cover year and the 2003 post-cover year.

2.5.2. Physical Parameters

The SWCC describes the relationship between the water content and matric suction, which can be related to the unsaturated hydraulic conductivity for a particular soil. Figure 2.4 shows three SWCC's: one derived from the matric suction and volumetric water content measurements (SWCC (field curve)), one based on a laboratory curve derived from a Tempe cell test (SWCC (laboratory curve)), and one estimated SWCC for the compacted waste rock cover. Both the field and the laboratory SWCC's were obtained from the minus 0.1 m portions of the waste rock and are more representative of the matrix material than the bulk waste rock. With the lower infiltration conditions observed following cover placement, water flow is likely to occur exclusively within the matrix material.

The hydraulic conductivity curves (HCC) derived from the field SWCC, the laboratory SWCC and the cover SWCC are shown in Figure 2.5. The relative position and slopes of the three curves show that at saturated conditions, the waste rock has a two-order of magnitude greater hydraulic conductivity than the compacted cover, and a much greater capacity to conduct water. With increasing matric suction, the difference between the unsaturated hydraulic conductivity of the waste rock and that of the cover decreased to within one-order of magnitude. Both the processes of sieving the waste rock to a minus 0.04 m size fraction and compacting during the construction of the cover did not increase the fines portion enough to allow the cover to act as a capillary break over the waste rock. Based on the estimated HCC's, the cover material will at no given value of matric suction have a greater capacity to conduct water than the non-compacted waste rock. For most values of matric suction, the field curve corresponds to a slightly lower hydraulic conductivity than the laboratory curve. The difference between the curves is in part a result of two different SWCC sample collection and preparation methods.

2.5.3. Numerical Modeling

Obtaining model convergence was a challenge when modeling unsaturated flow within the CPE. While convergence was obtained for the simulations using measured values of saturated hydraulic conductivity and porosity, convergence was not obtained for the largest and smallest values attempted during the sensitivity analysis. The most important factors affecting convergence were the steep SWCC functions, the contrast in the material properties of the waste rock and cover layers, and the rapid changes in water content with time. For example, as a result of the steep SWCC's, a large rainfall event following a dry period would result in non-convergence. To improve convergence, the near-surface nodal spacing was reduced to minimum possible values permitted by the code, and a high number of iterations were allowed.

The non-linear relationship between hydraulic conductivity and matric suction requires an iterative process to solve the equations for hydraulic head. With a steep SWCC, the degree of non-linearity increases and a small change in matric suction can result in a several-order of magnitude change in hydraulic conductivity (Figure 2.5). This highly non-linear relationship and a steep SWCC can result in the solution failing to converge. While the SWCC measured in the field and the SWCC determined in the laboratory both exhibit a steep slope, obtaining convergence was easier for the scenarios that used the laboratory SWCC to describe the waste rock because of a slightly lower slope and a characteristic curve more similar to the cover SWCC. Convergence was difficult to obtain when simulating large rainfall events, unless rainfall occurred in the previous few days. To promote convergence, the total volume of rain from large rainfall events were spread out over a few days. While this distribution of rainfall allowed the model to converge, it also artificially contributed to an elevated predicted AE and a reduced predicted net-percolation. The SoilCover model applies daily precipitation over a 24 hr period using a sinusoidal function, so that the near-surface waste rock had a high degree of saturation for a large portion of the days in which rainfall occurred. For the days with rainfall, SoilCover predicts a daily AE that is very close to the PE and an AE/PE ratio close to one. Yearly average AE/PE ratios of 0.38 and 0.27 were calculated for the 2002 and 2003 model run years using the predicted daily AE and PE for all rainless, non-freezing days. The AE/PE ratios for days where rainfall was artificially added to aid model convergence were calculated to be 0.70 and 0.66. A correction factor was determined by assuming that the AE/PE ratio for the days in which rainfall was artificially added should have been similar to the AE/PE ratio of a dry day. The predicted PE from the days with added rainfall was divided by the dry AE/PE ratio and the result was used as an estimate for AE for each of the days with artificially added rainfall. The amount of water that was determined to be over-predicted as evaporation was added to the predicted total surface infiltration for the day of the large rainfall, as if the rainfall was not distributed between days. The results of the base case simulations and the corrected evaporation and infiltration values are presented in Table 2.3 and discussed below.

2.5.4. Comparison of Model Results to Observational Data

Net-percolation and runoff values predicted using SoilCover were compared to measured rates from the CPE. All SoilCover results are presented in mm and as a percent of annual rainfall (Table 2.2). The comparison is used to evaluate how well the model reproduces the observed data, to provide confidence in the calculated value of evaporation for which no direct measurements exist, and to provide information about how to best characterize coarse waste rock using a SWCC.

2.5.4.1. Uncovered CPE

A suitable match to the observed outflow data was not obtained for either of the uncovered base case simulations. The SoilCover model under-predicted outflow and over-predicted AE from the uncovered waste rock. The adjusted SoilCover net-percolation predictions for the uncovered waste rock were 96 mm using the field curve and 115 mm using the laboratory curve, which are lower than the measured 167 mm by 30% and 19%, respectively. The predicted AE values were 219 mm using the field curve and 201 mm using the laboratory curve, which are higher than the calculated AE by 24% and 19%, respectively. SoilCover predicted that the majority of the losses to evaporation occurred from within the top meter of the waste rock pile.

Distinctive wetting fronts in the form of outflow spikes were observed to migrate the entire 5 m of the CPE following large rainfall events. Based on tracer test data, Nichol (2003) identified the fast flow spikes as macropore flow of event water through the entire 5 m of the CPE. As stated earlier, SoilCover cannot mechanistically account for this component of flow. In the simulations using the field SWCC, sharp wetting fronts were observed to a depth of approximately 2 m in response to the large surface infiltration events, and were not discernible at the base of the model unless porosity was adjusted to lower than realistic values (<15%). The reduction in porosity reduces the capacity of the waste rock to store water in the upper portion of the pile where it can be readily drawn out by evaporation and allows for deeper penetration of infiltration during single events. The results for net-percolation using the laboratory-derived SWCC are closer to measured values; however, the porosity that corresponds to the laboratory curve (22%) is lower than the field curve (30%), and lower than the waste rock porosity (30-35%). The 8% difference in porosity only accounts for 4 mm of the 19 mm difference between the laboratory curve and the field curve results (Table 2.3). The remainder of the difference is likely a result of the steeper hydraulic conductivity function that relates to the laboratory derived curve.

A better fit to the observed pre-cover net percolation could have been obtained by using a trial-and-error, or parameter optimization approach to adjust the SWCC (Adu-Wusu et al, 2007). The goal was not to develop a calibrated model of the uncovered CPE for future predictions, rather to determine how well the model predicted net percolation using the SWCC measured in the field and the SWCC determined in the laboratory. The difference between the simulation results and the observations for the uncovered models are related to the estimated amount of non-capillary preferential (macropore) flow occurring in the uncovered CPE, and gives credibility to the simulations for the covered CPE where macropore flow was less significant.

The differences between the simulations and observations for the uncovered models are likely related to macropore flow. The process of macropore flow deep into the pile was observed in the field (Nichol et al, 2005), and resulted in the transport of water to a depth where evaporative effects were minimized. SoilCover does not account for this mechanism, and it is likely that macropore flow could account for the 20 to 30% difference in net-percolation. While Nichol (2003) concluded that macropore flow only accounts for up to 5 to 9% of an observed outflow response from a single large rainfall event, he estimated that 30 to 40% of the flow within the CPE traveled through preferential pathways even if it was not observed at the base of the CPE during the event. Based on the model results it appears that the majority of the evaporative flux occurred within the top 1.5 m of the CPE. It is possible that non-capillary preferential flow of water to a depth of greater than 1.5 m could account for the discrepancy between model results and observations.

The results suggest that the exclusion of macropore and non-capillary processes will result in an under-prediction of net-percolation, and an over-prediction of AE when modeling coarse, uncovered waste rock with steep SWCC's. Without a mechanism that accounts for macropore flow of water in the pile, the model may tend to over-predict AE.

2.5.4.2. Covered CPE

The net-percolation values predicted by SoilCover using both the field curve and the laboratory curve are approximately 20% greater than measured outflow from the covered waste rock. The predicted values of runoff are 4% less than measured values and the predicted values of AE are 3% greater than the estimate derived from the water balance (Table 2.3). Given the heterogeneity in the waste rock hydrologic properties such as the water-holding capacity, all predicted values are thought to be within the expected range. The SWCC's used were appropriate for the covered models and presumably provided good estimates for the capillary component in the uncovered case.

2.5.5. Sensitivity Analysis

The sensitivity analysis was conducted by varying the saturated hydraulic conductivity ($K_{(sat)}$) and porosity of the waste rock and the cover material. The average saturated hydraulic conductivity of the matrix component of the waste rock as measured in the laboratory was 5 x 10^{-5} m/s and in the cover was 5 x 10^{-7} m/s. Figure 2.10 shows the results of the sensitivity analysis for both the uncovered and the covered base case simulations using the laboratory SWCC. $K_{(sat)}$ was varied one order of magnitude greater and one order of magnitude lower. The porosity of the waste rock was varied at 5% intervals between 15 and 35%, and the cover porosity was varied between 20 and 35%. Porosity values of 20 to 35% are plausible for the waste rock and cover material, and are consistent with both SWCC's. The analysis shows that the calculated net-percolation is sensitive to both the porosity and the $K_{(sat)}$ for the uncovered model simulations, and only sensitive to the $K_{(sat)}$ of the cover material in the covered model simulations.

In addition to changing soil properties, the effect of changing the thickness of the cover layer on the model net-percolation was evaluated. The net-percolation for the covered base case simulations was relatively insensitive to the range of evaluated cover thickness, and decreasing the cover thickness from 0.4 m to 0.1 m increased the net-percolation by only 3 mm/year. The sensitivity analysis shows that increasing the thickness of the compacted surface layer does not significantly reduce the net-percolation.

The sensitivity analysis shows that increasing the hydraulic conductivity of the cover material increases the net-percolation. The increase in net-percolation was equal to the decrease in predicted AE, and not related to a decrease in predicted runoff value until the unsaturated hydraulic conductivity was less than that of the underlying waste rock. The model indicates the partitioning between net-percolation, runoff, and evaporation was largely controlled by the sharp contrast in material properties at the lower boundary of the cover layer and the upper boundary of the waste rock layer. Decreasing $K_{(sat)}$ within the one-order of magnitude range resulted in a minimal increase in predicted runoff. The increase in runoff was minimal because the majority of rainfall occurred during low intensity events. Changing the thickness of the compacted cover layer resulted in less than a 3% difference in the predicted annual net-percolation. As a result of the compaction methods used during cover construction, the transition between the waste rock and the compacted cover in the field was gradational. Refining the model to make the interface between the cover and waste rock more gradual would likely further improve the model results, and result in fewer numerical instabilities. However, since the interface did not act as a capillary barrier in the field or in the base case model simulations, and since data to better define the interface in the simulation were not available, a distinct boundary between the cover and waste rock was used. The characteristics of the waste rock below the cover had a smaller effect on the predicted net-percolation than in the uncovered model simulations. In contrast, the characteristics of the cover, especially the saturated hydraulic conductivity, had a large effect on the output from the covered model simulations.

The SoilCover model is based on capillary flow, while water flow within the uncovered waste rock occurred by several mechanisms, including both capillary porous media flow and non-capillary flow. The difference between predicted and observed water balance components are observed to be larger in the uncovered waste rock model simulations than in the covered simulations and this is attributed to a greater amount of macropore and non-capillary flow. Because non-capillary preferential flow is reduced in the covered pile, the differences between the values predicted using SoilCover and values observed in the field are significantly smaller for the covered model simulations.

2.6. CONCLUSIONS

A detailed water balance for the experimental waste rock pile was determined from four years of hydrologic data measured in the field. A variably saturated, evaporative flux model was employed to assess calculated evaporation rates for the CPE and to gain insight into parameters that affect net infiltration and evaporation.

The appropriateness of a Richards based model for modeling flows through a covered heterogeneous waste rock pile was also evaluated. The water balance and the modeling provides data necessary to evaluate the mechanisms of water flow through waste rock and the relationship between flow mechanisms and surface conditions. Ultimately, a careful determination of the water balance is critical for understanding the factors controlling mass loading at the base of waste rock stockpiles. The specific conclusions from this analysis include:

- For years 2000, 2001 and 2002 when the CPE was uncovered, 44%, 51% and 55% of rainfall was measured as lysimeter outflow at the base of the waste rock pile. Following the placement of a compacted cover that resembled a traffic or haul surface, lysimeter outflow was reduced to less than 10% of rainfall and evaporation increased by 10%.
- As expected, the non-capillary preferential flow (non-Darcian) that has been observed in the CPE could not be simulated using a Darcian flow model. The model simulations for the uncovered pile over-predicted actual evaporation and under-predicted net-percolation as a result of the inability of the model to account for fast non-capillary flow that was observed in the field.
- The differences between the model predictions for the covered pile and field observations were shown to lie within the expected range (given the uncertainties in potential evaporation, and those associated with the

heterogeneous characteristics of the waste rock). The capillary-based SoilCover model was able to accurately predict water balance components based on observed field data from a highly heterogeneous, covered waste rock pile.

2.7. REFERENCES

Adu-Wusu, C., Yanful, E.K., Lanteigne, L., O'Kane, M., 2007. Prediction of the water balance of two soil cover systems. Geotech Geol Eng. v. 25. pp. 215-237.

Albright, W.H.,. Gee, G.W., Wilson, G.V., Fayer, M.J., 2002. Alternative Cover Assessment Project, Phase I Report. Desert Research Institute Report No. 41183.

Alpers, C.N. and Nordstrom, D.K., 1999. Geochemical modeling of water-rock interactions in mining environments, in Plumlee, G.S. and Logsdon, M.J. (eds.), The Environmental. Geochemistry of Mineral Deposits. Part A. Processes, Methods, and Health Issues. Society of Economic Geologists, Littleton, Colorado, Reviews in Economic Geology. v. 6A. Chapter 14. pp. 289-323.

American Society for Testing and Materials (ASTM), 1991. Test method for laboratory compaction characteristics of soil using standard effort (12,400 ft-lbf/ft3 (600 kN-m/m3)) (D698-91). Annual Book of ASTM Standards. v. 04.08.

Aubertin, M., Mbonimpa, M., Chapuis, R.P., 2003. A model to predict the water retention curve from basic geotechnical properties. Canadian Geotech. J. v.40. pp. 1104-1122.

Ayres, B.K., 1998. Field monitoring of soil-atmosphere fluxes through uranium mill tailings and natural surface soils at Cluff Lake, Saskatchewan, M.Sc. Thesis, University of Saskatchewan, Saskatoon, Saskatchewan, Canada.

Bain, J.G., Mayer, K.U., Molson, J.W., Blowes, D., Frind, E.O., Kahnt R. and Jenk, U., 2001. Modelling the closure-related geochemical evolution of groundwater at a former uranium mine, Journal of Contaminant Hydrology. v. 52. pp. 109-135.

Baldocchi, D.D., Hicks, B.B. and Meyers, T.P., 1988. Measuring biosphere-atmosphere exchanges of biologically related gases with micrometeorological methods. Ecology, v. 69. pp. 1331-1340.

Bowen, I.S., 1926. The ratio of heat losses by conduction and by evaporation from any water surface, Physics Review, vol. 27, pp. 779-787.

Brooks, R.H. and Corey, A.T., 1964. Hydraulic properties of porous media. Colorado State University (Fort Collins), Hydrology Paper No. 3.

Carey, S.K., Barbour, S.L. and Hendry, M.J., 2005. Evaporation from a waste-rock surface, Key Lake, Saskatchewan, Canadian Geotechnical Journal. v. 42. pp. 1189-1199.

Christiansen, J.E., Irrigation by sprinkling, University of California Agricultural Experimental Station Bulletin, 670., 1942.

Cogema Resources, 2001. Cluff Lake Project Comprehensive Study Report for decommissioning. January 15, 2001.

Durham, A., 2002. Design and optimization of a waste rock cover system for arid environments, MSC. Thesis, University of Saskatchewan, 258 p.

Fayer, M.J. and Jones, T.L., 1990. UNSAT-H version 2.0: Unsaturated soil water and heat flow model. PNL-6779, Pacific Northwest Laboratory, Richland, Washington.

Fredlund, D.G. and Xing, A., 1994. Equations for the soil-water characteristic curve, Canadian Geotechnical Journal. v 31. pp. 521-532.

Fredlund, D.G., Xing, A. and Huang, S. 1994. Predicting the permeability function for unsaturated soils using the soil-water characteristic curve, Canadian Geotechnical Journal. v 31. pp. 533-546.

Fredlund, M., Fredlund, D.G., Wilson, G.W., 1997. Prediction of the soil-water characteristic curve from grain–size distribution and volume-mass properties. In: Proc 3rd Brazilian Symp on Unsaturated Soils, Rio de Janerio.

Frostad, S., Klein. B. and Lawrence, R.W., 2005. Determining the weathering characteristics of a waste dump with field tests, International Journal of Surface Mining, Reclamation and Environment. pp. 132-143.

Geo-Slope International Ltd. 2004. VADOSE/W on-line help version 1.18.

Grigg, A.H., Sheridan, G.J., Pearce, A.B. and Mulligan, D.R., 2003. The effect of organic mulches on crusting, infiltration and salinity in the revegetation of a saline-sodic coal mine spoil from central Queensland, Australia.

Paper presented at the 2003 National Meeting of the American Society of Mining and Reclamation and the 9th Billings Land Reclamation Symposium, Billings, Montana. 3-6 June 2003. pp. 292-310.

Guan, Y., 1996. The measurement of soil suction. Ph.D. Thesis, University of Saskatchewan, 353 p.

Holmes, R.M., 1961. Estimation of soil moisture content using evaporation data. In: Evaporation, Proceedings of Hydrological Symposium 2, Toronto. Queen's Printer, Ottawa. pp. 184-196.

Kabwe, L.K., Wilson, G.W. and Hendry, M.J., 2005. Effects of rainfall events on waste-rock surface-water conditions and CO2 fluxes across the surfaces of two waste-rock piles. Journal of Environmental Engineering and Science Review. v. 4. pp. 469-480.

Kempton, H. and Atkins, D., 2000. Delayed environmental impacts from mining in semi-arid climate, in Proceedings from the 5th International Conference on Acid Rock Drainage ICARD 2000, Society for Mining Metallurgy and Exploration, Inc. Proceedings Fifth International Conference on Acid Rock Drainage. pp. 1299-1308.

Khire, M., Benson, C.H. and Bosscher, P.J., 1997. Water balance modeling of earthen final covers. Journal of Geotechnical and Geoenvironmental Engineering. pp. 744-757.

Kowalewski, P.E., 1999. Design and evaluation of engineered soil covers for infiltration control in heap leach closure. Closure, remediation and management of precious metals heap leach facilities. Edited by Dororthy Kosich and Glenn Miller. pp. 21-29.

Leong, E.C., He, L., Rahardjo, H., 2002. Factors affecting the filter paper method for total and matric suction measurements Geotechnical Testing Journal, ASTM 25. pp. 321-332.

Lopez, D.L., Smith, L. and Beckie, R., 1997. Modeling water flow in waste rock piles using kinematic wave theory, in 4th International Conference on Acid Rock Drainage. pp. 497-513.

Nichol, C.F., Smith, L. and Beckie, R., 2000. Hydrogeologic behavior of unsaturated mine waste rock: An experimental study. In Proceedings of the 5th International Conference on Acid Rock Drainage, Denver, Colorado, 21-24 May. Society for Mining, Metallurgy, and Exploration Inc. (SME),. pp. 215-224.

Nichol, C.F., 2003. Transient flow and transport in unsaturated heterogeneous media: Field experiments in mine waste rock. Ph.D. dissertation, University of British Columbia, Vancouver.

Nichol, C.F., Smith, L. and Beckie, R., 2005. Field scale experiments of unsaturated flow and solute transport in a heterogeneous porous medium, Water Resources Research. v. 41.

Nicolau, J.M., 2003. Trends in relief design and construction in opencast mining reclamation. Land Degradation & Development. v. 14. no. 2. pp. 215-226.

Noel, M.N., Rykaart, E.M., 2003. Comparative study of surface flux boundary models to design soil covers for mine waste facilities. Sixth International Conference Acid Rock Drainage. pp. 703-710.

O'Kane, M.A., Porterfield, D., Weir, A. and Watkins, L., 2000. Cover system performance in semi arid climate on horizontal and sloped waste rock surfaces, in 5th International Conference on Acid Rock Drainage. pp. 1309-1317.

Penman, H.L., 1948. Natural evapotranspiration from open water, bare soil, and grass. Proceedings of the Royal Society of London Series A. v. 193. pp. 120-145.

Rykaart, M., Fredlund, M.D. and Stianson, J., 2001. Solving tailings impoundment water balance problems with 3-D seepage software. Geotech. News. v. 12. pp. 50-54.

Simunek, J., M. Sejna and van Genuchten, M.Th., 1996. HYDRUS-2D: Simulating water flow and solute transport in two-dimensional variably saturated media. International Groundwater Modeling Center, Colorado School of Mines, Golden, CO.

Shurniak, R.E., 2003, Predictive modeling of moisture movement within soil cover systems for saline/sodic overburden piles, MS Thesis, University of

Saskatchewan, Saskatoon, Canada. pp. 1-129.

SoilCover, 1997. The design of soilcover systems. SoilCover Version 4.0 User Manual. Unsaturated Soils Group, Department of Civil Engineering, University of Saskatchewan, Saskatoon.

SoilVision Systems Ltd., 1997. User's guide for a knowledge-based database program for estimating soil properties of unsaturated soils for use in geotechnical engineering. SoilVision Systems Ltd., Saskatoon, Saskatchewan, Canada.

Stockwell, J.E., 2002. Investigation of hydrological and geochemical properties and spatial relationships of an unsaturated waste rock pile, Key Lake, Saskatchewan, Masters Thesis, University of British Columbia.

Swanson, D.A., Kempton, J.H., Travers, C. and Atkins, D.A., 1998. Predicting long-term seepage from waste-rock facilities in dry climates, Society for Mining, Metallurgy, and Exploration, Inc. pp. 98-135.

Swanson, D.A., Barbour, S.L., Wilson, G.W., O'Kane, M., 2003. Soil-atmosphere modelling of an engineered soil cover for acid generating mine waste in a humid, alpine climate, Canadian Geotechnical Journal. v. 40. pp. 276-292.

Torres, R., W.E. Dietrich, D.R., 1998. Montgomery, S. P. Anderson, K. Loague, Unsaturated zone processes and the hydrologic response of a steep, unchanneled catchment, Water Resources Research. v. 34. no.8. p. 1865.

U.S. Army Corps of Engineers, 1994. The Hydrological Evaluation of Landfill Performance (HELP) Model, Version 3.03.

U.S. EPA, 1999. Mine waste technology program, 1999 Annual Report. Prepared for the U.S. EPA and the U.S. DOE. Inter agency agreement management committee: IAG ID NO. DW89938513-01-0.

Van Dam, J.C., J. Huygen, J.G. Wesseling, R.A. Feddes, P. Kabat, P.E.V. van Walsum, P. Groenendijk and C.A. van Diepen, 1997. Theory of SWAP version 2.0. Simulation of water flow, solute transport and plant growth in the Soil-Water-Atmosphere-Plant environment. Report 71, Subdep. Water Resources, Wageningen University, Technical document 45, Alterra Green World Research, Wageningen.

van Genuchten, M.Th. 1980. A closed-form equation for predicting the hydraulic conductivity of unsaturated soils. Soil Sci. Soc. Am. J. v. 44. pp. 892-898.

Wels, C., O'Kane, M., Fortin,S. and Christensen, D., 2001. Infiltration test plot study for mine rock piles at Questa Mine, New Mexico. Paper presented at the 2001 National Meeting of the American Society for Surface Mining and Reclamation. Pub. By ASSMR 3134 Montavesta Rd., Lexington KY 40502.

Wilson, G.W., 1990. Soil Evaporative Fluxes for Geotechnical Engineering Problems. Ph.D. Thesis, University of Saskatchewan, Saskatoon, Saskatchewan, Canada.

Wilson, G.W., Fredlund, D.G. and Barbour, S.L., 1994. Coupled soil-atmosphere modelling for soil evaporation, Canadian Geotechnical Journal. v. 31. no.2. pp. 151-161.

Wilson, G.W., Fredlund, D.G. and Barbour, S.L., 1997. The effect of soil suction on evaporative fluxes from soil surfaces. Canadian Geotechnical Journal. v. 34. no.2. pp. 145-155.

Yang, H., Rahardjo, H., Leong, E., Fredlund, D.G., 2004. Factors affecting drying and wetting soil-water characteristic curves of sandy soils. Canadian Geotechnical Journal. v. 41. pp. 908-920.

Zegelin, S.J. and White, I., Jenkins, D.R., 1989. Improved field probes for soil water content and electrical conductivity measurement using time domain reflectrometry, Water Resources Research. v. 25. no. 11. pp. 2367-2376.

Rainfall (mm), 2000 – 2004

Year	Jan	Feb	Mar	Apr	May	Jun	Jul	Aug	Sep	Oct	Nov	Dec	Year
2000		0.0	0.0	4.6	32.4	24.6	151.5	93.8	45.2	10.0	0.0	0.0	363.1
2001	0.2	0.8	0.0	0.4	31.2	32.2	92.6	17.4	44.2	46.0	8.6	0.4	275.2
2002	1.8	0.4	0.0	10.2	57.0	29.2	64.4	101.1	48.8	5.6	0.0	0.0	316.5
2003	0.2	0.0	0.0	4.0	69.6	30.4	92.8	20.6	23.8	47.6	0.0	0.2	289.8
2004	0.0	0.6	0.2	0.0	0.2								
Ave	0.6	0.4	0.0	3.8	38.1	29.1	100.3	58.2	40.5	27.3	2.2	0.2	311.2

Table 2.1. Monthly precipitation values measured on the top of the waste rock pile for the period between January 2000 and May of 2004. Yearly totals are based on April 01 to March 31 for each of the four years. Snowfall is excluded.

Year	Rainfall	Net-Percolation		AE Calculated		Runoff	
	mm	mm	%	mm	%	mm	%
2000-2001	363	160	44	203	56	0	0
2001-2002	275	145	51	130	49	0	0
2002-2003	316	167	55	149	45	0	0
2003-2004	289	30	10	170	60	89	30

Table 2.2. Summary of measured water balance components. The annual measurements are reported as water years between April 01 and March 31 of the following year. All percentages are reported as percent of precipitation for the same time period.

	Year	Precip	Measured		Model FC				Model LC			
					Uncorrected		Corrected		Uncorrected		Corrected	
	٢٠٠٠		**mm**	**%**	**mm**	**%**	**mm**	**%**	**mm**	**%**	**mm**	**%**
Net Perc	**٠٢-٠٣**	٣١٦	١٦٧	٥٥	٧٨	٢٥	٩٦	٣٠	٩٦	٣٠	١١٥	٣٦
	٠٣-٠٤	٢٨٩	٣٠	١٠	٢٧	٩	٣٦	١٢	٢٩	١٠	٣٨	١٣
AE	**٠٢-٠٣**	٣١٦	١٥٠	٤٥	٢٣٨	٧٥	٢١٩	٦٩	٢٢٠	٦٩	٢٠١	٦٤
	٠٣-٠٤	٢٨٩	١٧٠	٦٠	١٨٤	٦٤	١٧٥	٦١	١٨٣	٦٣	١٧٤	٦٠
Runoff	**٠٢-٠٣**	٣١٦	٠	٠	٠	٠			٠	٠		
	٠٣-٠٤	٢٨٩	٨٩	٣١	٧٨	٢٧			٧٧	٢٧		
PE	**٠٢-٠٣**	٣١٦			٥١٠	١٦١			٥١٠	١٦١		
	٠٣-٠٤	٢٨٩			٨٣٥	٢٨٩			٨٣٦	٢٨٩		

Table 2.3. Comparison of field measurements with SoilCover results. Results from two simulations are presented for both of the two run years. FC refers to the field SWCC and LC to the laboratory derived SWCC both shown in Figure 2.1. The annual measurements are reported from April 01 to March 31 for each of the four years. All percentages are reported as percent of precipitation.

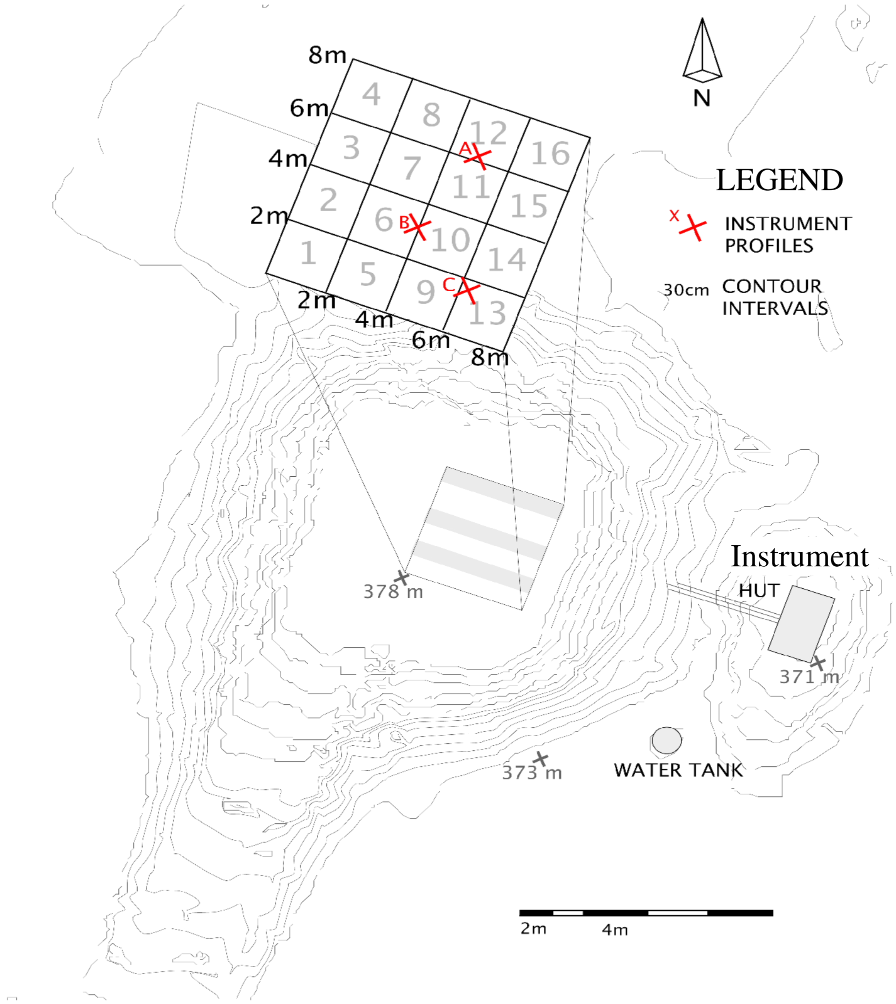

Figure 2.1. Schematic view of the top of the waste rock pile. The grid of sixteen lysimeters is shown in relation to the overlying waste rock. The origin of the grid is on the lower left (south west) side of lysimeter 1. The lysimeter grid is to scale and is superimposed on topographic contours of the constructed waste rock pile. The three instrument profiles are labeled with an X, and contour intervals are 30 cm.

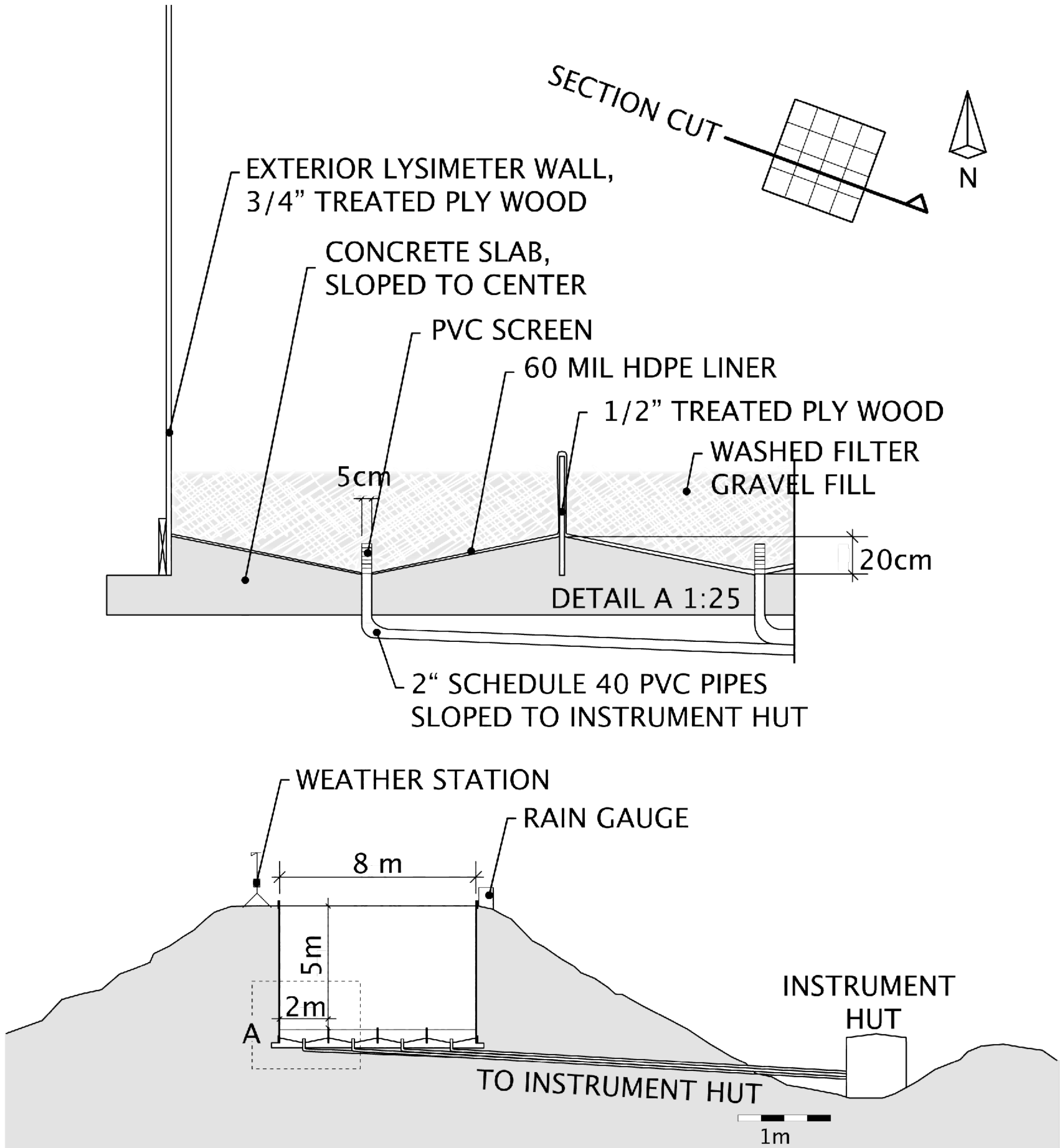

Figure 2.2. Cross-section of the constructed waste rock pile and a detail of the basal lysimeter design.

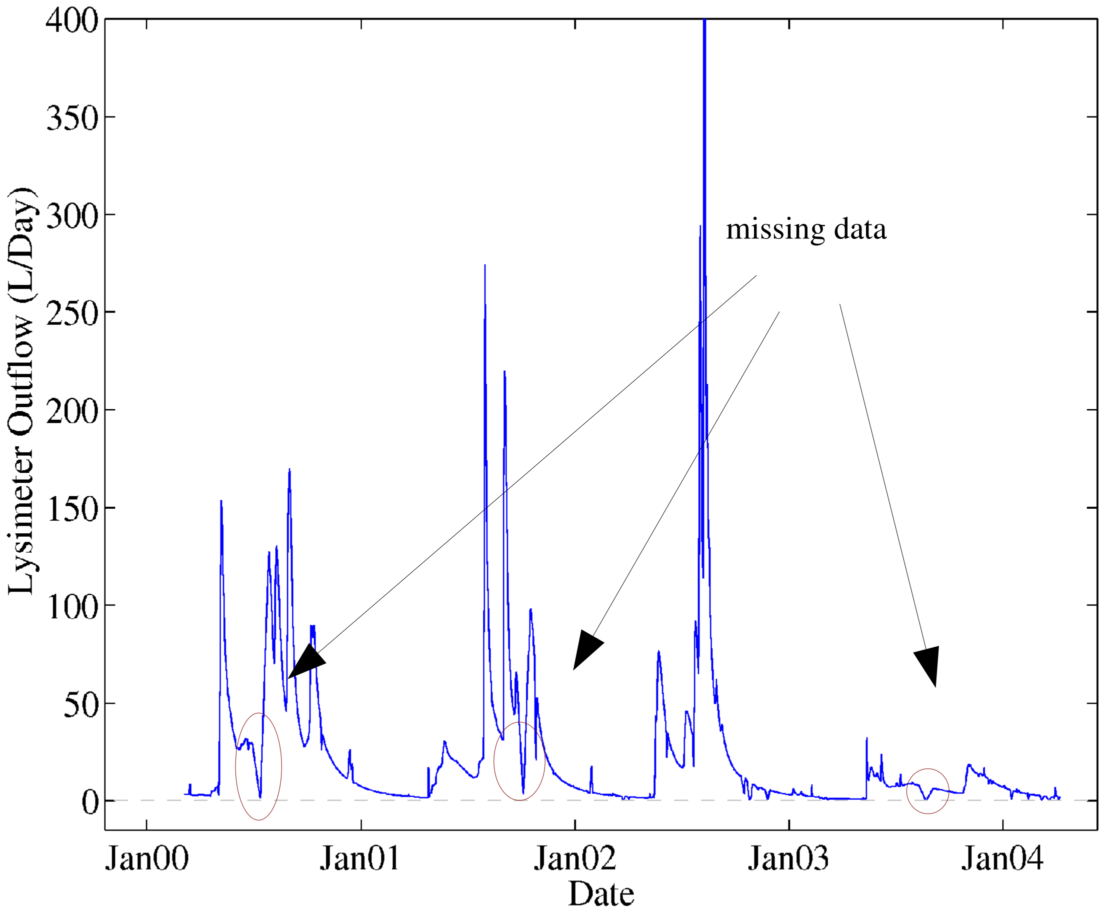

Figure 2.3. Hydrograph measured as combined outflow from the 16 lysimeters at the base of the CPE between January of 2000 and May of 2004. The 'dips' in the hydrograph, as identified by the red circles, are artificial and result from periods when the data from one or more of the lysimeters are missing. The large, short-lived (less than one day) 'spikes' in the outflow from lysimeter 6 were removed for clarity. Lysimeter 6 alone exhibited spikes in flow rate greater than 300 L/day.

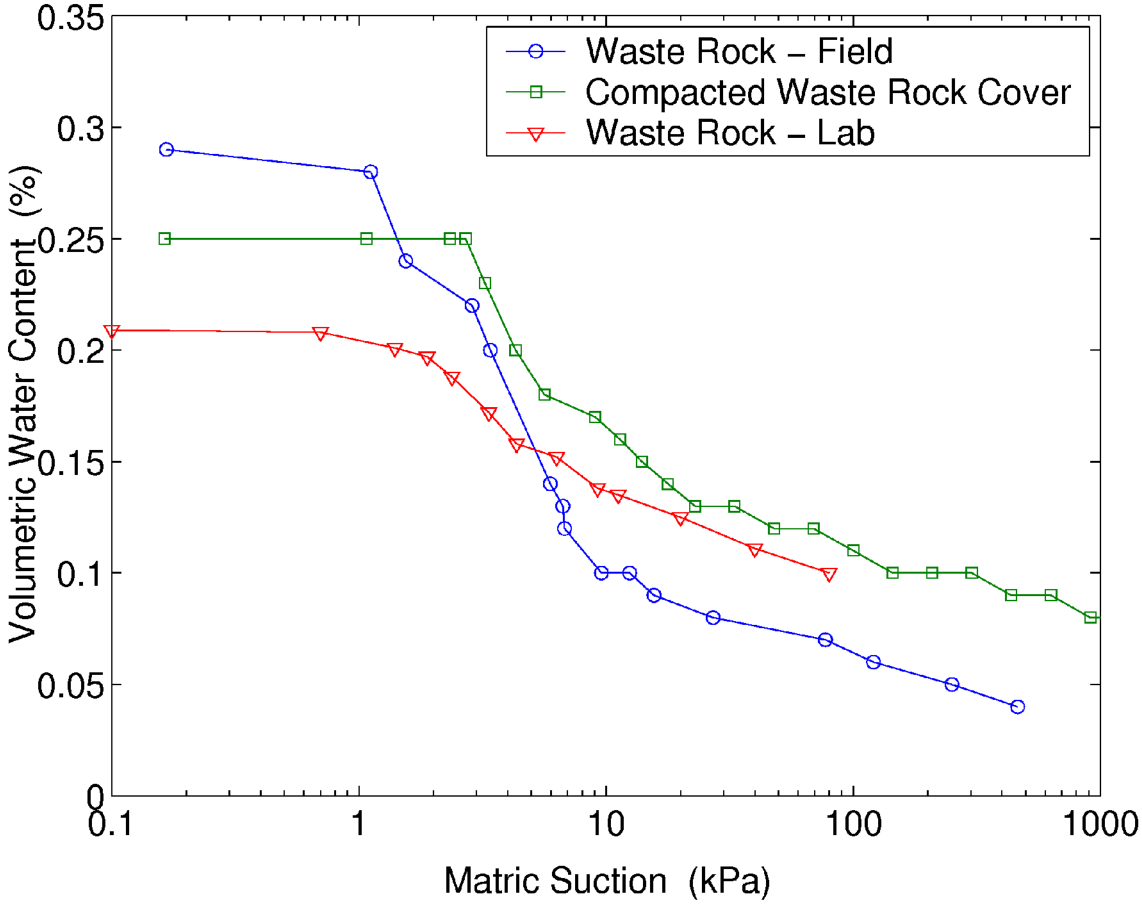

Figure 2.4. Soil water characteristic curves (SWCC) for the waste rock and cover material. The blue curve (○) is a SWCC for the waste rock based on field data. The matric suction values were determined indirectly using the filter paper method and the volumetric water content measurements were obtained from direct, in-situ measurements. The red curve (∇) is a SWCC for the waste rock based on laboratory data using a Tempe cell. The green curve (□) is an estimated SWCC for the waste rock cover based on the Fredlund and Xing (1994) equation.

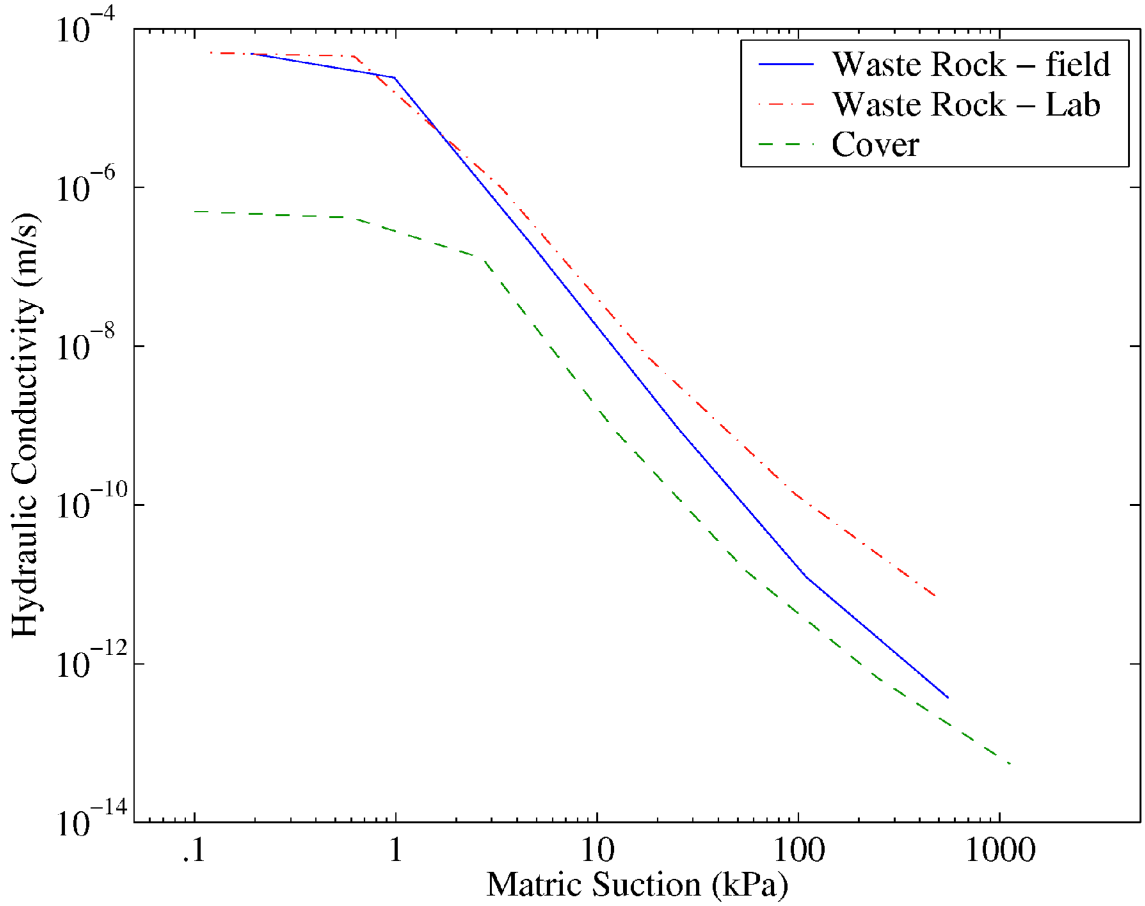

Figure 2.5. Hydraulic conductivity curves for the waste rock and cover material. The blue curve (solid) is the HCC for the waste rock based on field data. The red curve (dashed) is the HCC for the waste rock based on laboratory data. The green curve (dash-dot) is the HCC for the waste rock cover. All three curves are based on the Fredlund et al (1994a) equation.

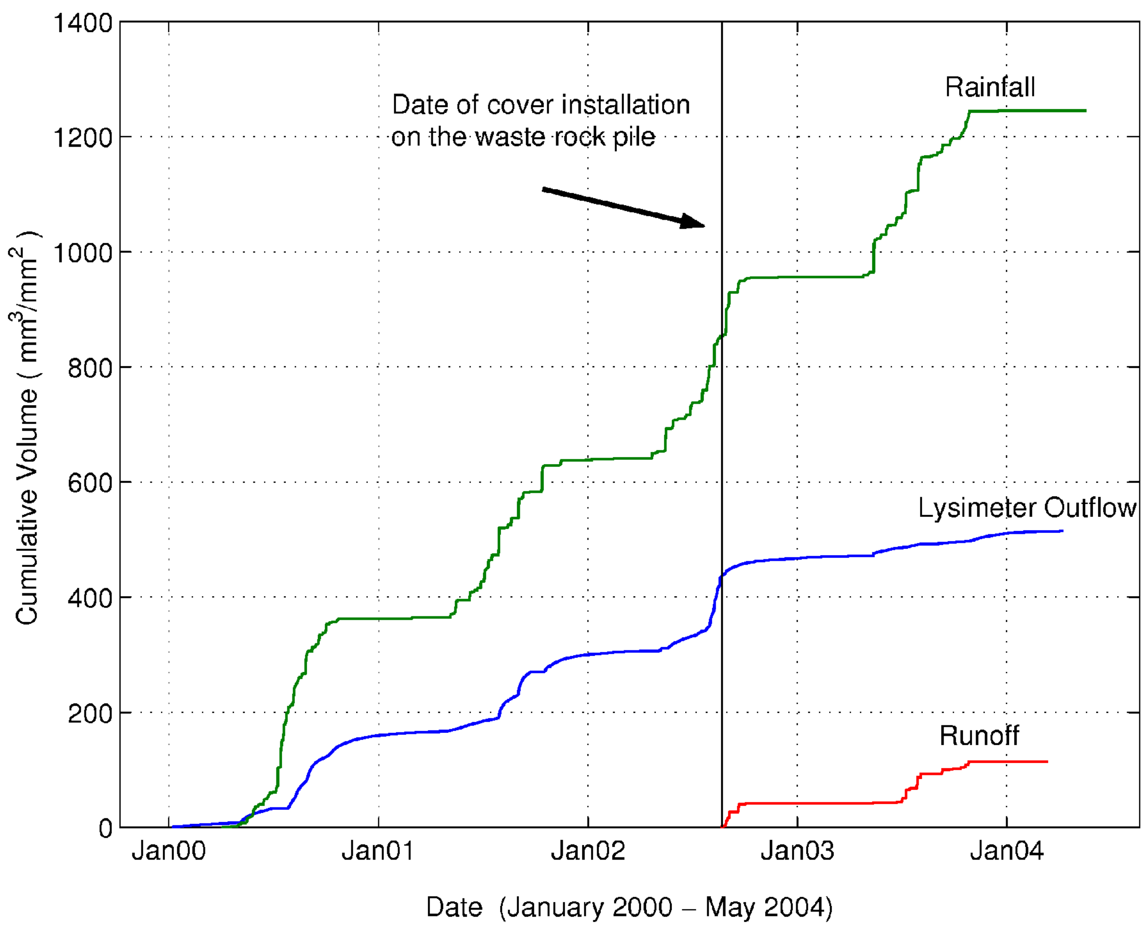

Figure 2.6. Annual precipitation and lysimeter outflow for the four years of the experiment. The solid vertical line marks the completion of the compacted waste rock cover in the fall of 2002.

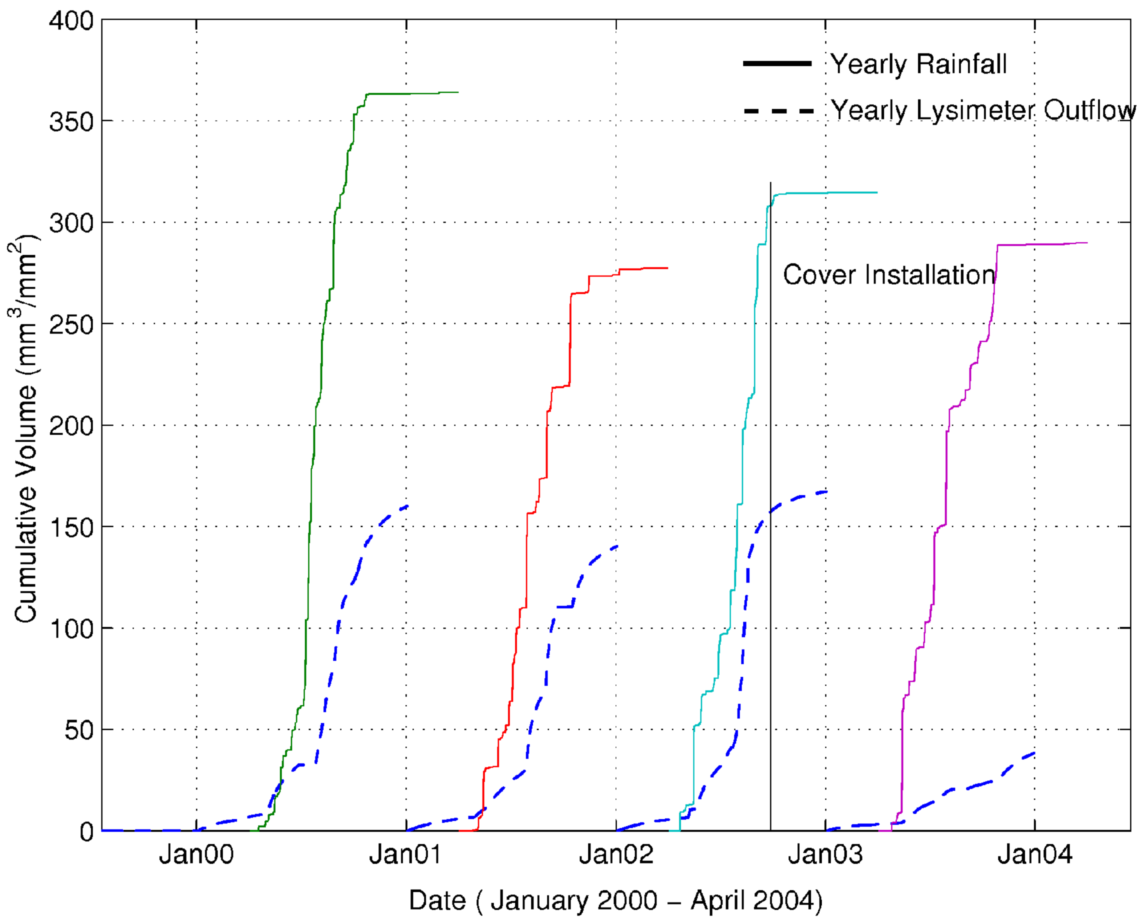

Figure 2.7. Annual cumulative precipitation and lysimeter outflow between January 2000 and January 2004. The accumulated rainfall excludes snowfall.

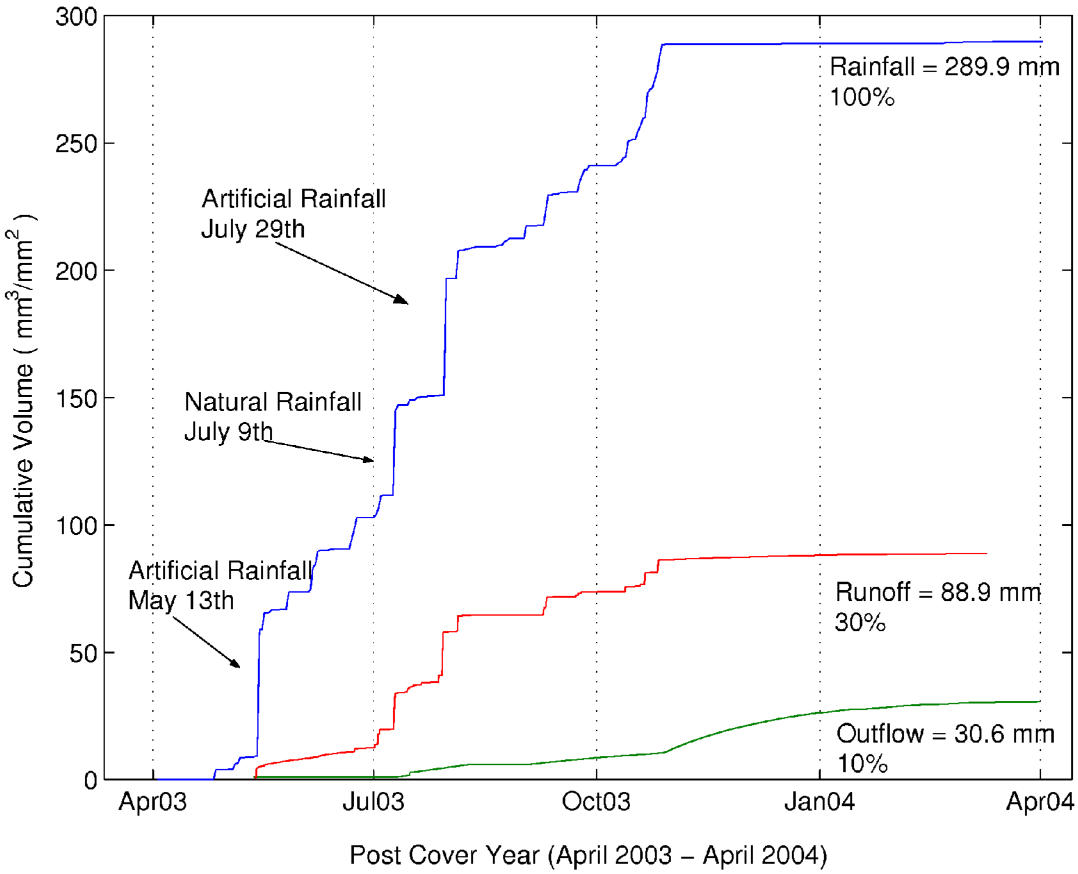

Figure 2.8. Cumulative precipitation, outflow and runoff for the year following the construction of the compacted cover. Little runoff was associated with the artificial rainfall events due to the lower than natural application rates.

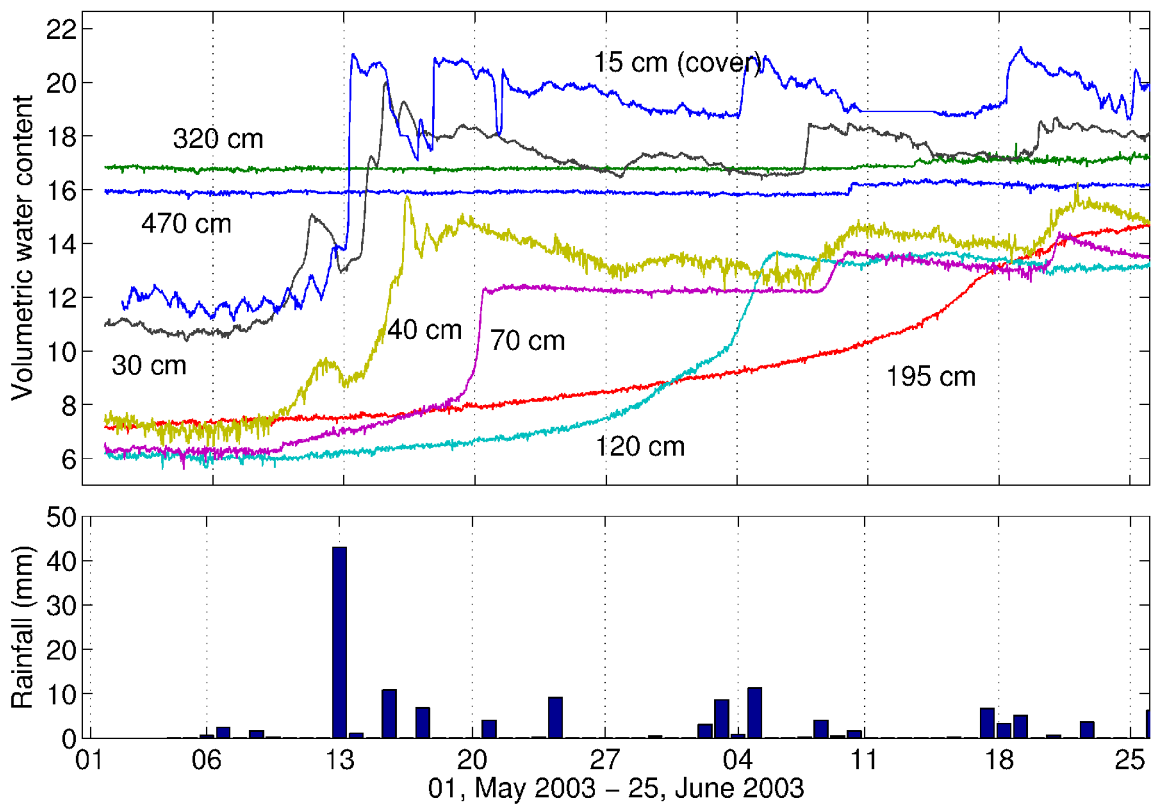

Figure 2.9. The volumetric water content as measured by TDR probes at 8 different depths within the waste rock pile between May 01, 2003 and June 25, 2003. The data are an average from the probes at the same depth in all three profiles. The sub-plot shows the rainfall record for the same period.

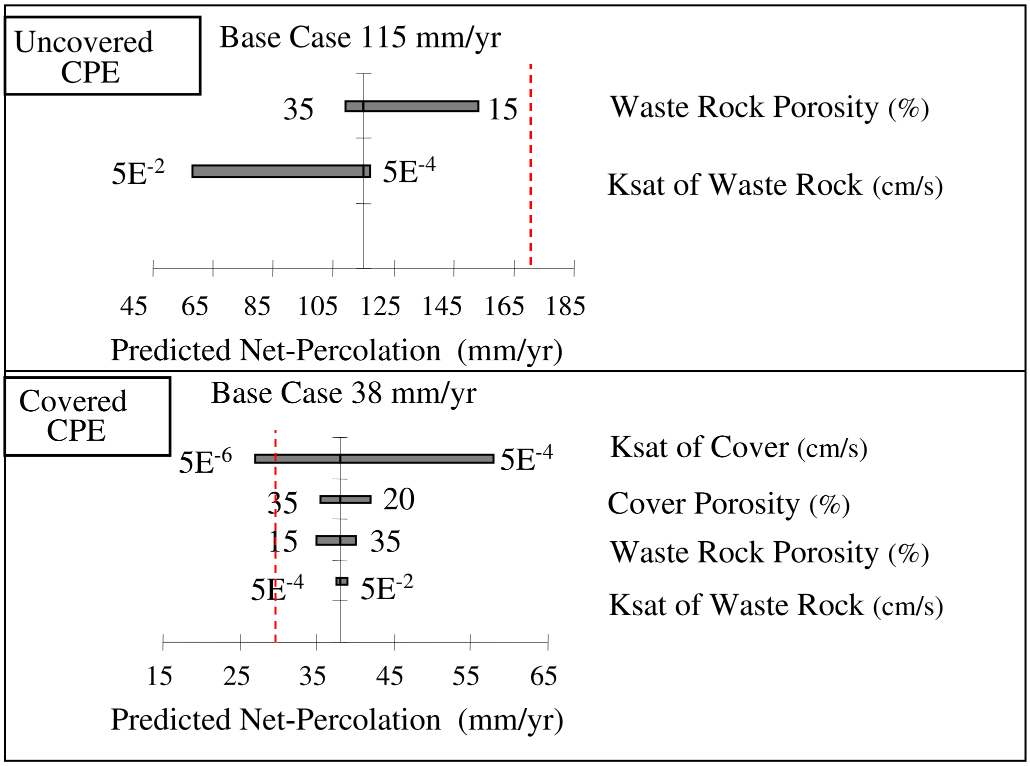

Figure 2.10. Sensitivity of net percolation to key parameters on the predicted net-percolation for the uncovered and covered waste rock scenarios. Both plots are from base case model simulations using the laboratory SWCC for the waste rock. The end member values for each parameter are listed. The red dashed lines represent the net-percolation as measured in the basal lysimeters for the model year.

CHAPTER 3: THE EFFECT OF SURFACE CONDITION ON INTERNAL WATER FLOW IN WASTE ROCK

3.1. INTRODUCTION

Low quality drainage is released from many operational and reclaimed mine waste rock piles and is a potential source of environmental liability. The need to minimize acid rock drainage (ARD) during operations and after closure has spurred an emphasis on the evaluation of waste management technologies and reclamation alternatives. Waste rock piles typically remain uncovered during the life of a mine, and exhibit a range of surface conditions and textures. Often waste rock piles have an irregular top surface resulting from free-dump construction techniques. Numerous waste rock piles at copper, gold and sandstone-type uranium mines have at some time been used as heap leach piles and will have a ripped and leveled surface, while others have a pavement-like surface, intentionally compacted or compacted by haul trucks and other mine traffic.

Design alternatives to modify the hydrologic behavior of waste rock piles or to limit chemical and transport processes within waste rock have been investigated (Fortin et al, 2000, Winter Syndor et al, 2002, Fines et al, 2003a, Maddocks, 2003, Mbonimpa et al, 2003, Williams et al, 2003). A commonly applied technology is an engineered cover system designed to limit moisture and/or oxygen flux into the

---

A version of this chapter will be submitted for publication. Marcoline, J.R., The effect of surface condition on water flow in waste rock.

waste rock and thus reduce loadings at the base of a waste rock pile. The manner in which the surface texture of an uncovered pile or a cover system influences fluid flow and geochemical processes inside a waste rock pile is poorly understood due to the lack of observational data, compounded by the spatial heterogeneity in particle size (ranging from clays to boulders). A better understanding of fluid flow in waste rock can be attained by examining drainage from a pile subject to successive surface modifications. Re-working of the upper surface will change the spatial distribution of infiltration and construction of a low-permeability cover can substantially reduce infiltration into waste rock. Both changes may lead to a change in dominant fluid pathways within the pile, water residence times and outflow chemistry. The term pathway is used in this research to describe a single mechanism, or group of mechanisms, that result in a distinct wetting front arrival at the base of a waste rock pile. Wetting front arrivals are identified as a sharp increase in the outflow rate observed at the base of the waste rock pile, or as a sharp increase in volumetric water content as measured by instrumentation inside the pile.

3.2. OBJECTIVES

The primary objective of this paper is to document the changes in fluid pathways and magnitude of flow through a waste rock pile as its surface condition is modified. Two hypotheses underlie the design of the experiments:

- The substantial spatial and temporal variability in outflow from the experimental waste rock pile was primarily a result of the influence of the surface condition on infiltration rates into the pile and to a lesser degree, to the heterogeneous internal structure of the pile. The influence of the surface condition on infiltration rates was inferred from the highly irregular surface topography and the variations in waste rock grain sizes across the surface.
- The addition of a lower permeability cover could greatly decrease spatial and temporal variability in outflow. The flat, homogeneous lower permeability cover was void of topography and large variations in surface texture and the resulting rate of infiltration across the surface was expected to be constant. With a constant surface infiltration rate, and flow through the matrix material, variability of basal outflow was expected to be significantly reduced.

3.3. METHODS

The hypotheses are tested using an intermediate-scale constructed waste rock pile experiment (CPE) built and instrumented at the Cluff Lake Mine in northern Saskatchewan. To investigate these questions, the basal lysimeter outflow and surface runoff were observed for each of three surfaces: i) the original free-dumped surface, ii) the surface ripped to an approximate depth of 0.3 m to 0.4 m and leveled and iii) the surface covered by a layer of 0.1 m to 0.15 m of compacted waste rock.

3.3.1. Experimental Design

The CPE was constructed and instrumented at the Cluff Lake Mine in northern Saskatchewan. The pile was 32 m by 32 m-wide, with an 8 m by 8 m-wide by 5 m-high central core. Run-of-mine waste rock was free-dumped on a grid of sixteen, 2 m by 2 m lysimeters (Figure 3.1) using an excavator and backhoe. Three vertical profiles, each containing automated temperature, soil moisture (TDR) and matrix suction sensors (tensiometers and thermal dissipation sensors) were installed in the waste rock pile. Outflow volume and rate were measured and recorded continuously from each lysimeter. Detailed results from infiltration and tracer experiments on the uncovered waste rock pile between 1998 and 2000 are described in Nichol et al (2000), (2003a) and Nichol et al (2005).

Hydrographs from the sixteen lysimeters show a large range of wetting front arrival times, outflow volumes, and multiple wetting fronts at a 2 m by 2 m scale (Nichol et al, 2000, 2002, 2003a, Marcoline et al, 2003).

The original surface of the experimental pile was approximately level, with numerous cobbles exposed at the surface. With differential settlement over a three-year period, the surface evolved into a set of variably-sized “basins” with a topographic relief of up to 0.45 m across the surface (Figure 3.2.). Particles from silts to cobbles (0.4 m in diameter) were present at the surface (Figure 3.3.a). The majority of the surface had a matrix-supported structure with numerous cobbles. Small portions of the surface were clast-supported, consisting primarily of 0.05 m to

0.3 m cobbles and a few boulders as large as 0.5 m in diameter, with a minimal amount of visible fine-grained material between the cobbles.

The surface of the waste rock pile was ripped and leveled in October 2001. To prevent damage to near-surface instruments and because the top of the pile was inaccessible to standard mining equipment, the surface was homogenized to a depth of 0.3 m to 0.4 m using a hand pick. The surface ripping was designed to minimize the variability in texture across the top layer of the pile and to eliminate any pre-existing preferential flow paths in the top 0.3 m to 0.4 m of the CPE. Following ripping, the surface was surveyed at a 0.45 m grid and leveled to ensure that large topographic depressions were eliminated. To facilitate leveling, approximately 1.0 m^3 of waste rock from the surface immediately outside the lysimeters was added as fill to replace all of the coarse waste rock greater than 0.3 m that was removed and to fill in depressions. The resulting surface was non-compacted, visually homogeneous, matrix-supported, and absent of mappable catchment areas (Figure 3.3.b).

In late August 2002, a compacted layer of waste rock was placed on the surface (Figure 3.3.c) to create a lower permeability layer at the surface of the pile. An eight meter-long gutter drain collection system was incised into the compacted layer on the north side, adjacent to the lysimeter wall. The system was designed to collect surface runoff without interception of direct precipitation. Before placement of the cover, there was no runoff generated at the surface. Runoff from the surface during natural and artificial rainfall events flowed from the gutter drain through a 50 mm down pipe into a series of four, 200 liter retention drums. The flow from the drums was trickle fed through two independent tipping bucket rain gauges located in the instrument hut. The system allowed for accurate measurement of runoff volume up to approximately 1900 L/day, a value just below the maximum calibrated capacity of the rain gauges. Flow from the drums to the tipping bucket rain gauges was limited to 1900 L/day. When runoff rates exceeded 1900 L/day, the four, 200 liter retention drums filled and automatically allowed a greater time for the water volume to be measured.

3.3.2. Cover Construction

The compacted layer was constructed with waste rock located from within the waste rock pile but outside of the lysimeter grid. Approximately 23 m^3 of waste rock was sieved through a minus 0.1 m screen. Four Zegelin-type time domain reflectomety (TDR) probes (Zegelin, 1989) with a high resistance coating on the center rod (Nichol et al, 2003) and two thermistors were installed on the surface just prior to placing the cover. The screened waste rock was manually placed onto the waste rock pile with shovels, moisture was added and the surface compacted.

The sieved waste rock used for the compacted surface was well graded and had a particle size distribution of approximately 3% cobbles, 40% gravel, 40% sand and 17% silt and clay (Figure 3.4). The particle size distribution was determined on splits of two samples according to ASTM test method D442 (ASTM, 1990), although hydrometer tests were not conducted. The thickness of the compacted layer was approximately 25% greater than the diameter of the largest cobbles within the cover to minimize direct short circuiting or preferential flow through the layer.

Compacted layers installed as part of cover systems typically lay beneath a non-compacted, non-acid generating layer of material. One function of the overlying layer is to protect the compacted layer from drying and from freeze-thaw cycles. Here, the compacted layer placed on the CPE was located at the surface without any additional material placed above the compacted layer and was designed to promote a uniform infiltration rate across the entire surface. The cover design and the method of construction were selected to minimize the formation of desiccation cracks that result from drying of the compacted layer. Such failures would promote preferential flow through the cover and potentially through the constructed pile as well. The justification for the cover design is discussed below.

Compacted layers in ARD cover applications are typically installed wet of the optimum water content in order to promote the creation of a layer of permanently saturated material. The optimum water content is the moisture content that allows for the highest dry-density at a given compaction effort. Materials compacted dry of optimum will have a more open structure (Fleureau et al, 2002), and consequently, their soil water characteristic curve (SWCC) will have a slightly lower water content for a given suction than if compacted wet of optimum. The compacted layer, if saturated, will also minimize the ingress of oxygen into covered waste (Nicholson et al, 1989, Yanful et al, 1993, Wilson et al, 1997). For oxygen barrier systems, compaction on the wet side of optimum is more appropriate since the layer will remain close to saturation under higher suctions (Vanapalli et al, 1996). Holtz and Kovacs (1981) and O'Kane (2001) suggest that compaction on the wet side of optimum will allow for a greater level of compaction and a higher moisture content. However, it has been suggested that in all climates including semi-arid climates, compacted layers constructed wet of optimum are ineffective at limiting oxygen and water due to drying and cracking of the material (Dwyer, 1997).

For the experimental pile, the goal was to achieve a durable compacted surface layer and not to achieve a layer with a high moisture content. This was accomplished by ensuring that the cover material was at optimal, or slightly dry of optimal water content. Compaction at optimum or slightly dry of optimum reduced the potential for desiccation defects in the compacted surface layer while creating a layer that was effective in reducing the net-infiltration of water. Standard Proctor laboratory compaction tests following ASTM method D689 (ASTM, 1991) were conducted on the minus 20 mm fraction of the sieved waste rock to determine the relationship between dry density and water content. Water content and dry density were corrected to account for the 21 mm to 100 mm particles following ASTM method 4718 (ASTM, 1994). The corrected maximum dry density for the cover material was determined to be 2280 kg/m^3, at an optimum water content of 7.0%. Based on two samples collected just prior to compaction, the cover was placed at an average water content of 6.9%.

Compaction was carried out on August 15, 2002, in one lift and three passes with a standard free-standing rammer compactor delivering approximately 3100 pounds/blow over a 0.34 m by 0.36 m pad. The compacted layer was constructed with an overall slope of 1% towards the north edge of the waste rock pile to remove surface runoff during higher intensity storms.

Two test pits through the compacted layer were logged to visually inspect the degree and depth of compaction. Compaction appeared homogeneous to a depth of approximately 0.12 m with a slightly lesser degree of compaction between 0.12 m and 0.15 m. Below 0.2 m, the waste rock appeared to be non-compacted. On October 10, 2002, six measurements of moisture content and density were made on the compacted waste rock surface using a Troxler nuclear densometer gauge with a probe depth of 0.15 m. In addition, three samples were collected from the compacted layer for laboratory moisture testing. Average field density and moisture content for the compacted surface as measured by the Troxler gauge were 2114 kg/m^3 and 6.1%, respectively, and the moisture content values measured on the laboratory samples were 6.0%, 7.1% and 5.8%. Compaction was similar to that achieved during compaction trials on the DJN and Claude waste rock material (Cogema, 2001) and during compaction trials on the Claude waste rock pile at Cluff Lake using various mine equipment (O'Kane Consultants, 2001).

A few topographic lows were identified following a rain event on May 13, 2003.

In June of 2003, a small quantity of waste rock was added to low areas in the surface above lysimeters 1, 2, 13 and 14 and compacted with a hand tamper.

3.4. DATA

Event-specific hydrographs for the basal lysimeters from a natural and an artificial rainfall event on each of the three surface conditions are presented. The six rainfall events were chosen based on the completeness of the data record, the size of the rainfall event, and because each had a period of dry weather preceding the rainfall event. The three artificial rainfall events were similar to larger, high intensity rainfalls commonly observed in the area during the later summer months. The natural rainfall events were lower intensity, longer duration events common to the region during the spring and early summer months. The first two rainfall events occurred prior to surface ripping and leveling. The third and fourth occurred on the ripped and leveled surface and the final two on the covered surface. Table 3.1 provides details of the six rainfall events and the lysimeter responses are described below.

3.4.1. Individual Lysimeter Responses

The outflow response to rainfall events was unique for each of the sixteen lysimeters and varied from one rainfall event to another. Hydrographs from 11 of the 16 lysimeters are presented. The quality of data from the tipping buckets that metered outflow from lysimeters 12 and 15 began to deteriorate in 2002 and the resulting hydrographs are noisy. Hydrographs from lysimeters 4, 8 and 16 were omitted from all plots because evidence exists for bypass flow along the external wall of the experimental waste rock pile, an experimental artifact, following large rainfall events on the covered surface.

Outflow hydrographs for the precipitation events on the free-dumped surface are shown in Figures 3.5.a and 3.5.b. The hydrographs are for 9 days following a 40.8 mm natural rainfall event on July 30, 2001 and a 32.2 mm artificial rainfall event on September 01, 2001.

Outflow hydrographs for two precipitation events on the ripped and leveled surface are plotted for three days following a 25 mm natural rainfall event on July 01, 2002 and for 9 days following a 39.9 mm artificial rainfall event on the August 08, 2002 (Figures 3.6.a and 3.6.b).

Figures 3.7.a and 3.7.b show outflow hydrographs for two precipitation events on the lower permeability cover surface. The hydrographs are plotted for 40 days following a 49.8 mm artificial rainfall event on of May 13, 2003 and for 40 days following a 33.2 mm natural rainfall event on July 09, 2003. Note the Y-axis is in liters per day and the flow rate is an order of magnitude smaller than that in Figures 3.5. and 3.6.

3.5. RESULTS AND DISCUSSION

Nichol (2003) observed spatial variability in lysimeter outflow and found that the relative pattern of outflow response observed for each individual lysimeter was consistent from event to event. Spatial variability in outflow response of individual lysimeters and between lysimeters were observed and hypothesized to be affected by the irregular surface configuration on the waste rock pile (Marcoline et al, 2003). This section presents a discussion of the characteristics of the outflow response in relation to the rainfall characteristics and the surface configuration of the waste rock pile.

For similar size precipitation events under the free-dump surface configuration, the relative magnitude and timing of the wetting front responses recorded in individual basal lysimeters remained constant (Nichol et al, 2002 and Nichol, 2003). Lysimeter 6, for example, consistently shows the largest flow rate and appears as a single, large wetting front that returns to pre-event flows after approximately 10 days (Figures 3.5.a and 3.5.b). It is likely that the large response in lysimeter 6 obscures the observation of secondary wetting front arrivals at the base of the CPE. The shape of the hydrographs from lysimeters 1, 7 and 13 are similar to 6, however, they consistently show a lower magnitude initial response, followed by one or more wetting front arrivals. In contrast, the outflow hydrographs from lysimeters 3 and 5 are often the last to respond, and typically show the lowest magnitude response following large rainfall events on the free-dumped surface.

Following ripping and leveling of the waste rock surface, the patterns observed in the hydrographs from lysimeters 5 and 9 do not change, while several hydrographs change following rainfall events on the ripped and leveled surface. Following ripping and leveling, the hydrograph from lysimeter 6 is still the first to show a response following rainfall events, and has the largest magnitude flow rate, but no longer has the uniquely large spike in flow rate. Lysimeter 1 no longer shows a rapid response to rainfall events. Lysimeter 3 shows a delayed, and low magnitude response following the 25 mm rainfall event, and shows a high magnitude, rapid response following the 39.9 mm rainfall event (Figure 3.6.b).

Three distinctive patterns are evident in the outflow hydrographs following rainfall on the covered surface (Figures 3.7.a and 3.7.b). The majority of the lysimeters show a very gradual increase in flow rate without distinctive spikes or wetting front arrivals and cannot be linked to the rainfall event. Lysimeters 1, 2 and 3 exhibit wetting front arrivals that are in response to the rainfall events, but may in part, be an experimental artifact related to bypass flow along the wall of the lysimeters. Hydrographs from lysimeters 13 and 14 have a distinctive response to the rainfall events characterized by a 15 to 20 day gradual increase in flow rate.

3.5.1. Spatial Variability in Rate and Total Magnitude of Infiltration

Nichol (2002) observed the variability in outflow at the base of the waste rock pile and suggested that localized runoff resulting from an irregular surface topography may have been one factor contributing to the observed variability in outflow. Earlier, Bellehumeur (2001) documented the initiation of preferential flow beneath "catchment drains" on the surface of the Claude waste rock pile at Cluff Lake. The result was a more localized, faster and deeper wetting front beneath the catchment drains. Similar to the observations of Bellehumeur (2001), and reported in Smith and Beckie (2003), when the precipitation rate exceeds the infiltration capacity of the surface of the CPE, overland flow to low areas and ponding of water will occur in the topographically defined basins.

Altering the surface configuration of the waste rock pile was hypothesized to affect the amount, rate and spatial variability of infiltration into the waste rock. The surface modification from the free-dumped surface to the ripped and leveled surface removed topographic relief, eliminating localized runoff and ponding effects that were observed during highest intensity artificial rainfall events. Creating this change permitted an investigation of the relationship between the spatial variability of surface infiltration into the material and the spatial variability in basal outflow. The hydrographs showed that both the infiltration rate and the degree of spatial variability in outflow were a function of the magnitude of the rainfall event, and it appears that, in addition, the pattern of the spatial variability changes with rainfall magnitude under the first two surface configurations. Thus, the subsequent modification from the ripped and leveled surface to a smooth, compacted surface allowed for the investigation of the effect of a significantly reduced infiltration rate on spatial distribution of outflow.

Rainfall events with precipitation rates lower than the infiltration capacity of the surface provide additional data to investigate the relative importance of surface topography and surface texture on the outflow distribution. During these events, localized runoff and surface redistribution are minimized and the surface topography has limited to no effect on the distribution of the rate and volume of surface infiltration into the pile. At these lower precipitation rates, any variability in wetting front arrival times and the flow rates at the base of the pile following the removal of topography must principally reflect differences in waste rock characteristics inside of the pile, assuming that the evaporative losses are uniform across the surface of the pile. The variability then results from lateral redistribution of water within the waste rock pile and preferential flow.

Figure 3.8 shows two outflow hydrographs for each of the 11 lysimeters following the two natural lower intensity events, both having a fairly similar rainfall rate (Table 3.1). The data are for the same rainfall events as shown in Figures 3.5.a and 3.6.a. The solid lines are the outflow hydrographs following a rainfall event on the free-dumped surface and the dashed lines are the hydrographs following the rainfall on the ripped and leveled surface. The time axis for the July 30, 2001 event is plotted along the bottom of this figure; the time axis for the July 1, 2002 event is plotted along the top of this figure. All lysimeters except 3, 7 and 11, exhibit significant differences between the outflow hydrographs for the two surface conditions. The time interval between the initiation of the rainfall event and the outflow response recorded in each of the basal lysimeters varied from lysimeter to lysimeter. Several lysimeters responded faster to rainfall events prior to ripping and leveling of the surface while others appeared to respond slower. With the exception of one lysimeter, the outflow responses observed following rainfall on the free-dumped surface exhibit a steeper rise in flow rate and a higher initial peak regardless of the duration between the start of the rainfall event and the outflow response. The rainfall event on the free-dumped surface resulted in sharp outflow peaks in lysimeters 1, 6, 9 and 13 that were not present following rainfall events on the ripped and leveled surface. Both events had rainfall rates lower than the infiltration capacity of the surface, ruling out surface topography and texture as the dominant controlling factors.

The initial water content of the waste rock in the CPE and the duration of the rainfall event cannot explain the absence of the fast peaks from the hydrographs for the ripped and leveled surface condition. The average initial water content of the waste rock pile prior to the event on the ripped and leveled surface was higher than the water content prior to the event on the free-dumped surface. A higher volumetric water content with the same precipitation rate could allow for a greater degree of fast preferential flow and earlier flow peaks, which is the opposite to what was observed. Furthermore, elimination of the fast flow spikes cannot be explained by the additional volume of infiltration following the rainfall event on the free-dumped surface, which lasted 16 hours compared to the 9-hour event on the ripped and leveled surface, unless the rainfall was heavily weighted towards the beginning of the 16-hour period. The flow spikes reach their maximum value in approximately eight hours, before half of the total precipitation on the free-dumped surface occurred. While the outflow rates following rainfall events with a lower precipitation rate indicate little about the effects of surface topography during higher intensity rainfall events, they do suggest that a large portion of the variability was unrelated to the surface topography and must be a result of internal, or near-surface waste rock structure.

The larger natural rainfall events and the majority of the artificial rainfall events on the experimental waste rock pile occurred at a rate close to, or below the infiltration capacity, based on the absence of runoff and ponding. During the largest artificial rainfall event the infiltration capacity of the irregular free-dumped surface was exceeded. Following the rainfall, a few localized areas on the surface appeared to be saturated and isolated ponding with a water depth of less than 2 mm was observed. Prior to ripping, the surface elevation of the waste rock pile was surveyed to 0.1 cm on a 30 cm by 30 cm grid in September of 2001. Ten variably-sized basins with a maximum topographic relief of up to 0.45 m across the free-dumped surface condition were identified (Figure 3.2). This surface relief was then examined in relation to the hydrographs from the underlying lysimeters. Basins with a drainage area greater than the 2 m by 2 m lysimeter area were located above lysimeters 6, 7 and 13. Topographic highs or sloped surfaces existed on the surface above lysimeters 2, 3, 10, 11 and 14 and little to no ponding was observed above the lysimeters.

Lysimeters beneath several of the largest drainage basins exhibit larger flows and earlier wetting front arrivals following high intensity rainfall events on the free-dumped surface than on the ripped and leveled surface. Figure 3.9 shows an outflow hydrograph for each of the 11 lysimeters from two similar-sized, large rainfall events, one in 2001 and the other in 2002 (Table 3.1). The time axis for the September 01, 2001 event is plotted along the top of this figure; the time axis for the August 08, 2002 event is plotted along the bottom of this figure. The solid line is the hydrograph for the free-dumped surface and the dashed line is the hydrograph for the ripped and leveled surface. Note that the scale on the Y-axis for lysimeter 6 is different than the other lysimeters. Prior to ripping and leveling, hydrographs from lysimeter 6, 7, 11 and 13 exhibit short-lived, large flow spikes shortly after large rainfall events began. In addition, lysimeter 6 was centered beneath the largest catchment basin and typically responded to large rainfall events with an outflow rate between three and five times higher than that of any other lysimeter (Figure 3.5 a and b). Lysimeters 7, 11 and 13 are also located below the low point of a basin and show a sharp spike in flow rate following the rainfall on the free-dumped surface. The maximum flow rates were significantly reduced following a similar size rainfall event on the ripped and leveled surface (Figure 3.6). Lysimeter 6 recorded a three-fold decrease in flow rate following ripping and leveling and flow to lysimeters 1, 7 and 13 were reduced by approximately 50%. The fast pathways responsible for the high flow rate of lysimeter 6 in October 2001 are not as prominent following ripping and leveling, and the cumulative outflow volume was consequently less. While the maximum flow rate for lysimeter 6 decreased with ripping and leveling, the lysimeter was still the first to respond, and had a rapid spike in outflow rate double that of any other lysimeter. The sustained dominance of lysimeter 6 flow over that from other lysimeters suggests that in addition to the surface configuration, other mechanisms within the waste rock pile have a significant influence on the observed preferential flow. Other than the initial spike in flow rate, it was difficult to determine which differences in the outflow are related to the topography and which are related to the internal material characteristics at high infiltration rates.

Similar to lysimeter 6, a decrease in peak flow rate was observed in lysimeters 1, 7, 11 and 13. In addition, the cumulative volume of outflow from lysimeters 2, 3, 7, 9, 10, 11, 13 and 14 increased following similar magnitude rainfall events after ripping and leveling (Figure 3.9). The two-to three-fold increase in outflow volume following ripping and leveling is interpreted to result from the removal of topographic highs, and potentially from the activation of new fluid flow pathways. Lysimeters 2, 3, 9 and 14 were located beneath topographic highs or sloping surfaces on the free-dumped surface and experienced higher flow rates following ripping and leveling. It is inferred that the increase in relative flow rates following ripping and leveling are in part, a response to the elimination of localized ponding on the surface above the respective lysimeters. The increased outflow volume in these lysimeters is not related to a change in the water balance, rather it relates to a redistribution of water from other lysimeters that experienced higher relative volumes prior to ripping and leveling.

The topographically controlled variations in flow most notably effect the initial spike which occurred during the rainfall event. The concentrated flow volume in the three basins allowed for the activation of fast flow paths within the waste rock. In the case of lysimeters 7 and 13, the preferential flow appears to be activated beneath the basins as a result of the larger flow and not as a result of differing sub-surface waste rock properties above the lysimeters and below the surface. In contrast, a similar outflow behavior is still observed in lysimeter 6 when the infiltration is more uniformly distributed across the surface of the waste rock pile. Lysimeter 6 appears to have preferential flow paths that are coincidental with the overlying basin and that are related specifically to the structure or character of the waste rock column above the lysimeter. The same sharp spikes in flow rate observed in lysimeters 6, 7 and 13, were also observed in lysimeters 1 and 11 which lie beneath topographic highs, and therefore cannot be explained by a topographically-controlled, localized, higher infiltration rate.

In addition to surface topography, surface texture could account for the observed spikes in flow. Changing the texture or physical properties of the material at the surface would result in a varying infiltration capacity. The process of ripping and leveling likely created a loose 'sponge-like' surface layer with a more uniform distribution of waste rock surface texture. The resulting surface likely had a more open pore structure and a higher (less negative) air-entry value than the underlying waste rock, allowing a more uniform distribution of infiltration deeper into the waste rock during rainfall events. While the ripped layer may have enhanced infiltration in some areas, it may also have reduced the infiltration capacity in other areas. The area above lysimeter 6 and 13 on the free-dumped surface consisted of cobbles and boulders 0.05 m to 0.50 m in diameter and were nearly void of matrix material across the entire 0.40 m ripped depth. The surface in these areas had a clast-supported structure while the majority of the surface of the CPE had a matrix-supported structure. During the ripping and leveling process, the surface material was homogenized to promote a similar particle size distribution across the entire surface. As with the removal of topography, the process of ripping and leveling eliminated all observable variation in surface texture on different portions of the surface which may have resulted in a minor, non-systematic change in outflow distribution. To minimize the disturbance of the CPE, particle size distributions of the waste rock at the surface were not measured prior to ripping and leveling, so this effect cannot be quantified.

A relationship between topography and the spatial variability of basal outflow exists for lysimeters 2, 3, 6, 7, 9, 13 and 14 and a potential relationship between the surface texture and flow spikes in lysimeters 6 and 13 exists. However, elimination of the topographic and textural differences together cannot explain the spatial distribution of outflow and therefore must be a result of internal structure.

3.5.2. Infiltration Rate

In addition to an irregular surface topography and surface texture, the rate of infiltration into the waste rock plays a role in influencing the magnitude, character and distribution of outflow in the basal lysimeters. The compacted cover was designed to significantly reduce the rate and volume of infiltration into the waste rock pile. The cover reduced surface infiltration 30% (lost to runoff) and reduced net-infiltration (net-percolation) from approximately 50% to 6% of precipitation. Hydrographs from all lysimeters following construction of the cover exhibit a small increase in flow rate during the summer of 2003 following the winter drain down, but the rapid response and high flow rates observed following precipitation events on the free-dump or ripped and leveled surface were absent.

Figure 3.10 shows 11 outflow hydrograph sets following an artificial and a natural rainfall event on the covered surface. Figure 3.10 differs from Figures 3.8 and 3.9 and compares two events on the same surface, not two different surfaces. The time axis for the July 09, 2003 event is plotted along the bottom of this figure; the time axis for the May 13, 2003 event is plotted along the top of this figure. The solid lines depict the 30 day hydrographs following the May 13th event plotted on the same scale as the 30 day hydrographs following the July 09th rainfall event (dashed lines). The time axes span the same duration, and are aligned to the initiation of the rainfall event. The artificial rainfall on May 13, 2003 was applied at a rate of 7.7 mm/hr while the rate of the natural event on July 09, 2003 was lower at 4.2 mm/hr. For the first 1.5 months following the April thaw, the majority of hydrographs continue to follow the winter drain down curve even though greater than 100 mm of rainfall had fallen on the top of the pile. The hydrographs from the six central lysimeters 5, 6, 7, 9, 10 and 11, show a gradual increase in flow rate at the base of the pile during July and August of 2003, without the distinctive wetting fronts observed pre-cover. This outflow from the six lysimeters likely consists of older, slow moving pore water in the pile and potentially a small amount of matrix flow associated with the large rainfall event in May.

Distinctive wetting fronts are observed in lysimeters 1, 2, 3, 13 and 14 following both rainfall events shown in Figure 3.10 and can be associated with surface ponding. During the May 13th event, an area of less than 0.5 m^2 of ponding was observed above each of lysimeters 1, 2 and 3. Larger ponded areas of approximately 1.0 m^2 above lysimeter 13 and an area of 2.0 m^2 above lysimeter 14 were observed. Wetting fronts were recorded in lysimeters 1, 2 and 3, approximately 15 days following the rainfall event. The elevated flow that followed the wetting fronts was observed for 4 to 14 days. In lysimeters 13 and 14, the first wetting front was observed within 5 days of the rainfall event and the elevated flow that followed the wetting fronts lasted 26 days. Following the May 13th rainfall event, additional material was added to the cover and compacted in the areas where ponding was observed. In rainfall events following the cover repair, surface ponding was eliminated above lysimeters 1, 2 and 3 and a minor amount of ponding was still observed in the area above lysimeter 13 and 14. The hydrographs from lysimeters 13 and 14 still show a response to the ponded water at the base of the pile approximately 14 days following the July rainfall event.

Tracers were used to examine the presence of event water in outflow. Deuterium tracer was applied on May 13, 2003 and a bromide tracer was applied on July 29, 2003. Neither tracer was detected in amounts above background levels in outflow water from early August of 2003. The lack of either tracer is significant because it confirms that the water comprising the wetting fronts observed in basal lysimeter 13 and 14 was old water and did not contain water from the large May 13th, July 9th, or the July 29th rainfall events.

The distinctive wetting fronts observed in lysimeters 1, 2, 3, 13 and 14 for the covered pile are interpreted to be a result of a pressure wave, or a kinematic wave as described by Torres (1998), Rasmussen et al (2000) and Williams et al (2002), and not as preferential flow. This is different than the kinematic wave discussed by Germann and Beven (1985), Germann (1990), Singh (2002), modeled by Lopez et al (1997), Poyck et al (2005), and observed in column and field experiments by Smith (1983), which is equated to actual water movement in macropores. Rainfall events may result in the propagation of a pressure wave that can be transmitted vertically through the pile. Following a rainfall event, the volumetric water content of the waste rock at the surface increases, the matric potential or suction decreases and the increased local gradient causes a redistribution of pore water. Depending on the initial conditions and the characteristics of the rainfall event, the pressure wave may propagate to the base and result in outflow.

Nichol (2003) documented that water flow in preferential flow paths in the CPE moves at rates far greater than the average fluid velocity. In addition to preferential flow of water, a pressure wave typically moves at a rate far greater than the average fluid velocity. Both water flow in preferential flow paths and pressure waves appear as basal outflow in response to transient infiltration events, and it is important to differentiate pressure wave propagation from preferential flow. Close to saturation, the moisture content changes rapidly for small changes in pressure head, therefore the addition of water to the uncovered pile would result in a small decrease in suction and a large increase in hydraulic conductivity. If the infiltration rate is high enough, the combination of the additional water and the higher conductivity will activate macropore flow and rapidly conduct water from the rainfall event into, or through the pile. The primary difference is that preferential flow is a physically controlled process that allows for new water to bypass the matrix water, while a pressure wave propagates through existing pore water and the pressure change causes redistribution of the existing water.

At low water contents, such as those occurring in the covered waste rock, the soil water characteristic curve (SWCC) for the waste rock is relatively flat (Figure 3.11). A small change in volumetric water content from a rainfall event will result in a large change in suction, or hydraulic head. As the pressure wave propagates through the pile, water from surrounding smaller pores is redistributed into larger pores in response to the higher pressure gradients. Based on the relationship between the soil water characteristic curve and the hydraulic conductivity curve (HCC) (Figure 3.12), the same small increase in volumetric water content of the waste rock while it is near residual saturation will only result in a small increase in the hydraulic conductivity. The pressure wave will propagate vertically in response to the head gradient, however, vertical percolation is still relatively small because of the low hydraulic conductivity. Depending on the water content, some of the redistributed pore water can drain down but much of it is drawn into the fine pores as the pressure stabilizes. In a pure pressure wave response, the water reporting to the lysimeters is older pore water from within the pile and not newly-infiltrated rain water. Without high frequency tracer data it is difficult to distinguish between the two processes. Based on the theory above, a critical threshold in the water content and particle size should exist above which water from a transient infiltration event will result in the activation of macropore flow in addition to pressure waves. Regardless of whether the field derived, or laboratory derived SWCC (Figure 3.11) is used, the average volumetric water content (vwc) of the covered waste rock is apparently below this threshold. In other words, the properties of the covered waste rock plot in a steep region of the matric suction versus conductivity plot (Figure 3.12) and this region corresponds to a very low hydraulic conductivity.

The antecedent or initial water content of the pile affects both the velocity of the water and the propagation of pressure waves. After extended periods of drain down the residual volumetric water content of the upper portion of the waste rock within the CPE was between 5 and 9% (Figure 3.13). Under such conditions, such as in the spring of 2003, the likelihood of preferential flow to reach to the base of the CPE is significantly less than under wetter summer, or pre-cover conditions and the observed responses were likely a result of pressure waves. In comparison to the average pore water velocity of 0.001 m/day calculated from the deuterium tracer (Marcoline et al, 2006) and the measured water flux, the 0.14 to 1 m/day wetting front velocity measured by TDR are thought to be localized water redistribution in response to pressure waves. The wetting front progressions as measured by TDR are evident in the 1.95 m TDR probes, but not in the 3 m and deeper probes. While the observed responses are more likely to result from pressure waves than from preferential flow under the drier conditions, they also can dissipate faster because of the less continuous and more torturous path of filled pores for the wave to be transmitted. Furthermore, the pressure wave is dissipated faster as the energy is used to redistribute the water to the larger pores. The pressure wave speed will be controlled by the unsaturated hydraulic conductivity and the slope of the moisture content versus matric suction curve at the prevailing pressure head. When the water content is higher, even if it is not high enough to activate preferential flow, the wave propagates faster and further as a result of less lateral water redistribution and the more continuous network of water pores, and is more likely to reach the base of the pile.

Rasmussen et al (2000) applied kinematic theory to the unsaturated hydraulic conductivity model and predicted that pressure wave travel times should be between two and fifteen times the tracer velocity regardless of the particular form of the SWCC (Brooks-Corey, van Genuchten-Mualem, Broadbridge-White, or the Galileo formulation). In column experiments, Rasmussen et al (2000) observed pressure wave velocities up to 1000 times faster than tracer velocities. Nichol et al (2003) documented preferential flow of water to the base of the waste rock pile shortly following large rainfall events and suggested that the kinematic wave theory may explain some of the fast outflow. While Nichol did not attempt to differentiate between preferential flow rates and pressure wave travel times, it can be inferred based on his chloride tracer and outflow data that pressure wave velocities were on the order of 100 times faster than the average pore water velocities in the uncovered waste rock pile. In comparison to the estimated pressure wave rates through the uncovered waste rock pile, a reduction in pressure wave velocities was observed following placement of the lower permeability cover.

3.5.3. Variability of Outflow

The reduction in variability of basal lysimeter outflow following cover placement can be observed by comparing pre- and post-cover cumulative outflow (Figure 3.14). The process of ripping and leveling the surface of the waste rock pile activated some pathways and closed other pathways for fast flowing water relative to the three-year old free-dumped surface. As evident in Figures 3.7.a, 3.7.b and 3.11, spatial variability of outflow does exist between lysimeters post-cover, but in general, the outflow response of all lysimeters was within a few liters per day. It is proposed that with the modification of the surface from ripped and leveled to one with a lower permeability compacted layer, a large portion of the variability in outflow was removed from the system by significantly limiting infiltration and not allowing water to access the fast pathways.

3.6. CONCLUSIONS

In the free-dumped waste rock, the combined effects of the large range in particle size distribution (ranging from clays to boulders), surface topography, and internal structures, resulted in highly variable outflow distributions measured in the basal lysimeters. The topographically-controlled variations in flow most notably affect the initial spike which occurred during the rainfall event. However, the high degree of spatial variability in basal outflow observed from the CPE with the free-dumped surface appears to result from preferential flow associated with the internal structure of the CPE.

The modification of the surface from free-dumped to a ripped and leveled surface had an effect on outflow by removing large topographic and particle size heterogeneity from the top 0.4 m of the pile, that in-turn reduced the variation in infiltration rate across the surface. The process of ripping and leveling the surface of the waste rock pile activated some pathways and closed other pathways for fast flowing water relative to the three-year old free dump surface. The changes observed following precipitation events on the ripped and leveled surface support a model in which the internal waste rock heterogeneities and structure are the dominant factors controlling the outflow distribution and wetting front arrival times. Surface configuration was important, but only a secondary factor.

The compacted surface reduced the spatial variability of water infiltrating into the waste rock. The modification of the surface from a ripped and leveled to one with a lower permeability compacted layer reduced the surface infiltration and removed a large portion of the variability in outflow from the system. The total basal lysimeter outflow was reduced from 54% to 10% of precipitation. Data from the covered, low infiltration experiments suggest that in this case surface configuration, especially related to ponding, was the dominant control on outflow variability. The construction of the lower permeability cover marked the beginning of a gradual drain down of the waste rock pile, not unlike that seen in the late fall when the surface freezes. In addition, wetting front arrival times were approximately doubled in the 5 m-high waste rock pile following cover placement.

The reduction of the large degree of heterogeneity of material participating in flow and the elimination of macropore flow may allow for more accurate assessment of net-infiltration and internal flow mechanisms and result in a more predictable system.

Specifically, the first hypothesis was that the large spatial and temporal variability in outflow observed from the uncovered CPE was primarily a result of the surface condition of the waste rock pile and to a lesser degree, related to the heterogeneous internal structure of the pile. As discussed above, this was shown to not be the case for either the free-dumped surface or the ripped and leveled surface. However, data from the covered experiments suggested that surface configuration, especially related to localized ponding, was the dominant control on outflow variability in this lower-infiltration condition.

The second hypothesis was that the addition of a lower permeability cover would greatly decrease spatial and temporal variability in outflow by eliminating preferential flow. The lower permeability compacted layer removed a large portion of the spatial and temporal variability in outflow from the system, however, a large amount of preferential flow was still observed in the system.

3.7. REFERENCES

American Society for Testing and Materials (ASTM), 1990. Standard test method for particle size analysis of soils (D422-63; re-approved 1990). Annual Book of ASTM Standards. v. 04.08.

American Society for Testing and Materials (ASTM), 1991. Test method for laboratory compaction characteristics of soil using standard effort (12,400 ft-lbf/ft3 (600 kN-m/m3)) (D698-91). Annual Book of ASTM Standards. v. 04.08.

American Society for Testing and Materials (ASTM), 1994. Standard practice for correction of unit weight and water content for soils containing oversize particles (D4718-87; reapproved 1994). Annual Book of ASTM Standards. v. 04.08.

Bellehumeur, T.M., 2001. Mechanisms and spatial variability of rainfall infiltration on the Claude waste rock pile. MA Sc thesis, University of British Columbia, Vancouver.

Cogema Resources, 2001. Cluff Lake Project Comprehensive Study Report for decommissioning. January 15, 2001.

Dwyer, S.F., 1997. Large-scale field study of landfill covers at Sandia National Laboratories. Conference Proceedings Landfill Capping in the Semi-Arid West: Problems, Perspectives, and Solutions, T.D Reynolds and R.C. Morris (eds). Grand Teton National Park, May 1997. pp. 27-38.

Fines, P., Wilson, G.W., Landriault, D., Langetine, L. and Hulett, L., 2003a. Co-mixing of tailings, waste rock and slag to produce barrier cover systems, Proceedings Sixth International Conference Acid Rock Drainage.

Fines, P., Wilson, G.W., Willams, DJ., Tran, A.B. and Miller, S., 2003. Field Characterization of two full-scale waste rock piles. Proceedings Sixth International Conference on Acid Rock Drainage.

Fleureau, J.M., Verbrugge, J.C., Huergo, P.J., Correia, A.G. and Kheirbek-Saoud, S., 2002. Aspects of the behaviour of compacted clayey soils on drying and wetting paths. Canadian Geotechnical Journal. v. 39. pp. 1341-1357.

Fortin, S., Lamontagne, A., Tasse, N. and Poulin, R., 2000. The use of basic additives to tailings in layered co-mingling to improve AMD control. Paper presented at the 6th SWEMP 2000, May 30th-June 2nd 2000, Calgary, Alberta.

Germann, P.F., 1990. Macropores and hydrologic hillslope processes. In: Anderson, M.G. and T.P. Burt (eds.) Process Studies in Hillslope Hydrology. pp. 327-363; John Wiley and Sons.

Germann, P.F. and Beven, K., 1985. Kinematic wave approximation to infiltration into soils with sorbing macropores. Water Resources Research. v. 21. pp. 990-996.

Holtz, R.D. and Kovac, W.D., 1981. An Introduction to Geotechnical Engineering, Prentice Hall, New Jersey.

Lopez, D.L., Smith, L. and Beckie, R., 1997. Modeling water flow in waste rock piles using kinematic wave theory, in 4th International Conference on Acid Rock Drainage. pp. 497-513.

Mbonimpa M., Aubertin M., Aachib M., Bussière B., 2003. Diffusion and consumption of oxygen in unsaturated cover materials. Canadian Geotechnical Journal. v. 40. no. 5. pp. 916-932.

Maddocks, G., 2003. Preliminary assessment of remediated sulfidic waste rock using Terra B™. National Meeting of the American Society of Mining and Reclamation and the 9th Billings Land Reclamation Symposium. 30 p.

Marcoline, J.R., Beckie, R.D., Smith, L. and Nichol, C.F., 2003. Mine waste rock hydrogeology - The effect of surface configuration on internal water flow. Sixth International Conference Acid Rock Drainage..

Nichol, C.F., 2003. Transient flow and transport in unsaturated heterogeneous media: Field experiments in mine waste rock. Ph.D. dissertation, University of British Columbia, Vancouver.

Nichol, C.F., Smith, L. and Beckie, R., 2000. Hydrogeologic behavior of unsaturated mine waste rock: An experimental study. In Proceedings of the 5th International Conference on Acid Rock Drainage, Denver, Colorado, 21-24 May. Society for Mining, Metallurgy, and Exploration Inc. (SME). pp. 215-224.

Nichol, C.F., Smith, L. and Beckie, R., 2002. Evaluation of uncoated and coated time domain reflectometry probes for high electrical conductivity systems. Soil Sci. Soc. Am. Journal. v. 66. pp. 1454-1465.

Nichol, C.F., Smith, L. and Beckie, R., 2003. Water Flow in Uncovered Waste Rock - A Multi-Year Large Lysimeter Study. Sixth International Conference Acid Rock Drainage.

Nichol, C.F., Smith, L. and Beckie, R., 2005. Field scale experiments of unsaturated flow and solute transport in a heterogeneous porous medium, Water Resources Research. v. 41.

Nicholson, R.V., Gillham, R.W., Cherry, J.A. and Reardon, E.J., 1989. Reduction of acid generation in mine tailings through the use of moisture-retaining cover layers as oxygen barriers, Canadian Geotechnical Journal. v. 26. pp. 1-8.

O'Kane Consultants, 2001. Development of compacted specifications for the Claude Waste Rock Pile surface - Draft - Cluff Lake Project, Submitted to Cogema Resources, O'Kane Consultants Inc., December 2001.

Poyck, S., Troch, P.A., A de Rooij, G.H. and Hilberts, A.G.J., 2005. Simple hillslope hydrology model based on 1D kinematic wave unsaturated flow and the hillslope-storage Boussinesq equation. Geophysical Research Abstracts. v. 7.

Rasmussen, T.C., Baldwin, R.H., Dowd, J.F. and Williams, A.G., 2000. Tracer vs.

pressure wave velocities through unsaturated saprolite. Soil Sci. Soc. Am. Journal. v. 64. pp 75-85.

Singh, V.P., 2002. Is hydrology kinematic? Hydrol. Process. v. 16. pp. 667-716.

Smith, L. and Beckie, R., 2003. Hydrological and geochemical transport processes in mine waste rock, Ch 3 in Environmental Aspects of Mine Wastes, Mineral. Assoc. Canada, Short Course Series. v. 31. pp. 51-72.

Smith, R.E., 1983. Approximate soil water movement by kinematic characteristics. Soil Sci. Soc. Am. v. 47. pp. 3-8.

Torres, R., W.E. Dietrich, D.R., 1998. Montgomery, S. P. Anderson, K. Loague, Unsaturated zone processes and the hydrologic response of a steep, unchanneled catchment, Water Resources Research. v. 34. no.8. p. 1865.

Vanapalli, S.K., Fredlund, D.G., Pufahi, D.E., 1996. The Relationship Between the Soil-Water Characteristic Curve and the Unsaturated Shear Strength of a Compacted Till. Geotechnical Testing Journal. v. 19. Issue 3. p. 10.

Williams, A.G., Dowd, J.F. and Meyles., E.W., 2002. A new interpretation of kinematic stormflow generation. Hydrological Processes. v. 16. pp. 2791-2803.

Wilson, G.W., Fredlund, D.G. and Barbour, S.L., 1997. The effect of soil suction on evaporative fluxes from soil surfaces. Canadian Geotechnical Journal. v. 34. no.2. pp. 145-155.

Winter Syndnor, M.E. and Redente, E.F., 2002. Reclamation of high-elevation, acidic mine waste with organic amendments and topsoil. Journal of Environmental Quality. v. 31. pp. 1528-1537.

Yanful, E.K., Bell, A.V. and Woyshner, M.R., 1993. Design of a composite soil cover for an experimental waste rock pile near Newcastle, New Brunswick, Canada. Canadian Geotechnical Journal, v. 30. pp. 578-587.

Zegelin, S.J. and White, I., Jenkins, D.R., 1989. Improved field probes for soil water content and electrical conductivity measurement using time domain reflectrometry, Water Resources Research. v. 25. no. 11. pp. 2367-2376.

Date	Event Type	Surface Configuration	Precipitation (mm)	Duration (hrs)	Rate (mm/hr)	Runoff runoff (%)
30. Jul. 2001	Natural	Free-Dumped	41	16.0	3	0
1. Sep. 2001	Artificial	Free-Dumped	32	2.4	13	0
1. Jul. 2002	Natural	Ripped and Leveled	25	9.1	3	0
8. Aug. 2002	Artificial	Ripped and Leveled	40	2.9	14	0
13. May. 2003	Artificial	Covered	50	6.5	8	12
9. Jul. 2003	Natural	Covered	33	8.0	4	22

Table 3.1. Summary of the six isolated rainfall events on the top of the constructed waste rock pile.

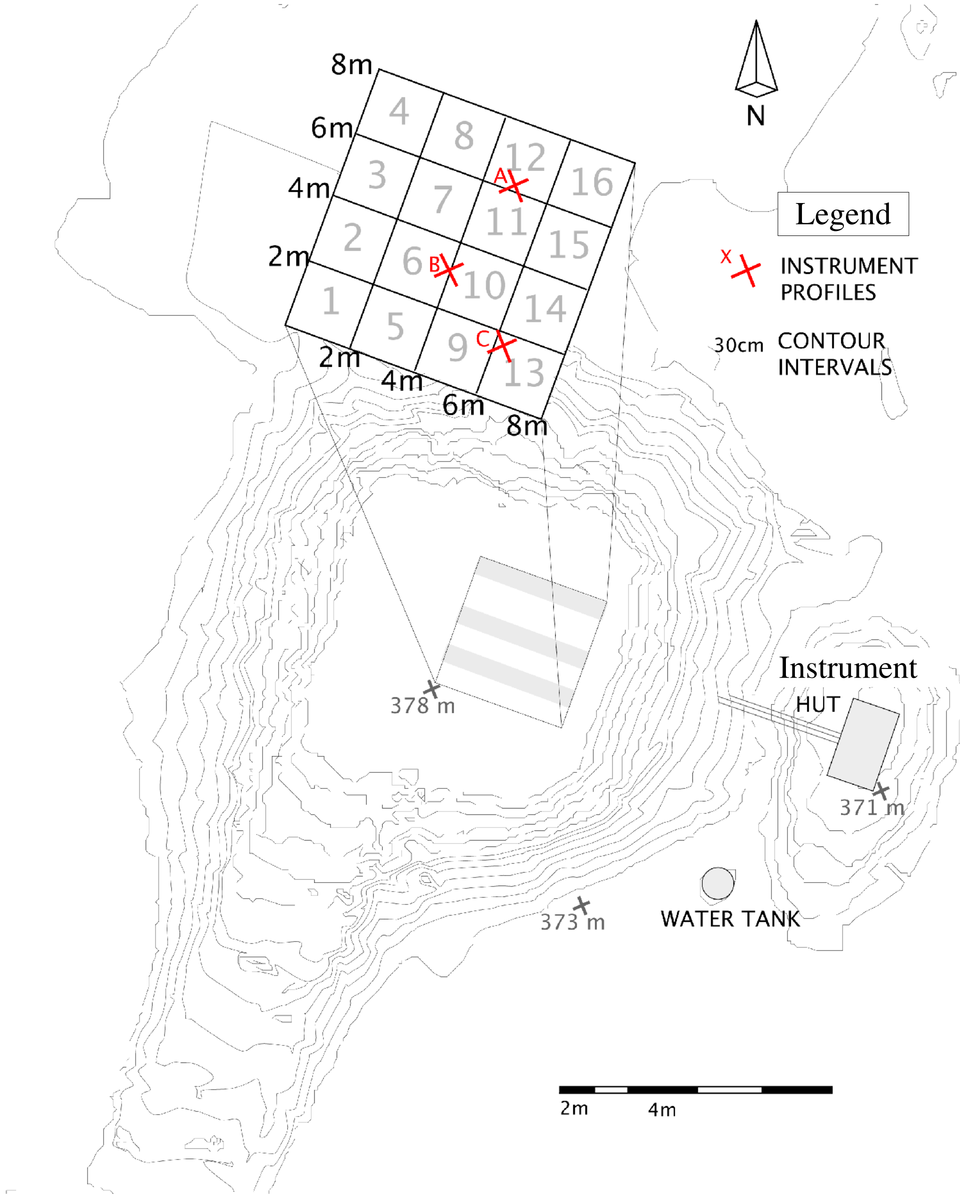

Figure 3.1. Schematic plan view and cross section of the constructed waste rock pile. The grid shows the relative location of the 16 lysimeters.

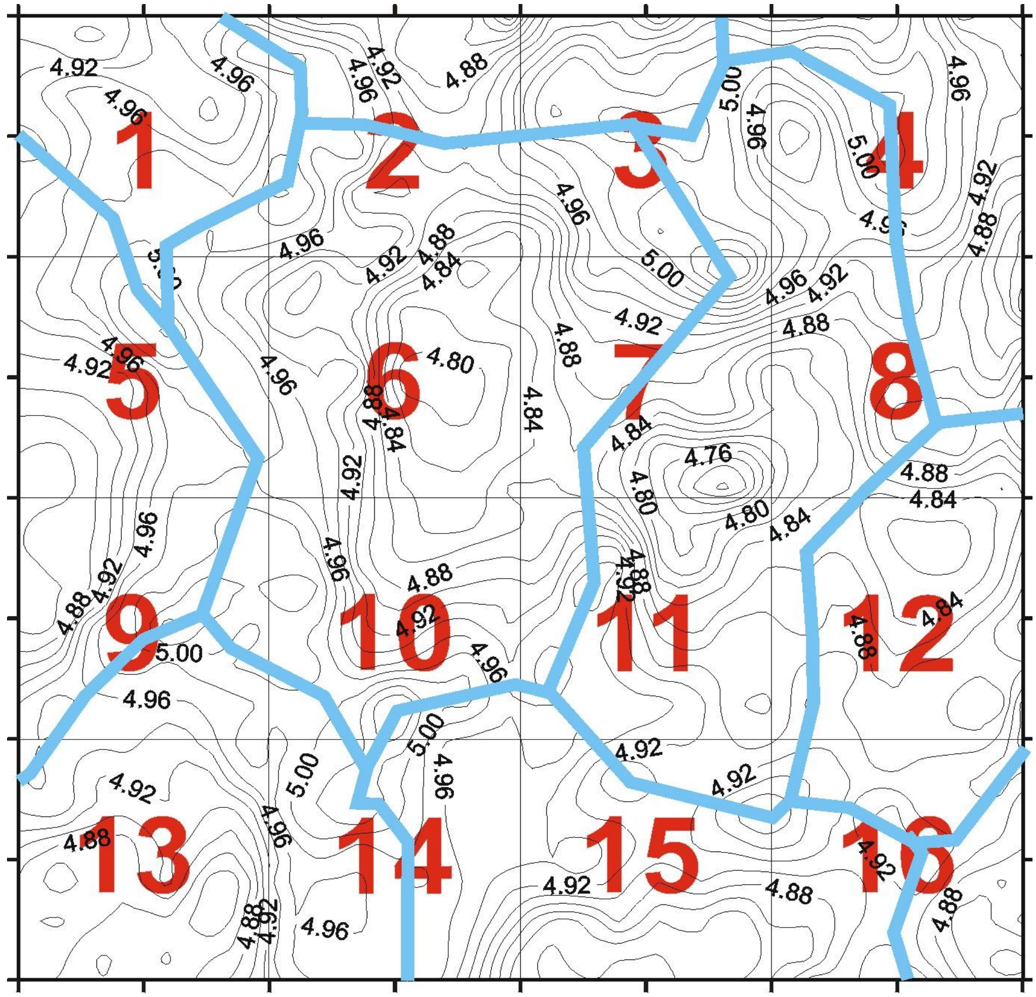

Figure 3.2. Topography of the free-dumped surface as surveyed in the Fall of 2001. The drainage basin boundaries were modified from Nichol (2003) and overlain on the surface topography. The thick boundary lines follow the topographic highs and define the basin divides.

a)

b)

c)

Figure 3.3. a) Photograph of the 3.5 year-old free-dumped top surface looking northwest. b) Photograph looking north-northeast at the ripped and leveled waste rock surface. c) Photograph looking north at the surface following construction of the compacted waste rock layer.

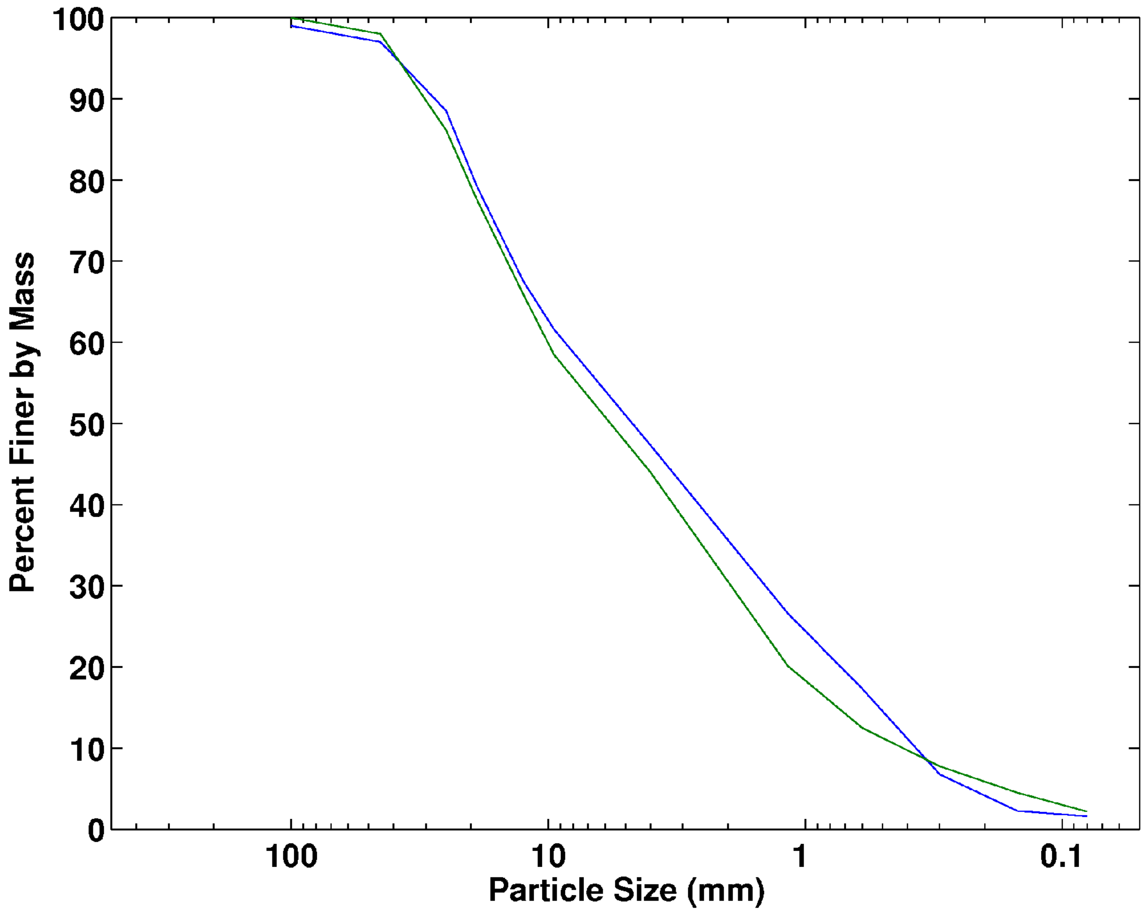

Figure 3.4. Particle size distribution curves from the waste rock cover material before compaction (two samples were collected).

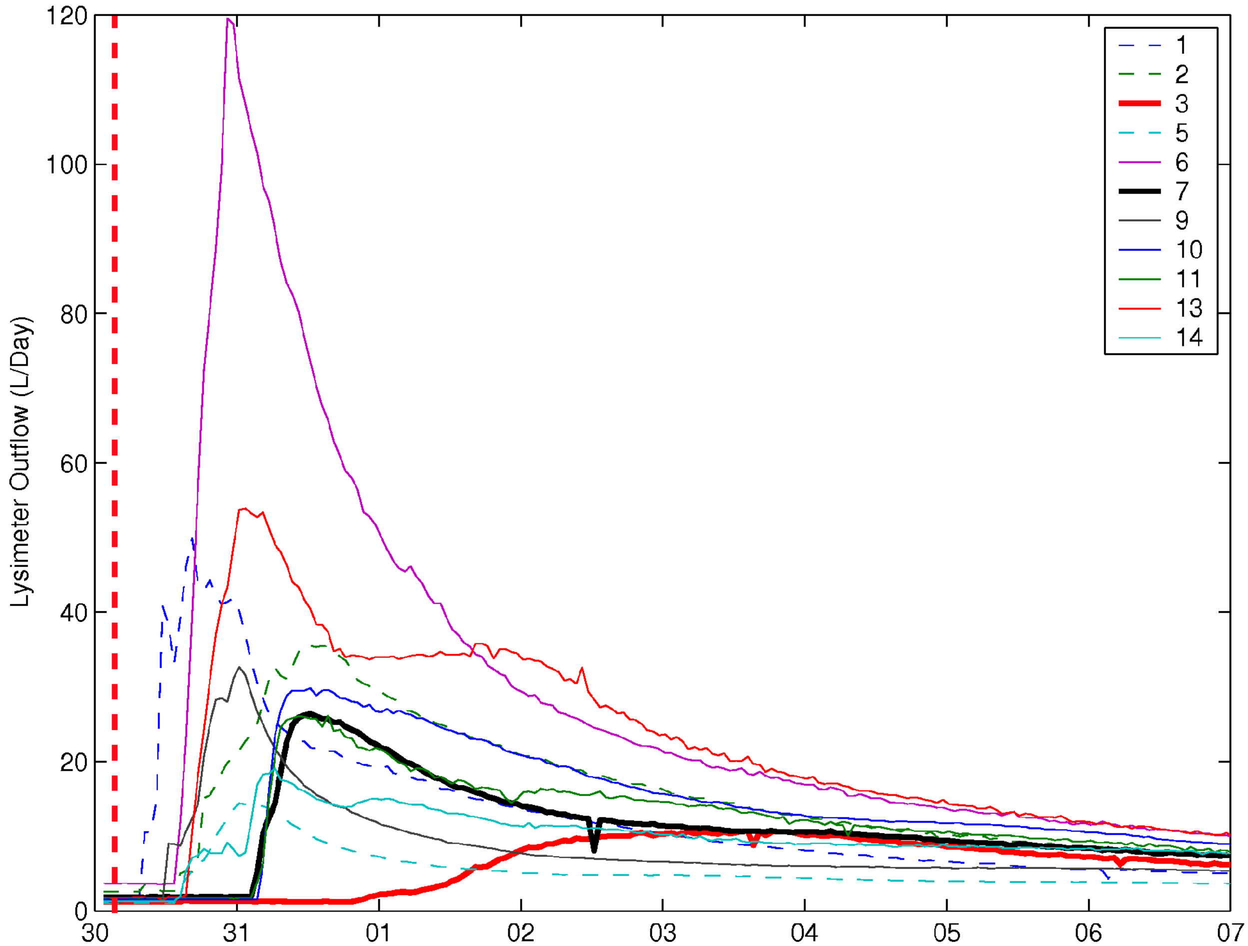

July 30, 2001 - August 07, 2001

Figure 3.5.a. Outflow hydrographs for a precipitation event on the free-dumped surface. The hydrographs are in liters per day for 9 days following a 40.8 mm natural rainfall event on 30th of July 2001. The red dashed line marks the rainfall event.

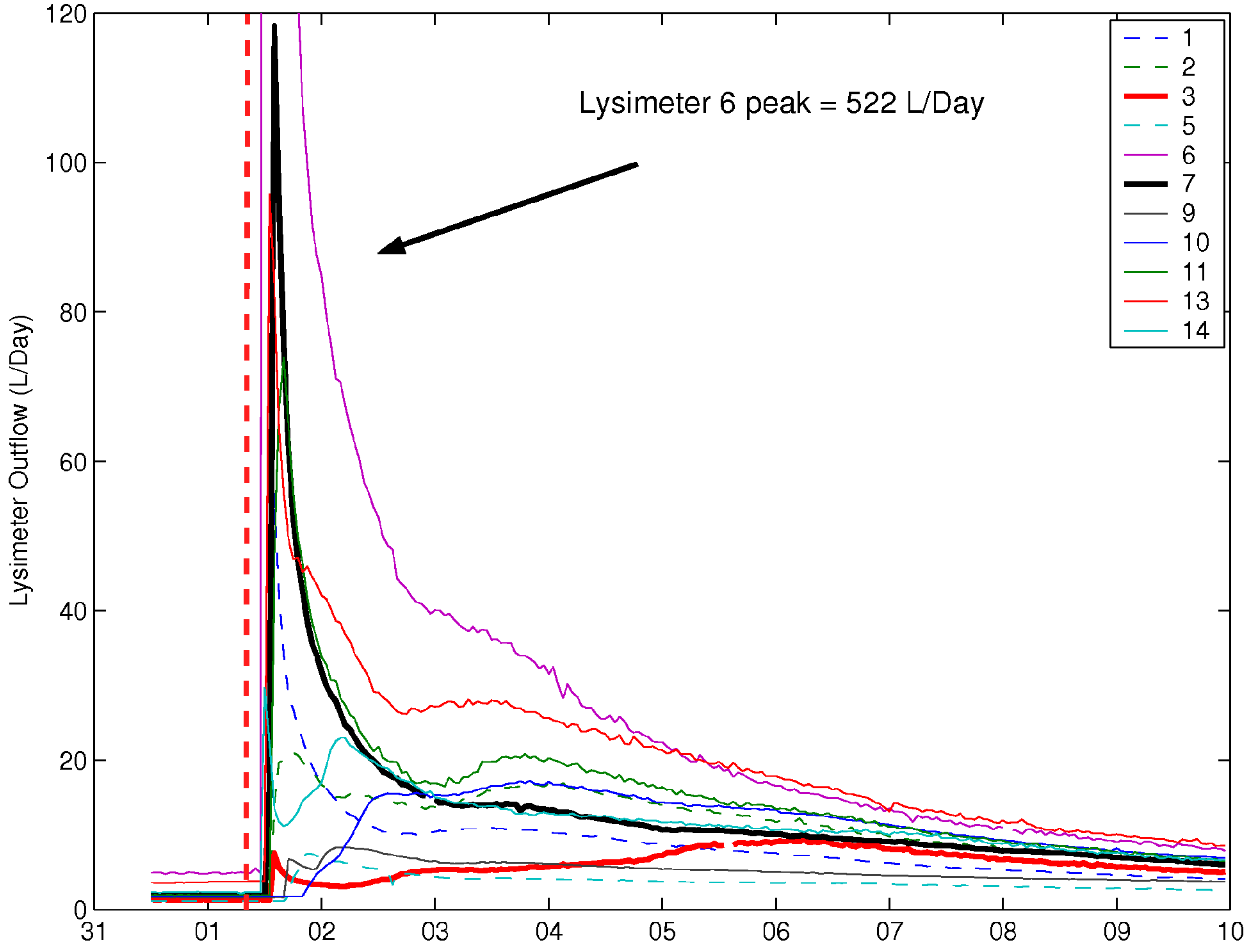

August 31, 2001 - September 10, 2001

Figure 3.5.b. Outflow hydrographs for a precipitation event on the free-dumped surface. The hydrographs are in liters per day for 9 days following a 32.2 mm artificial rainfall event on the 1st of September 2001. The red dashed line marks the rainfall event.

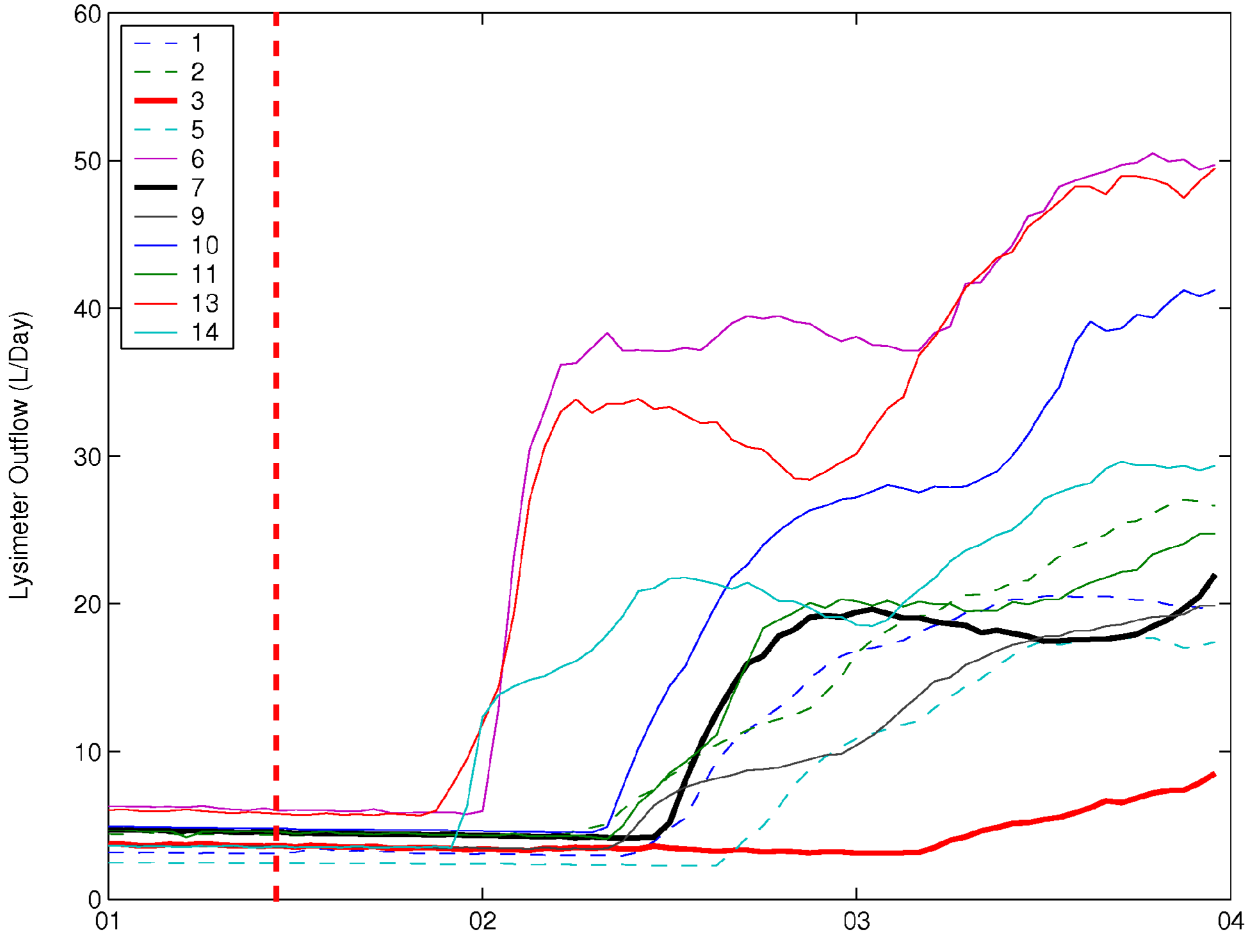

July 01, 2002 - July 04, 2002

Figure 3.6.a. Outflow hydrographs for a precipitation event on the ripped and leveled surface. The hydrographs are in liters per day for 3 days following a 25 mm natural rainfall event on July 01, 2002. As a result of equipment malfunction, data for the week starting on July 04 is missing. The red dashed line marks the rainfall event.

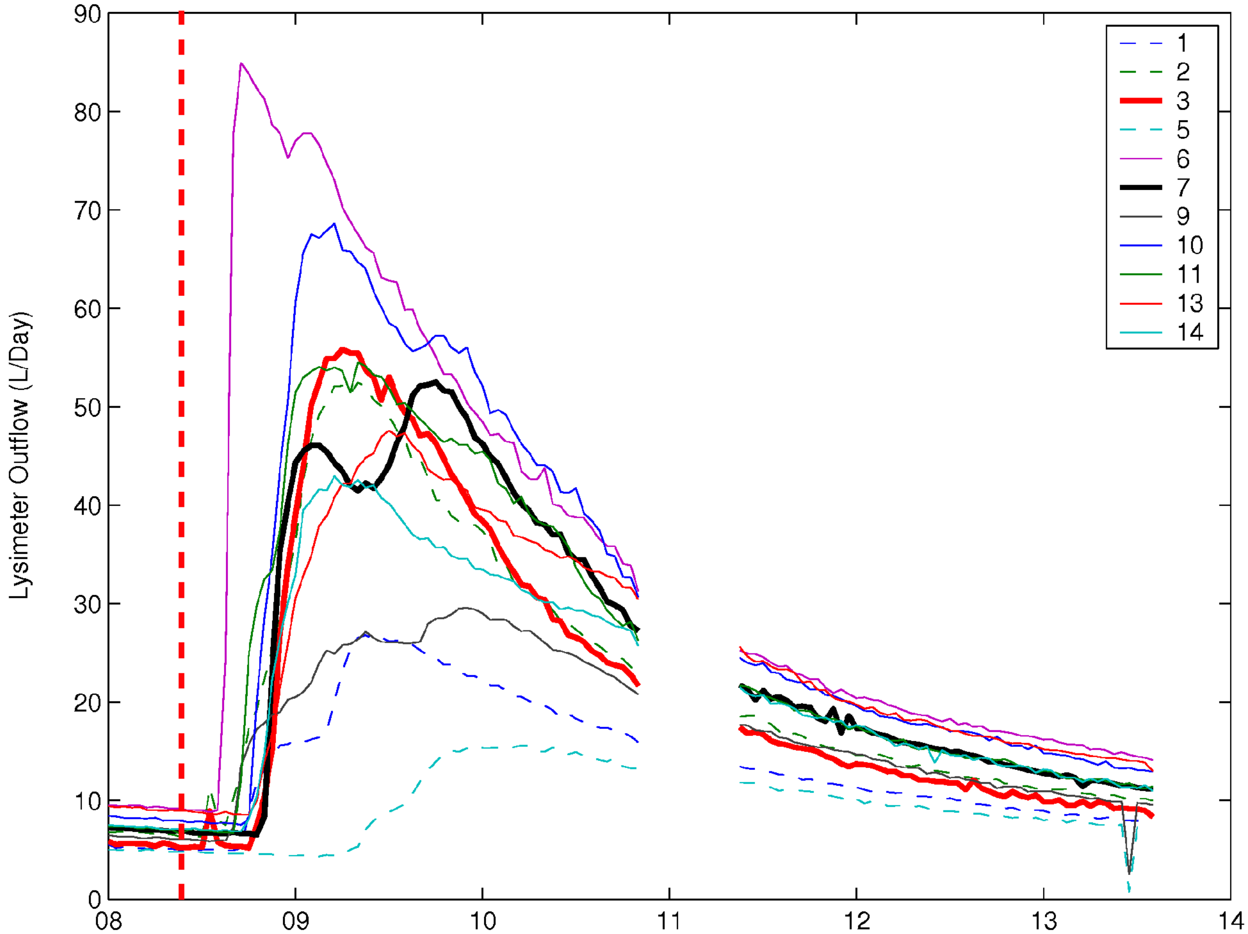

August 08, 2002 - August 13, 2002

Figure 3.6.b. Outflow hydrographs for a precipitation event on the ripped and leveled surface. The hydrographs are in liters per day for 5.5 days following a 39.9 mm artificial rainfall event on the 8th of August 2002. The red dashed line marks the rainfall event.

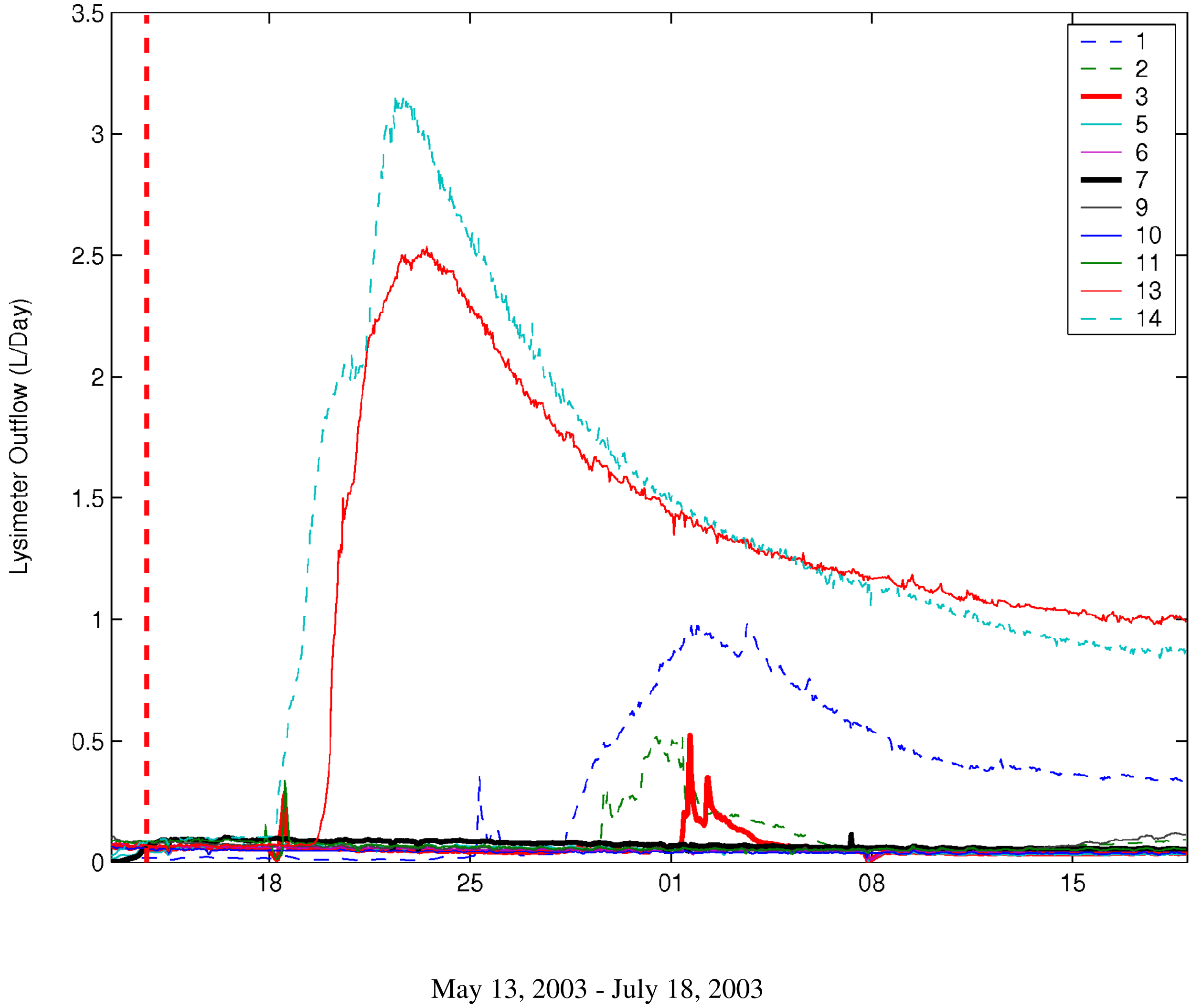

Figure 3.7.a. Outflow hydrographs for a precipitation event on the covered surface. The hydrographs are in liters per day for 35 days following a 49 mm artificial rainfall event on May 13, 2003. The red dashed line marks the rainfall event.

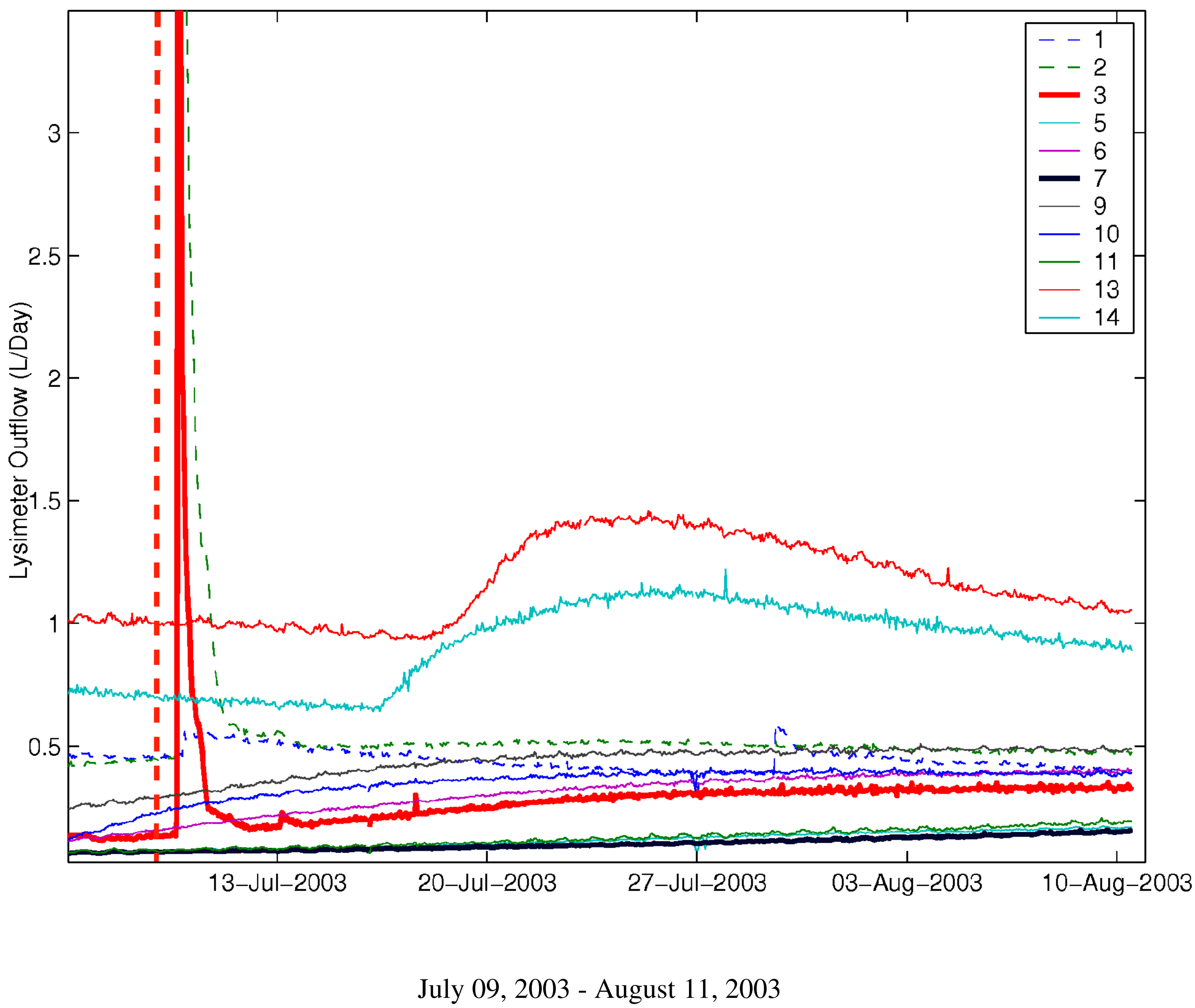

Figure 3.7.b. Outflow hydrographs for a precipitation event on the covered surface. The hydrographs are in liters per day for 32 days following a 33 mm artificial rainfall event on July 09, 2003. The red dashed line marks the rainfall event.

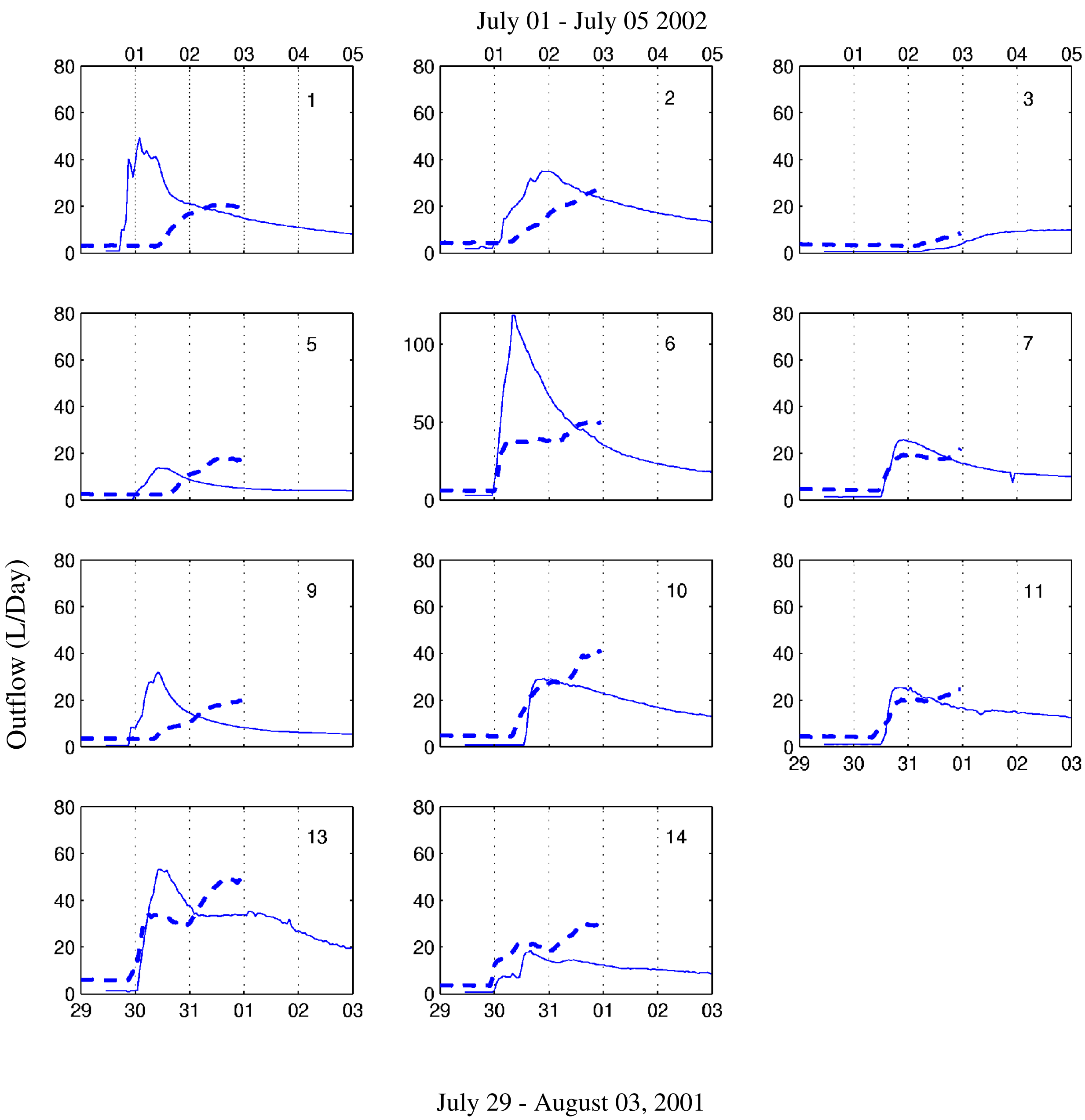

Figure 3.8. Two outflow hydrographs for each of the 11 lysimeters following two natural low intensity rainfall events. The solid lines are the outflow hydrographs following an event on the free-dumped surface (July 30, 2001) and the dashed lines are the hydrographs following the rainfall on the ripped and leveled surface (July 01, 2002).

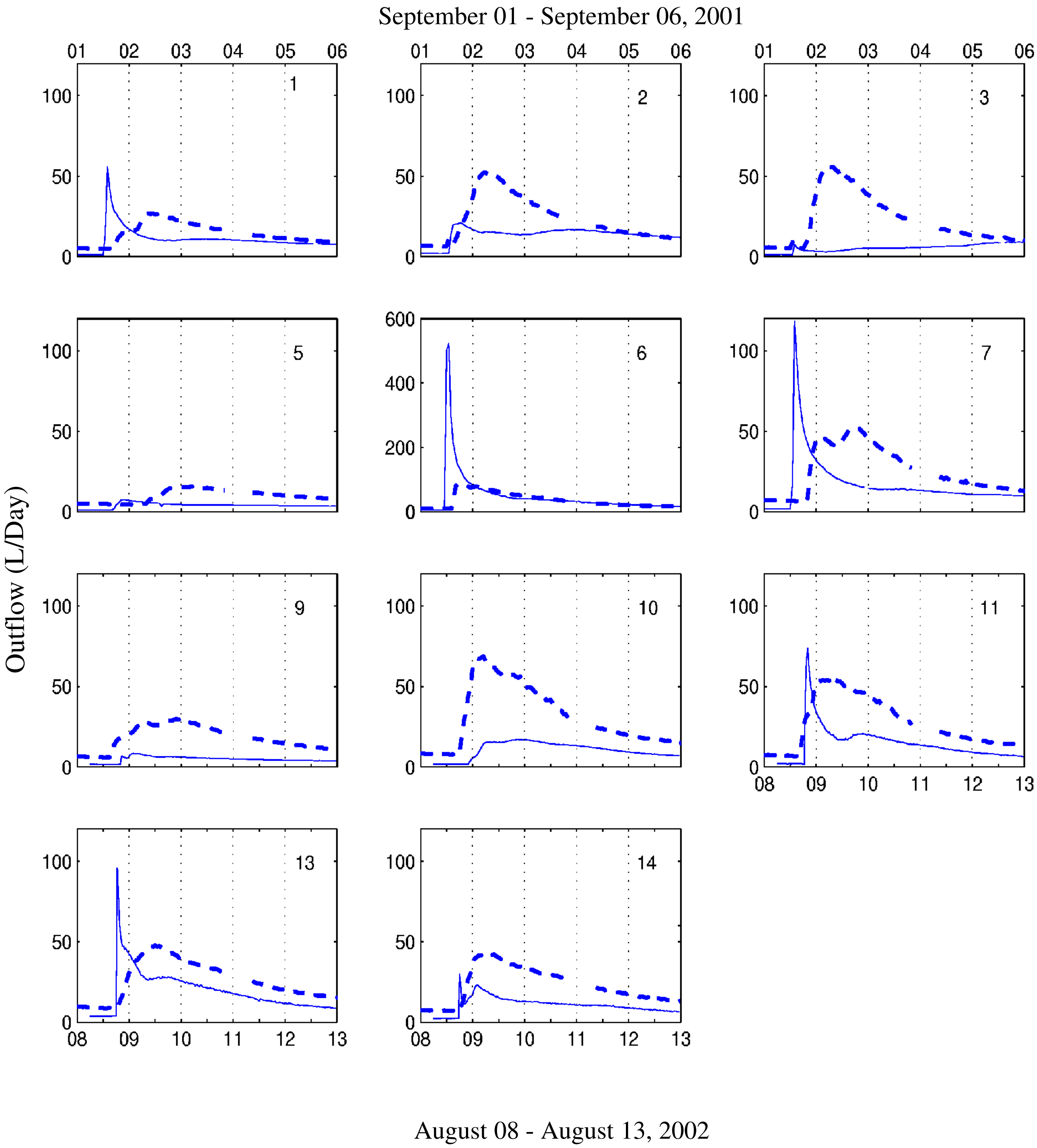

Figure 3.9. Two outflow hydrographs for each of the 11 lysimeters following two artificial high intensity events. The solid lines are the outflow hydrographs following an event on the free-dumped surface and the dashed lines are the hydrographs following the rainfall on the ripped and leveled surface.

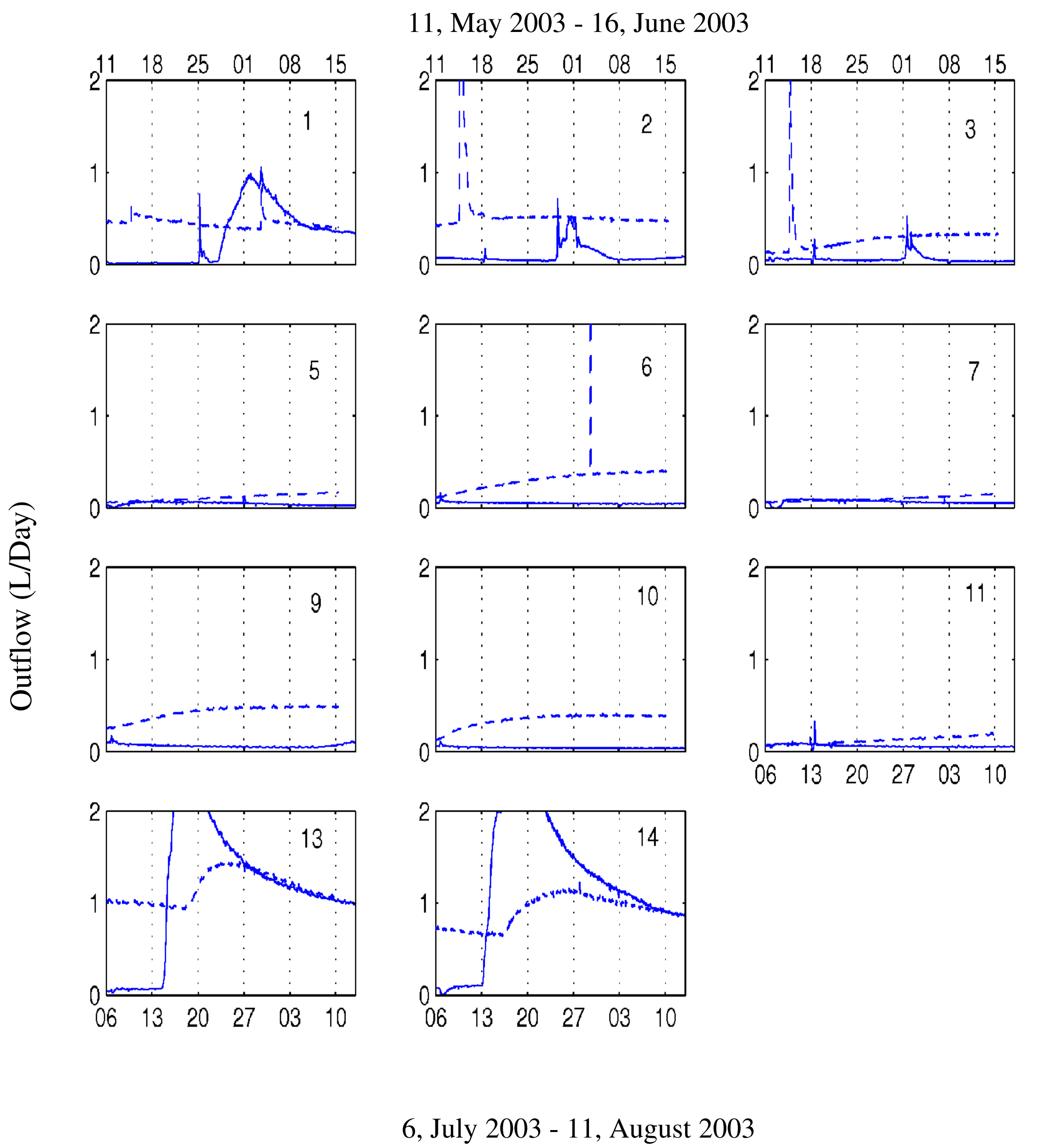

Figure 3.10. Two outflow hydrograph sets following an artificial and a natural rainfall event on the covered surface for each of the 11 lysimeters following an artificial high intensity events with fairly constant precipitation rates. The solid lines depict the 30 day hydrographs following the May 13th event and the dashed lines, 30 day hydrographs following the July 9th rainfall event.

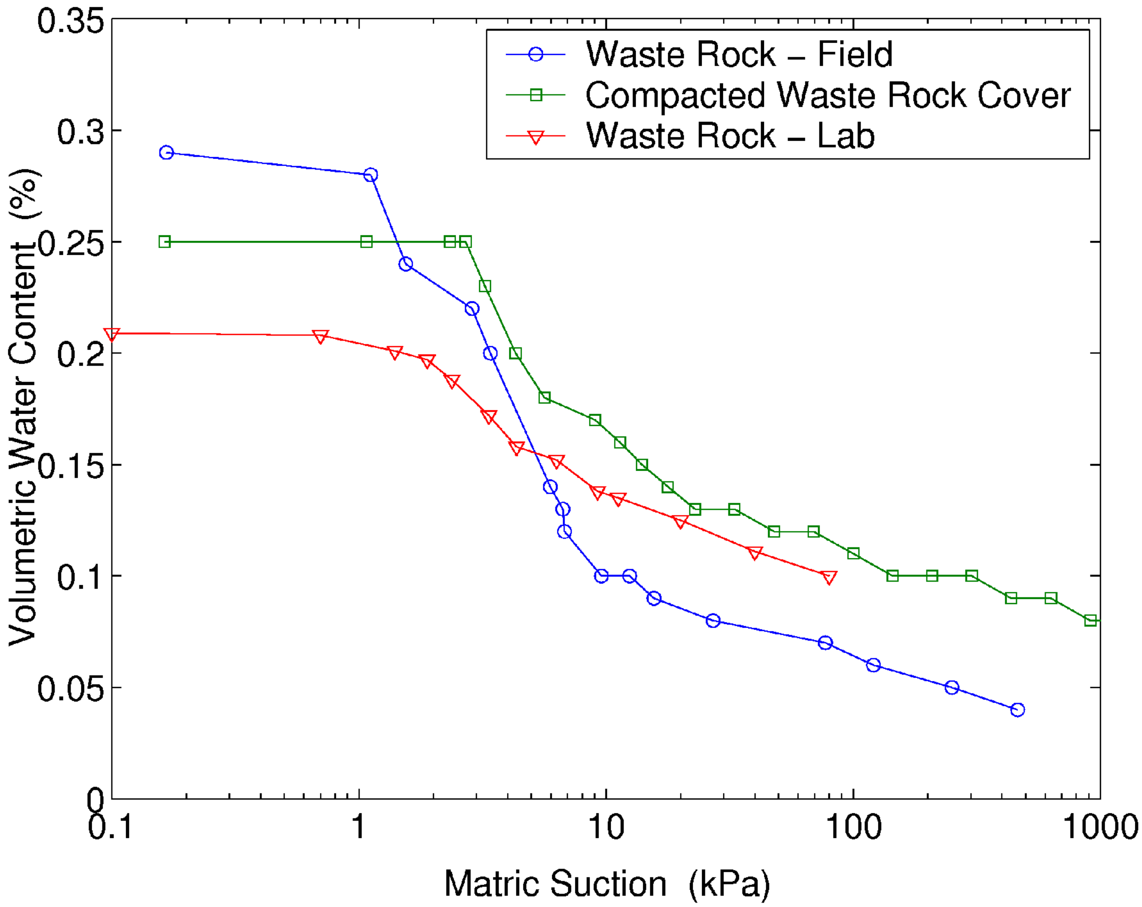

Figure 3.11. Soil water characteristic curves (SWCC) for the waste rock and cover material. The blue curve (◯) is a SWCC for the waste rock based on field data. The matric suction values were determined indirectly using the filter paper method and the volumetric water content measurements were obtained from direct, in-situ measurements. The red curve (∇) is a SWCC for the waste rock based on laboratory data using a Tempe cell. The green curve (□) is an estimated SWCC for the waste rock cover based on the grain size distribution and volume mass properties as calculated by the Fredlund and Xing (1994) equation.

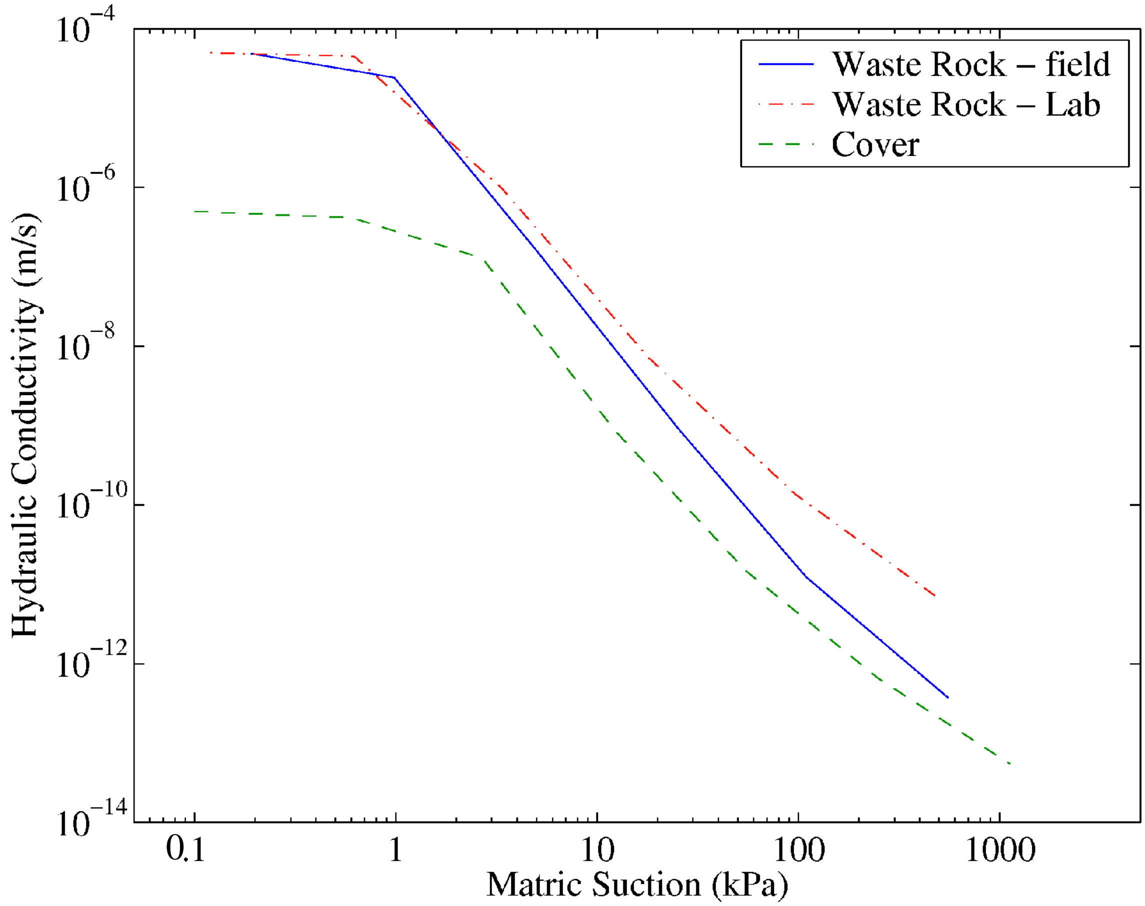

Figure 3.12. Hydraulic conductivity curves for the waste rock and cover material. The blue curve (solid) is the HCC for the waste rock based on field SWCC. The red curve (dashed) is the HCC for the waste rock based on laboratory SWCC. The green curve (dash-dot) is the HCC for the waste rock cover. All three curves are estimated using the Fredlund et al (1994a) equation.

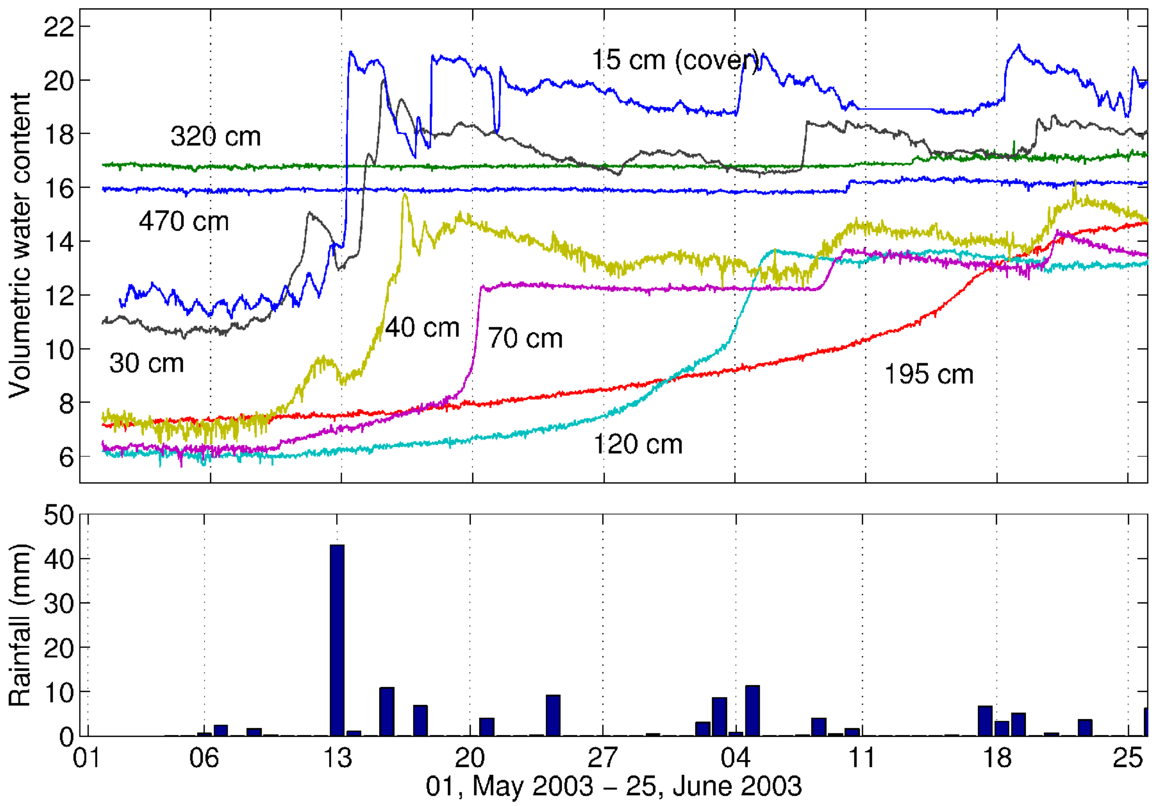

Figure 3.13. The volumetric water content as measured by TDR probes at 8 different depths within the waste rock pile between May 01, 2003 and June 25, 2003. The data are an average from the probes at the same depth in all three profiles. The sub-plot shows the rainfall record for the same period.

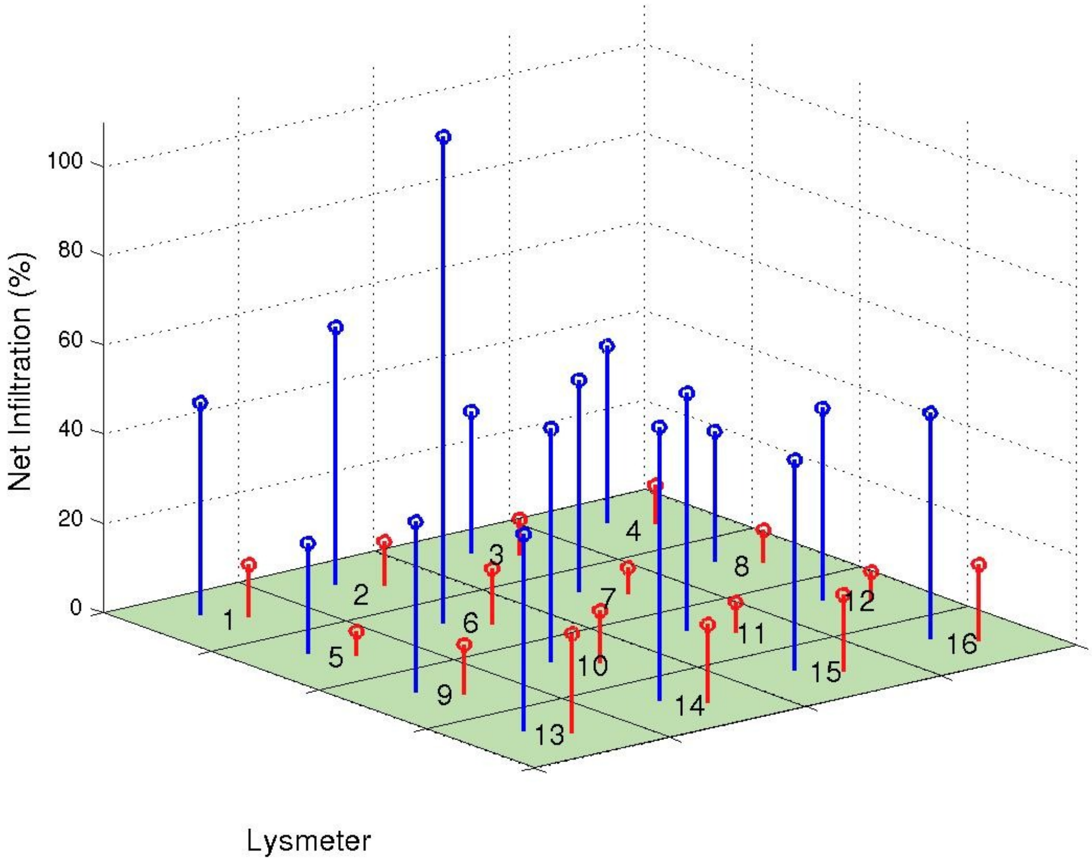

Figure 3.14. Cumulative outflow from each of the 16 lysimeters in percent relative to precipitation for the period between April 2001 and April 2002 on the uncovered waste rock in blue and the period between April 2003 and April 2004 on the covered waste rock in red.

CHAPTER 4: WATER MIGRATION IN COVERED WASTE ROCK: A DEUTERIUM TRACER STUDY

4.1. INTRODUCTION

The evaluation of the potential for acid rock drainage (ARD) and ground water contamination from mine waste rock piles is an issue at many hard rock mines worldwide (Lapakko, 2002, Batterham, 2003, Coeppicus et al, 2003). Measurement of the volume and chemistry of basal outflow from large waste rock piles is at best difficult and often not possible, which necessitates the use of some type of predictive tool as an evaluation method. In addition to mineralogical and geochemical information about the waste rock and the net-infiltration of water into the pile, information on the mechanisms that control where the water resides and flows inside the pile is important for prediction. The chemical processes related to ARD have been examined in numerous studies (eg. Alpers and Nordstrom, 1999, Jambor and Blowes, 1998, Hammarstrom and Smith, 2002), but there are fewer studies on the flow processes that control the degree of water-rock interactions and influence the amount and timing of solute transport (Bezuidenhout, 2002, Smith and Beckie, 2003, Nichol et al, 2003, Stockwell et al, 2003, Molson et al, 2005).

The character of the water-rock interactions will depend in part on the internal structure of the waste rock pile, which reflects the approach used to construct the

---

A version of this chapter will be submitted for publication. Marcoline, J.R., Water migration in covered waste rock.

pile. Two common methods of constructing waste rock piles are end-dumping and free-dumping; both result in piles with different internal structures. End-dumped piles often have an internal structure characterized by steeply inclined layers, situated between horizontal traffic surfaces. End-dumped piles have been referred to as structured, segregated or layered as a result of the fining upward textural segregation that occurs when the granular material is dumped over the tip face of the waste rock pile (Smith et al, 1995, Herasymuik, 1996, Fines, 2006). Free-dumped waste rock piles are constructed by truck dumping on a horizontal traffic surface followed by grading or leveling. Free-dumped piles often have a range of internal structures, such as traffic surfaces and localized layering as a result of the construction method and material properties, but often lack the segregation and sloped layering found in end-dumped piles. Some piles are composites of both types of construction.

Water flow in both uncovered and covered, end-dumped waste rock piles has been studied in the field and preferential flow has been modeled within the steeply inclined layers (Herasymuik, 1996, Fala et al, 2003, Fines, 2003, Tran et al, 2003). In contrast, preferential flow and the effect of cover systems on fluid flow and transport within heterogeneous, free-dumped waste rock are poorly understood (Smith et al, 1995). Since all waste rock piles are heterogeneous and many will ultimately be covered, a better understanding of waste rock hydrogeology in such a scenario is valuable for the prediction and minimization of acid rock drainage.

Soil covers are a common strategy to reduce infiltration into waste rock and thereby reduce long-term acidic drainage and metal loading to the receiving environment. Soil covers can be designed to: 1) slow down internal weathering reactions, and 2) limit the flushing of solubilized weathering products from a stockpile. Detailed discussions on the design and effectiveness of soil covers are available (U.S. EPA, 1994, Albright et al, 2002, Milczarek et al, 2003, O'Kane and Waters, 2003, MEND, 2004), however, information about the systematics of the water flow and of the transport of weathering products through covered waste rock is limited. Such information should lead to better ARD predictive methods and refined source control strategies.

4.2. HYPOTHESES

This paper describes the use of the stable isotope deuterium tracer to characterize infiltration into and the flow dynamics within a covered waste rock pile. The specific hypotheses are:

- That the addition of a lower-permeability surface cover would result in a significant reduction of distinctive preferential flow paths by limiting the flow to the finer grained matrix materials.
- That the surface cover would reduce the spatial variability of surface infiltration.
- That the lower-permeability surface cover would result in a more uniform flushing of weathering products from the pile.

- That a deuterium tracer would allow for the investigation of the depth and spatial distribution of infiltration into and water movement through the covered waste rock pile.

4.3. BACKGROUND

4.3.1. Preferential Flow In Unsaturated Media

Preferential flow in unsaturated media occurs as localized water flow at a rate much faster than the average pore water velocity. Preferential flow in unsaturated media can result either from the presence of large interconnected voids, at the transition from fine to coarse-textured soils, or from flow fingering at wetting fronts. Preferential flow paths are often characterized as a system of large, interconnected voids, rubble zones or large pore spaces (Beven and Germann, 1982, Morin et al, 1991, Flury et al, 1994, Newman, 1999, Li, 2000, Bellehumeur, 2001). The link between preferential flow paths and permeability variations or soil heterogeneity has been observed experimentally (Eriksson et al, 1997, Fines et al, 2003, Nichol, 2003) and examined numerically (Trapp et al, 1995, Birkholzer and Tsang, 1997, Eriksson and Destouni, 1997, Fala et al, 2003).

Heterogeneities within the soil matrix have also been shown to significantly affect flow and solute transport in unsaturated material and create preferential flow (Buczko et al, 2001, Hangen et al, 2004). For example, Parlange and Hill (1976) and Baker and Hillel (1990) documented small-scale preferential flow resulting from water flowing across a transition from fine to coarse-texture materials.

Preferential flow is also observed in materials that are devoid of obvious structural or physical heterogeneity (Parlange and Hill, 1976, Jury et al, 2003, Ghodrati and Jury, 1992, Wang and Jury, 2003, Cho et al, 2005). Preferential flow that is not directly related to material properties or texture can occur at the redistribution wetting front as the hydraulic gradient reverses following an infiltration event into a drier medium (Diment and Watson, 1985, Wang and Jury, 2003). The redistribution wetting front refers to the interface between initially dry material and the propagating soil water introduced during infiltration. Redistribution will continue until the water content in the soil is uniform. Wang et al (2004) and Jury et al (2003) suggest that all soils are likely to experience such preferential flow, or flow fingers. Wang et al (2003) observed flow fingers with a mean width of 0.13 m in coarse-textured, nonstructured soils and that the flow paths reappeared in the same location during subsequent infiltration events.

Coarse waste rock often has a low air-entry value and will rapidly drain far below the saturated water content after a dry period following an infiltration event. The air-entry value is the matric suction at which air first enters the largest pores during drying (Brooks and Corey, 1964, 1966), and the water-entry value is the matric suction at which the water content of the soil starts to increase significantly during wetting. The volumetric water content of coarse waste rock remains close to saturation on the soil water characteristic curve (SWCC) between 0 KPa and the air-entry value. Additionally, the difference in potential (matric suction) between the air-entry value and the water-entry value of the waste rock is often relatively small, which is favorable for the initiation of unstable flow fingers (Wang et al, 2004). The majority of water that infiltrates through a cover is likely to be contained within the finer matrix material and experience a gradient reversal due to evaporation after the rainfall event ceases. Even with relatively high matric suctions, mechanisms for preferential flow must exist (Pruess, 1999). Based on the work of Jury et al (2003) and Wang et al (2004) at the equivalence point between the downward gradient due to gravity and the upward gradient due to evaporation (capillarity), lateral redistribution of water into a finger will occur and gravity-driven preferential flow can be initiated.

4.3.2. Chemical Tracers Used in Waste Rock Studies

Tracers have been used to investigate flow and transport processes in uncovered mine waste rock. Murr (1979) and Nichol (2003) used chloride as a tracer, Eriksson et al (1997) used bromide, Bellehumeur (2001) used dye staining, and Hangen et al (2004) used bromide, terbuthylazine, and deuterium. Other than Guebert and Gardner (2001), who used a fluorescent dye, few tracer studies have been conducted on covered mine material.

Nichol (2003) described flow and transport of a chloride tracer through the same experimental waste rock pile that is discussed in this paper. On this basis, Nichol (2003) concluded that multiple flow paths (i.e. fast preferential flow paths, slower preferential flow paths and capillary-driven matrix flow paths) exist even within an area as small as 2 m by 2 m.

The choice of a tracer for this research was constrained by cost and by the ability to detect the tracer in high conductivity, low pH pore water within the CPE. Chloride was still present in the CPE from a tracer release in 1999 and deuterium was chosen as a tracer based on a low detection limit, a lack of chemical interference with other solutes in the pore water, and a low analysis cost. Bromide was also applied to the covered waste rock pile in 2003, however, it was not possible to accurately measure bromide in pore water extracted following the deconstruction of the pile. High sulfate concentrations (400-40,000 ppm) in pore water masked bromide in ion chromatography analyses and sample volumes were too small for colorimetric analysis.

4.3.3. Stable Isotopes as Tracers in Unsaturated Media

The oxygen and hydrogen isotopes of water can be effective tracers of water flow paths in unsaturated materials (eg. Newman et al, 1997, Singleton et al, 2003, USGS, 2003, DePaolo et al, 2004). Precise measurements of the stable isotopes of water are difficult and necessitate the measurement of the relative isotopic difference (δ) between the sample and a reference standard. The δ value is expressed as per mil (‰) and defined by:

$$\delta = [(Ratio_{(sample)} - Ratio_{(standard)}) / Ratio_{(standard)}] \times 10^3$$

where the standard is standard mean ocean water (SMOW) from Craig (1961) and the ratios are $^{18}O/^{16}O$ and $^{2}H/^{1}H$ for $\delta^{18}O$ and $\delta^{2}H$ (deuterium), respectively.

The main processes that dictate the oxygen and hydrogen isotopic compositions of water are the initial composition of the rainfall, mixing with other waters (pore water and subsequent rainfall), and fractionation. Mixing of water labeled by deuterium with either pore water already present in the porous medium, or meteoric water that infiltrates after the tracer release, will have an effect of diluting the ^{2}H in the tracer water. Fractionation is the disproportionate removal of the lighter isotopes of water into the gas phase, resulting in higher relative values of the heavier to lighter isotopes in the water phase.

Fractionation can result from phase changes such as evaporation, condensation and melting or from diffusion and water-rock interactions. In the CPE, water with a high deuterium value was applied as the water tracer. Following the tracer release, deuterium values in the pore water that are higher (heavier, enriched or more positive) than background may result from mixing with the applied deuterium tracer, by fractionation of pre-tracer water, or both (Figure 4.1). The enrichment resulting from phase changes can be an equilibrium effect which is strongly dependent on temperature, or a kinetic effect, which is strongly dependent on relative humidity (Gat, 1996). In unsaturated material, kinetic fractionation (diffusion controlled fractionation) is the dominant mechanism. Kinetic fractionation is caused by different diffusion rates of the heavy and light isotopes of water vapor in the layer of air immediately adjacent to the water surface. It is referred to as evaporative fractionation for the remainder of this chapter. Evaporative fractionation occurs with the disproportionate removal of the lighter isotopes (^{16}O and ^{1}H) resulting in enrichment of the $\delta^{18}O$ and δD isotope ratios in the water (more positive δ value).

The global meteoric water line (GMWL) is defined by $\delta^{18}O$ and δD values of global precipitation and is approximated by $\delta D = 8 * \delta^{18}O + 10$ (Craig, 1961). Equilibrium fractionation will result in a line offset to the right, but parallel to the GMWL (Figure 4.2), while kinetic fractionation will result in a line with a lower slope than the GMWL, as shown in Figure 4.1. The local water line, described in Section 4.5, is defined by background pore water values from within the CPE. If vapor that is concentrated in ^{16}O and ^{1}H migrates and condenses following evaporative fractionation, the δ value of the water will become more positive, as shown in Figure 4.1 (Sofer and Gat, 1975, Gonfiantini, 1986).

While oxygen and hydrogen isotopes of water can be effective tracers of water flow paths in unsaturated materials, fractionation effects must be considered when interpreting the tracer test results on the CPE.

4.4. METHODS AND EXPERIMENTAL DESIGN

4.4.1. Constructed Waste Rock Pile Experiment

The instrumented footprint of the constructed pile experiment (CPE) was 8 m by 8 m in plan and 5 meter-high. The test pile was built in 1998 upon a grid of sixteen contiguous lysimeters, each 2 m by 2 m in area. The design established a water table at the base of the CPE to allow for free drainage of the system. For the first 4 years, the waste rock was uncovered. Outflow at the base of the pile was recorded on a continuous basis. In the fall of 2002, a lower permeability surface layer was constructed on the CPE. In the spring of 2004, the waste rock pile was deconstructed, and samples were collected for particle size characterization and pore water extraction.

4.4.2. Lower Permeability Surface Layer

A compacted waste rock layer (cover) was placed on the top surface of the waste rock pile in September 2002. Compacted layers are often used as one component of a soil cover system, and are rarely used as a stand alone surface layer. The intent of the cover construction on the CPE was to reduce the infiltration through the surface and to study and observe the change in hydrology, and not to construct a robust cover system of the type used in mine closure. The surface layer was constructed with waste rock taken from the CPE outside of the lysimeter grid. Approximately 23 m^3 of waste rock was sieved through a minus 0.1 m screen and then hand shoveled onto the top surface.

Standard Proctor laboratory compaction tests following ASTM method D689 (ASTM, 1991) were conducted on the minus 20 mm fraction of the sieved waste rock to determine the relationship between dry density and water content. Water content and dry density were corrected to account for the 21 mm to 100 mm particles following ASTM method 4718 (ASTM, 1994). The corrected maximum dry density for the cover material was determined to be 2280 kg/m^3 at an optimum water content of 7.0%. Based on two samples collected just prior to compaction, the cover was placed at an average water content of 6.9%.

Compaction was carried out in one lift and three passes with a rammer compactor delivering approximately 3100 pounds per blow over a 34 cm by 36 cm pad. The covered surface was smooth and flat and resembled a haul truck traffic or "pavement" surface. Based on double ring infiltrometer tests, field saturated hydraulic conductivity of the compacted layer was estimated to be ~ 5 x 10 $^{-7}$ m/s.

Six measurements of moisture content and density were made on the compacted waste rock surface using a Troxler model 3411 nuclear densometer gauge with a probe depth of 0.15 m. Average field density and moisture content for the compacted surface were 2114±47 kg/m^3 and 6.1%, respectively. In addition, three samples from the compacted layer were collected for laboratory moisture testing. The moisture contents measured on the laboratory samples were 6.0%, 7.1% and 5.8%. Compaction at optimum or slightly dry of optimum reduces the potential for desiccation defects in the compacted surface layer and ultimately result in a layer that is more effective in reducing infiltration of water (Coons et al, 2000, Dwyer, 1997, 1999). Immediately following cover construction, two test pits through the compacted layer were logged to visually inspect the degree and depth of compaction. Compaction appeared homogeneous to a depth of approximately 0.12

m with a slightly lesser degree of compaction between 0.12 m and 0.15 m.

4.4.3. Tracer Application

The deuterium tracer was applied to the surface of the waste rock pile in a 49 mm artificial rainfall event over a 6.5-hour period on May 13, 2003 (~7.5 mm/hr). The applied water had a deuterium value (δD) of +213 per mil and a $\delta^{18}O$ value of -15.47 per mil. The rainfall rate was measured as water reaching the top surface of the CPE. Approximately 12% of the rainfall was recorded as runoff, resulting in an estimated surface infiltration of 43 mm. Based on subsequent evaporative flux modeling, as much as 4 mm of the applied rainfall may have evaporated during the day of May 13th. Throughout this paper, water that infiltrated during the test is referred to as “tracer water”, pore water in the CPE prior to the test is “pre-tracer water” and water infiltrating after the tracer release is referred to as “fresh water”.

4.4.4. Monitoring

The CPE was only monitored for one year until the experiment was terminated when the large waste rock pile beneath the constructed pile was relocated to an adjacent open pit. For the year following tracer application, water samples were collected from the 16 basal lysimeters on a weekly basis. During July and August of 2003, pore water samples were extracted using soil water solution samplers along three vertical profiles from 1.75 m, 3 m and 4.5 m below the cover. Based on pre-cover transport times of the Cl tracer, and on the very slow post-cover flow rate within the CPE, intensive monitoring for isotopes in the basal lysimeters was not undertaken. A suite of basal lysimeter samples from September 2003 and February 2004 and two samples from May 2004 were analyzed for their isotopic composition to identify if any tracer water migrated five meters to the basal lysimeters. The results were within the range of the pre-event baseline samples for both δD and $\delta^{18}O$, suggesting that no tracer reached the base. While only two outflow samples were analyzed just prior to deconstruction, little outflow (less than 150 liters) occurred between the February 2004 sampling and the waste rock pile deconstruction.

4.4.5. Deconstruction and Sampling of the Waste Rock Pile

The waste rock pile was deconstructed between May 17th and June 21st of 2004 in a series of five lifts. The first lift was 0.4 m deep. Twenty four pits were excavated from the cover. Samples of waste rock were collected from 8 of the 24 sample pits at 0.05 m increments through the cover. The physical properties of the compacted surface layer were re-evaluated during the deconstruction of the first lift. Based on visual inspection of the 24 pits, compaction appeared homogeneous to a depth of approximately 0.20 m. Sixteen samples were collected for volumetric water content and density from 0.25 m deep test pits. The average density was 1984±140 kg/m^3, 130 kg/m^3 lower than the average density of 2114±47 kg/m^3 measured in 2002. It is unclear whether the lower density measured in 2004 was related to averaging over a sample depth of 0.25 m as compared to 0.15 m in 2002, to measurement methods, or to actual changes in density of the cover. After the first winter, there were no observable defects or dessication cracks in the compacted surface. Following the second winter, a few hairline cracks were observed in the upper surface (less than 0.05 m in length) but they did not appear to extend into the layer. Double ring infiltrometer tests on the cover surface were not repeated prior to deconstruction so not to locally introduce water into the CPE.

The remaining 5 m of the waste rock pile was excavated in four lifts, each using three parallel 8 m by 1 m by 1.5 m (LxWxD) trenches across the core of the waste rock pile. One trench per day was cut across the full length of the waste rock pile along a surveyed grid for a total of 16 trenches (Figure 4.3). The location of trenches allowed for a cross sectional view of waste rock above each of the 16 lysimeters (Figure 4.4). The trenching methodology allowed for a dense sampling of each cut trench face immediately following excavation following the methodology outlined by Stockwell et al, (2006). Waste rock was sampled and the trench face mapped beneath an insulated tarp to minimize drying by evaporation from the fresh waste rock. Waste rock samples were collected at 0.10 m vertical increments from the trench walls along vertical profiles separated by 0.5 m. Each sample was collected by hand excavating an area approximately 0.15 m by 0.15 m wide by 0.10 m high from the trench faces. Waste rock samples were sealed in bags filled with nitrogen and transported to the University of British Columbia.

4.4.6. Data Collection and Sample Processing

Rainfall, runoff and lysimeter outflow were continuously monitored using an array of 20 tipping bucket rain gages. Volumetric water content was estimated using 28 time domain reflectrometry (TDR) probes programmed to collect data every 28 minutes. TDR probes were buried in four locations within the cover and along three vertical profiles with probes at depths of 0.15, 0.2, 0.3, 0.4, 0.7, 1.2, 1.95, 3.2, and 4.7 m in each profile.

Pore water was extracted from 174 waste rock samples obtained during deconstruction using an IEC Model K centrifuge operating at 2100 rpm. Approximately 800 g of waste rock was spun until sufficient water for analysis was obtained. Centrifuge spin times varied depending on the moisture content of the sample. All spins were less than 30 minutes and yielded a typical volume of 1.5 ml. Stable isotopes $\delta^{18}O$ and δD were determined at the New Mexico Tech Stable Isotope Laboratory and at the University of British Columbia Stable Isotope Laboratory. The hydrogen and oxygen isotopes are reported in delta (δ) notation, as per mil (‰) differences relative to the Vienna-Standard Mean Ocean Water (V-SMOW) international, and listed in Appendix C. Based on duplicate results, the analytical precision was (+/-) 0.6 ‰ for δD and as much as 0.3 ‰ for the very small (0.05 ml to 0.15 ml) $\delta^{18}O$ samples based on laboratory standards.

4.5. ISOTOPIC BASELINE

Values of local precipitation often have a slightly different slope and intercept than the GMWL, as a result of factors such as the degree of evaporation, local climate, humidity, distance from the ocean, latitude and altitude (Allison, 1982, Gat, 1996, Clark and Fritz, 1997). As a result of local variations, regional or local meteoric water lines (LMWL) are often developed to establish a site-specific isotopic baseline for ground water studies. Cluff Lake is located in an area without significant topography, at 58 degrees latitude in the center of the continent. Data to create a LMWL based on seasonal variations in precipitation are not available. To establish background isotope values for the study, the $\delta^{18}O$ and δD values of pre-tracer pore water samples were collected at a depth between 0 and 4.5 m within the experimental pile and from an artificial precipitation event. These pore water samples were collected over a period of two years using SoilMoisture soil water solution samplers. The measured $\delta^{18}O$ values for pore water and artificial precipitation (water from Cluff Lake) are within the range of values predicted for the geographic area by Bowen and Wilkinson (2002). The $\delta^{18}O$ pore water values are plotted against their δD values (Figures 4.2 and 4.5) and define an average pre-tracer isotope value with depth in the experimental waste rock pile. This line is defined by $\delta D = 6.9 * \delta^{18}O - 19$ and is referred to as the Cluff Lake pore water line (CPWL). The CPWL is used as a baseline for comparison of all samples collected following the tracer application. The CPWL was derived from samples collected at different depths within the CPE over a relatively short time and thus differs from a local meteoric water line that is typically derived from isotopic values of precipitation measured over a period of time. Evaporation effects are potentially incorporated within the CPWL.

The CPWL has a slope of 6.9, suggesting that some kinetic fractionation, as well as equilibrium fractionation relative to the GMWL has occurred. The entire CPWL is shifted to the right of the GMWL and is similar to evaporative lines observed in other unsaturated materials (Dincer, 1974). As discussed in Section 4.4, the degree of the shift is related to the relationship between the local rate of isotopic enrichment from equilibrium fractionation and dilution by rainfall (Barnes and Allison, 1982, Allison et al, 1983).

Based on the slope and location of the CPWL relative to the GMWL, the CPWL serves as a LMWL for the tracer experiments by identifying a background profile in the CPE. The background level of δD ranged from -133 ‰ to as high as -121 ‰, depending on depth (Figure 4.6), and $\delta^{18}O$ background values range between -16.2 ‰ and -15.0 ‰ (Figure 4.7). While any δD values larger than -121 ‰ observed after the tracer application likely contain water from the tracer application, it is possible such values are a result of further fractionation of the pore water.

4.6. RESULTS AND DISCUSSION

4.6.1. Basal Outflow and Tracer Recovery

Winter drain down in the CPE began approximately one month earlier following the construction of the lower permeability cover than in the previous years. The water flux from the sixteen basal lysimeters immediately prior to tracer application in May of 2003 varied from 2.7 to 4.5×10^{-10} m/s, slightly above the seasonal minimum. This flux rate is equivalent to a basal outflow rate of 1.5 to 2.3 L/d from the 8 m by 8 m core of the waste rock pile. The basal flux at the time of deconstruction was slightly lower, approximately 0.5 to 1.0 liter per day and the average volumetric water content of the waste rock derived from field samples was 8±2%. The basal outflow rate was fairly constant in the months prior to deconstruction and the outflow is assumed to be drainage water from the lowest 2 m of the CPE. This assumption is based on 1) the temperature data showing that the upper portion (between 0 and 1.5 m) of waste rock was frozen, and 2) the TDR data from January to April of 2004 shows a relatively constant volumetric water content in the mid-portion of the pile and a gradually decreasing water content at the 3.15 and 4.65 m depths. Between the time of the tracer application and deconstruction, a maximum volumetric flow of 14.6 L/day was observed. Three large (greater than 20 mm) rainfall events, two artificial and one natural, occurred in May, June, and August 2003 before pile deconstruction in May 2004. Since no deuterium above background was measured in the basal lysimeters, and since the basal lysimeters sample a composite of all water exiting the waste rock pile, it is clear that water from the tracer application did not infiltrate to a depth of 5 m during the year following the tracer application. While water labeled with the tracer was not detected in the lysimeter outflow, an increase in basal flow was observed in response to infiltration following the large rainfall events in May, July, and August 2003.

4.6.2. Internal Water Flow

The deuterium tagged rainfall event applied on May 13, 2003 was large for the season. The rainfall event was applied at a below average rate to ensure that the tracer water infiltrated into the low permeability waste rock surface, yet, a small amount of ponding was observed in a few localized areas. A response in outflow associated with the rainfall event was observed in 5 of the 16 lysimeters after approximately six days. The response was marked by a gradual (2 L/d) increase in combined lysimeter flow rate that lasted four days and peaked on May 23rd, 10 days after the rainfall event (Figure 4.8). The outflow response for the two other large rainfall events was characterized by a similar maximum flow rate, however, the response was slower and not as sharp. The timing and shape of the hydrograph responses were primarily associated with the amount of infiltration and with surface ponding. Distinctive responses in outflow were not observed for smaller (less than 20 mm) natural rainfall events.

In addition to basal outflow, water content was monitored along three vertical profiles using TDR probes following each of the rainfall events. Water content data were used to derive estimates of wetting front arrival times, to determine variability in wetting front progressions and to compare with outflow data.

Distinctive wetting fronts within the pile are evident in TDR data collected along the three vertical instrument profiles A, B, and C located as shown in Figure 4.3. Only profile C was located below a region with surface ponding and δD values above background were not observed in any of the soil water solution samplers, including those from within profile C. Figure 4.9.a shows TDR data from probes located in each profile at 0.70 m and 1.20 m within the pile for a period of 45 days following the tracer application, and Figure 4.9.b shows the wetting front profiles within and below the cover during and immediately following the tracer release. While there is variability in the wetting front arrival times within each profile, there is no clear evidence in the TDR or tracer data that wetting fronts progressed faster or deeper in profile C, over which ponding was observed, than in profiles A and B where ponding was not observed.

4.6.3. Deuterium Distribution of Pore Water

The δD values from 175 pore water extracts obtained from the deconstruction samples range from as heavy as -63 per mil (‰) to background levels of approximately -132 ‰ (Figure 4.6). The vertical and horizontal spatial distributions of pore water δD values in the waste rock pile are highly variable. In the region in which above-background tracer values are observed in pore water, there is no clear trend in δD values with depth from the 8 m by 8 m CPE and there is no correlation between depth and horizontal location. On the scale (0.15 m by 0.15 m) of the deconstruction samples, tracer values are observed to increase with depth in some areas and decrease with depth in other areas (Marcoline et al, 2006) and is discussed below. While multiple factors can affect the stable isotope concentrations, fractionation and mixing are most important (Figure 4.1).

The relative degree of fractionation caused by diffusive and evaporative effects cannot be distinguished. However, a distinction between the effects of fractionation and mixing can be made using oxygen isotopes, since the initial oxygen isotopic composition of the applied tracer was similar to that of the background pore water. Variations in the oxygen isotopic composition in the pore water samples reflect the combination of fractionation due to phase changes and to a greater degree kinetic effects. Any δD value in a sample beyond that which can be explained by fractionation or condensation must therefore come from the applied tracer. The meteoric water lines and the Cluff pore water line are used to establish the degree of fractionation and condensation following procedures of stable isotope fractionation of pore water in unsaturated soils established by Allison (1983), Barnes and Allison (1983 and 1984), and Allison and Barnes (1985 and 1990).

The lowest baseline δD value was -132 ‰ and the highest value measured from pre-tracer pore water was -120 ‰. The variability in δD values of baseline pore water samples is a result of seasonal variations in the δD value of the local rainfall and an undetermined amount of evaporative fractionation within the CPE. Assuming a simple model in which the pre-tracer pore water was within the range of the measured baseline values (the CPWL), and that evaporative fractionation results in shifting isotopic values parallel to the evaporative fractionation line (Figure 4.4); evaporative fractionation could account for δD values as high as -110 ‰. Therefore samples that have elevated $\delta^{18}O$ values, and δD values between -120 ‰ and -110 ‰

can be accounted for simply by fractionation. Several samples with higher δD values also had higher δ^{18}O values. Based on these results, it could be that either: 1) greater evaporative fractionation has occurred following cover placement, 2) greater diffusive fractionation has occurred following cover placement or 3) all samples with δD values greater than -110 ‰ contain water from the tracer event or re-distributed condensate water. Most likely, the observed post-cover δD values greater than -110 ‰ reflect a combination of these three factors. Samples that have elevated δD values and δ^{18}O values near their baseline plot along the 'mixing line' shown in Figure 4.1. It is clear that these samples contained both pre-tracer and tracer water and that little fractionation occurred. Samples that plot in this area above the baseline (CPWL) and below the applied tracer value are in the 'mixing zone' (Figure 4.1). Samples that have elevated δD values, greater than -110 ‰, and elevated δ^{18}O values, plot to the right of the mixing line have a component of the tracer, and have experienced fractionation.

Based on the distribution of δD and δ^{18}O values, it appears that more fractionation occurred in the post-cover samples relative to the pre-cover samples. The increased fractionation could be a result of a larger water residence times in the cover and evaporation. In addition, the increase in fractionantion is consistent with the idea that fractionation will increase with lower water content and is likely related to a larger diffusive component of fractionation. Craig and Gordon (1965) developed a model for the evaporative enrichment of δD and δ^{18}O from a free water surface. Their model explains the enrichment using primarily an equilibrium effect driven by a phase change and secondly, a kinetic effect caused by different diffusion rates of the heavy and light isotopes of water vapor in a layer of air immediately above the water surface. While the equilibrium effects dominate fractionation from a free water surface, Alison (1982) demonstrated that the kinetic effect is more pronounced in the unsaturated zone, and potentially more important than the equilibrium effect. The greater importance of the kinetic effect in the unsaturated zone is a result of a significantly increased layer thickness through which the water vapor must diffuse. The relationship between the degree of kinetic fractionation and volumetric water content in the unsaturated zone is two-fold. First, with a decreased volumetric water content, the pore water/air interface is increased, and the effective area for diffusive fractionation is increased. Second, by the definition of fractionation given above, the lower the volume of water is, the higher the relative isotopic shift in the water phase will be for the same amount of evaporation.

The isotopic ratios of pore water samples collected in the top one meter of waste rock below the cover are highly variable and difficult to interpret (Figure 4.6. and 4.7.). These pore water samples contain a mixture of pre-tracer water, tracer water and fresh (post-tracer infiltration) water. The samples in the top meter also show a range in the degree of evaporative fractionation from sample to sample. The near-surface samples that have high δD values and high $\delta^{18}O$ values are believed to consist primarily of pre-tracer water that have experienced significant fractionation. Samples that have high δD values and have near background $\delta^{18}O$ values consist of non-fractionated tracer water. In contrast, a few near-surface samples have isotopic ratios that plot along the near-surface CPWL and are characteristic of more recent rain water with little subsequent fractionation. At these locations, the amount of fresh water gradually decreases, and the amount of tracer water increases with depth along the vertical sample profiles. Based on the variability of this relationship evident in these data, it appears that the infiltration of fresh water in the time period between the tracer application and the deconstruction was highly localized. As a result of the spatial complexity of the data in the top meter of waste rock, only general conclusions can be drawn based on the samples in this depth range. First, it appears that some water infiltrated through the cover to a depth of up to 1 m during the rainfall event that contained the tracer, and that fresh water infiltrated to the same depth during the two rainfall events following tracer application. These pathways were highly localized. Second, as observed in the elevated $\delta^{18}O$ values (Figure 4.7), it appears that the majority of the evaporation occurred to a depth of approximately one meter below the cover and that the degree of evaporation within the top meter of the waste rock pile was spatially variable. The one meter depth of evaporation is similar to that observed in isotope data from the Hanford site in Washington State (Singleton et al, 2004).

The pore water samples collected below a depth of one meter show a localized and lesser degree of evaporative fractionation. Based on the observed δD distribution, it is clear that little to no tracer migrated to a depth of greater than three meters. A few samples deeper than three meters (4 out of 174) have δD values between -120 ‰ and -115 ‰. As discussed above, while fractionation can theoretically account for values as high as -110 ‰, these four samples appear to have undergone little to no fractionation based on the near background $\delta^{18}O$ values. The samples suggest that a small quantity of tracer water migrated as deep as 4.0 m in the waste rock pile in a few isolated locations, and in small quantities.

4.6.4. Condensation and Convection

Convection and condensation of fractionated water vapor is another process that has a potential influence on the isotopic distributions in the waste rock pile (Sracek et al, 2004). The density difference between cold dry air and warm wet air can result in air convection with warm air rising and cold air sinking toward the bottom of the convection cell. Convection of the air and isotopically light water vapor followed by the condensation of water vapor within the CPE could lead to values of $\delta^{18}O$ higher than background in the deeper portion of the pile and lower values between 1.5 m and 2.0 m in the pile. With a lower relative humidity, kinetic fractionation and equilibrium fractionation can occur at depth in the waste rock pile. It is possible that thermal convection occurred for up to one half of the calender year in the covered waste rock pile. While numerous waste rock piles have a reaction (ie. sulphide oxidation) driven thermal gradient from the interior to the surface (Lu and

Zhuang, 1997), the proposed gas convection in the CPE was driven by climatic conditions. Figure 4.10 shows the temperature profiles within the experimental waste rock pile. While not related to oxidation reactions, a steep thermal gradient existed between October 2003 and May 2004 as a result of the heat-traced basal lysimeters in the core of the experimental pile. The temperature at the base of the waste rock pile remained at appropriately 15 degrees Celsius even though ambient temperatures were below freezing. The upward gradient was larger and existed for approximately two weeks longer in the covered waste rock than in the uncovered waste rock of previous years. The larger gradient and longer duration is attributed to the addition of the compacted cover and the reduction of air flow across the compacted layer in the weeks before freezing and after thaw of the upper portions of the waste rock.

It is hypothesized that freezing of the upper layer of waste rock also reduced the amount of vapor flow moving across the surface. In the fall, it was common to have periods of below freezing temperatures during which time the shallow (0.2 m - 0.5 m) thermistors recorded sub-zero temperatures, followed by short periods of above freezing surface temperatures and small rainfall events. The rainfall infiltrated into the thawed surface but did not thaw the waste rock in or below the cover. This and any near-surface pre-freeze infiltration would be frozen in place, reducing the effective porosity for air-flow. The depth of the freeze layer increased as the winter progressed and the region in which air convection may occur decreased. If the heat across the CPE was dissipated via conduction, the redistribution of the water vapor would be minimal compared to the amount of redistribution that would occur if the heat transfer was dominated by convection. Whether air convection will occur or not depends on the thermal gradient and is described by the dimensionless Rayleigh number. The Rayleigh number is the ratio of the viscous and buoyancy forces which are controlled by the temperature gradient across the cell and the cell geometry. The critical Rayleigh number is the number at which the forces are equal and convection begins. Lu (2001) documented the onset of convection in mine waste following the addition of a cover. He also conducted model simulations based on the field data that predicted the onset of convection in the waste rock. In comparison to the data from Lu's case study and modeling simulations, a much larger thermal gradient and a smaller cell geometry existed in the constructed waste rock pile during the winter months, both of which would lead to a higher Rayleigh number and ultimately a higher potential for a convection-driven heat dissipation system. Based on the large gradients in the Cluff Lake system, Lu suggested that a convection-dominated heat and air transfer system likely existed, and that the temperature amplitude decay and phase lag characteristic of a conduction only system was not present in the Cluff Lake data (Lu, personal communication, March, 2006).

Without non-isothermal isotopic modeling, the degree of the shift in isotopic ratios resulting from fractionation, convection and condensation cannot be determined, however, the redistribution of the fractionated water vapor by convection could account for the samples in the lower portion of the pile that plot to the right of the background $\delta^{18}O$ line, and help explain the samples that have low δD and $\delta^{18}O$ values between 1.5 m and 2.0 m in the pile (Figures 4.6 and 4.7).

4.6.5. Water Travel Times

Estimating the velocity and residence time of mobile water in a waste rock pile is important for predicting mass loading from waste rock, and is in part, the reason for investigating flow mechanisms within the CPE. Multiple independent methods for estimating water travel times exist. Water travel times within the CPE were estimated using 1) deuterium tracer data, 2) TDR wetting front data, and 3) estimated using the total flux through the pile and the average volumetric water content. As a consequence of the measurement method, the sampling scale of each of the measurements, and the degree of heterogeneity in the system, the variability in water travel time estimates derived from the tracer data and the TDR data is greater than that based on the average flux data. Each method estimates fundamentally different properties relative to the water and solute travel times. A summary of water travel time estimates is provided in Table 4.1. A discussion of each method, including the strength of each is presented below.

4.6.5.1. Water Velocities Estimated from Tracer Data

Isotopic concentrations of pore water and the sample depth beneath the cover were used to estimate an upper and a lower bound on the pore water velocity in the

CPE. Often the average pore water velocity is calculated using the elapsed time and depth to the observed tracer median concentration (Rasmussen et al, 2000). However, as a result of the limited number of samples, the uneven distribution of samples with depth, and the high spatial variability of the measured tracer maxima in each profile, the depth of the median tracer mass could not be readily identified to calculate the average velocity of the tracer. Instead, a range of pore water velocities was bracketed using the elapsed time between the tracer application and 1) the deepest occurrence of tracer (3.2 m), and 2) the center of mass of the shallowest (0.2 m) tracer maximum (defined below).

Samples 3.2 m below the surface of the cover were used to estimate an upper bound on pore water velocity. These samples were collected during deconstruction and had δD values between -109 ‰ and -92 ‰, and $\delta^{18}O$ values near background. An upper bound estimate of pore water velocity of 0.017 m/d (6.4 m/y) was calculated assuming a constant flow rate and a 183 above freezing days between the tracer application and the deconstruction. The estimate assumes that no water flow occurred in the upper portion of the pile during the winter of 2003 and that the tracer did not move beyond the frost front during the onset of freezing conditions.

The high tracer values identified 0.2 meters below the cover were used to estimate a lower-bound pore water velocity of 0.001 m/d (0.39 m/y) in the CPE. These samples had a maximum δD value of -83 ‰ with a near-background $\delta^{18}O$ values. The samples from the vertical profiles immediately below the samples with the high δD values, had δD values near-background (-121 ‰ to -118 ‰), suggesting that tracer did not migrate below 0.2 m at these locations.

A large range in pore water velocities was expected as a result of both the high degree of heterogeneity of the waste rock and because of the observed preferential flow within the waste rock. While tracer data are often used directly to estimate water travel times in unsaturated materials, it is necessary to differentiate between piston flow and preferential flow, and to differentiate between mobile and immobile water. The water velocities presented above likely reflect a combination of matrix flow and preferential flow. With matrix flow, the isotopic tracer will progress downward as a single slug of water. As a result of the variation in velocities of water within the heterogeneous CPE, mixing of the tracer with the surrounding water will occur. The redistribution of $\delta^{18}O$ and δD into the pore water adjacent to preferential flow fingers or flow paths results in water that does not participate in the flow having a tracer component. In the waste rock with a lower water content, the water contained in the immobile fraction may be significant. An under-estimate of the average pore water velocity and an over-estimate of the average residence time will result if the accrual of immobile water is discounted in the calculation. Such may be the case with the pore water velocity estimate of 0.001 m/d if the tracer sample was extracted from a zone of relatively immobile water.

Preferential flow, mixing and diffusion, and waste rock heterogeneity will result in dispersion of the tracer slug. Preferential flow, regardless of the mechanism, may result in a much larger, potentially discontinuous and highly variable degree of dispersion of the tracer slug. Rather than moving as a single slug with dispersion about the center of mass, preferential flow fingers will result in multiple smaller fingers of tracer water. For example, tracer may be transported down in a flow finger at a rate faster than the average pore water velocity. While water is flowing in a finger, it has little interaction with the material adjacent to the finger. Lateral redistribution of the tracer water into the surrounding pore network occurs deeper in the profile at the cessation of the finger flow. In other locations, the tracer water may move slowly under both capillary and gravity forces with greater lateral dispersion occurring high in the profile. Since evidence for preferential flow in the CPE exists, the maximum water velocities based on observed tracer concentrations should be interpreted as a velocity of water in the preferential flow paths, or as an upper limit for pore water velocity, but not as a representative average velocity. This characterization is further complicated in the CPE as a result of mixing of water between the fine and coarser pores with time, in response to rainfall events and subsequent drying periods. It may not be possible to determine whether the tracer observed in a particular location arrived through matrix flow or traveled through preferential flow paths, even with methods such as sequential extractions which would pull water from different pore size fractions.

The tracer experiment documents the occurrence of event-driven preferential flow within the waste rock pile following placement of a lower permeability cover.

For conditions prior to placement of the lower permeability cover, Nichol (2003) estimated an average pore water velocity through the matrix materials of approximately 1.5 m/yr. Nichol (2003) and Marcoline et al (2003) documented maximum preferential flow velocities as high as 5 m/day through the uncovered waste rock. Based on the outflow hydrographs and TDR data, little flow was observed within the waste rock following placement of the cover, with the exception of that following the three large rainfall events described above. Deuterium tracer was observed to a maximum depth of 3.2 meters in the waste rock and was attributed primarily to preferential flow during and shortly after the three large rainfall events on the covered surface. Using the tracer data presented above, a maximum possible velocity of water moving in preferential flow paths is 3.2 m/d. The tracer data yields a large range in estimated water travel times and data from TDR probes and infiltration data are used to further refine the pore water, and preferential flow velocities in the waste rock.

4.6.5.2. Water Velocities Estimated from Wetting Front Data

The TDR probes provided reliable, high resolution water content data but do not provide data on water velocity. TDR probes buried along the three vertical profiles recorded wetting fronts in response to the three large rainfall events. Wetting fronts at similar depths across the waste rock pile had different arrival times (Figure 4.9.a).

The progression of wetting fronts to a depth of at least 1.95 m were observed in the TDR data following the three large events on the covered pile. In the weeks following these large events, there was no observable response in the TDR data at the 3.2 m and 4.7 m depths. The observations could be explained as a cessation of wetting front propagation in response to the high sorptivity of the material surrounding a flow finger or vertical zones with slightly larger pore geometries. Probes in the cover and 0.5 m below the cover record small perturbations in response to smaller rainfall events, but wetting fronts did not continue deeper into the pile. It is likely that much of this water was held in near-surface storage and subsequently removed by evaporation.

Based on a comparison of TDR wetting front progressions and outflow at the base of the CPE, Nichol (2003) hypothesized that the TDR probes were not in the pathways transmitting the fastest moving water in the uncovered waste rock. Similar to the conclusions of Nichol (2003), the TDR probes did not record the fast preferential flow that occurred within the CPE following cover placement. The fastest wetting front measured by TDR (up to 0.1 m/d) was significantly slower than the slowest estimate of the preferential flow velocity based on the tracer data. The post-cover location of the tracer maxima and the maximum depth of wetting fronts as observed by TDR from the year following tracer application are similar (Figure 4.11). However, the slowest wetting front velocity measured by TDR data was nearly identical to the fastest (unrealistically high) estimate of the pore water velocity based on the tracer data. This suggests that the TDR probes were measuring wetting front velocities slower than the preferential flow velocity yet much larger than the average pore water velocity. The observed TDR responses are interpreted to result from faster than average water flow and from pressure waves.

Prior to the deconstruction, the wetting front progressions and the outflow associated with ponding were the only direct evidence for flow deeper than 2 m in the covered pile. Both the outflow and TDR response associated with ponding are assumed to be a pressure wave response that was not manifested in the tracer data. The combination of the depth of observed tracer and the limited number of event-driven wetting fronts support the idea that the water in the CPE following covering was primarily moving in response to the large rainfall events. While this cannot be quantified, it appears that the maximum depth of the tracer corresponds with the maximum depth of the preferential flow that occurred in response to, or following the large rainfall event in which the tracer was applied and that the depth is not a cumulative result of the three large events. It has been documented that preferential flow will occur repeatedly in the same area in response to transient events even in the absence of observable structure (Wang et al, 2002), however, if this was the case, fresh water with near-background δD values would have been observed in the upper portion of profiles above the 3.2 m tracer maxima. This interpretation assumes that minimal lateral flow occurs during these events. It is also assumed that if the volumetric water content of the waste rock remained high between successive events, it would be more favorable for a second preferential flow finger to progress deeper in response to a similar size event. This is not the observed case since the water content drops back down to pre-rainfall levels prior to the subsequent large events. The second two (greater than 20 mm) rainfall events may have resulted in a slight progression of the leading edge of the tracer slug and an increased amount of dispersion. It is more likely that the subsequent two events resulted in a mixing and dilution of the isotopic tracer maxima and a progression of the preferential flow fingers.

4.6.5.3. Water Velocities Estimated from Flux Data

The third estimate of the average pore water velocity is calculated from the measured flux through the CPE and the average volumetric water content of the CPE during the year following placement of the cover. The pore water velocity within the covered waste rock calculated by this method is 0.001 m/d (0.5 m/y). The primary assumptions in this calculation ar that the infiltration rate equals the flux measured as outflow, that the flow was steady throughout the year, and that flow occurs through the entire volume of filled pores. A value of 10% was used as the volume of filled pores (volumetric water content), based on the long-term average from TDR data. While the flow was not steady throughout the year, the resulting pore water velocity calculated by this method still yields a better approximation of the average pore water velocity through the pile than the other methods as a result of the long period of time over which the measurements were made. The flux data provided the best estimate of pore water velocity through the CPE while the tracer and the TDR methods constrain the range of velocities calculated.

4.7. SUMMARY

Tracer maxima observed one year after tracer application were located at depths between 0.5 m and 3.2 m below the cover and are attributed to a combination of preferential flow and matrix flow during rainfall events. While many of the near-surface samples appear to have been fractionated, the majority of samples between 1.5 m and 3.2 m contain enriched water that can only be explained by mixing of pre-tracer water with the tracer. The high variability in tracer values results from different amounts of mixing with pre-tracer water and is suggestive of a combination of preferential flow and matrix flow. The combination of the lateral spatial variability of δD values and the occurrence of δD values at 3.2 m depth within the pile yield strong evidence for preferential flow, likely in the form of transient flow fingers. Based on the tracer values obtained from adjacent vertical profiles, distinctive preferential flow paths appear to be contained within an area of less than 0.15 m.

Prior to placement of the lower permeability cover, an average pore water velocity through the matrix materials of approximately 1.5 m/yr and maximum preferential flow velocities as high as 5 m/day were observed. Following placement of the cover, little flow within the waste rock was observed at depths greater than 1 m with the exception of during, and for a few weeks following, large rainfall events. An upper bound post-cover pore water velocity of 0.017 m/d (6.4 m/y) was estimated from the tracer data, the post-cover pressure wave velocity of 0.1 to 1 m/day was inferred from outflow and TDR data, and average pore water velocities of 0.39 m/y and 0.73 m/y (0.001 m/d) were calculated by the water flux and tracer methods, respectively.

In the covered waste rock, where the water flow appears to be active primarily during rainfall events, a single estimate of pore water velocity is unlikely to be representative. For models that require an average pore water velocity to describe flow, the estimate calculated from the flux data is most appropriate. However, in systems with preferential flow, it may be appropriate to use an upper bound estimate calculated using the tracer data as a preferential flow velocity in a two-domain model.

The observation that preferential flow occurs in covered and drained waste rock has significant implications for the prediction of water residence times, wetted surface area, and characterizing how dissolved metals are transported through covered waste rock. Since water flow in the covered waste rock appears to be dominantly associated with larger rainfall events, the water residence time, as well as the amount of deeper preferential flow is highly dependent on the amount and frequency of infiltration. Even with a low infiltration surface and little matrix flow, infiltration into the covered waste rock under certain climatic patterns may result in significant preferential flow fingers that could transport weathering products through a covered waste rock pile faster than the estimated average rate.

4.8. CONCLUSIONS

This paper provides a description of the post-cover water flow and the tracer distribution within the CPE. The relationships between the tracer distribution and the variable infiltration rate at the surface are established. Specifically, the first hypothesis was that the addition of a lower permeability surface cover would result in a significant reduction of distinctive preferential flow paths by limiting the flow to within the finer grained matrix materials. The tracer and outflow data shows that the addition of a lower permeability cover significantly reduced the amount of infiltration into the CPE and consequently resulted in a significant reduction in volume of water flowing through preferential flow paths within the system. Even though the volume of water flowing in the CPE was lower, the majority of water that infiltrated into the post-cover CPE was event-driven and transported through preferential flow paths similar to that observed by Pruess (1999). Thus, the lower permeability cover apparently increased the amount of preferential flow relative to the percentage of infiltration.

Deuterium was expected to act as an ideal tracer of water movement through a waste rock pile in which few other options for water tracers were available. Even though deuterium has been effectively used as a conservative tracer of water flow in other unsaturated systems, this was shown to be false for the covered, unsaturated mine waste rock. Deuterium has advantages in that it is inexpensive, has low detection limits and does not interfere with the water chemistry within the waste rock. However, as a result of the large amount of fractionation, deuterium in this context was non-conservative. As a result of fractionation, mixing with pre-tracer and post-tracer water, and preferential flow, the interpretation of the deuterium tracer data was difficult.

4.9. REFERENCES

Albright, W.H., Gee, G.W., Wilson, G.V., Fayer, M.J., 2002. Alternative cover assessment project, Phase I Report.

Allison, G.B., 1983. The relationship between ^{18}O and deuterium in water in sand columns undergoing evaporation, Journal of Hydrology. v. 55. pp. 163-169.

Allison, G.B. and Barnes, C.J., 1985. Estimation of evaporation from the normally "dry" Lake Frome in South Australia. Journal of Hydrology. v. 78. pp. 229-242.

Allison, G.B. and Barnes, C.J., 1990. Estimation of evaporation from non-vegetated surfaces using natural Deuterium. Nature. v. 301. pp. 143-145.

Allison, G.B., Barnes, C.J. and Hughes, M.W., 1983. Distribution of deuterium and oxygen-18 in dry soils: II Experimental. Journal of Hydrology. v. 64. pp. 377-397.

Alpers, C.N. and Nordstrom, D.K., 1999. Geochemical modeling of water-rock interactions in mining environments, in Plumlee, G.S. and Logsdon, M.J. (eds.), The Environmental. Geochemistry of Mineral Deposits. Part A. Processes, Methods, and Health Issues. Society of Economic Geologists, Littleton, Colorado, Reviews in Economic Geology. v. 6A. chapter 14. pp. 289-323.

American Society for Testing and Materials (ASTM), 1991a. Test method for laboratory compaction characteristics of soil using standard effort (12,400 ft-lbf/ft3 (600 kN-m/m3)) (D698-91). Annual Book of ASTM Standards. v. 04.08.

American Society for Testing and Materials (ASTM), 1994. Standard practice for correction of unit weight and water content for soils containing oversize particles (D4718-87; reapproved 1994). Annual Book of ASTM Standards. v. 04.08.

Barnes, C.J. and Allison, G.B., 1983. Distribution of deuterium and oxygen-18 in dry soil: I Theory. Journal of Hydrology. v. 60. pp. 141-146.

Baker, R.S. and Hillel, D., 1990. Laboratory tests of a theory of fingering during infiltration into layered soils. Soil Sci. Soc. Am. Journal. v. 54. pp. 20-30.

Barnes, C.J. and Allison, G.B., 1984. Distribution of deuterium and oxygen-18 in dry soils: III Theory for non-isothermal water movement. Journal of Hydrology. v. 74. pp. 119-135.

Batterham, R., 2003. The international network for acid prevention (INAP) - Addressing a global need. Plenary, Proceedings Sixth International Conference on Acid Rock.

Bellehumeur, T.M., 2001. Mechanisms and spatial variability of rainfall infiltration on the Claude waste rock pile. MA Sc thesis, University of British Columbia, Vancouver.

Beven, K., Germann, P., 1982. Macropores and water flow in soils. Water Resources Research. v. 18. no. 5. pp. 1311-1325.

Bezuidenhout, N., van Niekerk, A.M, and Vermaak, J.J.G., 2002. The effects of natural soil covers on geochemical processes associated with coal discard deposits-results from a pilot scale. In Proceedings of the 5th International Conference on Acid Rock Drainage.

Birkholzer, J. and Tsang, Chin-Fu, 1997. Solute channeling in unsaturated heterogeneous porous media. Water Resources Research. v. 33. no. 10. pp. 2221-2238.

Bowen, G.J. and Wilkinson, B, 2002. Spatial distribution of $D^{18}O$ in meteoric precipitation. Geology. v. 30. no. 4. pp. 315-318.

Brooks, R. H. and Corey, A. T., 1964. Hydraulic properties of porous media. Colorado State University (Fort Collins), Hydrology Paper No. 3.

Brooks, R. H. and Corey, A. T., 1966. Properties of porous media affecting fluid flow. Journal of the Irrigation and Drainage Division, ASCE. v. 92. pp. 61-89.

Buczko, U, Gerke, H,H, Huttl, R.F., 2001. Spatial distributions of lignite mine spoil properties for simulating 2-D variably saturated flow and transport Ecological Engineering. v. 17. no.2-3. pp. 103-114.

Cho, H., de Rooij, G.H. and Inoue, M., 2005. The pressure head regime in the induction zone during unstable nonponding infiltration: Vadose Zone

Journal. v. 4. pp. 908-914.

Coeppicus, S., Bauer, C., Grassmann, J., Ruhrberg, M. and Peiffer, S., 2003. A methodological approach towards a global environmental impact assessment of acid mine drainage using copper mining processes as an example. Proceedings Sixth International Conference on Acid Rock Drainage, Cairns, Australia.

Coons, L.M., Ankeny, M.D. and Bulik, Gary M., 2000. Alternative earthen final covers for industrial and hazardous waste trenches in Southwest Idaho. Unpublished article from cover workshop. p.14.

DePaolo, D.J., Conrad, M.E., Maher, K. and Gee, G.W., 2004. Oxygen and hydrogen isotopes in pore fluids from a 70 m-thick vadose zone soil section at Hanford, Washington: Implications for recharge and horizontal fluid movement: Vadose Zone Journal. v. 3. pp. 220-232.

Diment, G.A. and Watson, K.K., 1985. Stability analysis of water movement in unsaturated porous materials. v. 3: Experimental studies. Water Resources Research. v. 21. pp. 979-984.

Dincer, T., Al Mugrin, A., Zimmermann, U., 1974. Study of the infiltration and recharge through sand dunes in arid zones with special reference to the stable isotopes and thermonuclear tritium. Journal of Hydrology. v. 23. pp. 71-109.

Dwyer, S.F., 1997. Large-scale field study of landfill covers at Sandia National

Laboratories. Conference Proceedings Landfill Capping in the Semi-Arid West: Problems, Perspectives, and Solutions, T.D Reynolds and R.C. Morris (eds). Grand Teton National Park, May 1997. pp. 27-38.

Eriksson, N., Gupta, A. and Destouni, G., 1997. Comparative analysis of laboratory and field tracer tests for investigating preferential flow and transport in mining waste rock: Journal of Hydrology, v. 194. no. 1-4. pp. 143-163.

Eriksson, N., Destouni, G., 1997. Combined effects of dissolution kinetics, secondary mineral precipitation, and preferential flow on copper leaching from mining waste rock. Water Resources Research. v. 33. no.3. pp. 471-483.

Fala, O., Aubertin, M., Molson, J., Bussiere, B., Wilson, G.W., Chapuis, R. and Martin, V., 2003. Numerical modeling of unsaturated flow in uniform and heterogeneous waste rock piles, Sixth International Conference Acid Rock Drainage.

Fines, P., Wilson, G.W., Landriault, D., Langetine, L. and Hulett, L., 2003. Co-mixing of tailings, waste rock and slag to produce barrier cover systems, Proceedings Sixth International Conference Acid Rock Drainage.

Fines, P., Wilson, G.W., Willams, DJ., Tran, A.B. and Miller, S., 2003. Field characterization of two full-scale waste rock piles. Proceedings Sixth International Conference on Acid Rock Drainage.

Fines, P., 2006. Hydrologic characterization of two full-scale waste rock piles.

MSc. thesis, University of British Columbia, Vancouver.

Flury, M., Fluhler, H., Jury, W.A. and Leuenberger, J., 1994. Susceptibility of soils to preferential flow of water: A field study. Water Resources Research. v. 30. pp. 1945-1954.

Ghodrati, M., Jury, W.A., 1992. A field study of the effects of soil structure and irrigation. Method on preferential flow of pesticides in unsaturated soil. Journal of Hydrology. v. 11. pp. 101-125.

Gonfiantini R., 1986. Environmental isotopes in lake studies. In Handbook of Environmental Isotope Geochemistry A. v. 1 (ed. P. Fritz and J. C. Fontes). pp. 113-168.

Guebert, M.D., Gardner, T.W., 2001. Macropore flow on a reclaimed surface mine: infiltration and hillslope hydrology. Geomorphology. v. 9. pp. 151-169.

Hangen, E., Gerke, H.H., Schaaf, W., Huttl, R.F., 2004. Assessment of preferential flow processes in a forest-reclaimed lignitic mine soil by multicell sampling of drainage water and three tracers, Journal of Hydrology. v. 303. no. 1-4. pp. 16-37.

Hammarstrom, J.M. and Smith, K.S., 2002. Geochemical and mineralogic characterization of solids and their effects on waters in metal-mining environments, in Seal, R.R., II, and Foley, N.K., eds., Progress on geoenvironmental models for selected mineral deposit types: U.S Geological Survey Open-File Report 02-0195. pp. 8-54.

Herasymuik, G.M., 1996. Hydrogeology of a waste rock dump. M.Sc. Thesis. Department of Civil Engineering, University of Saskatchewan, Canada.

Jambor, J.L. and Blowes, D.W., 1998. Theory and application of mineralogy in environmental studies of sulfide-bearing mine wastes, in Modern Approaches to Ore and Environmental Mineralogy (Cabri, L.J. and Vaughan, D.J., Eds.), Mineralogical Association of Canada Short Course. v. 27. pp. 367-402.

Jury, W.A., Wang, Z. and Tuli, A., 2003. A conceptual model of unstable flow in unsaturated soil during redistribution. Vadose Zone Journal. v. 2. pp. 61-67.

Lapakko, K., 2002. Metal mine rock and waste characterization tools: An overview. Minesota Department of Natural Resources, US. Posted on the Acid Drainage Technology Initiative - Metal Mining Sector.

Li, M., 2000. Unsaturated flow and transport observations in large waste rock columns, in Proceedings Fifth International Conference on Acid Rock Drainage. pp. 247-256.

Lu, N. and Y. Zhang, 1997. Thermally induced gas convection in mine wastes, International Journal of Heat and Mass Transfer. v. 40, no. 11, pp. 2621-2636.

Lu, N., 2001. An analytical assessment on the impact of covers on the onset of air convection in mine wastes, International Journal for Numerical and

Analytical Methods in Geomechanics. v. 25. pp. 347-364.

Marcoline, J.R., Beckie, R.D., Smith, L. and Nichol, C.F., 2003. Mine waste rock hydrogeology - The Effect of Surface Configuration on Internal Water Flow. Sixth International Conference Acid Rock Drainage.

Marcoline, J.R., Smith, L, Beckie, R.D., 2006, Water migration in covered waste rock, Investigations using. deuterium as a tracer. Proceedings of the 7th International Conference Acid Rock Drainage.

MEND 2.21.4, 2004. Design, construction and performance monitoring of cover systems for waste rock and tailings, Prepared for the Mine Environmental Drainage Program (MEND) by: O'Kane Consultants Inc.

Milczarek, M, Yao, Tzung-mow, Vinson, J, Word, J, Kiessling, S, Musser B, and Mohr, R., 2003. Performance of mono-layer evapotranspirative covers in response to high precipitation and extended drought periods in the southwestern united states. Sixth International Conference Acid Rock Drainage.

Molson,.J.W., Fala, O., Aubertin, M., Bussiere, B., 2005. Numerical simulations of pyrite oxidation and acid mine drainage in unsaturated waste rock piles. Journal of Contaminant Hydrology. v. 78. pp. 343-371.

Murr, L.E., 1979. Observations of solution transport, permeability, and leaching reactions in large, controlled, copper-bearing waste bodies. Hydrometallurgy. v. 5. pp. 67-93.

Newman, B.D., Campbell, A.R. and Wilcox, B.P., 1997. Tracer-based. studies of soil-water movement in semiarid forests of New Mexico., Journal of Hydrology. v. 196. pp. 251-270.

Newman, L.L., Herasymuik, G.M., Barbour, S.L., Fredlund, D.G. and Smith T., 1997. The hydrology of waste rock dumps and a mechanism for unsaturated preferential flow., Proceedings, Fourth International Conference on Acid Rock Drainage. pp. 551-565.

Newman, L., 1999. A mechanism for preferential flow in vertically layered, unsaturated systems, MSc thesis, University of Saskatchewan, Saskatoon.

Nichol, C.F., 2003. Transient flow and transport in unsaturated heterogeneous media: Field experiments in mine waste rock. Ph.D. dissertation, University of British Columbia, Vancouver.

Nichol, C.F., Smith, L. and Beckie, R., 2003. Water flow in uncovered waste rock - A multi-year large lysimeter study. Sixth International Conference Acid Rock Drainage.

O'Kane, M. and Waters, P., 2003. Dry cover trials at Mt Whaleback - A summary of overburden storage area cover system performance. Sixth International Conference Acid Rock Drainage.

Parlange, J.Y. and Hill, D.E., 1976. Theoretical analysis of wetting front instability in soils. Soil Sci. no. 122. pp. 236-239.

Rasmussen, T.C., Baldwin, R.H., Dowd, J.F. and Williams, A.G., 2000. Tracer vs. pressure wave velocities through unsaturated saprolite. Soil Sci. Soc. Am. Journal. v. 64. pp 75-85.

Singleton, M.J., Sonnenthal, E.L., Conrad, M.E., DePaolo, D.J. and Gee, G.W., 2004, Multiphase reactive transport modeling of seasonal infiltration events and stable isotope fractionation in unsaturated zone pore water and vapor at the Hanford site. Vadose Zone Journal. v. 3. pp. 775-885.

Smith, L., Lopez, D., Beckie, R.D., Morin, K., Dawson, R. and Price, W., 1995. Hydrogeology of waste rock dumps. Report prepared for CANMET and BC Ministry of Energy, Mines and Petroleum Resources. pp. 1-130.

Smith, L. and Beckie, R., 2003. Hydrological and geochemical transport processes in mine waste rock, Ch 3 in Environmental Aspects of Mine Wastes, Mineral. Assoc. Canada, Short Course Series. v. 31. pp. 51-72.

Sofer, Z. and Gat, J.R., 1975. The isotopic composition of evaporating brines: Effect of the isotopic activity ratio in saline solutions. Earth and Planetary Science Letters. v. 26. pp. 179-186.

Sracek, O., Choquette, M., Gelinas, P., Lefebvre, R., Nicholson, R.H., 2004. Geochemical characterization of acid mine drainage from a waste rock pile, Mine Doyon, Quebec, Canada., Journal of Contaminant Hydrology. v. 69, pp. 45-71.

Stockwell, J., Beckie, R.D. and Smith, L., 2003. The hydrogeochemical characterization of an unsaturated waste rock pile, Key Lake, Saskatchewan, Canada. Sixth International Conference Acid Rock Drainage.

Stockwell, J., Smith, L., Jambor, J. and Beckie, R., 2006. Hydrogeochemistry of an unsaturated waste rock pile, Key Lake, Saskatchewan. Applied Geochemistry v. 21. pp. 1347-1361.

Tran, A.B., Fines P., Miller S., Williams, D.J. and Wilson, G.W., 2003. Hydrologic and geochemical characterization of two full-scale waste rock piles: a joint university/industry research program sponsored by INAP, Geotechnical News. v. 21, no. 3. pp. 36-42.

Trapp, G., Meyer-Windel, S., Lennartz, B., 1995. Cell lysimeter for studying solute movement as influenced by soil heterogeneity, BCPC Monograph 62: Pesticide Movement to Water. pp. 123-128.

U.S. EPA, 1994. Technical Document: Acid mine drainage prediction. EPA/530-R-94-036.

USGS, 2003, Isotope investigations in the middle Rio Grande Basin. Southwest Hydrology. January/February. pp. 26-29.

Wang, Zhi, T., A. and Jury, W.A., 2003. Unstable flow during redistribution in homogeneous soil. Vadose Zone Journal. v. 2, pp. 52-60.

Wang, Z, Wu, L., Harter, T., Lu, J. and Jury, W.A., 2003. A field study of unstable preferential flow during soil water redistribution. Water Resources

Research. v. 39. no. 4, p. 1074.

Wang, Z., Jury, W.A., Tuli, A. and Kim, D., 2004. Unstable flow during redistribution. Controlling factors and practical implications., Vadose Zone Journal. v. 3. pp. 549-559.

	Matrix Flow (average velocity)	Preferential Flow Paths
Uncovered	1.5 m/yr	5 m/day
Covered		
Tracer	0.4 to 0.7 m/yr	3.2 m/day
Flux-based	0.5 m/yr	

Table 4.1. Summary of water travel time estimates for both pre- and post-cover periods.

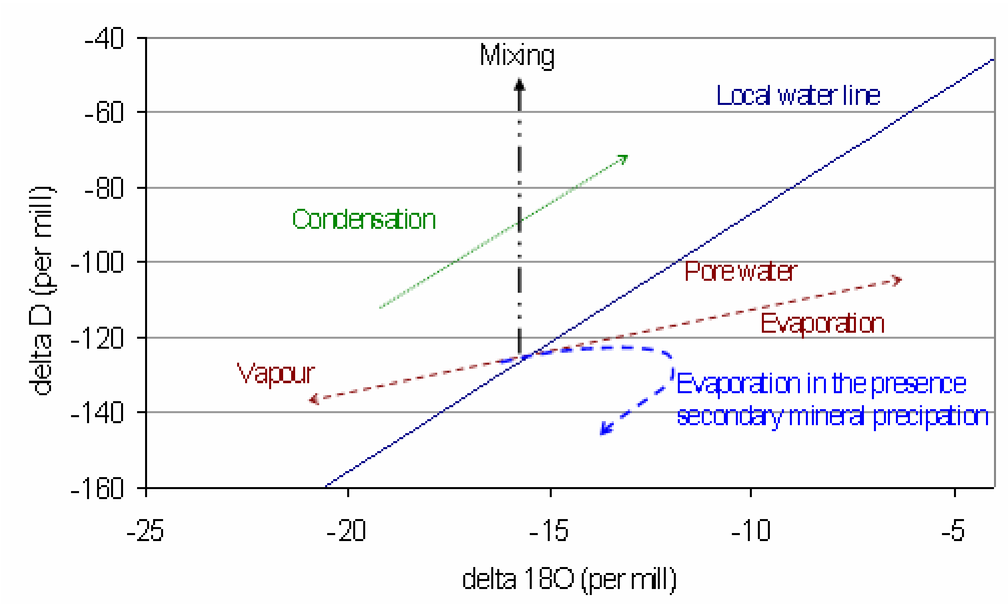

Figure 4.1. A local water line on a δD versus $\delta^{18}O$ plot showing potential isotopic evolution of pore water and water vapor resulting from equilibrium fractionation. Diffusive or kinetic fractionation would follow either the red dashed pore water evaporation trend line or the blue dashed trend line. The vertical mixing line shows the direction that a sample with background δD values would trend with increased mixing with tracer labeled water. This line is drawn between average baseline values and the tracer value which had a deuterium value (δD) of +213 per mil and a $\delta^{18}O$ value of -15.47 per mil.

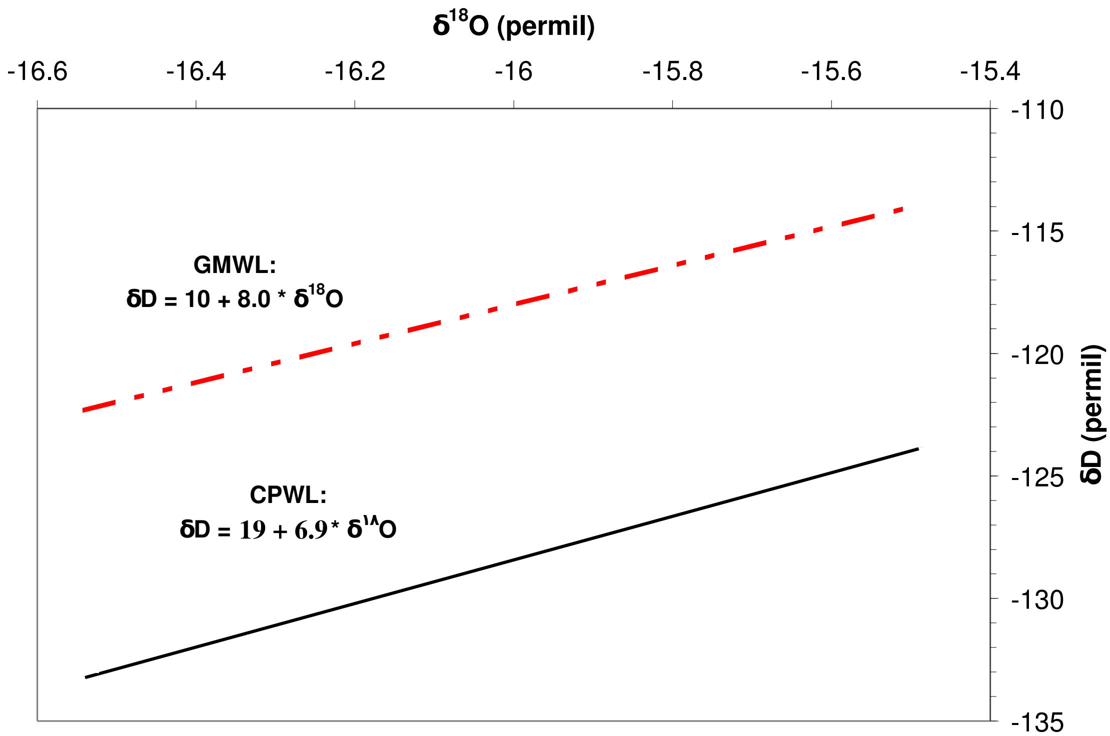

Figure 4.2. The global meteoric water line (GMWL) published by Craig (1961) is shown with the dashed line. The solid line (CPWL) represents the average background pore water isotope values measured from within the experimental waste rock pile. The CPWL is similar to a local meteoric water line and is offset from the GMWL as a result of equilibrium fractionation.

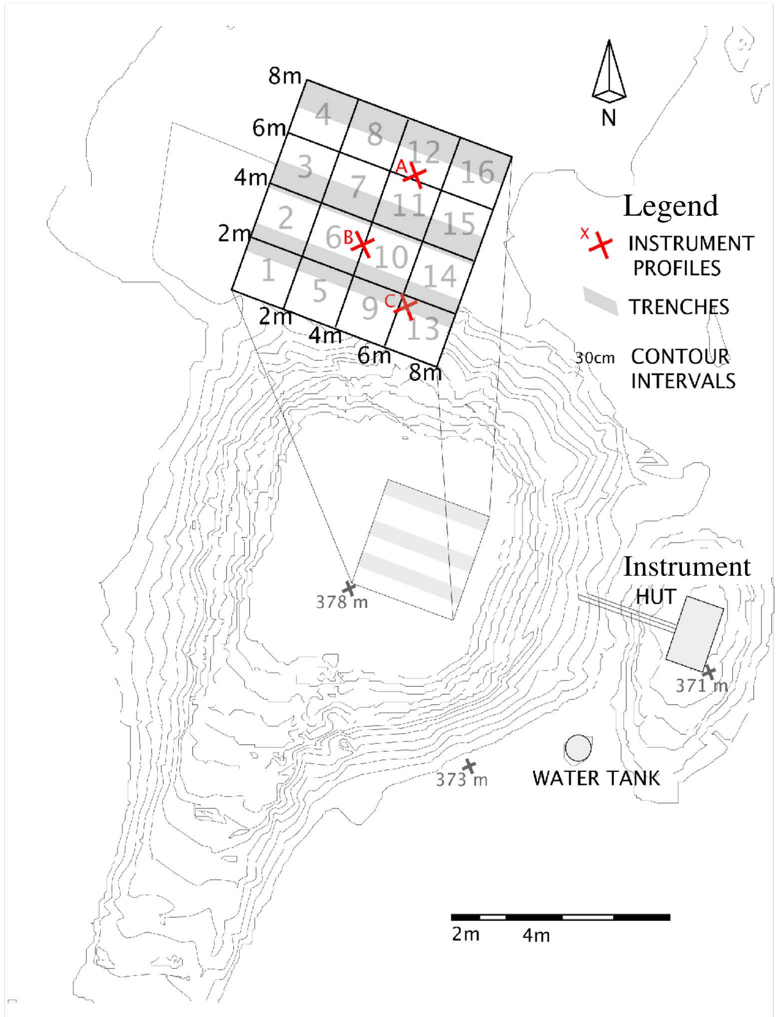

Figure 4.3. Schematic view of the top of the CPE. Instrument profile and trench locations within the lysimeter grid are shown. The trenches outside of the grid are not shown. The origin of the grid is on the lower left (southwest) side of lysimeter 1. The lysimeter grid is to scale and is superimposed on topographic contours of the CPE.

Figure 4.4. Photograph of a vertical trench face at the base of the experimental waste rock pile. Vertical (red) lines approximate boundaries of underlying lysimeters. Note the heterogeneity in waste rock texture.

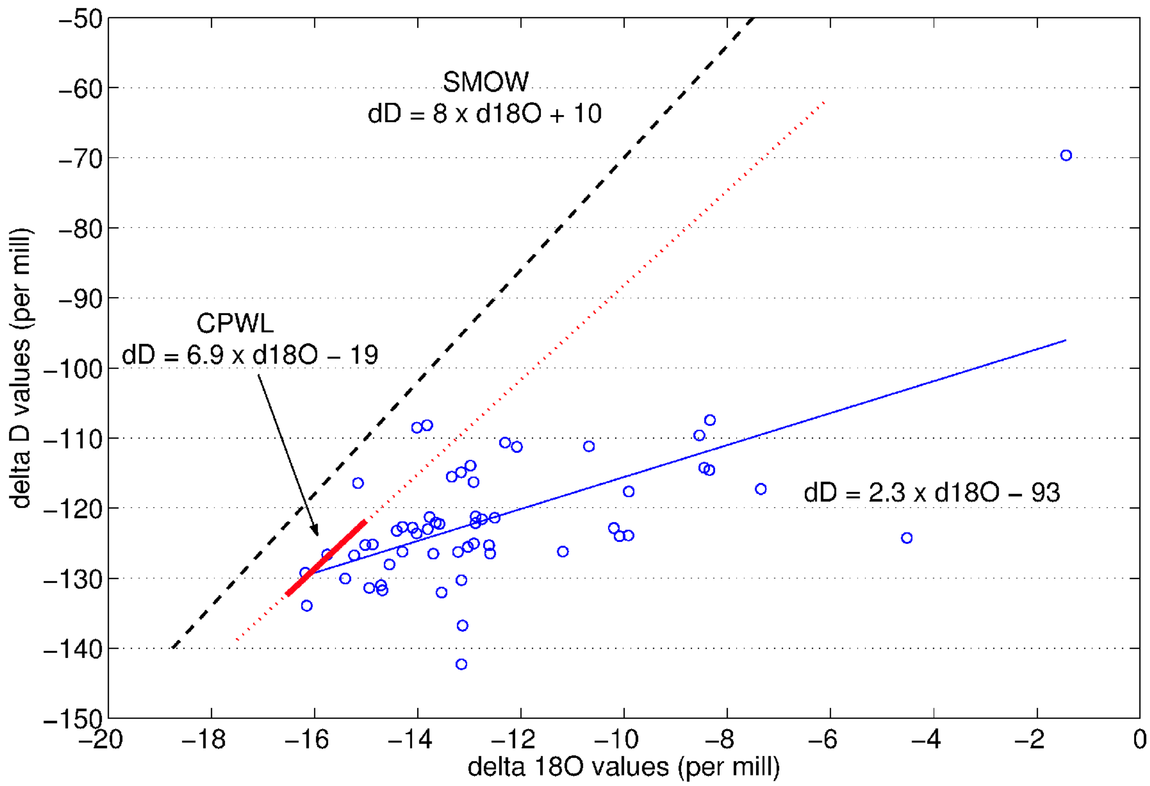

Figure 4.5. Plot of the global meteoric water line (SMOW) (Craig, 1961), the Cluff Lake background pore water line (CPWL) and an estimated fractionation line defined by pore water samples. Samples used to define the CPWL are not included on this plot.

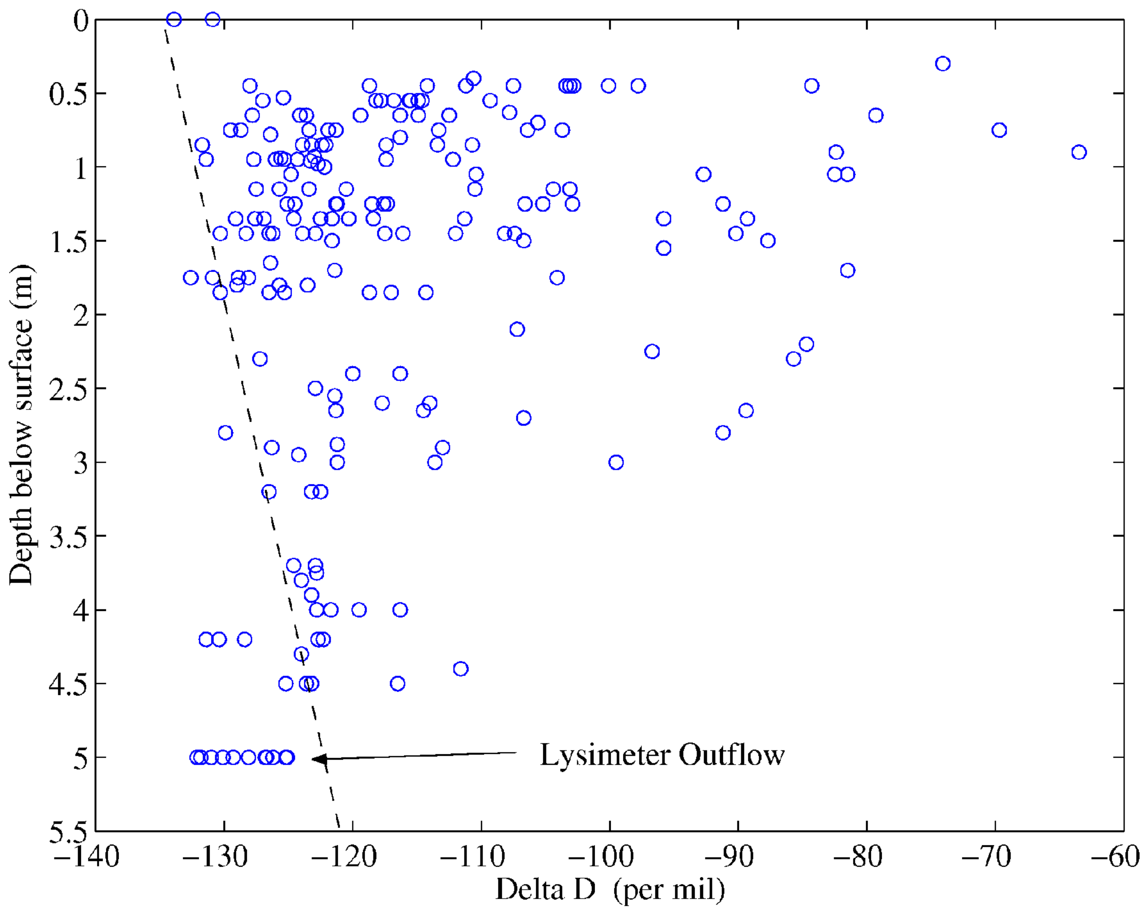

Figure 4.6. The vertical spatial distribution of 174 pore water δD values in the waste rock pile. The dashed line is defined by background pore water δD and δ18O values of pre-tracer pore water. The background samples were collected prior to tracer application and are the same data used to determine the background CPWL.

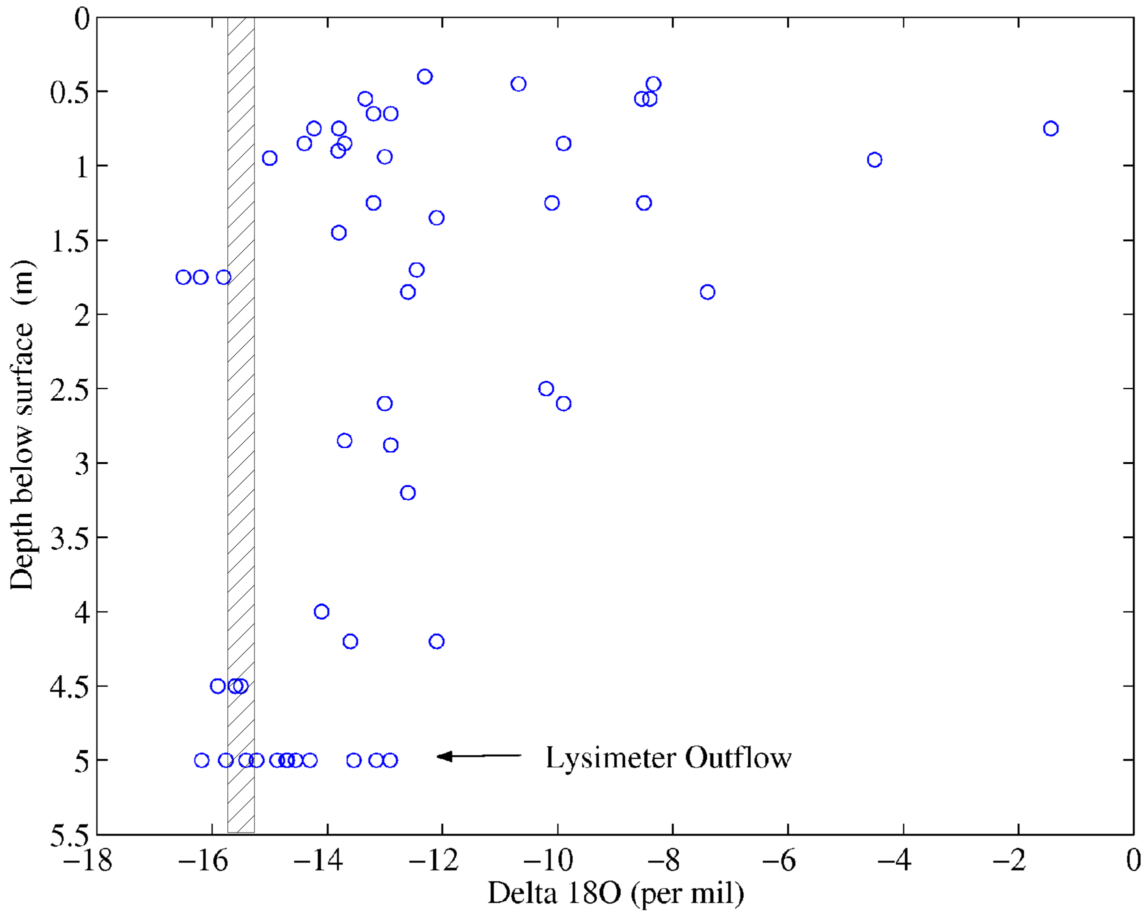

Figure 4.7. Plot of $\delta^{18}O$ values relative to depth in the waste rock pile. Samples plotting at 5 m below the surface were collected in the basal lysimeters. Hatched area represents background values.

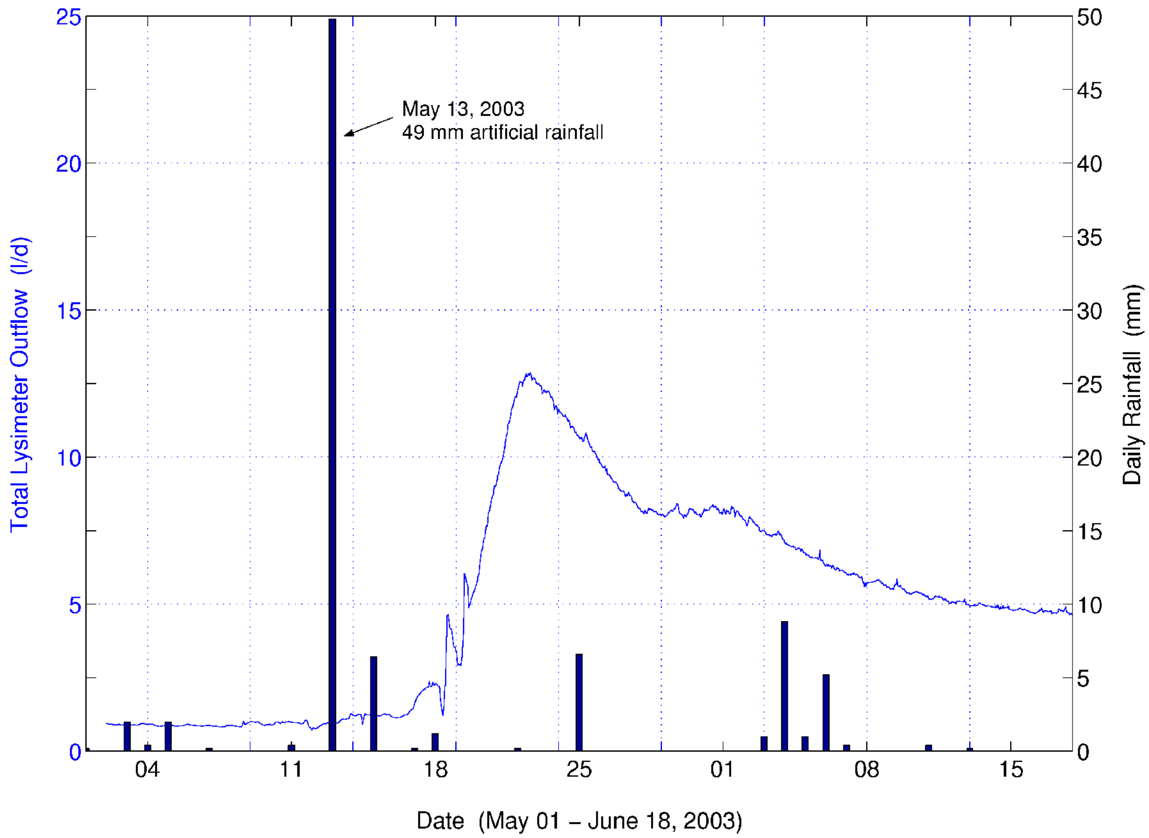

Figure 4.8. Plot showing the 49 mm rainfall event on the May 13, 2003 on the right Y-axis and the lysimeter outflow in liters per day from the 16 combined lysimeters for the period between May 01, 2003 and June 18, 2003. The dips and spikes in the outflow curve between the 18th and the 20th May are a result of a night time freeze and a thaw the following day of water in the exposed portion of the lysimeter drainage pipes.

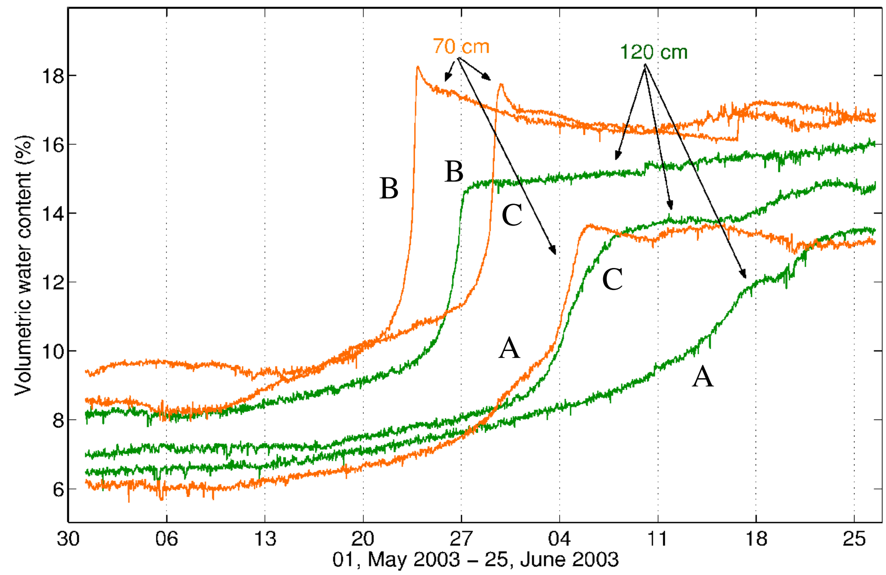

A

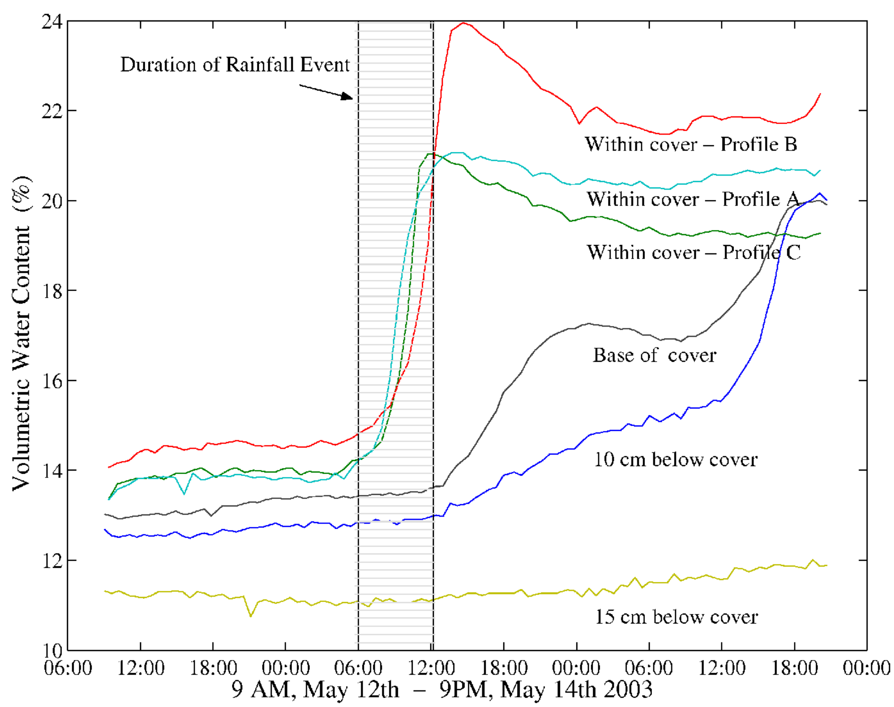

B

Figure 4.9.a) TDR data from probes located in profiles A, B and C at two depths within the pile for a period of 45 days following the May 13, 2003 tracer application. b) TDR data from different depths during the tracer test.

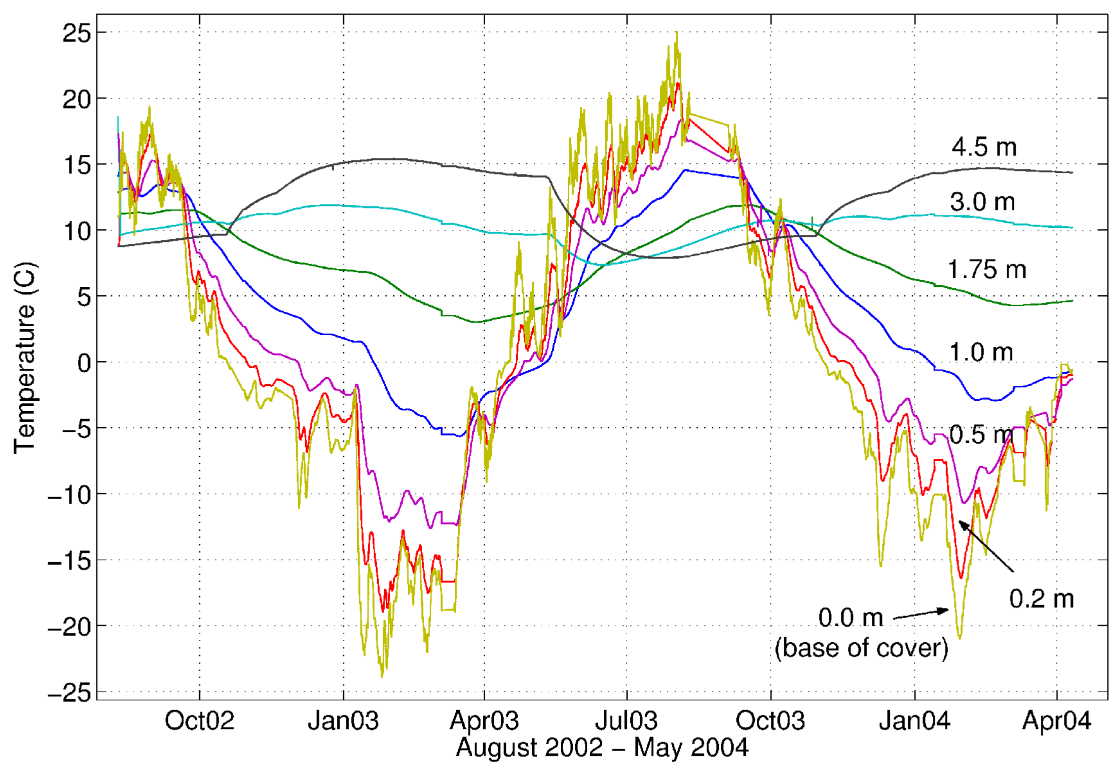

Figure 4.10. Temperature profiles for 7 depths within the waste rock pile. The profiles show the reversed thermal gradient in the pile during the winter months of 2003 and part of 2004.

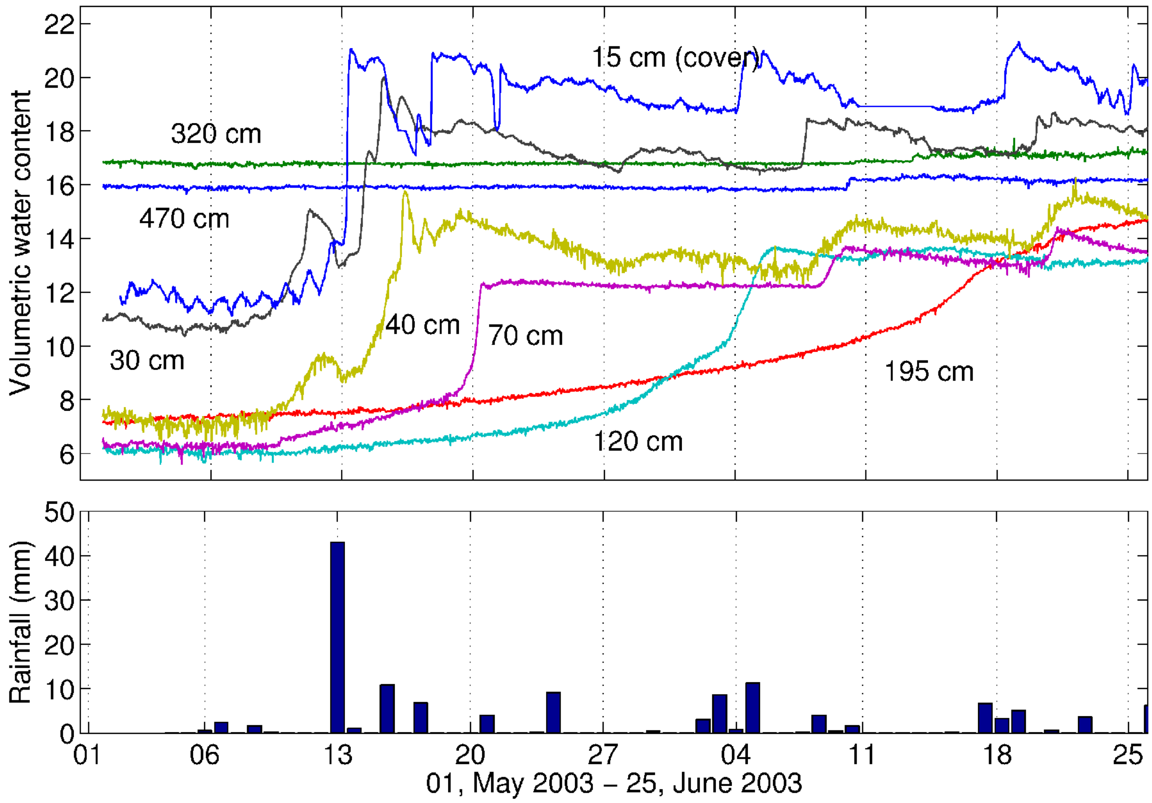

Figure 4.11. The volumetric water content as measured by TDR probes at 8 different depths within the waste rock pile between May 01, 2003 and June 25, 2003. The data are an average from the probes at the same depth in all three profiles. The sub-plot shows the rainfall record for the same period.

CHAPTER 5: DECONSTRUCTION OF THE EXPERIMENTAL WASTE ROCK PILE

5.1. INTRODUCTION

Physical and geochemical properties of waste rock piles are often characterized by compiling observational and geochemical data from composite surface and shallow trench samples (Higgs et al, 1997), drill cuttings (Shaw et al, 2002) and/or historic mine records (Soregaroli and Williams, 1997, Soregaroli and Lawrence, 1998). While perhaps adequate for screening of acid rock drainage (ARD), this approach yields little information on the structural properties of the waste rock and the arrangement of the coarse and fine material. Structural properties are thought to have a strong influence on fluid flow paths, water residence times and mass loading from a pile. The deconstruction of a mine waste rock pile offers the opportunity to observe the internal structure and investigate how the structures may relate to the hydrogeologic properties of the pile (Smith et al, 1995, Herasymuik, 1996, Wilson, 2000, Saretzky et al, 2000, Stockwell, 2002).

Although waste rock piles have been deconstructed in the past, none of them has been instrumented to the extent that allows an investigation of the role of structures in influencing outflow rates and mass loadings. A large waste rock pile at the Golden Sunlight Mine in Montana was excavated between 1994 and 1995

A version of this chapter will be submitted for publication. Marcoline, J.R., Deconstruction of a covered waste rock pile.

(Herasymuik, 1996). During the excavation, both the waste rock structure and the hydrogeologic properties of the waste rock were characterized in detail. Based on these field observations, Herasymuik developed a conceptual model for unsaturated flow through an end-dumped waste rock pile. He predicted that water will preferentially migrate in the sloping finer materials within the pile and gas flow will occur predominantly in the coarse layers. In 2002, a 12 meter-high waste rock test pile at the Key Lake Mine in northern Saskatchewan was deconstructed (Stockwell, 2002, Stockwell et al, 2006). Stockwell found significant variability in weathering products throughout the test pile as indicated by color, paste-pH, pore water chemistry and mineralogy. He evaluated the spatial relationship between pore water chemistry and particle size of the waste rock, and concluded that a relationship between the internal structure of the pile and the degree of local weathering either did not exist, could not be identified, or that the test-pile was too young for the relationship to evolve. Stockwell outlined recommendations to improve sampling methodology for future waste rock deconstruction projects.

Fines (2003) reported a physical and geochemical characterization of a waste rock pile at the Ridgeway Mine in South Carolina, and a waste rock pile at the Whistle Mine in Ontario. Fines concluded that water flow through waste rock and the amount of stored weathering products are spatially variable and depend on the pile structure, the variability of particle sizes, and the degree of weathering. Fines used observations from the excavations to develop a steady-state numerical model of water flow in layered waste rock. Based on the modeling, Fines concluded that preferential flow developed within the waste rock as a result of the textural differences between sloping layers. The deconstruction of the experimental rock pile (CPE) at Cluff Lake marks the first detailed deconstruction of a long-term, instrumented waste rock pile for which the water balance is well-characterized.

5.1.1. Objective

The experimental waste rock pile (Figure 5.1.a) has been used to investigate water flow and solute transport within unsaturated, heterogeneous waste rock since 1998 (Nichol et al, 2003, Marcoline et al, 2003, Nichol et al, 2005, Marcoline et al, 2006, Wagner et al, 2006). The CPE was constructed by free-dumping waste rock with an excavator and back-hoe on a grid of 16 lysimeters. The construction methodology resulted in a 5 m high pile of waste rock without pavement surfaces or angle of repose slopes. This work has led to the formation of a conceptual description of the physical mechanisms by which water moves through the waste rock, based on both natural and artificial rainfall experiments, tracer experiments, and the spatial and temporal variability in volumetric flow and solute concentrations in the basal lysimeter grid. The conceptual model includes mechanisms for the flow of water through the matrix material at approximately the average pore water velocity, and mechanisms for localized preferential flow of water at a rate much faster than the average pore water velocity. The conceptual model also invokes preferential flow to explain the localized presence of water and tracers deeper than anticipated based on uniform flow in finer grained matrix. Potential preferential flow mechanisms include non-capillary macropore flow and the formation of flow fingers during high intensity rainfall events on the uncovered CPE, and potentially unstable flow following infiltration events in the covered waste rock.

Heterogeneities in textural properties such as particle size distributions, specific structural features such as distinctive layers, and localized zones with distinctive textures affect unsaturated flow and transport processes within waste rock piles. The heterogeneity and presence of structures may promote preferential flow and a change of pore-scale transport processes, such as the initiation of a preferential flow finger from matrix water or the stagnation of water above a capillary break. Textural variations may result in localized immobile zones within the CPE that become isolated from water flow. Flow from fine to coarse-textured materials will promote flow fingers (Baker and Hillel, 1990) and flow instabilities (Su et al, 2004, Wang et al, 2004). Voids and coarse zones can result in localized capillary breaks and water content variations.

Following large rainfall events on the CPE prior to cover placement, one of the lysimeters (lysimeter 6) would record flow spikes within 20 minutes of the rainfall event, with flows up to five times greater in magnitude than any of the other 15 lysimeters. The variability in outflow on the 2 m by 2 m scale was observed in the outflow and it was concluded that this variability must be dominantly controlled by internal structures. Given the magnitude of the differences between lysimeter 6 and adjacent lysimeters (Figure 5.2), the structures were hypothesized to be large and observable.

The primary objective of the deconstruction was to determine if relationships could be identified between the physical properties of the waste rock pile, its internal structure, and the observations of spatially distributed outflow and tracers distribution at the base of the CPE. Multiple lines of evidence are examined, including mapping of structures, dye tracers, analysis of grain size distribution curves, and interpretation of deuterium and chloride distributions from pore water extractions.

5.2. BACKGROUND AND METHODOLOGY

5.2.1. Deconstruction

The experimental waste rock pile was located on the top bench of the Dominique-Jane North (D-JN) waste rock pile at the Cluff Lake Mine. In the fall of 2004, Cogema Resources Inc. (Cogema) relocated the entire D-JN waste rock pile to the Claude open pit. In the spring of 2004, prior to removal of the D-JN pile, the UBC experimental waste rock pile was deconstructed. Deconstruction and sampling followed the methodology described below and recommended by Stockwell (2002). The characterization of the hydrogeologic and physical properties followed procedures outlined by Carter (1993), Herasymuik (1996), Fines (2006) and the appropriate ASTM Guidelines. This chapter also details the mapping of the tracer distributions within the waste rock pile. The relationship between these internal observations and the observations of outflow and tracer arrival at the base of the waste rock pile between 2000 and 2004 are discussed.

Deconstruction of the experimental waste rock pile began following the thaw of the waste rock and prior to any spring rainfall events. At the time of the deconstruction, the low-permeability cover on the CPE had been in place for approximately 1.5 years. The construction of the cover in September of 2002 significantly reduced infiltration of water into the CPE and marked the beginning of a gradual drain down of the pile. Outflow into the basal lysimeters was at the lowest rate since the initial wet-up of the CPE in 1999, with a combined total of approximately one liter per day. Volumetric water contents as low as 4% were measured in the upper portions of the CPE, and as high as 30% just above the basal lysimeters. The lysimeter design effectively created a water table at the base of the CPE. Average volumetric water content in the region between 1 m and 3 m below the cover surface was approximately 7%.

The deconstruction occurred between May 17th and June 21st of 2004 in a series of five lifts. The first lift was 0.40 m deep and included sixteen sets of vertical profile samples through the compacted surface layer, collected in 0.05 m increments (Figure 5.1.b). The remaining five meters of the waste rock pile were excavated in four lifts using three parallel 8 m by 1 m by 1.3 m (LxWxD) trenches within and across the core of the CPE. In addition, a trench was dug on the north and south sides of the CPE, and the lysimeter walls were removed to allow for observation of the waste rock in contact with the walls. One trench per day was cut across the full length (8 m) of the waste rock pile along a surveyed grid. In total, 12 trenches through the core of the CPE were sampled (Figure 5.3). The location of trenches allowed for six complete cross-sectional views of the waste rock above the lysimeter pad, with at least one of the sections intersecting the material above each of the 16 lysimeters. The CPE was covered with a sheet of HDPE and an insulated tarp during the deconstruction to ensure that no rainfall entered the CPE once deconstruction began.

The southwest corner of lysimeter number one was designated as the origin of the grid surveyed for the deconstruction (Figure 5.3). Local "x" coordinates ran from lysimeter one to lysimeter 13 and local "y" coordinates ran from lysimeter one to lysimeter four. Prior to excavating waste rock above the lysimeter grid, the waste rock immediately outside of the northern wall of the pile was removed to a depth of approximately 1.3 m. The lysimeter wall was then removed to expose the waste rock beneath the runoff collection gutter above lysimeters 4, 8, 12 and 16.

The first one meter-deep trench was excavated across the waste rock pile between y = 8.0 m and 7.0 m. The structure of the waste rock along each trench face was described and a comprehensive set of photographs taken. The second excavation across the waste rock pile was 1.3 m deep and located between y = 3.9 m and 4.9 m. The third excavation across the waste rock pile was 1.3 m deep and located between y = 1.0 m and 3.0 m. Prior to excavating the third trench, the waste rock from immediately outside of the southern wall of the waste rock pile was removed to a depth of one meter. The lysimeter wall was removed to expose the waste rock above lysimeter 1, 5, 9 and 13. The third 1.3 m trench excavation was located between y = 1.0 m and 0.5 m. Following excavation of the third trench, the remaining waste rock was bladed off the pile with a small dozer to just above the surveyed elevation of the base of the trenches. The procedure was repeated with four new trenches. On the third lift, a dye stain was released over a three by three meter area centered between trench two and three (Figure 5.4). The entire area beneath the release was hand-excavated with shovels from the adjacent trenches.

5.2.2. Sampling

The trenching methodology allowed for a dense sampling and mapping of each cut trench face immediately following excavation. The trench face was mapped and sampled beneath an insulated tarp to minimize evaporation from the newly-exposed waste rock. Trench faces were surveyed and the textural differences, the presence of secondary minerals, discoloration and observable structures were mapped. Photographic documentation of each trench face and relationships between sample locations and observed waste rock characteristics were noted (Appendix B).

Samples for pore water extraction and gravimetric water content were collected along vertical profiles from both trench walls to allow for detailed characterization of pore water tracer concentrations. A surveyed grid was set at 0.5 m, but sampling varied locally to accommodate coarse rubble zones or large boulders. Each vertical sample was collected in 0.1 m vertical increments by hand excavating an area approximately 0.15 m by 0.15 m wide from the trench faces. Each waste rock sample was homogenized and split into sub-samples. Samples for water content and paste-pH measurements were collected from fine portions of waste rock. Samples were sealed in plastic sample bags, stored in a cooler and processed on-site the same day. Samples collected for pore water extraction and subsequent tracer analysis were sealed under nitrogen. For each vertical profile approximately 20 liters of waste rock was collected for particle size distribution analysis. In addition to the vertical profile sampling, 34 sample sets were collected from targeted locations within the CPE for measurement of a SWCC. Each sample set included a measurement of matric suction, bulk density and volumetric water content. SWCC sample locations were selected from areas within each lift where the waste rock was completely comprised of matrix material.

5.2.3. Pore Water Extractions - Deuterium and Chloride

In September of 1999, an artificial rainfall event containing 2100 mg/L of chloride (as LiCl) was applied to the top surface of the waste rock pile over a three-hour period (Nichol, 2003). In May of 2003, an artificial rainfall event containing +213 per mil of deuterium was applied to the top surface of the covered waste rock pile over a 6.5-hour period. A chloride concentration of 20 mg/L (Nichol et al, 2005) and deuterium values of -130 to - 121 per mil were identified as background for the pre-tracer pore waters. The 20 mg/L background chloride concentration was subtracted from all chloride concentrations presented in this chapter. In the months following the tracer applications, lysimeter outflow and samples from soil water solution samplers were collected and then analyzed for the applied tracers (Marcoline et al, 2006).

During the deconstruction, samples of the finer matrix materials were collected to identify the internal distribution of chloride remaining within the waste rock from the 1999 tracer release and the deuterium released in the 2003 tracer test. Pore water was extracted from 175 of the bulk samples using an IEC Model K centrifuge.

In the laboratory, the sealed bulk samples were opened and approximately 800 g of waste rock passing a 19 mm sieve was immediately packed into specially designed centrifuge inserts and spun at 2100 rpm. Centrifugation continued until sufficient water for two analyses was obtained, typically 1.5 ml (sample and duplicate). The inserts had a collection reservoir separated from the sample by a filter membrane. Extractions removed between 0.1% and 10% (by weight) of the total mass of water in the samples depending on the initial water content of the sample, the particle size distribution and the duration of the spin. All samples were spun for less than 30 minutes.

Sequential sampling was initially performed on four matrix samples by collecting water several times during an extended spin cycle to determine if the tracer concentration in the extracted water changed with an increase in the length of spin. It was hypothesized that sampling in this way might yield water from different networks of pores. If the tracer was not homogeneously distributed in all pore sizes, tracer concentrations would be different in the solution from the coarser pores released after relatively short centrifugation than the solution released from the finer pores of the sample after extended centrifugation. However, the process was discontinued since both the deuterium and chloride results from each extraction were nearly identical. A sequential sampling method may be more appropriate if the matrix material were undisturbed and extractions performed over a larger range of rpm's.

Chloride concentrations in pore water were determined using a HACH DR/2010 spectrophotometer, the mercuric thiocyanate spectrophotometric and known addition methods described by Eaton et al (1995) and Nichol (2003). Based on duplicate samples, the precision was (±) 1 mg/L. Stable isotopes $\delta^{18}O$ and δD in the pore water were determined at the New Mexico Tech Stable Isotope Laboratory and at the UBC Stable Isotope Laboratory. The hydrogen and oxygen isotopes are reported in delta (δ) notation, as per mil (‰) differences relative to the Vienna-Standard Mean Ocean Water (V-SMOW) international. Based on duplicate samples, the analytical precision was (±) 0.6 ‰ for δD and as much as 0.3 ‰ for the very small (0.05 ml to 0.15 ml) $\delta^{18}O$ samples based on laboratory standards.

5.2.4. Dye Staining

Visible and fluorescent dyes have been used to trace water flow paths through both saturated and unsaturated mine waste in columns (Cathles and Murr, 1980, McKnight and Bencala, 1998, Hangen et al, 2004) and at field sites (Hayes, 1993, Güebert and Gardner, 2001, Bellehumeur, 2001). In unsaturated systems, dye tracers are typically used to characterize the extent and amount of flow, and to distinguish between preferential flow and matrix flow. A comprehensive review of the use of dyes as tracers in hydrology is provided by Flury et al (2003).

Bellehumeur (2001) conducted a series of rhodamine dye staining experiments on the Claude waste rock pile at the Cluff Lake Mine. Bellehumeur identified several mechanisms of flow through the waste rock including flow on the surface of boulders and cobbles, lateral flow in coarser zones above compacted layers, macropore flow, and minor amounts of flow through fine grained matrix material. Hayes (1993) conducted 24 fluorescent dye tracer experiments and excavations at nine mine sites. Hayes determined that material texture plays a critical role in determining the properties of flow and the development of macropore networks. While the material at the nine mine sites appeared to be more similar to soil than waste rock, he postulated that the overall macropore length, depth and fluid flow rate were positively correlated to the percentage of grains larger than 2 mm and that 12 to 23% silt and clay was required for cohesive macropore wall development. Hayes observed a reduction in the physical dimensions and hydrologic effectiveness of the macropore if the silt and clay content was above 23%. Flow patterns observed by Hayes in materials with little to no silt and clay particles had little matrix flow, and appeared similar in character to the flow described as boulder hopping by Bellehumeur (2001).

During the deconstruction, attention was paid to identify any structures that might be responsible for preferential flow or that could act as conduits for fast flow. To help visual observations, a rhodamine dye stain was applied to the surface after the removal of the first two lifts (depths to ~2.5 m). Approximately 189 liters (21 mm) of rhodamine dye stain was sprayed on a 3 m by 3 m square area, centered 2 m directly above lysimeter six on the third lift to identify where the water flowed (Figure 5.4). The dye-stained water was sprayed by hand over a 1.5-hour period, during which no ponding occurred. The waste rock beneath the stained area was subsequently hand-excavated from trenches located on either side of the infiltration zone and visual observations of the dye distribution were made. The primary goal of the dye staining test was to identify any physical flow paths that might help explain the higher flow rates observed in lysimeter six.

5.3. RESULTS AND DISCUSSION

5.3.1. Flow and Waste Rock Structure

During the deconstruction, an attempt was made to identify structures within the CPE that might be responsible for the high degree of variability observed in basal outflow prior to placement of the low infiltration cover. Visibly identifiable structures that may have influenced the water flow paths were identified, including potential capillary breaks, localized sloping layers, large boulders and areas of finer grained matrix materials adjacent to rubble zones. In addition to the high density grid sampling along trench faces, target samples were collected from above, within, adjacent to and below identified structures for deuterium and chloride tracer analysis.

Physical characterization of waste rock was complicated because of the large range in particle sizes, from clays and silts to 1.2 m boulders. While variations in particle size and the relative locations of finer and coarser zones were noted, locations for measurement of in-situ waste rock properties and sample collection were only feasible from the finer grained portions of the waste rock. For example, maximum particle size for particle size analysis was approximately 0.1 m, as determined by the diameter of the sample containers. Samples for soil matric suction were constrained by the size of 500 ml jars used for the filter paper method, and samples for tracer extraction were limited to 0.025 m by the diameter of the centrifuge extraction inserts. In an attempt to link the water flow paths in the CPE to structures, the location and positioning of the fine grained samples relative to adjacent large structures were noted.

Bellehumeur (2001) documented specific water flow patterns in relation to boulders in coarse, unsaturated waste rock based on dye tracer observations. Bellehumeur identified the material located directly above the sloping surface of boulders as areas of focused flow where dye stain was concentrated. Waste rock on the underside of a sloping boulder surface was identified as shadow zones that experienced lower amounts of water flow, and waste rock below the lowest portion of boulders was identified as zones of concentrated flow, resulting from water 'dripping' off the boulders.

Boulders between 0.5 m and 1 m in diameter were common within the CPE. Boulders with large flat sloping surfaces that could have resulted in a lateral redirection of downward flowing water were targeted for sampling. Matrix samples were collected from above the boulders to represent the tracer pore water concentrations independent of the boulder and as a reference value for the samples below the boulder. Samples were also collected from the matrix material in a thin layer parallel to the top sloping surfaces, from the drip, shadow and focus zones.

In the top meter of the pile, the majority of the pore water samples include deuterium from the tracer event, and contain a fairly uniform, low concentration of chloride. Figures 5.5 and 5.6 show two boulders located at the same depth below the covered surface, together with the pore water sample collection points. The tabular data below each photograph provide the tracer concentrations that correspond to sample locations indicated in the photographs and describe the relationship between the structure and the adjacent matrix material using designations defined by Bellehumeur (2001). In the near-surface samples, the presence of chloride with an above average concentration is interpreted to represent a region having a lower pre-cover flow rate. In these areas, the chloride remained at a higher than average concentration of other samples at that depth. Similarly, the presence of elevated δD values suggest that post-cover flow occurred through this waste rock.

Figure 5.5 shows a boulder located approximately 0.5 m below the base of the cover, and above lysimeter 5. Sample point A had a δD value of approximately -102 ‰. Sample points B and C had elevated δD values of approximately -114 ‰. $\delta^{18}O$ data exist only for points A, B and D around the boulder shown in Figure 5.5, and were -10.2, -10.1 and -12.4 ‰, respectively. Assuming that the maximum δD shift that could result from evaporative fractionation alone is approximately -110 ‰, (Marcoline et al. 2006), deuterium from the tracer application in 2003 was observed in pore water in sample location A, located 0.15 m below the base of the cover. Since B has an $\delta^{18}O$ value of -10.1 ‰ and plots directly on the evaporative fractionation line, the elevated δD values in samples B and C are likely a result of evaporative fractionation. Similarly, water labeled with the δD tracer was not observed in sample points D, E or F. In this location, deuterium tracer traveled to a maximum depth of 0.15 m below the cover in the one-year following the tracer application, significantly less distance than in other areas in the CPE. Based on the high chloride concentration observed in the near-surface samples, A and B shown in Figure 5.5, it appears that the pre-cover water flux was also low in the vicinity of this boulder. Nichol (2003) documented chloride concentrations of pore water collected from tensiometers as high as 2000 mg/L in the top 0.2 m of the CPE shortly following the tracer release. Within nine months, concentrations dropped to less than 50 mg/L from the same three sample locations. While chloride concentrations of 80 and 82 mg/L are low compared to the source concentration of the tracer release, they are greater than three times the average chloride concentration observed in the top 0.5 meters of the CPE at the time of deconstruction. A low pre-cover water flux may explain why an elevated chloride tracer was retained within 0.15 m of the CPE surface.

Figure 5.6 shows a boulder located approximately 0.5 m below the base of the cover above lysimeters 12 and 16. Note, the blue vertical line in the photograph was a deconstruction marker and is irrelevant to the discussion. The relationship between tracer values from pore water and the location relative to the boulder are opposite of those observed around the boulder from the same depth shown in Figure 5.5. Deuterium indicative of the applied tracer was observed in all seven sample locations around this boulder without an obvious relationship to the boulder. The variability in δD values shows the highly heterogeneous nature of the post-cover water flow. All samples have lower than average chloride concentrations and high δD values suggesting mixing of both pre-cover and post-cover water. An above average pre-cover water flux and localized post-cover preferential flow may explain the pattern of pore water tracer concentrations around this boulder.

Flow patterns in relation to a particular structure will depend upon the rate and magnitude of the water delivered from above. This, in turn, is controlled by the characteristics of the waste rock above the structure, the water flow paths, the rate and magnitude of the infiltration and the water content of the waste rock prior to the infiltration event. The chloride tracer was applied in a high volume, high intensity event when the waste rock was already wet from previous rainfall events. Following the chloride application, greater than four years of artificial and natural precipitation fell on the uncovered waste rock and much of the chloride tracer was removed in outflow (Section 5.3.4). The remaining chloride was distributed throughout the entire pile with elevated concentrations associated with presumed very low flow zones. In contrast, the deuterium tracer was applied in a low intensity, low volume event on the covered surface of the CPE, when the waste rock had drained to less than 10% volumetric water content, near residual saturation, at the time the tracer was applied. The tracer application and subsequent rainfall resulted in limited infiltration into the waste rock and likely flow was dominantly through the finer matrix material. During the rainfall events on the covered CPE, when the waste rock was approaching residual saturation, it is likely that the water was diverted around the boulders and drawn by capillary forces into the matrix material instead of pooling and flowing on top of the surface of boulders.

While correlations of tracer concentrations and specific structures, for example, shadow zones versus drip zones and the collection of water on boulders, were ambiguous, several conclusions can be drawn. First, the δD values are variable within the upper one meter of the pile, even in areas without large structures such as boulders. Second, the relationship between boulders and remaining chloride concentrations suggests that the two tracers exist in different networks of pores in the upper one meter of the pile. For example, samples surrounding the boulder shown in Figure 5.5 have elevated chloride and low δD values, and samples surrounding the boulder shown in Figure 5.6 have elevated δD values and low chloride concentrations.

In addition to the boulders, coarse rubble zones and sloping layers were identified and target samples were collected. Relationships between these structures and tracer concentrations were not identified. Earlier experiments documented surface topography and surface texture as contributing factors to the flow behavior observed in highest flowing lysimeter 6 (Marcoline et al, 2003). Subsequent work showed that surface topography and surface texture could not alone be responsible for these observations (Chapter 3). As a result, it was concluded that in addition to topography and texture, a direct link between the internal structure and the high flow rates must exist. Contrary to initial expectations, there were no obvious structures in the waste rock above lysimeter 6, with the exception of a 1.2 m wide boulder above the corner of lysimeters 1, 2 and 6 (Figure 5.7.a). The waste rock above lysimeter 6 was matrix-dominated with no large rubble zones and was not noticeably different than the matrix-supported portions of the surrounding lysimeters, with the exception of a 2.5 m high coarse zone in lysimeter 10 (Figure 5.7.b.). The large boulder was located 2.4 m below the cover surface and sloped away from lysimeter 6, toward lysimeter 1. The coarse rubble zone in lysimeter 10 was located directly in the center of the lysimeter and is apparently unrelated to the high flows in lysimeter 6. Based on these observations, it is concluded that large observable structures may not be necessary for a structurally controlled flow system.

5.3.2. Dye Staining on the CPE

After removal of the top two lifts, no distinctive structures or differences in the waste rock characteristics above lysimeter 6 had been observed (Section 5.3.1) that might explain the large difference in volume reporting to each lysimeter as outflow. To further investigate the flow, a dye stain was applied on the top of the third lift to identify any physical flow paths that might help explain the higher flow rates observed in lysimeter six. The surface of the CPE was often far from saturated prior to the large rainfall events that induced preferential flow; in order to reproduce these conditions, the staining event was applied without saturating the waste rock. The waste rock had a volumetric water content of approximately 8% prior to the dye stain event and matric suctions were relatively high (-27 kPa) as inferred from the waste rock SWCC. As a result of the high matric suction, sorptivity was likely high and would have a significant effect on limiting the depth of the flow during the application of the dye.

The entire surface was stained a dark purple from the dye (Figure 5.4), however, much of the area had little to no staining below the top 1 cm of waste rock. Dye staining was observed in approximately 15% of the surface area at a depth of 5 cm. Below the 5 cm depth, the majority of dye was observed in four to five isolated locations with depth to width ratios between 3:1 and 10:1. The stained flow paths appeared to be between 5 and 10 cm wide and followed irregular paths for the first 20 to 30 cm (Figure 5.8). In the upper 20 cm to 30 cm, several of the stained flow paths were structurally controlled and exhibited a small degree of boulder hopping within the small, isolated, finger-shaped flow paths. Bellehumeur (2001) described boulder hopping as a thin layer of focused flow on the surfaces of adjacent boulders with little flow in the interstitial matrix material. The degree of staining of the matrix material was highly variable, and several of the stained flow paths were irregular and appeared to be independent of any observable structure. Below the 20 cm to 30 cm depth, the stained zones widened and predominantly existed in the finer grained matrix material (Figure 5.9).

The infiltration of the dye stain in the waste rock and the small amount of observed preferential flow was controlled by capillary forces. Even though light pink color was observed in the outflow of lysimeter 6, (2.4 m below the release) approximately eighty minutes after the beginning of the tracer application, no structures or macropores were observed to extend to the lysimeters.

The unstained waste rock beneath the release area was visibly wetter than the waste rock outside of the 9 m^2 area below the dye stain release. Several samples were collected for gravimetric water content. Two days after the application of the stain, the volumetric water content 70 cm below the stained area was 17%, approximately twice that of the average water content observed in the waste rock above the lysimeters surrounding the release area. The sample was collected from an area in which no stain was visible except the 1 cm surface layer 70 cm above. Based on a volumetric estimate, a homogeneous slug of water could have infiltrated to a depth of just under one meter following the stain application. Clearly the water did not move as a homogeneous slug below the stained area, and based on the dyed flow paths, it appears as if the 189 liters of stained water moved through the four to five isolated preferential flow paths. While many researchers consider rhodamine to be a conservative tracer, field evidence suggests that a separation of the dye and the carrier water was not only significant, but also occurred in a fairly short distance in the fine material. The sorption properties of rhodamine have been observed to increase with decreasing pH below 5 (Smart and Laidlaw, 1977, Bencala et al, 1986, Kasnavia et al, 1999). In a situation where the material is fairly dry (i.e., matric suctions are high, the dye application rate is moderate, and the pH is low (3.4)), the use of a dye stain may significantly over-accentuate the importance of preferential flow in the system. If the rhodamine is preferentially sorbed to the fines as a result of the high surface area, or if it is simply easier to visually identify in gravel or larger size particles, it will appear that preferential flow in the coarse material dominates even if volumetrically, it was insignificant. Without a separation of the dye and the carrier water, it is difficult to explain why so little dye was observed in the basal lysimeters below these preferential flow paths and to explain the elevated water content of the unstained waste rock below the dye stain release area. The applicability of using rhodamine as a visual dye stain in low pH, unsaturated materials is questionable.

5.3.3 Particle Size Analysis

Figure 5.10 shows the range of particle size distribution curves from 24 samples of waste rock collected during the deconstruction of the CPE. The dashed lines show the range in particle size distribution of 60 samples collected during the construction of the CPE in 1998, from the same size fraction of waste rock (Nichol, 2003). Hydrometer tests were not conducted and the fine silt and clay (less than 0.075 mm) material is undifferentiated. The table below the figure provides a summary of the average D10, D25, D50 and D90 values calculated for the 1998 and the 2004 samples. Based on the degree of weathering documented by Wagner et al (2006), an overall reduction in waste rock particle sizes was expected in the CPE over the 5.5 year-period. A reduction is not observed in the particle size distribution curves. The 1.5 mm to 100 mm size fractions cannot be distinguished statistically. In contrast, a decrease in the relative percentage of sub-1.5 mm size fractions was observed within the CPE after the 5.5 year-period and as shown by the decrease in D10 fraction between 1998 to 2004. Presumably, a percentage of the fine silt and clay was washed from the CPE over the course of the experiment. The assumption of migration of the fine silt and clay is reasonable based on the high turbidity observed in outflow following large rainfall events, and based on the large amount of fines observed in the washed gravel drainage layer during the deconstruction.

While obvious structures influencing flow were not observed, a potential correlation between lysimeters recording higher outflow rates and increased coarseness of the waste rock is evident in the particle size distribution curves. Figure 5.11 shows eight of the 24 particle size distribution curves collected from vertical profiles. An expanded view of the eight curves shows the relative position of samples from waste rock located above lysimeters 1, 3, 5, 6, 9, 7, 11 and 13. The minus 1 mm portions of the eight curves curves shown are nearly identical. The waste rock from samples above lysimeters 6, 7, 11 and 13 have a coarser texture in the 1 mm to 20 mm size fractions relative to waste rock above lysimeters 1, 3, 5 and 9, and were observed to have flow spikes following large rainfall events on the uncovered waste rock pile (Figure 5.5). Samples from above lysimeters 1, 3, 5 and 9 are finer in texture, and correspond with lysimeters that typically did not exhibit the large flow spikes, or had a lower cumulative outflow following large rainfall events. The same relationship between lower flow and finer particle sizes is also evident in particle size curves measured from waste rock collected within lysimeters 2, 3, 4, 8 and 10. The remaining 10 particle size distribution curves not shown here plot between the two groups shown in Figure 5.11. To better examine correlation between the lysimeters exhibiting fast flow spikes and the rock mass above the lysimeters containing the coarsest texture, SWCC's and HCC's were estimated based on the 24 particle size distribution curves using the Fredlund and Xing (1994) method. The SWCC's all had a nearly identical slope and residual saturation, and the estimated air entry value varied less than a tenth of a kPa. Similarly, the hydraulic conductivity curves were nearly identical in the 0 to 100 kPa range. While it is not evident in the estimated soil hydraulic properties, it appears likely that the higher percentage of 1 mm to 20 mm particle sizes contribute to the spikes in flow rate following large rainfall events and that the majority of fast outflow observed in lysimeter six likely flowed through the coarse end of the fine fraction. A larger number and a more comprehensive coverage of particle size analyses might help to strengthen this relationship between the percentage of 1 mm to 20 mm particle sizes and the spikes in flow rate. However, if the structure of the coarser fraction controls the outflow response, this relationship would not be evident in the SWCC's estimated from the particle size curves.

An attempt was made to relate the particle size distribution curves with values of post-cover deuterium tracer measured from pore water extractions. No correlation between relative particle size and deuterium tracer values were evident. Likely, the post-cover water flow was contained within the matrix material (<1 mm) for which all measured particle distribution curves are similar (Figure 5.11).

5.3.4. Tracer Distributions

Nichol (2003) estimated that 34% of the chloride tracer exited the base of the uncovered pile in the first year, based on data from lysimeter outflow and from soil water solution samplers. While Nichol estimated the mean residence time of chloride in the CPE was between 1.8 and 2.4 years, he predicted that the breakthrough curve would have a long tail caused by dispersive effects and diffusive transfer into immobile zones. Using this estimate of chloride residence time for the pre-cover condition as the minimum value for post-cover conditions, the deuterium tracer would be expected to be contained in the upper portion of the waste rock pile at the time of deconstruction. Based on TDR data from within and immediately below the compacted cover layer, wetting fronts and likely water infiltrating during the deuterium tracer event migrated at least to the base of this layer during the 6-hour tracer application (Figure 5.12). Unfortunately, it was not possible to extract sufficient water from the compacted cover samples using the centrifugal method to determine their deuterium tracer values.

The distribution of the deuterium (δD) tracer and the chloride (Cl) tracer within the waste rock pile at the time of deconstruction as a function of sample depth is plotted in Figure 5.13. Samples with δD values above background are located as deep as 3.2 m below the cover and range from -121 ‰ to as high as -63 ‰ at the time of deconstruction. There is high spatial variability in the δD values, however, deuterium was not observed in the bottom 1.5 m of the CPE. The distribution of chloride in the pile at the time of deconstruction also varies in the horizontal plane, as well as with depth. The chloride concentrations of 160 pore water extractions range from 0 to 107 mg/L after subtracting the background concentration of 20 mg/L. Independent of depth, the distribution of chloride concentrations exhibit a slight positive skew with the majority of values between 5 and 40 mg/L and a geometric mean of 24 mg/L. In the portion of the pile less than 2 m in depth, the concentrations follow a Gaussian distribution with an arithmetic mean of 22 mg/L, close to the geometric mean of 24 mg/L for all samples. The uniform distribution of chloride values in the upper portion of the pile five years after tracer release is evidence for exchange of the tracer with less mobile zones within the CPE.

The samples below 2 m exhibit a higher degree of skewness, with an arithmetic mean of 34 mg/L and a geometric mean of 23 mg/L as a result of a few samples with higher chloride concentrations. A peak outflow concentration of chloride of approximately 600 mg/L, and flux-averaged chloride concentration of approximately 150 mg/L occurred in July of 2000, nine months after tracer application (Nichol, 2003). Peak concentrations are the highest observed concentration among the 16 basal lysimeters, while the flux-averaged concentration is determined by outflow and concentration from all 16 lysimeters. July of 2000 was the beginning of the decline in both peak and flux-averaged chloride concentrations measured in the basal lysimeters. Nichol measured peak chloride concentrations in pore water from soil water solution samplers of approximately 2000 mg/L in the fall of 1999 at 0.2 m below the surface. Peak concentrations of 300 mg/L were measured at a depth of 4.5 m below the surface in July of 2000. While the in-situ chloride concentrations at the time of deconstruction do not define a trend of increasing chloride with depth, the higher chloride concentrations in the lower portion of the CPE are consistent with a tail of an instantaneous tracer release. A larger number of chloride analyses from the waste rock below 2 m in the CPE would have provided the data necessary to better characterize the chloride distribution in pore water. It is suggested that with additional time, the chloride concentrations throughout the pile would have become evenly distributed about the average value observed in the upper portion of the pile. To better understand the pattern of observed chloride concentrations with depth, the relationship between the distribution of pore water chloride concentrations and the in-situ δD values from the same samples was evaluated.

A cross plot of the chloride pore water concentrations and the δD values is shown in Figure 5.14. All samples plotted contain a component of the water released during the chloride tracer test. The three zones in the plot identify which samples contain, potentially contain, and do not contain water from the deuterium tracer test. The shaded zone has δD values below the background values of -121 ‰, which likely have no deuterium from the tracer event. The hatched zone contains approximately 40 samples with elevated deuterium between -120 ‰ and -110 ‰, as well as chloride from the 1999 tracer event. In these samples, the elevated δD may have resulted from the 2003 tracer event or from either evaporative fractionation or diffusive fractionation with the surrounding water. The relative proportions of the contribution from the tracer event, or from fractionation, cannot be distinguished without the corresponding $\delta^{18}O$ value. Samples plotting in the unshaded zone have δD values greater than -110 ‰ and contain a component of the water released during the tracer test. Given the three years between the two tracer releases, and given that the deuterium tracer was applied following placement of the cover, a trend from higher (less negative) deuterium and lower chloride concentrations near-surface to lower deuterium and higher chloride concentrations at depth would be expected. A range of the amount of interaction between the two tracers is observed, however, a single, well-defined trend line cannot be drawn. Despite a lack of a strong trend in these data, patterns are evident. Samples are observed with low chloride and a full range of deuterium values, and no samples are observed with both high chloride concentrations and high deuterium values. Each of these patterns are described below.

Samples with low chloride concentrations are observed to have both low and high δD values. The subset of these samples with near-background chloride and near-background deuterium are thought to identify areas that have experienced low to no post-cover flow, and likely low pre-cover flow. Several samples with near average chloride concentrations are also observed to have both low and high δD values and can be explained simply by the higher degree of spatial variability of the deuterium tracer relative to the slightly less variable nature of the chloride concentrations within the CPE. It is suggested that an average residual chloride concentration of approximately 22 mg/L (discussed above) is distributed throughout the finer-grained portions of pile and is characteristic of water in the pre-cover slower flow zones. In contrast, only a few samples exist with both high chloride concentrations and δD values greater than -110 ‰ and these samples are perhaps the most difficult to interpret. The paucity of samples exhibiting this relationship is attributed to the difference in depth of the peak concentrations.

Figure 5.15 (a and b) show δD values and chloride concentrations of pore water extractions versus depth in the CPE. Samples from two depths within the CPE contain a near-background (low) chloride concentration and high deuterium value. These samples are located between 0.5 m and 1 m deep and between 2 m and 3 m deep in the CPE. It is proposed that these samples from the 2 m to 3 m depth were collected from zones with faster pre-cover and post-cover flow. The high deuterium values at this depth result from preferential flow paths, even though the lower permeability cover was in place. These same pathways were likely fast flowing prior to cover application, resulting in much of the chloride tracer being flushed out. In contrast, a few samples with low chloride and high deuterium located between 0.5 m and 1 m deep are from areas of low flow that never contained chloride from the tracer event, and in which the deuterium remained near- surface due to very slow flow rates.

In summary, the pore water extractions from the upper half of the pile that contained high δD values typically contained lower-than-average chloride concentrations. Additionally, samples from this region with near-background δD values had chloride concentrations near the average value. Because of the small number of post-cover wetting fronts that moved through the CPE, and due to the relatively short duration between tracer application and deconstruction, limited interaction between the mobile and immobile zones occurred. As a result, a limited amount of mixing and/or diffusion of chloride occurred with younger δD labeled water. Interpretations of the chloride and δD results below 3 m are complicated because the majority of the samples that have δD values above background could be explained by fractionation of water that entered the pile prior to the deuterium tracer test. It appears that little tracer-derived deuterium exists at depths greater than 3.2 m below the surface. For the chloride remaining in the upper 2 m of the CPE to have not been flushed deeper in the pile, it is proposed that the transport is dominantly controlled by either diffusion or by very slow flow through fine portions of the CPE.

5.3.5. Chloride Mass Balance

Following the chloride tracer application in the fall of 1999, water samples from the outflow lysimeters and soil water solution samplers were collected for total tracer recovery calculations. Nichol (2002) estimated the total chloride mass flux through the CPE between August 1999 and October 2000 using flux-averaged chloride concentrations. As of October 2000, it was estimated 34% of the applied tracer had reported to the basal lysimeters. Nichol concluded that the peak chloride concentrations arrived at the base of the waste rock pile in July 2000, after only 0.5 pore volumes of water flowed through the pile. In this instance, the pore volume is defined relative to the average volumetric water in the CPE. Since the volumetric water content of the CPE as a whole changes with time, a long-term average water content of 16% was used. Nichol noted that July 2000 marked the beginning of a gradual decline in the chloride flux at the base of the waste rock pile. Chloride analyses of outflow samples collected at a high frequency (between every 15 minutes and three times per week) were not conducted after the summer of 2000, and therefore, the tracer outflow rate between 2000 and the time of CPE deconstruction cannot be determined. Based on the CPE deconstruction samples, 2.2% (by mass) of the applied chloride tracer remained in the waste rock pile after five years (Figure 5.16). During these five years, 1.9 pore volumes of water flowed through the CPE. Pore volumes were calculated using an average resident pore water volume within the CPE as estimated by TDR, and cumulative lysimeter outflow. The calculation of the mass of chloride remaining in the CPE is based on the chloride concentrations of pore water at the time of deconstruction, the measured volumetric water content and porosity. To account for the increased chloride concentrations with depth, the concentration of pore water is calculated as the mean of the average chloride concentration of each of the five, one-meter deep intervals within the CPE. The chloride remaining could be as low as 2% and as high as 6% using the estimated minimum and maximum possible values of volumetric water content and porosity.

In the first year following the application of the chloride tracer, the concentration in outflow varied greatly in response to outflow derived from higher intensity rainfall events. Periods of highest water flux corresponded to periods of highest chloride flux, as shown in Figure 7.8 of Nichol (2003), and a large percentage of the chloride tracer was transported down deeper in the pile during the larger flow events. Considering that the average water residence time was estimated to be between 1.8 and 2.4 years, preferential flow pathways were likely responsible for the rapid chloride transport. Nichol (2003) noted that chloride concentration increased in the outflow water following large rainfall events between 1999 and the summer of 2000, and that the opposite was observed after July 2000. By July of 2000, 0.3 pore-volumes of water had flowed through the CPE (Figure 5.16). After this time, the outflow response following large rainfall events showed decreasing chloride concentrations and a higher percentage of post-tracer water. The change in the relationship resulted from a shift in the dominant mechanism of chloride transport. Following this change, the flux-averaged concentration of the chloride tracer arriving at the base of the pile decreased in the summer months with the increase in preferential flow and increased in the winter months (Nichol et al, 2005). While a positive correlation between the tracer recovery and resident pore volumes in the first year can be made, after 2000, mass flux appears to have been more dependent on the rate of matrix flow within the CPE than on total volume of flow through the CPE.

This finding has practical implications for field rinsing and natural drain down of mine materials and is often neglected in studies. Large column studies by Cathels and Murr (1980), leach drain down studies by BOM (1984), and post-operational rinsing studies by the U.S. EPA (1994a), Logsdon and Mudder (1995) and Brown et al (2003) correlate the volume of incident rain water or applied solution to measured mass in basal outflow to make loading or recovery predictions. In contrast, some studies (O'Kane and Haug, 2000) stress the importance of the effect of flow rate, rather than flow volume, on leaching efficiency, but few include an evaluation of the effects of preferential flow. In other words, the investigation of mass recovery versus pore volumes of flow does not allow for the differentiation between flow processes which are flow-rate dependent and likely to occur in natural systems. In the CPE, numerous wetting and drying cycles likely resulted in a redistribution of the chloride tracer into the matrix material throughout the pile as discussed above. Following the redistribution of the chloride tracer within the pile, a higher percentage of the incident rainfall would preferentially flow through the uncovered pile in response to large rainfall events without an increase in tracer recovery rate at the base. Following covering of waste rock, the relationship between pore volume and mass flux again becomes more representative of the dominant flow processes, assuming that a fairly homogeneous distribution in chloride concentrations already exist within the mobile fraction of the pore water, and assuming that fast flow paths that can deliver fresh water deep into the pile are no longer active.

Figure 5.16 presents the cumulative release of chloride tracer from the waste rock pile as a function of time. The first 11 data points are from measured mass fluxes at the base of the CPE by Nichol (2003) and Nichol et al (2005). The final point is based on the measured chloride in pore water at the time of deconstruction. There are no data to justify the shape of the curve between 0.5 and 1.9 pore volumes, however, because the majority of the chloride was exiting the CPE in matrix flow paths, it is suggested that chloride concentrations in outflow after October of 2000 would not exhibit a pattern of higher seasonal mass flux. It seems likely that the mass flux continued on a similar trend to that observed in the later portion of 2000, with a gradual flattening of the slope before 2004. At what time and how fast the chloride concentrations flattened out is unknown and depends on the mass of chloride located in the mobile matrix material relative to the mass in the slowest flow zones, or the immobile zones. Since chloride was observed in the same network of pores as the mobile deuterium tracer, it appears that chloride is still being advectively transported in these portions of the pile. It is unclear whether diffusive transport or slow advective transport of chloride is dominant in the top two meters of the CPE. It is unlikely that the addition of the cover had a significant affect on the rate of the chloride mass flux at the base of the CPE.

Caution must be used in translating the chloride tracer data to metal loadings at the base of the CPE. The chloride model presented assumes that the chloride has been rinsed from the fraction of material through which the fast flow occurred and only exists in a portion of the fine matrix material. Weathering products associated with ARD may be continuously produced and the ARD in outflow would be expected for a much longer time. Since ARD generation occurs primarily in the finer as well as in the coarser pore spaces, a break in slope of the loading curve would be expected following the addition of the cover. The cover would limit the flow in the coarser pores, and the flushing of any weathering products within them. The manner in which the mass flux from a waste rock pile is evaluated may have significant implications on long-term predictions of effluent quality, as well as the practicality of rinsing leach heaps and on closure designs.

5.4. CONCLUSIONS

Detailed deconstruction of the experimental waste rock pile at the Cluff Lake Mine has allowed for greater understanding of the fluid flow paths and the mechanisms influencing transport of the deuterium and the chloride tracer within the CPE. Water flow and tracer transport was spatially variable in the uncovered and covered waste rock pile and preferential flow resulted in deuterium as deep as 3.2 m in the CPE. The location of the remaining chloride tracer (2.2% by mass) in the waste rock pile after five years was variable and appeared to be located in the portions of the waste rock that experienced the slowest water flow. The presence of high chloride concentrations in a few isolated locations near the surface of the CPE, and the lack of deuterium in the same samples suggests that portions of the waste rock may have been largely isolated from post-cover water flow.

While a consistent correlation between observed tracer values and specific structures did not exist at the time of deconstruction, the in-situ spatial distribution of chloride and deuterium tracer allow for a physically-based understanding of water flow at a local scale. The internal structure of the waste rock was highly variable with coarse rubble zones, lenses of fine matrix material and variably oriented, discontinuous textural boundaries, yet a direct link between intermediate-scale waste rock structure and spatial distribution of basal outflow could not be established. Intermediate-scale structures such as boulders had a localized influence on water flow as observed from dye stain patterns and tracer patterns, but a minimal influence on the bulk water flow and bulk transport of tracers through the waste rock. The use of rhodamine as a dye tracer in acidic, unsaturated waste rock with low water contents may be misleading and over-emphasize the role of preferential flow. Variations of the particle size distribution, specifically higher percentages of the waste rock between 1.5 mm and 20 mm may have had the largest effect on the presence of the fast flow spikes, and on the large degree of variability in spatial distribution of the lysimeter outflow.

5.5. REFERENCES

American Society for Testing and Materials (ASTM), 1990. Standard test method for particle size analysis of soils (D422-63; re-approved 1990). Annual Book of ASTM Standards. v. 04.08.

American Society for Testing and Materials (ASTM), 1994. Standard practice for correction of unit weight and water content for soils containing oversize particles (D4718-87; reapproved 1994). Annual Book of ASTM Standards. v. 04.08.

Aubertin, M., Mbonimpa, M., Chapuis, R.P., 2003. A model to predict the water retention curve from basic geotechnical properties. Canadian Geotech. J. v.40. pp. 1104-1122.

BOM, 1984. US Department of the Interior, Bureau of Mines, Gold and Silver Leaching Practices in the United States, Information Circular No. 8969, Washington, DC.

Baker, R.S. and Hillel, D., 1990. Laboratory tests of a theory of fingering during infiltration into layered soils. Soil Sci. Soc. Am. Journal. v. 54. pp. 20-30.

Bellehumeur, T.M., 2001. Mechanisms and spatial variability of rainfall infiltration on the Claude waste rock pile. MA Sc thesis, University of British Columbia, Vancouver.

Bencala, K.E., McKnight, D.M., Zellweger, G.W. and Goad, J., 1986, The stability of rhodamine WT dye in trial studies of solute transport in an acidic and metal-rich stream: U.S. Geological Survey Water Supply Paper 2310.

Beven, K., Germann, P., 1982. Macropores and water flow in soils. Water Resources Research. v. 18. no. 5. pp. 1311-1325.

Bowen, G.J. and Wilkinson, B, 2002. Spatial distribution of $D^{18}O$ in meteoric precipitation. Geology. v. 30. no. 4. pp. 315-318.

Brooks, R. H. and Corey, A. T., 1964. Hydraulic properties of porous media. Colorado State University (Fort Collins), Hydrology Paper No. 3.

Brooks, R. H. and Corey, A. T., 1966. Properties of porous media affecting fluid flow. Journal of the Irrigation and Drainage Division, ASCE. v. 92. pp. 61-89.

Brown, P.L., Garvie, A., Davidson, P., Deans, B., Pocock, B., 2003. Decommissioning, closure and rehabilitation of the heap leach system at the Girilambone Copper Mine, Central New South Wales, Australia Heap Leach Closure Workshop. Elko, Nevada.

Carter, M.R., ed., 1993. Soil sampling and methods of analysis. Canadian Society of soil Science, Lewis Publishers.

Cathles, L.M. and Murr, L.E., 1980. Evaluation of an experiment involving large column leaching of low grade copper sulfide waste: a critical test of a model of the waste leaching process Schlitt, W.J., Ed.; Society of Mining Engineers. pp. 1-19.

Eaton, A.D., Clesceri, L.S., Greenberg, A.E., 1995. Standard methods for the examination of water and wastewater, 19th ed., American public health association, American water works association, water environment federation.

Fines, P., Wilson, G.W., Willams, DJ., Tran, A.B. and Miller, S., 2003. Field Characterization of two full-scale waste rock piles. Proceedings Sixth International Conference on Acid Rock Drainage.

Fines, P., 2006. Hydrologic characterization of two full-scale waste rock piles. MSc. thesis, University of British Columbia, Vancouver.

Flury, M., Fluhler, H., Jury, W.A. and Leuenberger, J., 1994. Susceptibility of soils to preferential flow of water: A field study. Water Resources Research. v. 30. pp. 1945-1954.

Flury, M. and Wai, N.N., 2003. Dyes as tracers for vadose zone hydrology, Rev. Geophys., v. 41(1), p. 1002.

Fredlund, D.G. and Xing, A., 1994. Equations for the soil-water characteristic curve, Canadian Geotechnical Journal. v 31. pp. 521-532.

Fredlund, D.G., Xing, A. and Huang, S. 1994a. Predicting the permeability function for unsaturated soils using the soil-water characteristic curve, Canadian Geotechnical Journal. v 31. pp. 533-546.

Guebert, M.D., Gardner, T.W., 2001. Macropore flow on a reclaimed surface mine: infiltration and hillslope hydrology. Geomorphology. v. 9. pp. 151–169.

Hangen, E., Gerke, H.H., Schaaf, W., Huttl, R.F., 2004. Assessment of preferential flow processes in a forest-reclaimed lignitic mine soil by multicell sampling of drainage water and three tracers, Journal of Hydrology. v. 303. no. 1-4. pp. 16-37.

Hayes, K.R., 1993. Minesoil texture, macropore development and the evolution of minesoil hydrology on reclaimed surface mines in Pennsylvania. MS Thesis, The Pennsylvania State Univ., University Park, PA. 107 pp.

Herasymuik, G.M., Wilson, G.W., Barbour, S.L. and Smith T., 1995. The characterization of hydrologic properties and moisture migration pathways of a waste rock pile., Proceedings of the Nineteenth Annual British Columbia Mine Reclamation Symposium. pp. 234-244.

Herasymuik, G.M., 1996. Hydrogeology of a waste rock dump. M.Sc. Thesis. Department of Civil Engineering, University of Saskatchewan, Canada.

Higgs, H.A., Simons, T.W., Murphy, F.M., Stewart, C.J., 1997. ARD assessment program from exploration to operation: Case Studies from the Eskay Creek Mine. Proceedings of the Fourth International Conference on Acid Rock Drainage. v. 1. Vancouver, British Columbia. pp. 387-398.

Kasnavia T., Vu, D. and Sabatani, D.A., 1999. Fluorescent dye and media properties affecting sorption tracer selection. Ground Water. v. 37. pp. 376-381.

Logsdon, M.J. and Mudder, T.I., 1995. Geochemistry of spent ore and water treatment issues, Proceedings of the Tailings and Mine Waste 1995 Meeting and Summitville Forum, Ft. Collins, Colorado, USA, January.

Marcoline, J.R., Beckie, R.D., Smith, L. and Nichol, C.F., 2003. Mine waste rock hydrogeology - The effect of surface configuration on internal water flow. Sixth International Conference Acid Rock Drainage.

Marcoline, J.R., Smith, L, Beckie, R.D., 2006, Water migration in covered waste rock, investigations using. deuterium as a tracer. Proceedings of the 7th International Conference on Acid Rock Drainage, R.I. Barnhisel (ed.). The American Society of Mining and Reclamation. pp. 1142-1156.

Murr, L.E., 1979. Observations of solution transport, permeability, and leaching reactions in large, controlled, copper-bearing waste bodies. Hydrometallurgy. v. 5. pp. 67-93.

Nichol, C.F., Smith, L. and Beckie, R., 2002. Evaluation of uncoated and coated time domain reflectometry probes for high electrical conductivity systems. Soil Sci. Soc. Am. Journal. v. 66. pp. 1454-1465.

Nichol, C.F., 2003. Transient flow and transport in unsaturated heterogeneous media: Field experiments in mine waste rock. Ph.D. dissertation, University of British Columbia, Vancouver.

Nichol, C.F., Smith, L. and Beckie, R., 2003. Water Flow in Uncovered Waste Rock - A Multi-Year Large Lysimeter Study. Sixth International Conference Acid Rock Drainage.

Nichol, C.F., Smith, L. and Beckie, R., 2005. Field scale experiments of unsaturated flow and solute transport in a heterogeneous porous medium, Water Resources Research. v. 41.

O'Kane, M. and Haug, A., 2000. Demonstration of the Application of Unsaturated Zone Hydrology for Heap Leach Optimization Industrial Research Assistance Program Contract # 332407.

Saretzky, G.T. and Wilson, G.W., 2000. Hydrological characterization of a sulphide waste rock dump. Proceedings of the 52nd Canadian Geotechnical Conference. pp. 495-592.

Shaw, S., Wels, C., Robertson, A. and Lorinczi, G., 2002. Physical and geochemical characterization of mine rock piles at the Questa Mine, New Mexico: An Overview. Proceedings of the Ninth International Conference on Tailings AMD Mine Waste, Fort Collins, Colorado. pp. 447-458.

Smart, P. L. and Laidlaw, I. M. S., 1977. An evaluation of some fluorescent dyes used for water tracing. Water Resources Research.. v. 13. no. 1. pp. 15-33.

Smith, L., Lopez, D., Beckie, R.D., Morin, K., Dawson, R. and Price, W., 1995. Hydrogeology of waste rock dumps. Report prepared for CANMET and BC Ministry of Energy, Mines and Petroleum Resources. pp. 1-130.

Smith, L. and Beckie, R., 2003. Hydrological and geochemical transport processes in mine waste rock, Ch 3 in Environmental Aspects of Mine Wastes, Mineral. Assoc. Canada, Short Course Series. v. 31. pp. 51-72.

Soregaroli, B.A. and Lawrence, R.W., 1998. Update on waste characterization studies, paper presented at Mine Design, Operations & Closure Conference, Polson, MT, 10 p.

Stockwell, J.E., 2002. Investigation of hydrological and geochemical properties and spatial relationships of an unsaturated waste rock pile, Key Lake, Saskatchewan, Masters Thesis, University of British Columbia.

Stockwell, J., Beckie, R.D. and Smith, L., 2003. The hydrogeochemical characterization of an unsaturated waste rock pile, Key Lake, Saskatchewan, Canada. Sixth International Conference Acid Rock Drainage.

Stockwell, J., Smith, L., Jambor, J. and Beckie, R., 2006. Hydrogeochemistry of an unsaturated waste-rock pile, Key Lake, Saskatchewan, Applied Geochemistry. v. 21. pp. 1347-1361.

Su, G.W., Geller, J.T., Hunt, J.R. and Pruess, K., 2004. Small-scale features of gravity-driven flow in unsaturated rock fractures, Vadose Zone Journal, v. 3. n. 2. pp 592-601.

U.S. EPA, 1994a. Technical Document: Treatment of cyanide heap leaches and tailings. EPA 530/R-94-037.

Wagner, K., Beckie, R.D. and Smith, L., 2006, Geochemical characterization of mine waste rock, Cluff Lake, Saskatchewan., ICARD 7, St. Louis MO. Published by ASMR, 3134 Montavesta Rd., Lexington, KY.

Wang, Z., Jury, W.A., Tuli, A. and Kim, D., 2004. Unstable flow during redistribution. Controlling factors and practical implications., Vadose Zone Journal. v. 3. pp. 549-559.

Wilson, G.W., 2000. Embankment hydrology and unsaturated flow in waste rock., Slope Stability in Surface Mining, Chapter 33, Hustrulik, W.A., McCarter, M., Van Zyl, D.J.A., Editors. pp 305-310.

A)

B)

Figure 5.1. Photographs of the CPE. A) Side view. B) Top covered surface of the waste rock pile. The large grid lines approximate the 2 m by 2 m boundaries of underlying lysimeters. The smaller (16 red and 8 blue) squares mark the locations of sample pits and density test pits, respectively.

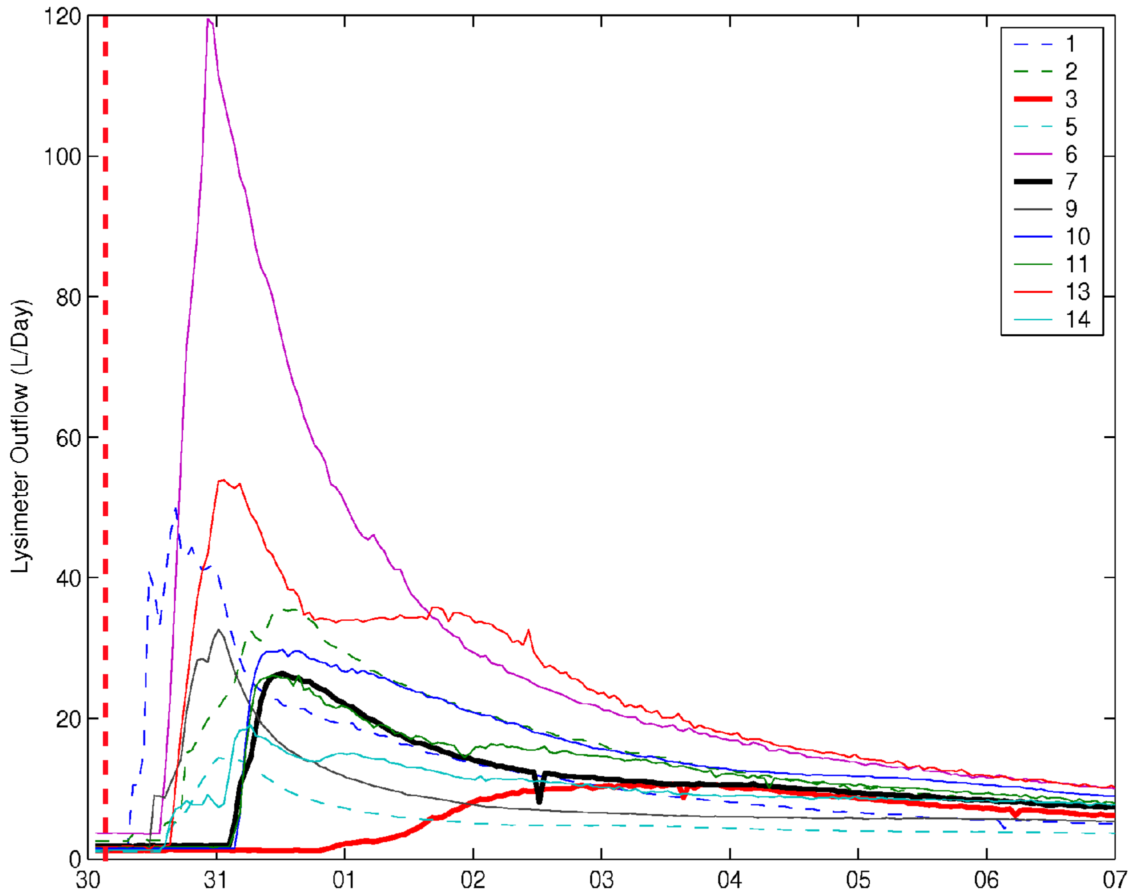

July 30, 2001 - August 07, 2001

Figure 5.2. Outflow hydrographs for a precipitation event on the free-dumped surface. The hydrographs are in liters per day for 9 days following a 40.8 mm natural rainfall event on 30th of July 2001. The red dashed line marks the rainfall event.

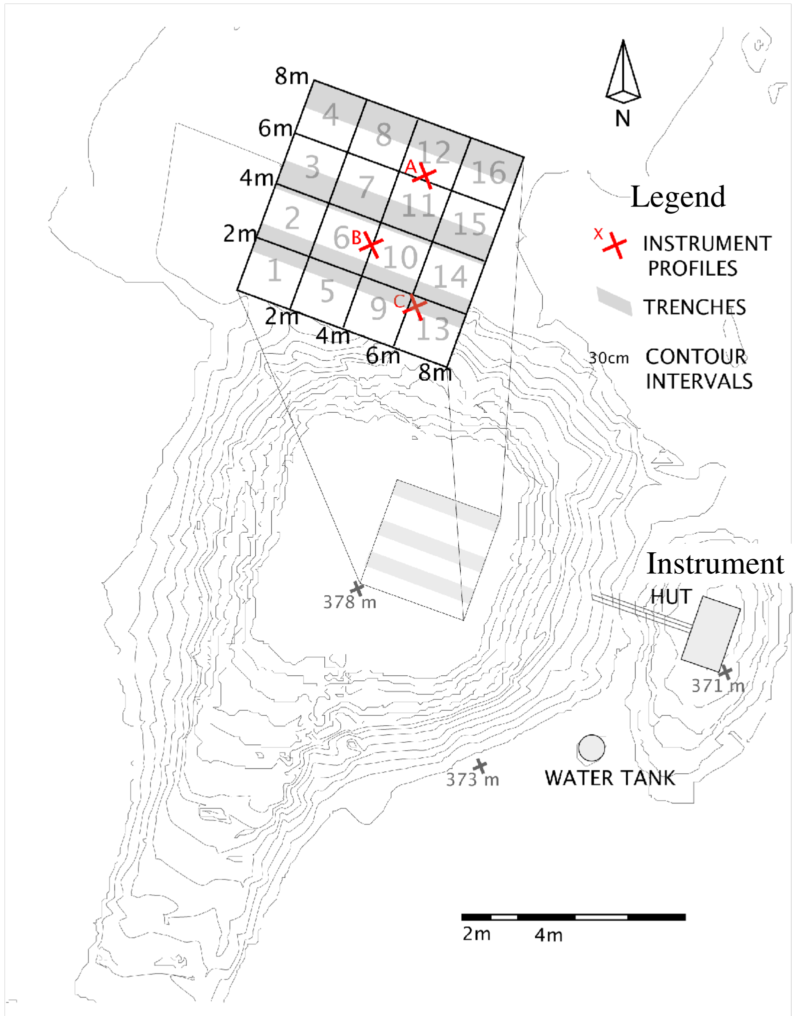

Figure 5.3. Schematic view of the top of the waste rock pile. Three trench locations within the lysimeter grid are shown. The trenches outside of the grid are not shown. The lysimeter grid is to scale and is superimposed topographic contours of the constructed waste rock pile. Contour intervals are intervals are 30 cm.

Figure 5.4. Photograph of the dye-stained area. The orange lines represents an outline of the underlying lysimeter grid. The dye stain was applied in the square shaded area that was centered above lysimeter 6. An area of 0.5 m overlap of the surrounding four lysimeters was included in the event that a focusing structure outside of the 2 m by 2 m area was present.

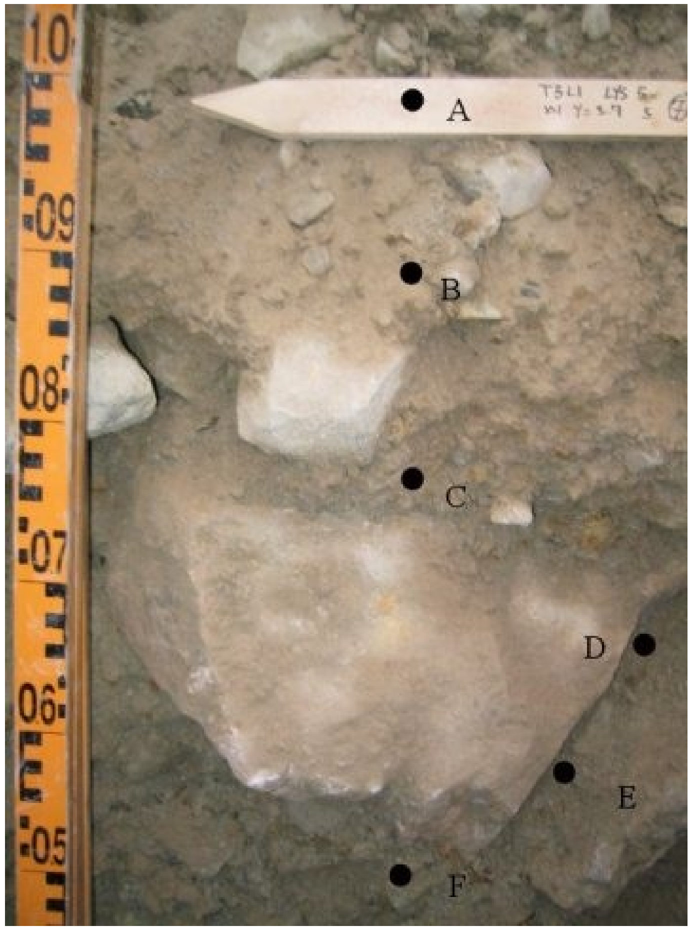

Sample	δD (per mill)	Cl (mg/L)	Notes
A	-۱۰۲.۸	۸۲	Matrix Above Rock
B	-۱۱۴.۹	۸۰	Gravel Zone Above Rock
C	-۱۱۴.۹	۴۹	Top Concave Surface
D	-۱۲۱.۳	۴۸	Shadow Zone Matrix
E	-۱۲۲.۱	۳۴	Shadow Zone Matrix
F	-۱۲۵.۳	۳۳	Potential Drip Zone

Figure 5.5. An intermediate size, matrix-supported boulder located approximately 0.5 m below the base of the cover. The δD values and the chloride concentrations of pore water are listed for each sample in the table above.

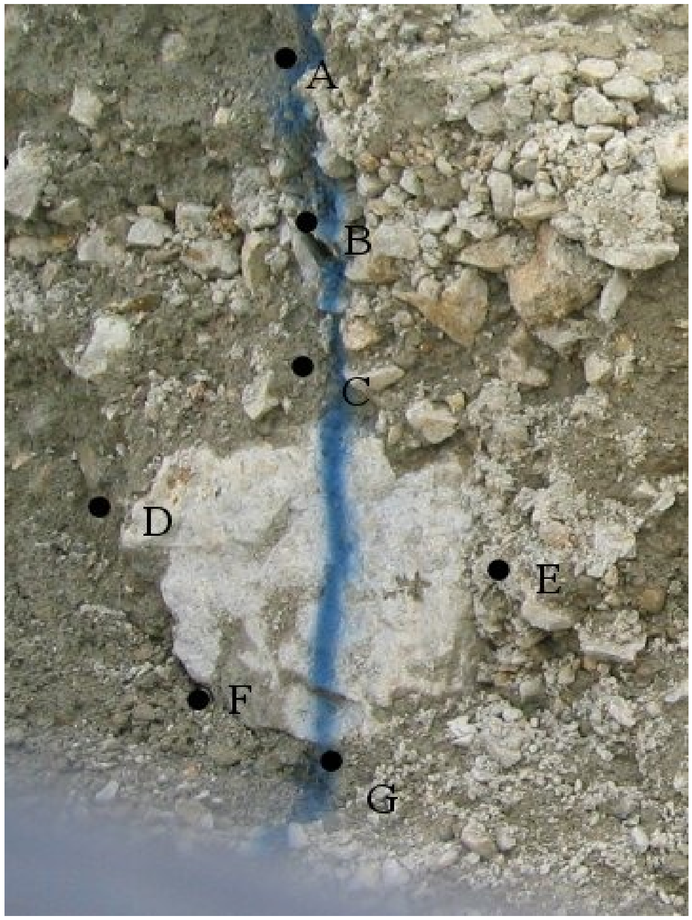

Sample	δD (per mill)	Cl (mg/L)	Notes
A	-۹۹.۵	۱۴	Above Capillary Barrier
B	-۸۹.۴	۱۹	Gravel Zone
C	-۱۰۷.۲	۶	Below Capillary Barrier, Above Rock
D	-۱۱۳	۱۲	Matrix on Side of Rock
E	-۸۵.۷	۲۱	Matrix on Side of Rock
F	-۹۱.۲	۱۵	Martrix Shadow Zone
G	-۱۰۶.۷	۱۲	Below Rock

Figure 5.6. An intermediate size boulder and gravel-supported by fine-grained matrix material located approximately 0.5 m below the base of the cover. The δD values and the chloride concentrations of pore water are listed for each sample in the table above. The blue line is a deconstruction marker with no relationship to the structure.

a)

b)

Figure 5.7 a) Photograph of 1.2 m boulder located above lysimeters 1, 2 and the southwestern corner of lysimeter 6. b) Coarse rubble zone in lysimeter 10. The coarse material continues below the photograph.

Figure 5.8. Photograph of trench face cut through the dye-stained area. Note the stained area directly beneath the application area is approximately 1 cm to 2 cm thick. The majority of stain observed below the surface is in localized zones, with depth to width ratios of greater than 3:1. The survey rod is one meter-long with 1 cm increments.

Figure 5.9. Photograph of trench face cut through the dye-stained area. Dye stains were narrow near the surface becoming more diffuse with depth.

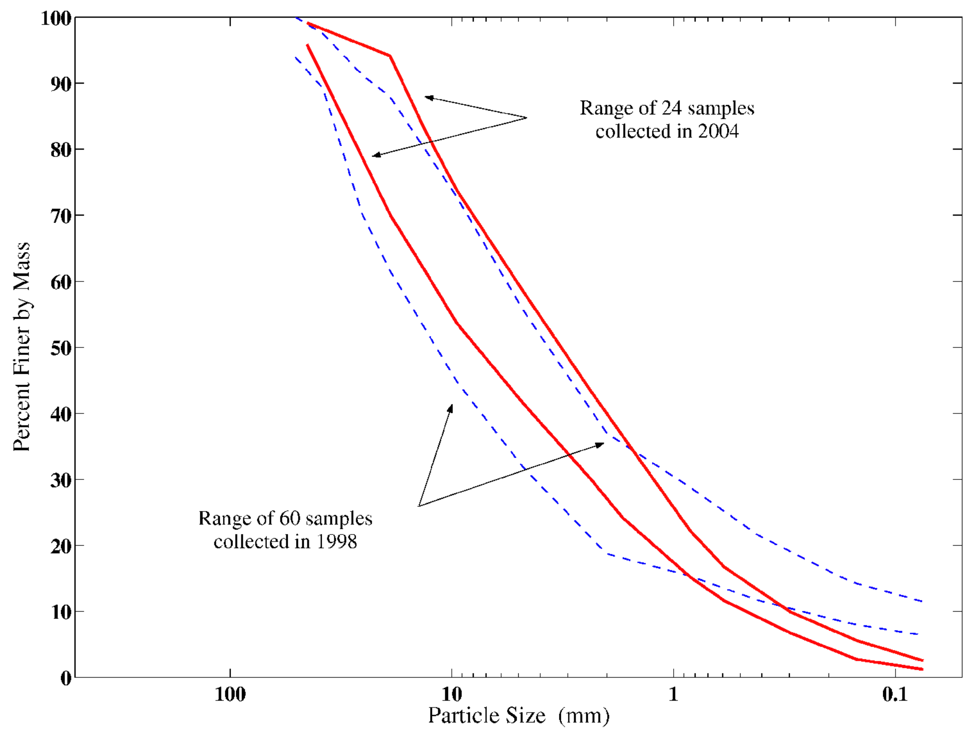

Size Fraction	۲۰۰۴			۱۹۹۸		
	mean	StDev	Std. error	mean	StDev	Std. error
D۱۰ (mm)	۰.۴	۰.۱	۰	۰.۱	۰.۱	۰
D۲۵ (mm)	۰.۶	۱.۴	۰.۳	۱.۷	۱.۸	۰.۳
D۵۰ (mm)	۵.۷	۳.۸	۰.۷	۵.۸	۷.۸	۱
D۹۰ (mm)	۲۱	۵.۶	۱.۱	۲۷	۲.۸	۰.۴

Figure 5.10. The solid (red) curves show the range of 24 particle size distribution curves from samples collected during the deconstruction of the CPE in 2004. The dashed (blue) curves show the range of 60 particle size distribution curves from samples collected during the construction of the CPE in 1998. The table shows the average D10, D25, D50 and D90 values and the corresponding particle sizes in millimeters.

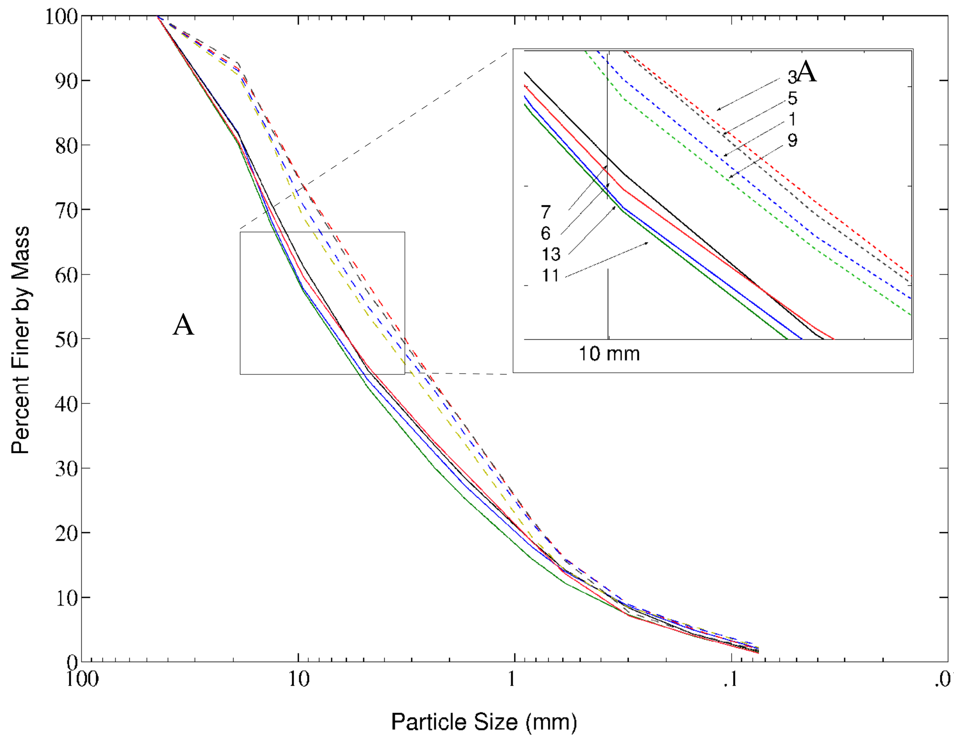

Figure 5.11. Particle size distribution curves for eight samples from within the CPE. The dashed lines are curves from material above lysimeters 1, 3, 5 and 9, and the solid lines are curves from samples collected above lysimeters 6, 7, 11 and 13.

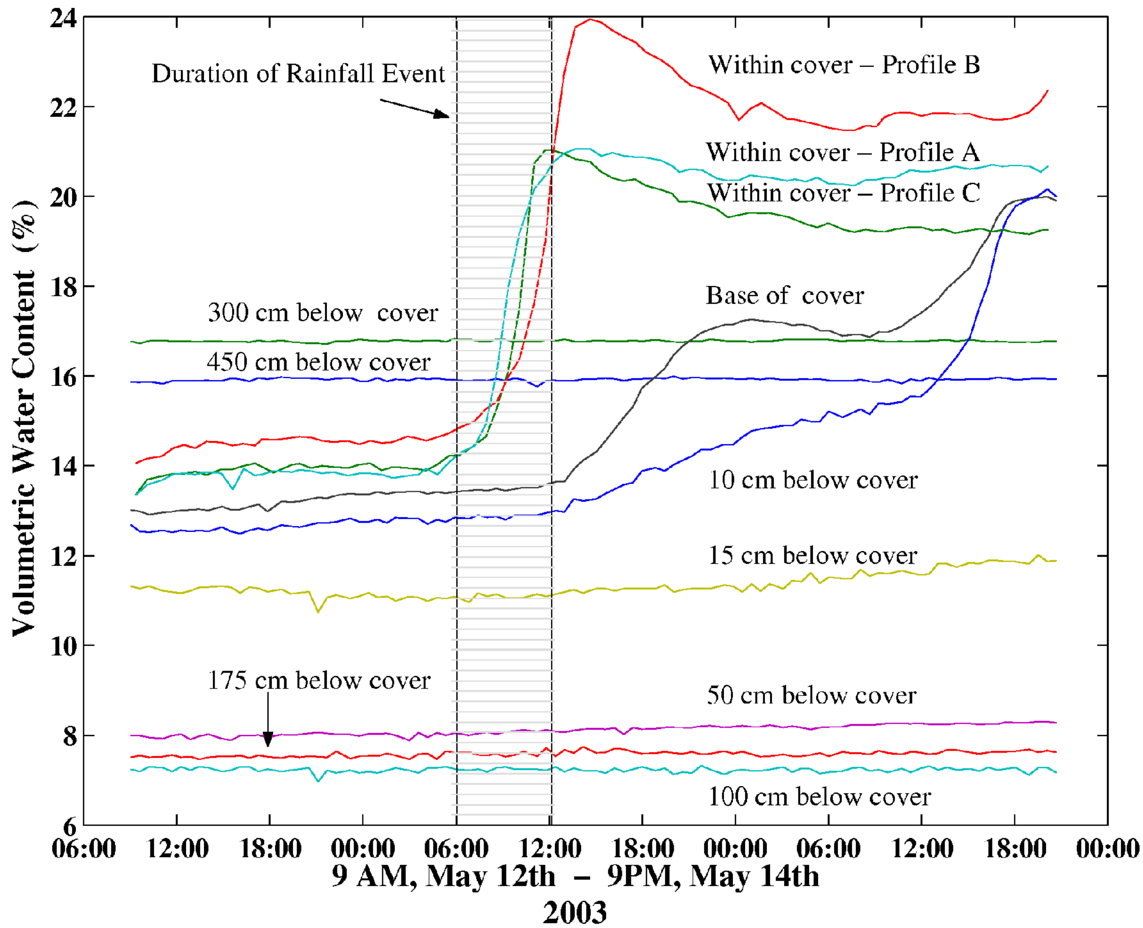

Figure 5.12. Volumetric water content as measured by TDR probes for a 60-hour period in 2003. A 49 mm artificial rainfall event was applied to the covered surface between 6 AM and 12 PM on May 13th as shown by the hatched zone.

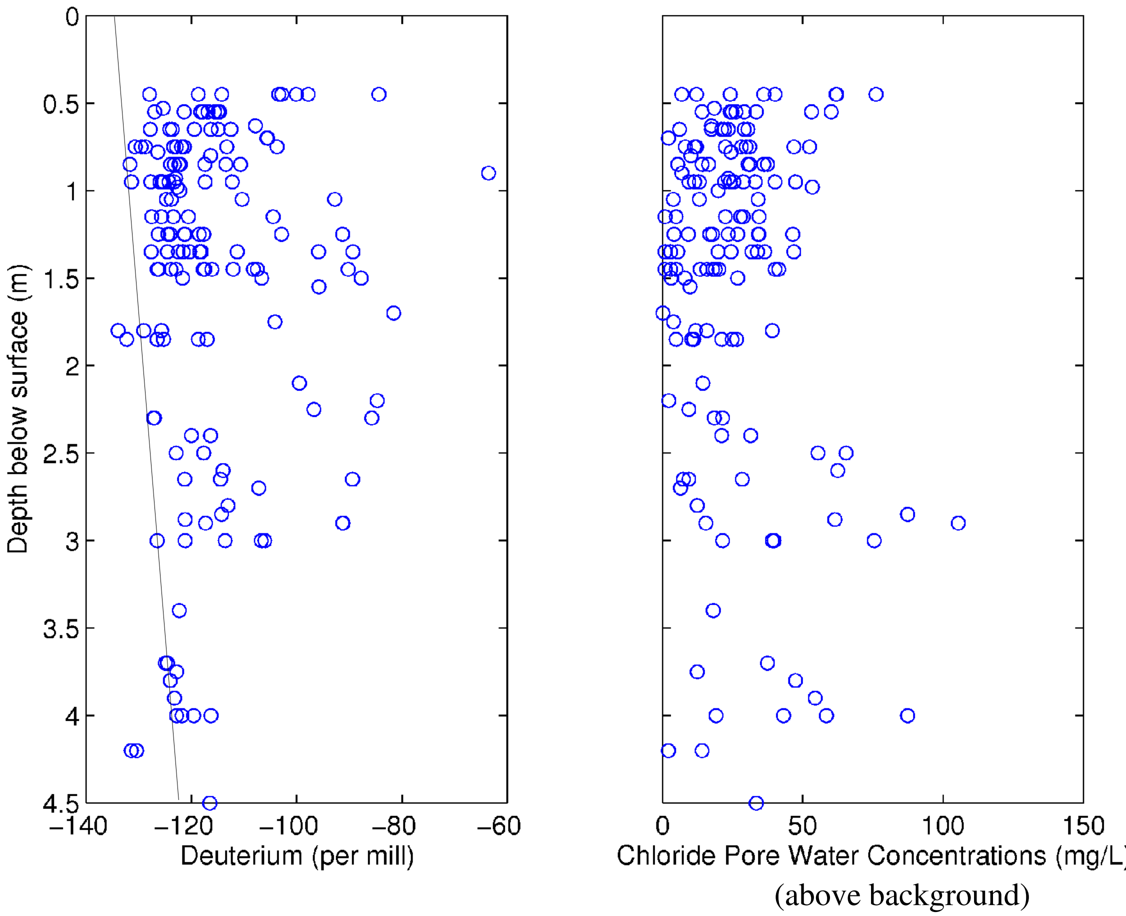

Figure 5.13. Concentration in mg/L chloride, and deuterium values plotted with depth in the waste rock pile. The solid line in the deuterium versus depth plot indicates background. Chloride data are plotted as concentrations above background value of 20 mg/L.

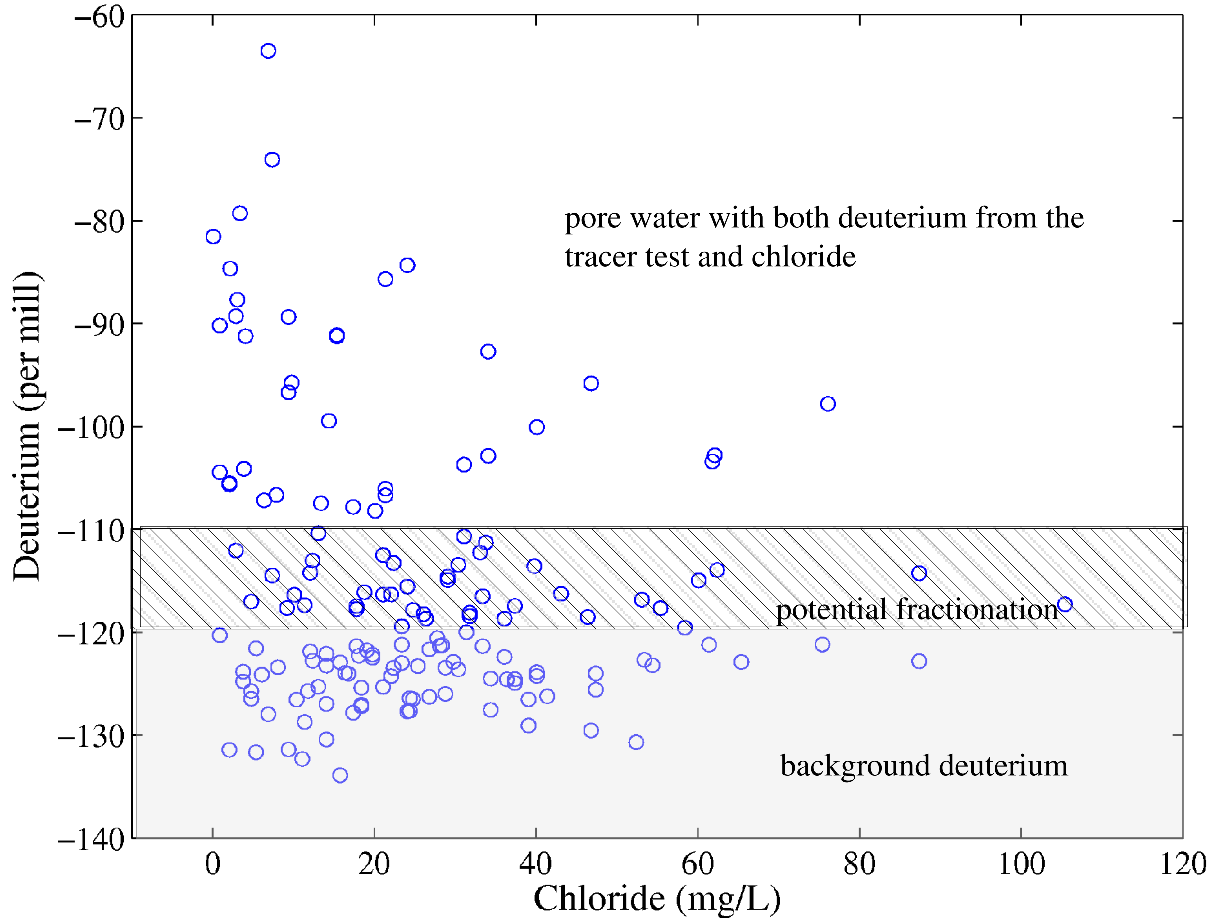

Figure 5.14. Plot of the δD value and the Cl concentration of 160 pore water samples within the waste rock pile at the time of deconstruction. Chloride data are plotted as concentrations above background value of 20 mg/L.

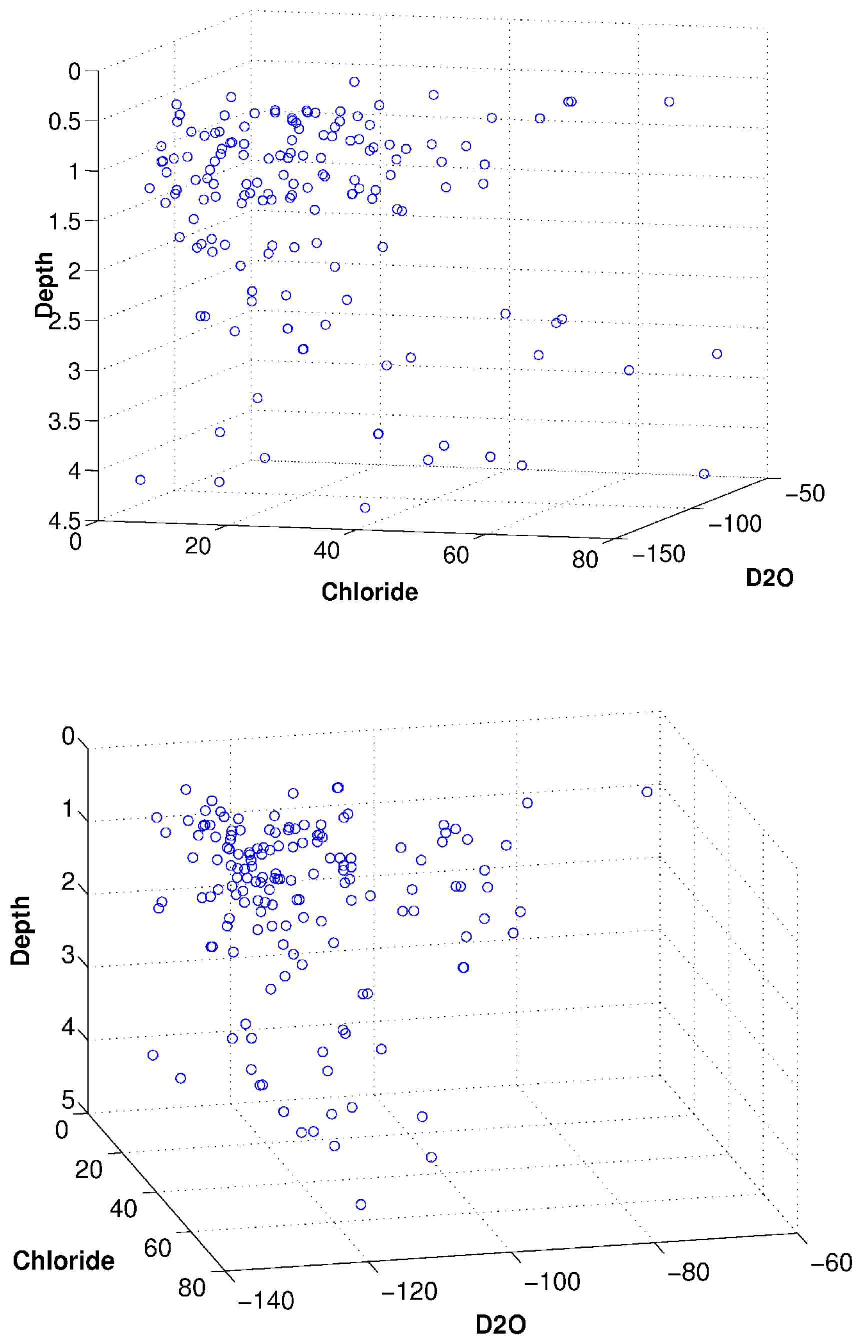

Figure 5.15. δD values and the Cl concentrations of pore water samples with depth in the waste rock pile at the time of deconstruction. Two views of the same plot are shown for clarity.

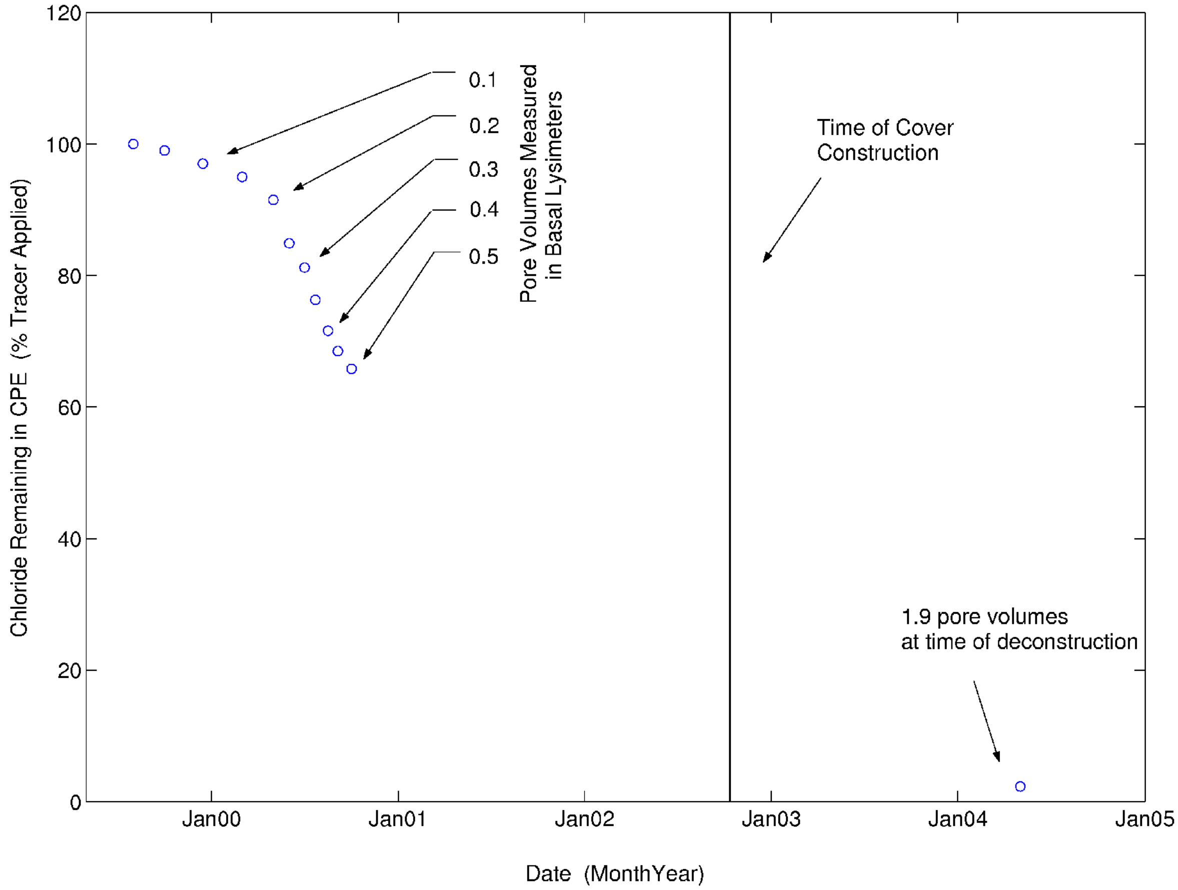

Figure 5.16. Plot of the chloride tracer remaining in the waste rock pile on the Y-axis and time on the X-axis. The completion of the compacted surface layer is marked by a line. The resident pore volumes measured as basal outflow are labeled. There are no data to justify the shape of the curve between 0.5 and 1.9 pore volumes.

CHAPTER 6: SUMMARY OF DISSERTATION

The thesis presents a comprehensive water balance for the CPE (Chapter 3) from data collected over a 5-year period. Chapter 3 includes a discussion of the procedures used for the measurement and prediction of the individual water balance components, and a discussion of the changes in the water balance resulting from the construction of a reduced permeability compacted cover. The water balance provides the framework to evaluate the hydrogeology of the waste rock pile. An investigation of how the unsaturated flow processes occurring within a free-dumped, coarse waste rock pile changed following a surface modification, and following the installation of a reduced permeability compacted cover is presented in Chapter 4. Results from the investigation of flow processes and surface configuration suggest that surface configuration alone cannot explain the complex patterns of outflow variability, and that mechanisms within the waste rock pile are important. Chapter 5 presents the results of a stable isotope tracer test, and provides a discussion of water and tracer migration within the covered CPE. The tracer test was designed to investigate the flow and transport mechanisms within the waste rock. Chapter 6 discussed the deconstruction of the CPE. Visual observations of particle size distributions and tracer concentrations obtained during the deconstruction of the CPE were compiled and attempts were made to link the observations to outflow data observed in the basal lysimeters, as well as to internal TDR and temperature measurements. The main research objectives and conclusions of each chapter are described below.

6.1. SUMMARY OF CHAPTER 2: Water Balance of the Constructed Waste Rock Pile

The primary objective of this study was to establish the water balance for an unsaturated mine waste rock pile over the time period from 2000 to 2004. The four years include a three-year period when the pile was uncovered, and a one-year period after a compacted cover was placed. Specifically, the first objective was to quantify the change in water balance components following the placement of a lower permeability cover that resembled a traffic, or haul surface.

The primary conclusions of this study were as follows:

- For years 2000, 2001 and 2002, 44%, 51% and 55% of rainfall was measured as lysimeter outflow at the base of the waste rock pile. Following the placement of a compacted cover that resembled a traffic or haul surface, lysimeter outflow was reduced to less than 10% of rainfall and evaporation increased by 10%.
- The differences between the covered model predictions and field observations were shown to lie within the expected range (given the uncertainties in potential evaporation, precipitation, and especially those associated with the heterogeneous characteristics of the waste rock). The model was able to accurately predict water balance components based on

observed field data from a highly heterogeneous, covered waste rock pile and realistically simulated the physical processes that affect water movement in the covered CPE.

6.2. SUMMARY OF CHAPTER 3: The Effect of Surface Condition on Internal Water Flow in Waste Rock

The primary objective of this study was to document the changes in fluid pathways and magnitude of flow through waste rock as its surface condition is modified. Specific initial hypotheses were:

- That the large spatial and temporal variability in outflow observed from the CPE were primarily a result of the surface condition of the waste rock pile and to a lesser degree related to the heterogeneous internal structure of the pile.
- That the addition of a lower permeability cover would greatly reduce spatial and temporal variability in outflow.

The primary conclusions of this study were as follows:

The surface condition of the waste rock pile was shown to affect the spatial and temporal variability in outflow from both the free-dumped surface and the ripped and leveled surface of the CPE, however, the internal waste rock heterogeneities and structure were the dominant factors controlling the outflow distribution and wetting front arrival times. In contrast, data from the covered, low infiltration experiments suggested that surface configuration, especially related to ponding, was the dominant control on outflow variability.

The second hypothesis was that the addition of a lower permeability cover would eliminate spatial and temporal variability in outflow. A large portion of the variability in outflow was removed from the system following construction of the lower permeability compacted layer, however, preferential flow was not eliminated from the system.

6.3. SUMMARY OF CHAPTER 4: Water Migration in Covered Waste Rock: A Deuterium Tracer Study

The deuterium tracer study was designed to investigate water flow and solute transport within waste rock beneath a lower-permeability surface cover. It was hypothesized that the lower-permeability cover would result in a significant reduction of distinctive preferential flow paths by limiting the flow to within the finer grained matrix materials. The surface cover would also reduce the expression of spatial variability of surface infiltration. It was assumed that deuterium might be an ideal tracer of water movement through a waste rock pile in which few other options for water tracers were available.

The primary conclusions of this study were as follows:

This deuterium tracer study provided a description of the post-cover water flow and the tracer distribution within the pile. The addition of a lower permeability cover significantly reduced the amount of infiltration into the CPE, and consequently, resulted in a significant reduction in volume of water flowing through preferential flow paths within the system. However, the lower permeability cover apparently increased the amount of preferential flow relative to the percentage of infiltration. Even though the volume of water flowing in the CPE was lower, the majority of water that infiltrated into the post-cover CPE was event-driven and transported through preferential flow paths.

Deuterium has advantages in that it is inexpensive, has low detection limits and does not interfere with the water chemistry within the waste rock, however, as a result of the large amount of fractionation, deuterium in this context was non-conservative. Deuterium was found to not be an ideal tracer of water movement through the waste rock pile.

6.4. SUMMARY OF CHAPTER 5: Deconstruction of the Experimental Waste Rock Pile

It was initially thought that the deconstruction of the waste rock pile would provide an opportunity to directly examine relationships between the structural features of the CPE and the outflow responses that were observed during the earlier experiments at the base of the pile. The primary objective of the deconstruction was as follows:

- To identify the relationships between the physical properties, internal structures, and observations of outflow and tracers at the base of the CPE. For example, to identify the physical properties or structures responsible for the large flows in lysimeter 6, and to identify what structures control the distribution of outflow observed at the base of the CPE.

Data collected during the deconstruction included observations of coarse rubble zones, lenses of fine matrix material, and variably-oriented, discontinuous textural boundaries, however, a direct link between these intermediate-scale structures and spatial distribution of basal outflow could not be established. Similarly, a consistent correlation between in-situ tracer values and these specific structures did not exist. These intermediate-scale structures did have a localized influence on water flow as observed from dye stain patterns and tracer patterns, however, based on the relationship between location in the CPE and variability of outflow, had a minimal influence on the bulk water flow and transport of constituents through the waste rock. Variations of the particle size distribution, specifically higher percentages of the waste rock between 1.5 mm and 20 mm apparently had the largest effect on the presence of the fast flow spikes, and on the large degree of variability in spatial distribution of the lysimeter outflow.

6.5 IMPLICATIONS FOR PRACTICE

All mine waste rock piles, stockpiles and heap leach piles have unique physical and structural characteristics, geochemical compositions, and experience site-specific climate patterns. However, general construction techniques are often similar, as are techniques often used for closure. Many of these unsaturated waste piles may at some point require measures to limit water and/or oxygen ingress into the waste, and/or may require monitoring or control of outflow and predictions of future loadings. While many of the observations from the CPE may be different from waste rock piles elsewhere, parallels can be drawn.

The compacted surface layer placed on the CPE was intended to resemble a traffic surface, and not a multi-layer cover system, yet was effective at reducing the infiltration of water into the waste rock. Because the surface was small (64 m^2) and care was used to ensure that minimal surface defects and heterogeneities existed, preferential flow was minimized. However, preferential flow was still observed to result from very small topographic differences. While a reduction in surface infiltration and a reduction of preferential flow were observed on the CPE, it is unlikely that the same reductions could be achieved on a large scale simply by installing a compacted layer without significant ground work and large compaction equipment. Such an attempt would likely make compaction a costly and ineffective interim method of controlling the infiltration of water into waste rock. In contrast, many of the observations of flow within the CPE following covering are more similar to that expected from within a waste rock pile that has been covered with a well designed cover system.

Based on SoilCover model results, evaporation from the uncovered waste rock becomes limited in dry periods between rainfall events when a continuous supply of water is not available to the surface for evaporation. Ensuring that the top one to two meters of a pile consists of fine material will help maintain a network of water filled pores that act as pathways for water to the evaporating surface, resulting in a significant reduction in net-percolation from uncovered waste rock. This concept has two practical implications. First, coarse rubble layers are sometimes placed on the surface of store and release cover systems to armor against erosion. Such a layer may result in a lower annual evaporation, decreasing the effectiveness of the cover. Second, ensuring that the top one to two meters of waste rock below a cover consist of fine materials could potentially result in cost savings including thinner storage layers by utilizing the near-surface waste rock as part of the cover system.

The observation of localized preferential flow within covered and drained waste rock has significant implications for prediction of water residence times, and characterizing how metals are transported through reclaimed waste rock. Even with a low infiltration surface and little matrix flow, infiltration into the covered waste rock under certain climatic patterns may result in preferential flow fingers that could transport weathering products through a covered waste rock pile at a faster than expected rate.

The characterization of the particle size distributions and of preferential flow within waste rock did not provide data adequate to reliably calculate the amount of a waste rock pile that could be expected to interact with water flow and contribute to metal loadings. The characterization methods employed in this research could provide such data for an end-dumped style waste rock pile in which a model with a more predictable geometry of particle size distributions exist. It is highly recommended that characterization techniques be improved so that such an analysis can be completed on a field scale heterogeneous free-dumped waste rock pile.

Over a five-year period, a change in the waste rock properties was observed and is hypothesized to have influenced flow within the waste rock. For long-term predictions of water flow, this effect of the evolution of the waste rock, particularly the change in particle size distributions and how the water flow paths and solute transport mechanisms change as the waste rock pile ages should be evaluated.

APPENDIXES:

APPENDIX A: SOILCOVER INPUT FILES

Run Day (#)	Calender Day (mon d, yr)	Max. AirTemp (C)	Min. AirTemp (C)	Net Rad. (MJ/m2-day)	Max. RH (%)	Min. RH (%)	Wind Speed (km/hr)	Daily Rainfall (mm)	Bot. Temp (C)
1	Apr 1, 02	-14.0	-28.3	4.36	85.0	45.4	4.98	0	7.9
2	Apr 2, 02	-7.4	-22.4	5.62	79.3	33.8	7.06	0	7.9
3	Apr 3, 02	-12.5	-23.1	6.35	93.2	33.6	4.99	0	7.9
4	Apr 4, 02	-11.9	-26.2	4.79	79.4	34.4	4.78	0	8.0
5	Apr 5, 02	-6.9	-22.6	5.78	80.8	31.4	8.93	0	8.0
6	Apr 6, 02	-10.3	-18.1	6.91	94.8	40.4	11.44	0	8.0
7	Apr 7, 02	-8.8	-25.5	7.16	91.3	33.8	8.64	0	8.0
8	Apr 8, 02	-6.0	-28.5	5.51	70.3	24.0	12.78	0	8.1
9	Apr 9, 02	-1.0	-12.5	7.24	80.1	31.4	15.81	0	8.1
10	Apr 10, 02	4.3	-7.0	6.35	96.7	43.4	12.36	0	8.1
11	Apr 11, 02	2.2	-9.2	3.45	99.8	48.8	9.78	0	8.1
12	Apr 12, 02	0.4	-7.8	11.10	100.0	67.2	11.94	0	8.1
13	Apr 13, 02	-1.4	-13.1	11.11	84.1	34.8	19.21	0	8.2
14	Apr 14, 02	-7.1	-16.9	10.69	69.0	22.2	12.57	0	8.2
15	Apr 15, 02	-6.1	-17.8	4.43	83.8	45.0	11.04	0	8.2
16	Apr 16, 02	-6.6	-12.2	9.21	95.4	62.5	8.94	0	8.2
17	Apr 17, 02	-5.8	-15.7	10.40	91.3	36.0	10.87	0	8.3
18	Apr 18, 02	2.8	-15.4	8.87	71.8	23.5	13.12	0	8.3
19	Apr 19, 02	9.2	-4.4	8.81	51.8	21.4	10.07	0	8.3
20	Apr 20, 02	9.2	-1.7	0.76	100.0	33.2	15.17	0	8.3
21	Apr 21, 02	5.7	-14.4	1.15	100.0	94.1	21.41	9.2	8.4
22	Apr 22, 02	-14.5	-19.4	3.29	94.3	78.8	12.03	0	8.4
23	Apr 23, 02	-10.2	-21.1	3.00	80.4	33.5	7.85	0	8.4
24	Apr 24, 02	-2.0	-22.0	3.97	76.9	22.7	5.50	0	8.4
25	Apr 25, 02	-3.9	-16.8	6.75	89.9	31.4	13.95	0	8.4
26	Apr 26, 02	3.1	-10.4	8.23	94.6	15.9	17.17	0	8.5
27	Apr 27, 02	0.8	-4.5	7.49	99.5	45.2	16.94	0.4	8.5
28	Apr 28, 02	2.6	-7.4	11.22	99.1	44.5	17.63	0.6	8.5
29	Apr 29, 02	-7.3	-16.1	12.58	82.0	44.9	12.71	0	8.5
30	Apr 30, 02	-1.7	-16.7	1.78	81.9	24.1	28.38	0	8.6

Run	Calender	Max.	Min.	Net	Max.	Min.	Wind	Daily	Bot.
Day	Day	AirTemp	AirTemp	Rad.	RH	RH	Speed	Rainfall	Temp
(#)	(mon d, yr)	(C)	(C)	(MJ/m2-day)	(%)	(%)	(km/hr)	(mm)	(C)
31	May 1, 02	3.7	-14.8	6.67	97.7	36.9	17.82	2.4	8.6
32	May 2, 02	11.3	-19.2	7.55	87.6	49.1	6.44	0	8.6
33	May 3, 02	-8.6	-21.6	11.10	92.9	34.8	6.52	0	8.6
34	May 4, 02	-6.9	-19.6	11.77	77.5	35.5	9.34	0	8.7
35	May 5, 02	-4.5	-16.7	12.62	84.9	30.7	6.22	0	8.7
36	May 6, 02	0.5	-13.3	3.45	70.2	22.1	6.38	0	8.7
37	May 7, 02	2.2	-7.2	8.53	55.8	12.9	3.10	0.2	8.7
38	May 8, 02	6.3	-9.4	8.53	60.6	11.3	3.92	0	8.7
39	May 9, 02	7.0	-4.7	9.42	48.2	20.8	8.14	0	8.8
40	May 10, 02	8.9	-3.3	3.98	84.8	24.4	6.90	0	8.8
41	May 11, 02	10.3	-2.9	3.45	100.0	25.0	10.01	0	8.8
42	May 12, 02	10.6	0.7	14.78	73.8	35.2	16.05	0.2	8.8
43	May 13, 02	2.9	-4.5	6.95	93.1	40.8	7.70	0	8.9
44	May 14, 02	8.4	-6.4	6.95	96.0	22.2	13.44	2	8.9
45	May 15, 02	12.5	-1.8	6.40	50.5	14.5	15.72	38.6	8.9
46	May 16, 02	15.1	1.0	6.95	32.9	10.7	19.98	0	8.9
47	May 17, 02	15.4	2.6	3.98	30.0	9.9	22.46	0	8.9
48	May 18, 02	11.6	4.5	9.35	73.8	14.2	10.84	0.4	9.0
49	May 19, 02	11.0	0.3	8.53	68.2	34.8	15.48	0	9.0
50	May 20, 02	1.6	-6.3	8.53	75.5	24.7	15.84	0	9.0
51	May 21, 02	0.6	-8.9	14.88	65.1	23.8	4.66	0	9.0
52	May 22, 02	5.2	-9.2	13.22	70.3	13.3	8.48	0	9.1
53	May 23, 02	10.0	-4.5	6.95	40.7	12.2	9.14	0	9.1
54	May 24, 02	4.7	-2.7	6.95	94.6	34.2	16.73	0.8	9.1
55	May 25, 02	10.9	-2.9	9.15	74.1	15.3	9.95	0	9.1
56	May 26, 02	4.6	-2.0	3.98	86.7	27.1	6.73	0.8	9.2
57	May 27, 02	14.9	-1.7	3.35	60.2	26.0	11.38	0	9.2
58	May 28, 02	13.6	4.7	6.75	100.0	41.3	15.10	12.2	9.2
59	May 29, 02	4.8	-1.0	6.51	100.0	71.9	5.50	0.8	9.2
60	May 30, 02	2.7	-1.2	9.49	98.8	66.6	5.03	0.4	9.2
61	May 31, 02	7.4	-1.3	6.95	100.0	52.5	5.49	0.2	9.3
62	Jun 1, 02	12.9	-3.5	6.51	93.6	31.4	5.40	0	9.3
63	Jun 2, 02	17.2	-0.4	8.53	66.5	14.8	6.64	0	9.3

Run	Calender	Max.	Min.	Net	Max.	Min.	Wind	Daily	Bot.
Day	Day	AirTemp	AirTemp	Rad.	RH	RH	Speed	Rainfall	Temp
(#)	(mon d, yr)	(C)	(C)	(MJ/m2-day)	(%)	(%)	(km/hr)	(mm)	(C)
64	Jun 3, 02	19.8	5.1	9.57	59.1	21.7	9.05	0	9.3
65	Jun 4, 02	20.9	7.9	10.09	82.4	22.3	7.77	0	9.4
66	Jun 5, 02	18.3	6.4	6.40	98.8	34.7	10.36	1.6	9.4
67	Jun 6, 02	18.8	3.5	13.72	99.7	14.8	7.22	0	9.4
68	Jun 7, 02	19.0	4.3	8.53	61.2	17.3	9.43	0	9.4
69	Jun 8, 02	17.7	3.7	8.53	87.8	14.6	12.23	0	9.5
70	Jun 9, 02	20.9	7.8	8.53	41.0	8.2	8.56	0	9.5
71	Jun 10, 02	22.0	8.4	12.22	44.9	8.2	10.43	0	9.5
72	Jun 11, 02	23.9	9.8	6.95	43.3	8.4	15.16	0	9.5
73	Jun 12, 02	15.7	7.9	6.95	75.0	21.3	10.84	0	9.5
74	Jun 13, 02	14.4	1.0	6.40	96.6	26.8	6.85	0	9.6
75	Jun 14, 02	14.3	1.2	4.83	71.0	14.7	9.29	0	9.6
76	Jun 15, 02	10.8	3.3	12.43	85.5	47.3	10.98	0.2	9.6
77	Jun 16, 02	11.8	1.7	13.56	93.8	22.1	3.20	0	9.6
78	Jun 17, 02	16.5	0.7	9.29	89.2	14.3	11.44	0	9.7
79	Jun 18, 02	15.5	2.5	11.02	95.6	28.6	9.59	3.4	9.7
80	Jun 19, 02	17.2	1.0	12.73	97.3	23.2	9.02	0	9.7
81	Jun 20, 02	15.6	3.2	8.53	89.9	43.8	7.69	3	9.7
82	Jun 21, 02	21.7	2.0	12.37	100.0	24.5	15.79	0	9.7
83	Jun 22, 02	25.2	15.5	8.81	45.2	21.9	12.79	0	9.8
84	Jun 23, 02	23.4	10.2	8.53	92.3	33.4	10.80	0	9.8
85	Jun 24, 02	23.4	9.2	14.84	92.0	22.1	7.80	0	9.8
86	Jun 25, 02	25.4	10.9	12.86	66.4	21.2	13.58	0	9.8
87	Jun 26, 02	29.9	14.3	8.53	68.5	9.8	5.18	0	9.9
88	Jun 27, 02	22.1	9.3	12.70	98.3	35.6	3.98	12	9.9
89	Jun 28, 02	18.9	8.5	5.16	100.0	51.1	7.48	4.4	9.9
90	Jun 29, 02	13.5	6.7	6.40	99.8	73.6	11.17	0	9.9
91	Jun 30, 02	7.8	3.9	12.03	99.8	85.5	6.03	4.6	10.0
92	Jul 1, 02	14.4	3.5	14.56	99.2	34.6	11.31	0.2	10.0
93	Jul 2, 02	17.9	4.0	5.08	87.7	23.2	15.08	0	10.0
94	Jul 3, 02	14.7	8.8	5.08	94.9	44.5	15.56	0.2	10.0
95	Jul 4, 02	15.5	7.3	11.13	97.7	28.9	13.54	0	10.0
96	Jul 5, 02	17.2	6.5	6.95	99.9	29.3	8.59	0.2	10.1

Run	Calender	Max.	Min.	Net	Max.	Min.	Wind	Daily	Bot.
Day	Day	AirTemp	AirTemp	Rad.	RH	RH	Speed	Rainfall	Temp
(#)	(mon d, yr)	(C)	(C)	(MJ/m2-day)	(%)	(%)	(km/hr)	(mm)	(C)
97	Jul 6, 02	19.9	6.3	6.95	92.6	21.2	4.10	0	10.1
98	Jul 7, 02	25.9	9.8	5.41	54.9	15.1	14.50	0	10.1
99	Jul 8, 02	24.4	13.3	6.95	53.4	11.8	17.08	0	10.1
100	Jul 9, 02	25.3	14.8	10.47	56.1	14.0	5.10	0	10.2
101	Jul 10, 02	25.5	10.6	6.40	63.4	27.8	11.67	0	10.2
102	Jul 11, 02	23.2	13.6	6.40	80.6	25.5	10.80	0	10.2
103	Jul 12, 02	17.0	8.3	3.78	84.4	41.4	15.32	0	10.2
104	Jul 13, 02	16.1	10.3	10.02	98.2	58.4	19.39	2.2	10.3
105	Jul 14, 02	13.9	6.5	10.37	98.2	44.3	10.41	0	10.3
106	Jul 15, 02	13.2	4.5	6.40	98.5	50.4	8.23	0.4	10.3
107	Jul 16, 02	17.2	5.1	2.45	85.8	35.9	12.25	0	10.3
108	Jul 17, 02	14.1	8.7	3.97	95.7	48.9	6.13	1	10.3
109	Jul 18, 02	12.0	8.5	2.71	100.4	92.6	15.76	17	10.4
110	Jul 19, 02	13.6	9.8	6.40	99.3	59.1	10.98	1	10.4
111	Jul 20, 02	17.4	5.3	6.40	82.1	33.9	5.63	0	10.4
112	Jul 21, 02	22.7	6.8	11.21	85.3	19.3	8.81	0	10.4
113	Jul 22, 02	22.0	11.7	12.34	87.6	36.7	6.68	0	10.5
114	Jul 23, 02	21.6	10.3	11.22	95.3	37.9	8.87	0	10.5
115	Jul 24, 02	25.1	11.7	10.53	83.7	31.5	8.97	0	10.4
116	Jul 25, 02	19.5	13.0	6.84	81.4	31.1	8.85	0	10.4
117	Jul 26, 02	13.9	10.1	8.81	100.0	68.8	9.22	6.2	10.4
118	Jul 27, 02	16.4	9.0	5.41	99.9	49.5	7.72	9.8	10.4
119	Jul 28, 02	11.9	7.0	4.17	97.5	55.0	13.77	0	10.3
120	Jul 29, 02	10.7	5.8	4.11	100.0	87.9	24.25	16.2	10.3
121	Jul 30, 02	7.7	2.6	7.93	99.2	93.7	20.88	10	10.3
122	Jul 31, 02	6.5	0.3	10.71	98.1	59.5	14.66	0	10.3
123	Aug 1, 02	6.3	-1.4	7.83	98.8	55.6	7.85	0	10.2
124	Aug 2, 02	7.8	-1.0	11.77	93.7	38.8	3.57	0	10.2
125	Aug 3, 02	11.7	-1.6	3.18	100.0	40.7	7.55	0	10.2
126	Aug 4, 02	12.9	3.6	3.78	99.5	47.9	11.91	0.2	10.2
127	Aug 5, 02	15.9	5.0	6.40	97.9	41.0	9.04	0	10.2
128	Aug 6, 02	21.5	8.2	12.78	68.7	24.3	8.13	0	10.1
129	Aug 7, 02	22.9	8.7	11.04	66.6	25.5	11.42	0.2	10.1

Run	Calender	Max.	Min.	Net	Max.	Min.	Wind	Daily	Bot.
Day	Day	AirTemp	AirTemp	Rad.	RH	RH	Speed	Rainfall	Temp
(#)	(mon d, yr)	(C)	(C)	(MJ/m2-day)	(%)	(%)	(km/hr)	(mm)	(C)
130	Aug 8, 02	21.2	10.3	6.76	90.3	34.7	13.58	36.3	10.1
131	Aug 9, 02	12.9	7.7	10.89	98.7	65.8	12.43	0.4	10.1
132	Aug 10, 02	12.8	5.6	10.94	100.0	50.8	4.71	0.4	10.0
133	Aug 11, 02	16.3	3.8	6.61	98.2	40.6	9.05	0	10.0
134	Aug 12, 02	15.5	8.1	8.31	98.1	61.5	13.69	0.4	10.0
135	Aug 13, 02	12.3	7.2	8.86	100.0	60.0	6.30	4.8	10.0
136	Aug 14, 02	11.7	3.9	4.97	97.2	50.9	11.49	0	10.0
137	Aug 15, 02	7.2	2.0	11.95	99.6	62.9	3.87	4.8	9.9
138	Aug 16, 02	11.6	-1.0	7.65	100.0	34.1	10.62	0.2	9.9
139	Aug 17, 02	14.1	2.6	9.21	97.2	45.5	12.55	0	9.9
140	Aug 18, 02	6.5	-0.6	12.67	99.8	42.9	8.12	4.6	9.9
141	Aug 19, 02	10.0	-3.1	9.28	99.6	32.8	10.10	0	9.8
142	Aug 20, 02	18.8	2.6	10.77	71.7	34.7	11.26	0	9.8
143	Aug 21, 02	17.9	9.3	10.61	78.0	40.6	5.80	0	9.8
144	Aug 22, 02	20.9	7.8	11.45	86.8	33.2	13.41	0	9.8
145	Aug 23, 02	18.5	8.3	10.24	88.0	24.3	4.40	0	9.7
146	Aug 24, 02	20.2	3.7	7.59	94.5	29.8	4.78	1.5	9.7
147	Aug 25, 02	18.5	10.3	10.51	96.9	60.6	6.60	0.7	9.7
148	Aug 26, 02	18.8	9.6	5.23	97.7	52.0	7.88	0	9.7
149	Aug 27, 02	22.4	10.4	10.18	85.1	40.1	6.35	0	9.7
150	Aug 28, 02	25.1	13.3	3.47	92.8	32.8	6.35	0	9.6
151	Aug 29, 02	15.3	9.4	9.63	99.9	61.8	4.01	44.2	9.6
152	Aug 30, 02	17.9	7.7	9.05	99.1	43.7	7.09	0	9.6
153	Aug 31, 02	15.5	8.1	6.42	100.0	48.9	4.22	2.4	9.6
154	Sep 1, 02	11.9	7.1	3.96	100.0	72.8	13.44	1.6	9.5
155	Sep 2, 02	8.5	6.3	2.59	100.0	83.5	14.63	4.4	9.5
156	Sep 3, 02	6.9	4.3	6.71	99.1	88.1	10.49	18.2	9.5
157	Sep 4, 02	8.1	3.5	8.18	100.0	62.1	1.79	2.6	9.5
158	Sep 5, 02	10.3	1.9	8.30	100.0	47.8	9.71	0.2	9.4
159	Sep 6, 02	12.9	3.4	8.99	90.6	38.1	11.98	0	9.4
160	Sep 7, 02	13.5	5.3	9.47	80.5	32.9	9.46	0	9.4
161	Sep 8, 02	15.5	4.7	9.20	94.1	40.5	13.88	0	9.4
162	Sep 9, 02	17.0	7.4	9.05	73.2	27.7	13.11	0	9.4

Run	Calender	Max.	Min.	Net	Max.	Min.	Wind	Daily	Bot.
Day	Day	AirTemp	AirTemp	Rad.	RH	RH	Speed	Rainfall	Temp
(#)	(mon d, yr)	(C)	(C)	(MJ/m2-day)	(%)	(%)	(km/hr)	(mm)	(C)
163	Sep 10, 02	13.4	5.6	8.52	81.3	35.5	6.65	0	9.3
164	Sep 11, 02	13.1	2.6	8.43	86.6	29.9	7.83	0	9.3
165	Sep 12, 02	11.8	2.7	8.19	93.3	35.7	7.20	0	9.3
166	Sep 13, 02	14.9	0.3	5.99	98.4	29.9	8.78	0	9.3
167	Sep 14, 02	13.0	5.7	5.10	99.6	57.7	14.10	0	9.2
168	Sep 15, 02	14.7	5.6	7.54	94.6	48.9	9.77	0	9.2
169	Sep 16, 02	11.5	5.1	8.02	98.4	50.7	10.22	0	9.2
170	Sep 17, 02	12.6	2.4	3.07	83.1	36.9	8.49	0	9.2
171	Sep 18, 02	7.3	2.6	3.43	99.7	59.1	19.57	6.2	9.1
172	Sep 19, 02	4.5	0.2	5.19	100.0	87.4	17.02	9.4	9.1
173	Sep 20, 02	2.7	-1.4	3.01	97.8	57.6	11.89	2.4	9.1
174	Sep 21, 02	-0.7	-3.9	3.70	100.0	61.3	16.61	1	9.1
175	Sep 22, 02	2.4	-5.5	1.70	93.9	47.2	16.61	0	9.1
176	Sep 23, 02	-4.3	-6.2	1.93	89.2	54.9	15.25	0	9.0
177	Sep 24, 02	-3.1	-6.8	2.50	99.1	64.0	10.24	0.2	9.0
178	Sep 25, 02	-2.2	-5.0	3.21	99.2	63.5	7.20	0	9.0
179	Sep 26, 02	-0.5	-4.6	3.70	87.3	46.6	12.34	0	9.0
180	Sep 27, 02	7.4	-3.3	4.12	100.0	58.6	9.09	0	8.9
181	Sep 28, 02	4.9	-2.2	3.29	100.0	62.0	6.03	0.4	8.9
182	Sep 29, 02	1.1	-5.1	3.92	100.0	72.5	4.70	0.6	8.9
183	Sep 30, 02	0.7	-5.0	2.56	100.0	61.6	13.93	1.6	8.9
184	Oct 1, 02	6.4	-2.2	3.19	99.7	62.8	17.36	0.2	8.9
185	Oct 2, 02	0.3	-5.0	1.45	100.0	59.4	7.52	2	8.9
186	Oct 3, 02	5.1	-7.4	3.63	99.0	62.1	5.35	0	8.8
187	Oct 4, 02	-1.2	-7.6	4.99	99.8	52.3	7.27	0.2	8.7
188	Oct 5, 02	1.1	-6.4	5.52	97.3	36.2	7.84	0	8.6
189	Oct 6, 02	1.2	-4.1	4.63	97.6	28.5	14.07	0.2	8.4
190	Oct 7, 02	9.5	-3.6	2.34	79.1	42.0	7.86	0	8.3
191	Oct 8, 02	4.8	-1.9	4.03	100.0	46.8	13.25	0.4	8.2
192	Oct 9, 02	1.6	-5.6	3.77	100.0	68.7	20.74	0.4	8.1
193	Oct 10, 02	-5.0	-10.5	3.28	81.1	37.9	8.79	0	8.0
194	Oct 11, 02	-7.6	-14.1	0.36	91.9	33.9	10.74	0	7.9
195	Oct 12, 02	1.0	1.0	1	100.0	100.0	1	0	7.9

Run	Calender	Max.	Min.	Net	Max.	Min.	Wind	Daily	Bot.
Day	Day	AirTemp	AirTemp	Rad.	RH	RH	Speed	Rainfall	Temp
(#)	(mon d, yr)	(C)	(C)	(MJ/m2-day)	(%)	(%)	(km/hr)	(mm)	(C)
365	Apr 1, 03	-8.97	-23.72	4.36	0.44	0.18	8.98	0	7.9

Run	Calender	Max.	Min.	Net	Max.	Min.	Wind	Daily	Bot.
Day	Day	AirTemp	AirTemp	Rad.	RH	RH	Speed	Rainfall	Temp
(#)	(mon d, yr)	(C)	(C)	(MJ/m2-day)	(%)	(%)	(km/hr)	(mm)	(C)
1	Apr 1, 03	-8.97	-23.72	4.36	0.44	0.18	8.98	0	7.9
2	Apr 2, 03	-7.61	-17.09	5.62	0.36	0.2	11.06	0	7.9
3	Apr 3, 03	-7.72	-17.42	6.35	0.43	0.27	8.99	0	7.9
4	Apr 4, 03	-5.60	-16.85	4.79	0.44	0.29	8.78	0	8.0
5	Apr 5, 03	-3.41	-13.35	5.78	0.59	0.39	12.93	0	8.0
6	Apr 6, 03	2.07	-9.79	6.91	0.7	0.37	15.44	0	8.0
7	Apr 7, 03	7.54	-4.07	7.16	0.68	0.3	12.64	0	8.0
8	Apr 8, 03	6.47	-6.34	5.51	0.87	0.39	16.78	0	8.1
9	Apr 9, 03	-6.37	-11.35	7.24	0.77	0.61	19.81	0	8.1
10	Apr 10, 03	1.68	-14.79	6.35	0.79	0.35	16.36	0	8.1
11	Apr 11, 03	5.00	-4.59	3.45	0.71	0.29	13.78	0	8.1
12	Apr 12, 03	0.07	-5.47	11.1	0.89	0.47	15.94	0	8.1
13	Apr 13, 03	-1.52	-7.58	11.11	0.83	0.27	23.21	0	8.2
14	Apr 14, 03	0.34	-11.97	10.69	0.7	0.26	16.57	0	8.2
15	Apr 15, 03	-0.47	-3.23	4.43	0.81	0.57	15.04	0	8.2
16	Apr 16, 03	8.70	-2.05	9.21	0.81	0.25	12.94	0	8.2
17	Apr 17, 03	8.92	-4.04	10.4	0.8	0.33	14.87	0	8.3
18	Apr 18, 03	11.74	-1.98	8.87	0.75	0.12	17.12	0	8.3
19	Apr 19, 03	13.93	0.71	8.81	0.44	0.18	14.07	0	8.3
20	Apr 20, 03	15.35	4.21	0.76	0.4	0.24	19.17	0	8.3
21	Apr 21, 03	17.25	2.41	1.15	0.83	0.2	25.41	0	8.4
22	Apr 22, 03	13.57	-1.49	13.29	0.89	0.17	16.03	0	8.4
23	Apr 23, 03	4.44	-4.85	13	0.89	0.67	11.85	0	8.4
24	Apr 24, 03	2.04	3.60	13.97	0.89	0.66	9.5	0.2	8.4
25	Apr 25, 03	1.00	3.00	16.75	0.89	0.01	17.95	3.8	8.4

Run	Calender	Max.	Min.	Net	Max.	Min.	Wind	Daily	Bot.
Day	Day	AirTemp	AirTemp	Rad.	RH	RH	Speed	Rainfall	Temp
(#)	(mon d, yr)	(C)	(C)	(MJ/m2-day)	(%)	(%)	(km/hr)	(mm)	(C)
26	Apr 26, 03	3.52	3.00	12.23	0.67	0.36	21.17	0	8.5
27	Apr 27, 03	5.09	-12.62	7.49	0.69	0.09	20.94	0	8.5
28	Apr 28, 03	8.44	-7.35	11.22	0.39	0.19	21.63	0	8.5
29	Apr 29, 03	4.06	-6.83	12.58	0.49	0.06	16.71	0	8.5
30	Apr 30, 03	13.13	-5.21	11.78	0.84	0.16	32.38	0	8.6
31	May 1, 03	1.59	3.00	6.67	0.86	0.76	21.82	0.2	8.6
32	May 2, 03	2.00	3.00	12.55	0.87	0.74	10.44	0	8.6
33	May 3, 03	0.00	3.00	11.1	0.85	0.46	10.52	2	8.6
34	May 4, 03	1.22	3.00	11.77	0.78	0.58	13.34	0.4	8.7
35	May 5, 03	2.77	-2.77	12.62	0.89	0.8	10.22	2	8.7
36	May 6, 03	6.58	-2.00	13.34	0.88	0.48	10.38	0	8.7
37	May 7, 03	3.78	-3.94	13.59	0.82	0.38	7.1	0.2	8.7
38	May 8, 03	8.44	-3.10	10.95	0.76	0.21	7.92	0	8.7
39	May 9, 03	13.64	0.21	9.42	0.35	0.1	12.14	0	8.8
40	May 10, 03	18.03	3.33	14.04	0.33	0.08	10.9	0	8.8
41	May 11, 03	21.22	6.03	14.04	0.3	0.06	14.01	0.9	8.8
42	May 12, 03	18.68	8.41	14.78	0.23	0.09	20.05	4.2	8.8
43	May 13, 03	16.58	4.64	16.46	0.78	0.19	11.7	7	8.9
44	May 14, 03	12.67	2.60	16.11	0.85	0.06	17.44	33	8.9
45	May 15, 03	12.15	3.00	15.42	0.89	0.31	19.72	4.4	8.9
46	May 16, 03	14.50	3.00	15.37	0.9	0.93	23.98	1.4	8.9
47	May 17, 03	12.00	3.00	13.98	0.87	0.77	26.46	0	8.9
48	May 18, 03	15.02	3.00	13.35	0.88	0.27	14.84	0	9.0
49	May 19, 03	12.92	3.00	16.03	0.48	0.23	19.48	0	9.0
50	May 20, 03	13.11	-0.79	16.34	0.71	0.16	19.84	0	9.0
51	May 21, 03	13.30	4.50	14.88	0.85	0.24	8.66	0	9.0
52	May 22, 03	16.64	-1.51	13.22	0.85	0.11	12.48	1.2	9.1
53	May 23, 03	21.25	7.52	6.95	0.31	0.17	13.14	0	9.1
54	May 24, 03	26.91	11.28	15.07	0.63	0.2	20.73	4	9.1
55	May 25, 03	15.43	7.26	9.15	0.86	0.38	13.95	4.6	9.1
56	May 26, 03	18.05	2.93	14.2	0.77	0.1	10.73	0	9.2
57	May 27, 03	18.03	4.18	3.35	0.69	0.13	15.38	0	9.2

Run Day (#)	Calender Day (mon d, yr)	Max. AirTemp (C)	Min. AirTemp (C)	Net Rad. (MJ/m2-day)	Max. RH (%)	Min. RH (%)	Wind Speed (km/hr)	Daily Rainfall (mm)	Bot. Temp (C)
58	May 28, 03	14.76	2.72	6.75	0.57	0.25	19.1	1.2	9.2
59	May 29, 03	19.29	2.50	6.51	0.79	0.2	9.5	0	9.2
60	May 30, 03	20.22	8.98	9.49	0.62	0.25	9.03	0	9.2
61	May 31, 03	22.11	9.47	15.5	0.58	0.17	9.49	0	9.3
62	Jun 1, 03	18.35	9.14	15.14	0.73	0.3	9.4	0	9.3
63	Jun 2, 03	18.03	7.66	13.29	0.86	0.37	10.64	1	9.3
64	Jun 3, 03	15.03	7.79	9.57	0.88	0.4	13.05	2.8	9.3
65	Jun 4, 03	13.02	3.46	10.09	0.88	0.41	11.77	4	9.4
66	Jun 5, 03	14.35	2.93	10	0.87	0.49	14.36	3	9.4
67	Jun 6, 03	19.96	2.67	13.72	0.86	0.49	11.22	5.2	9.4
68	Jun 7, 03	13.53	2.72	13	0.85	0.23	13.43	0.4	9.4
69	Jun 8, 03	16.24	1.29	15	0.8	0.15	16.23	0	9.5
70	Jun 9, 03	14.39	4.15	14	0.78	0.28	12.56	0	9.5
71	Jun 10, 03	18.31	3.87	12.22	0.83	0.2	14.43	0	9.5
72	Jun 11, 03	12.09	-1.47	12.12	0.85	0.43	19.16	0.4	9.5
73	Jun 12, 03	15.86	-3.68	15.88	0.76	0.36	14.84	0	9.5
74	Jun 13, 03	8.53	2.33	15.3	0.89	0.68	10.85	0.2	9.6
75	Jun 14, 03	18.51	2.16	12	0.89	0.17	13.29	0	9.6
76	Jun 15, 03	15.32	6.33	12.43	0.59	0.25	14.98	0	9.6
77	Jun 16, 03	20.35	4.18	13.56	0.84	0.12	7.2	2	9.6
78	Jun 17, 03	25.74	10.05	9.29	0.38	0.17	15.44	0	9.7
79	Jun 18, 03	21.17	10.60	11.02	0.73	0.07	13.59	0	9.7
80	Jun 19, 03	18.27	7.36	12.73	0.73	0.11	13.02	1	9.7
81	Jun 20, 03	10.89	3.18	17.17	0.87	0.34	11.69	3	9.7
82	Jun 21, 03	13.18	0.02	12.37	0.88	0.84	19.79	3.6	9.7
83	Jun 22, 03	12.63	-2.69	8.81	0.88	0.4	16.79	0	9.8
84	Jun 23, 03	16.85	3.27	14.58	0.82	0.22	14.8	3	9.8
85	Jun 24, 03	19.54	6.94	14.84	0.65	0.2	11.8	4.6	9.8
86	Jun 25, 03	19.25	9.15	12.86	0.72	0.25	17.58	0	9.8
87	Jun 26, 03	15.08	7.65	8.53	0.85	0.49	9.18	0	9.9
88	Jun 27, 03	15.16	6.46	12.7	0.88	0.32	7.98	0.2	9.9
89	Jun 28, 03	13.99	3.40	15.16	0.86	0.24	11.48	0	9.9

Run	Calender	Max.	Min.	Net	Max.	Min.	Wind	Daily	Bot.
Day	Day	AirTemp	AirTemp	Rad.	RH	RH	Speed	Rainfall	Temp
(#)	(mon d, yr)	(C)	(C)	(MJ/m2-day)	(%)	(%)	(km/hr)	(mm)	(C)
90	Jun 29, 03	17.28	4.53	16.4	0.56	0.19	15.17	0	9.9
91	Jun 30, 03	12.67	5.88	12.03	0.87	0.36	10.03	1	10.0
92	Jul 1, 03	11.39	6.15	14.56	0.87	0.69	15.31	2.4	10.0
93	Jul 2, 03	11.95	5.14	5.08	0.89	0.53	19.08	5	10.0
94	Jul 3, 03	15.72	5.85	11.06	0.88	0.41	19.56	0.2	10.0
95	Jul 4, 03	15.31	4.97	11.13	0.77	0.39	17.54	0	10.0
96	Jul 5, 03	16.81	5.79	16.81	0.67	0.22	12.59	1	10.1
97	Jul 6, 03	19.80	5.85	15.77	0.65	0.18	8.1	1	10.1
98	Jul 7, 03	18.67	8.36	13.76	0.61	0.28	18.5	4	10.1
99	Jul 8, 03	15.02	9.34	15.56	0.88	0.67	21.08	22.2	10.1
100	Jul 9, 03	18.92	9.21	10.47	0.88	0.28	9.1	5.2	10.2
101	Jul 10, 03	23.65	6.12	15.48	0.77	0.26	15.67	3	10.2
102	Jul 11, 03	19.42	7.66	14.73	0.7	0.41	14.8	0	10.2
103	Jul 12, 03	19.68	2.39	15	0.79	0.28	19.32	0	10.2
104	Jul 13, 03	20.69	3.61	16.02	0.88	0.31	23.39	0.2	10.3
105	Jul 14, 03	21.53	5.17	10.37	0.88	0.46	14.41	2	10.3
106	Jul 15, 03	23.83	5.00	15.21	0.79	0.22	12.23	0	10.3
107	Jul 16, 03	19.97	8.86	12.45	0.88	0.39	16.25	0	10.3
108	Jul 17, 03	14.27	7.93	13.97	0.88	0.54	10.13	0.8	10.3
109	Jul 18, 03	15.60	8.82	12.71	0.89	0.66	19.76	0.2	10.4
110	Jul 19, 03	18.03	6.36	11.58	0.89	0.54	14.98	0.2	10.4
111	Jul 20, 03	20.56	9.21	15.61	0.86	0.29	9.63	0	10.4
112	Jul 21, 03	23.47	11.39	14.21	0.77	0.2	12.81	0	10.4
113	Jul 22, 03	20.56	10.42	12.34	0.8	0.16	10.68	0.2	10.5
114	Jul 23, 03	18.07	8.45	11.22	0.83	0.43	12.87	0	10.5
115	Jul 24, 03	20.86	8.84	10.53	0.88	0.24	12.97	0	10.4
116	Jul 25, 03	23.69	9.57	16.84	0.85	0.24	12.85	0.2	10.4
117	Jul 26, 03	26.52	12.74	8.81	0.8	0.18	13.22	0	10.4
118	Jul 27, 03	17.74	11.42	15.41	0.74	0.42	11.72	0.2	10.4
119	Jul 28, 03	22.91	9.70	14.17	0.84	0.22	17.77	1	10.3
120	Jul 29, 03	25.43	12.00	14.11	0.56	0.18	28.25	1.5	10.3
121	Jul 30, 03	26.01	14.34	12.93	0.52	0.27	24.88	7	10.3

Run	Calender	Max.	Min.	Net	Max.	Min.	Wind	Daily	Bot.
Day	Day	AirTemp	AirTemp	Rad.	RH	RH	Speed	Rainfall	Temp
(#)	(mon d, yr)	(C)	(C)	(MJ/m2-day)	(%)	(%)	(km/hr)	(mm)	(C)
122	Jul 31, 03	27.57	15.18	16.71	0.58	0.23	18.66	26	10.3
123	Aug 1, 03	21.52	12.21	15.83	0.73	0.3	11.85	9	10.2
124	Aug 2, 03	20.09	8.46	11.77	0.8	0.25	7.57	2	10.2
125	Aug 3, 03	15.60	4.50	13.18	0.89	0.52	11.55	2	10.2
126	Aug 4, 03	17.82	3.27	14.8	0.89	0.29	15.91	0.2	10.2
127	Aug 5, 03	18.63	9.08	14.37	0.85	0.54	13.04	0	10.2
128	Aug 6, 03	17.49	7.68	12.78	0.89	0.56	12.13	0.4	10.1
129	Aug 7, 03	20.81	8.86	11.04	0.89	0.29	15.42	0.2	10.1
130	Aug 8, 03	21.70	8.12	6.76	0.81	0.28	17.58	0.2	10.1
131	Aug 9, 03	19.58	8.32	10.89	0.86	0.51	16.43	0.2	10.1
132	Aug 10, 03	19.00	5.40	10.94	0.88	0.58	8.71	0.4	10.0
133	Aug 11, 03	18.88	3.87	6.61	0.81	0.3	13.05	0	10.0
134	Aug 12, 03	19.84	7.90	8.31	0.82	0.4	17.69	0	10.0
135	Aug 13, 03	18.67	10.52	8.86	0.75	0.34	10.3	0.5	10.0
136	Aug 14, 03	25.24	9.79	14.97	0.68	0.24	15.49	1	10.0
137	Aug 15, 03	25.27	15.19	11.95	0.58	0.21	7.87	0.5	9.9
138	Aug 16, 03	20.65	11.49	13.65	0.72	0.2	14.62	0	9.9
139	Aug 17, 03	18.75	7.78	13.21	0.88	0.26	16.55	0	9.9
140	Aug 18, 03	14.21	7.97	12.67	0.88	0.58	12.12	0	9.9
141	Aug 19, 03	13.70	7.22	15.28	0.88	0.6	14.1	0.4	9.8
142	Aug 20, 03	17.20	6.52	10.77	0.89	0.27	15.26	0.2	9.8
143	Aug 21, 03	18.55	7.16	10.61	0.72	0.29	9.8	0	9.8
144	Aug 22, 03	13.13	7.47	11.45	0.85	0.62	17.41	1.4	9.8
145	Aug 23, 03	11.32	5.57	10.24	0.8	0.43	8.4	0.4	9.7
146	Aug 24, 03	7.65	3.95	12.59	0.84	0.7	8.78	0.8	9.7
147	Aug 25, 03	12.66	3.99	10.51	0.87	0.38	10.6	0	9.7
148	Aug 26, 03	16.04	3.30	5.23	0.83	0.32	11.88	0	9.7
149	Aug 27, 03	14.68	3.73	10.18	0.8	0.31	10.35	0.5	9.7
150	Aug 28, 03	18.25	3.18	13.47	0.83	0.38	10.35	1	9.6
151	Aug 29, 03	15.76	4.65	9.63	0.89	0.34	8.01	0	9.6
152	Aug 30, 03	18.35	5.27	9.05	0.68	0.28	11.09	0	9.6
153	Aug 31, 03	11.73	7.59	6.42	0.89	0.7	8.22	5	9.6

Run	Calender	Max.	Min.	Net	Max.	Min.	Wind	Daily	Bot.
Day	Day	AirTemp	AirTemp	Rad.	RH	RH	Speed	Rainfall	Temp
(#)	(mon d, yr)	(C)	(C)	(MJ/m2-day)	(%)	(%)	(km/hr)	(mm)	(C)
154	Sep 1, 03	15.68	6.67	13.96	0.89	0.43	17.44	0	9.5
155	Sep 2, 03	21.20	8.47	14.59	0.74	0.32	18.63	0	9.5
156	Sep 3, 03	15.65	6.64	6.71	0.87	0.35	14.49	0	9.5
157	Sep 4, 03	13.01	6.30	8.18	0.82	0.59	5.79	0	9.5
158	Sep 5, 03	15.12	7.97	8.3	0.88	0.53	13.71	0.2	9.4
159	Sep 6, 03	20.78	7.93	8.99	0.84	0.4	15.98	0	9.4
160	Sep 7, 03	13.77	8.70	9.47	0.84	0.54	13.46	1	9.4
161	Sep 8, 03	13.87	5.92	9.2	0.88	0.54	17.88	4.8	9.4
162	Sep 9, 03	9.76	5.12	9.05	0.89	0.74	17.11	6	9.4
163	Sep 10, 03	9.92	3.89	8.52	0.89	0.66	10.65	0	9.3
164	Sep 11, 03	8.34	3.59	8.43	0.89	0.47	11.83	0.4	9.3
165	Sep 12, 03	12.46	-1.35	8.19	0.9	0.34	11.2	0.2	9.3
166	Sep 13, 03	10.82	2.30	5.99	0.86	0.56	12.78	0	9.3
167	Sep 14, 03	2.39	-2.49	5.1	0.87	0.62	18.1	0.4	9.2
168	Sep 15, 03	1.33	-3.00	7.54	0.89	0.55	13.77	0	9.2
169	Sep 16, 03	1.29	-2.44	8.02	0.84	0.58	14.22	0	9.2
170	Sep 17, 03	4.74	-1.93	3.07	0.87	0.55	12.49	0.2	9.2
171	Sep 18, 03	7.07	1.73	3.43	0.73	0.53	23.57	0	9.1
172	Sep 19, 03	4.48	-0.39	5.19	0.88	0.76	21.02	0	9.1
173	Sep 20, 03	6.55	-3.86	3.01	0.86	0.31	15.89	0	9.1
174	Sep 21, 03	8.06	-3.94	3.7	0.87	0.59	20.61	0	9.1
175	Sep 22, 03	4.40	0.82	16.7	0.89	0.75	20.61	4.2	9.1
176	Sep 23, 03	0.82	-1.27	12.93	0.9	0.78	19.25	2.4	9.0
177	Sep 24, 03	1.57	-0.65	12.5	0.89	0.82	14.24	2.2	9.0
178	Sep 25, 03	0.49	-1.81	13.21	0.89	0.78	11.2	0	9.0
179	Sep 26, 03	2.32	-3.44	13.7	0.89	0.58	16.34	1.8	9.0
180	Sep 27, 03	1.48	-3.00	14.12	0.88	0.56	13.09	0	8.9
181	Sep 28, 03	1.32	-3.00	13.29	0.83	0.44	10.03	0	8.9
182	Sep 29, 03	9.60	-3.00	13.92	0.8	0.24	8.7	0	8.9
183	Sep 30, 03	12.53	0.57	12.56	0.83	0.38	17.93	0	8.9
184	Oct 1, 03	12.34	-2.01	13.19	0.9	0.47	21.36	0.5	8.9
185	Oct 2, 03	18.35	0.82	11.45	0.84	0.28	11.52	0.5	8.9

Run	Calender	Max.	Min.	Net	Max.	Min.	Wind	Daily	Bot.
Day	Day	AirTemp	AirTemp	Rad.	RH	RH	Speed	Rainfa ll	Temp
(#)	(mon d, yr)	(C)	(C)	(MJ/m2-day)	(%)	(%)	(km/hr)	(mm)	(C)
186	Oct 3, 03	19.88	6.17	3.63	0.56	0.25	9.35	1	8.8
187	Oct 4, 03	17.78	2.69	4.99	0.74	0.28	11.27	0	8.7
188	Oct 5, 03	19.50	3.79	5.52	0.69	0.26	11.84	0	8.6
189	Oct 6, 03	18.06	6.47	4.63	0.59	0.25	18.07	0	8.4
190	Oct 7, 03	10.19	3.81	2.34	0.81	0.62	11.86	0	8.3
191	Oct 8, 03	6.08	1.71	4.03	0.89	0.84	17.25	1	8.2
192	Oct 9, 03	3.79	-0.17	3.77	0.9	0.87	24.74	0.4	8.1
193	Oct 10, 03	4.33	-1.57	3.28	0.89	0.72	12.79	1.4	8.0
194	Oct 11, 03	0.41	-3.07	10.36	0.9	0.78	14.74	0.6	7.9
195	Oct 12, 03	1.51	-3.65	10.71	0.9	0.91	17.96	6	7.9
196	Oct 13, 03	1.40	-3.00	10.97	0.89	0.84	9.52	0.4	7.9
197	Oct 14, 03	2.81	-3.00	10.54	0.9	0.68	15.53	0.4	7.9
198	Oct 15, 03	0.54	-2.80	10.71	0.88	0.54	19.03	0	7.9
199	Oct 16, 03	1.77	-3.00	10.48	0.9	0.69	7.88	3.2	7.9
200	Oct 17, 03	0.25	-2.89	0.47	0.9	0.74	4.56	1.8	7.9
201	Oct 18, 03	1.26	-1.96	0.92	0.89	0.87	4.48	3	7.9
202	Oct 19, 03	0.24	-0.95	0.81	0.9	0.83	5.53	0.6	7.9
203	Oct 20, 03	2.47	-2.25	1.14	0.89	0.88	15.37	9.2	7.9
204	Oct 21, 03	0.51	-3.12	0.88	0.89	0.83	15.08	1.8	7.9
205	Oct 22, 03	1.74	-3.00	0.74	0.9	0.84	12.62	1.6	7.9
206	Oct 23, 03	2.00	-3.00	0.86	0.9	0.92	16.89	2.2	7.9
207	Oct 24, 03	2.00	-3.00	0.91	0.89	0.91	8.3	3	7.9
208	Oct 25, 03	0.04	-3.00	1.39	0.89	0.91	11.37	4.2	7.9
209	Oct 26, 03	1.16	-3.00	0.79	0.89	0.79	9.49	4.6	7.9
210	Oct 27, 03	1.00	-3.00	1.79	0.88	0.77	9.79	2	7.9
211	Oct 28, 03	1.00	-3.00	0.69	0.87	0.71	7.65	0.7	7.9
212	Oct 29, 03	-1.00	-5.00	1.04	0.86	0.66	9.77	0	7.9
213	Oct 30, 03	-2.00	-9.00	0.28	0.83	0.78	6.82	0	7.9
214	Oct 31, 03	-4.00	-14.00	0.2	0.78	0.58	8.55	0	7.9
365	Mar 31, 04	1.00	1.00	1	1	1	1	0	7.9

Max.Change Suction	Max.Change Temperature	Suction Dampening	Temperature Dampening	Max.Change Suction	Max.Change Temperature	Minimum Time Step	First Time Step	Maximum Time Step	Maximum Iterations
(%)	(%)	(%)	(%)	(%)	(%)	(secnds)	(secnds)	(secnds)	(#)
10	10	50	0	5	5	20	1	3000	50

APPENDIX B: PHOTO DOCUMENTATION

a)

b)

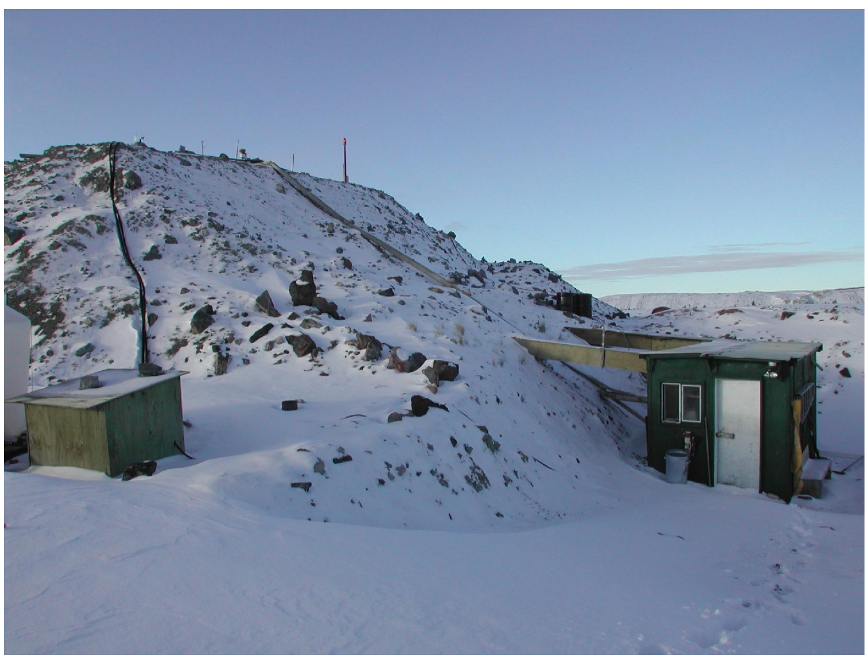

Photographs of the CPE. a) Side view of CPE with tracer tank, runoff collection drums and weather station shown. b) View of instrument hut and irrigation pump house.

a)

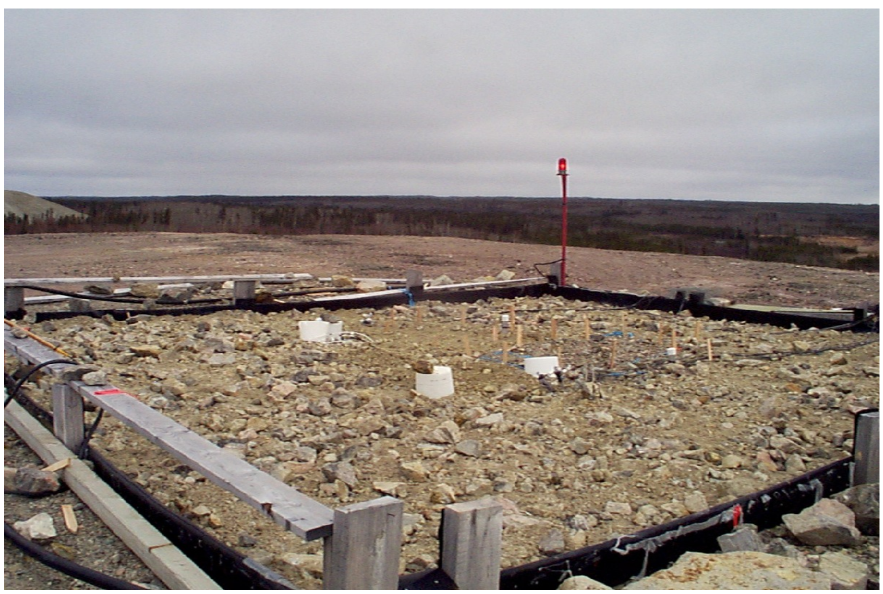

b)

Photographs of the pre-cover surface of the CPE. a) free-dumped surface of the CPE. b) ripped and leveled surface of the CPE.

a)

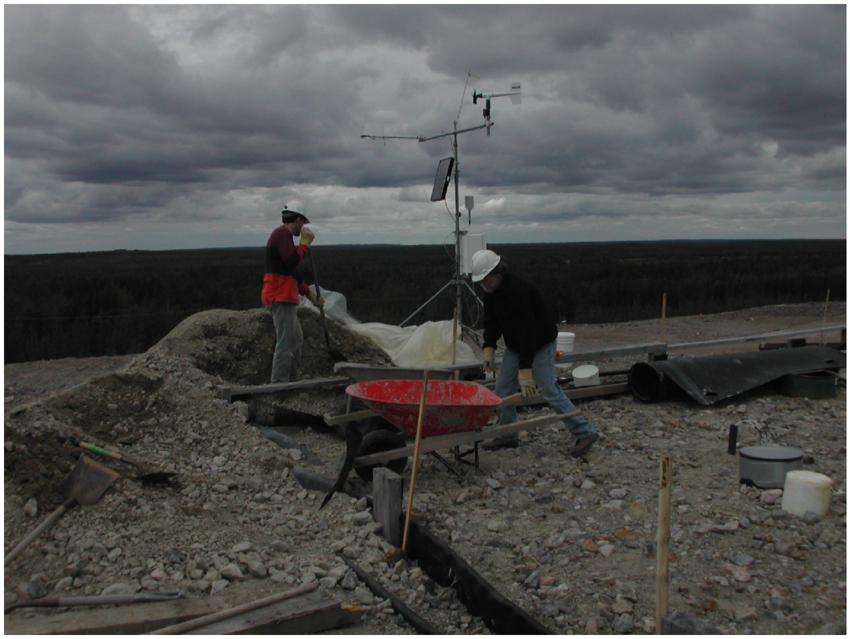

b)

Photographs of the construction of the compacted surface layer. a) Minus 10 cm waste rock is hand shoveled on to the surface of the CPE. b) Newly designed TDR probes are placed at the waste rock/cover interface and within the cover.

a)

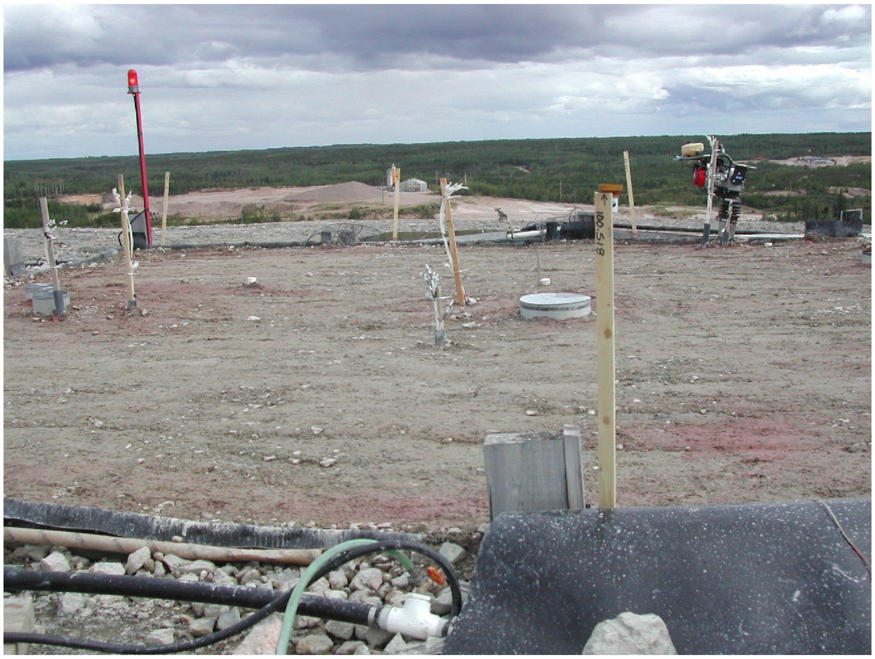

b)

Photographs of the of the compacted surface layer. a) A 'jumping jack' plate tamper was used to compact the surface. b) Final compacted waste rock surface.

a)

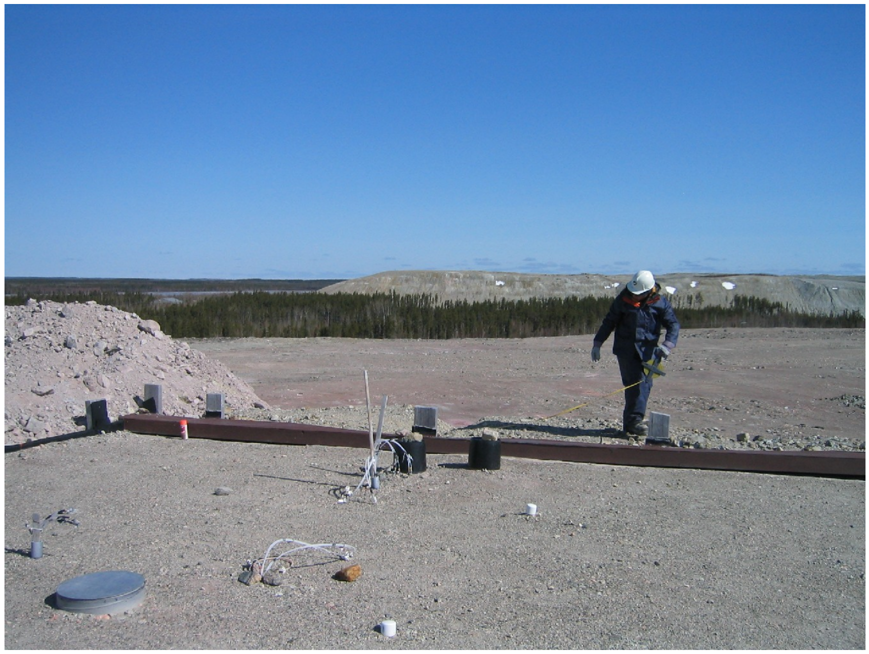

b)

Photographs of the construction of the deconstruction of the surface layer. a) Surface layer one year after construction. b) Initial test pit and cover sample pits.

a)

b)

Photographs of test pits in the surface layer. a) Initial test pit dug after cover placement. b) Test pit dug one year after construction.

a)

b)

Photographs of CPE deconstruction. a) trenched were dug with a backhoe. b) Trench walls were cleared for sampling.

a)

b)

Photographs of CPE deconstruction. a) Fine grained matrix material. The side of an older coated TDR probe is shown. b) Matrix material and boulder in lysimeter 8.

a) 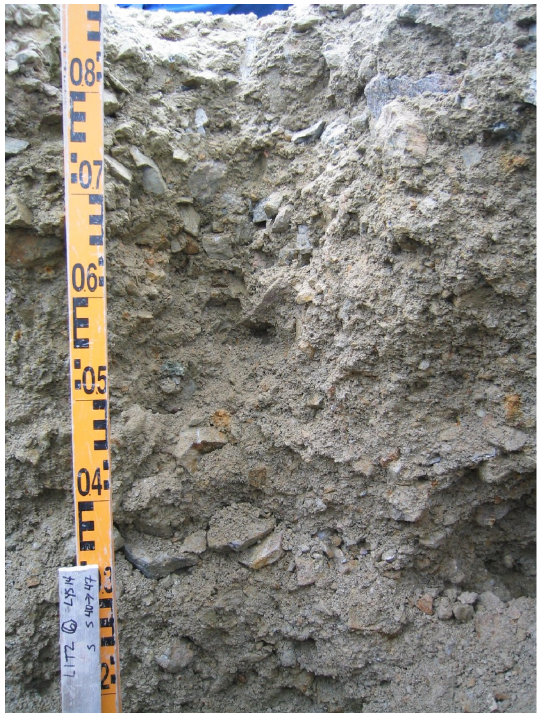

b) 

Photographs of CPE deconstruction. a) Matrix material above lysimeter 14. b) Heterogeneous waste rock above lysimeter 3.

a)

b)

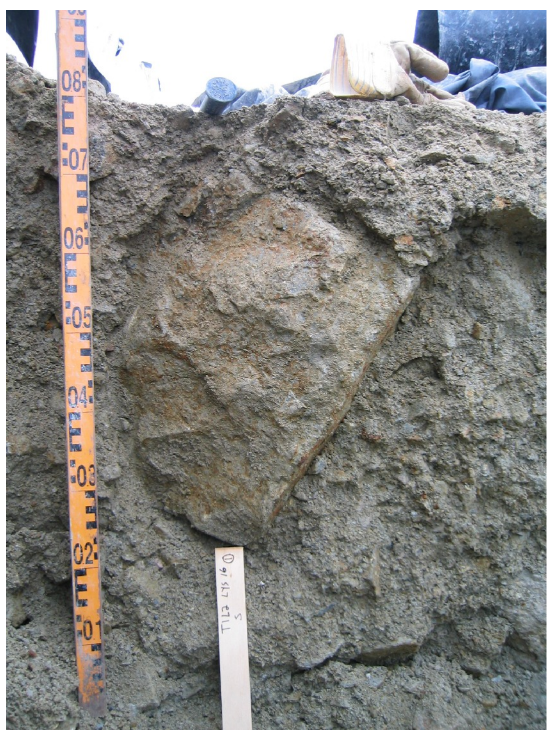

Photographs of CPE deconstruction. a) Heterogeneous waste rock above lysimeter 8. b) Large boulder above lysimeter 16.

a)

b)

Photographs of CPE deconstruction. a) Coarse waste rock above lysimeter 11. Note the dipping layer. b) Coarse waste rock layer dipping towards lysimeter wall above 14.

a)

b)

Photographs of CPE deconstruction. a) Northern most trench immediately above lysimeters 16, 12, 8 and 4 (from left to right). The cement pad is visible, as is the top of the inner lysimeter walls. b) Close up of waste rock above lysimeter 4.

a)

b)

Photographs of CPE deconstruction. a) Close up of waste rock above lysimeter 8. b) Close up of waste rock above lysimeter 12.

APPENDIX C: TRACER RESULTS

Sample ID	δD	depth	Cl	$\delta^{18}O$	Laborator y	pH
	‰	m	ppm	‰	Isotopes	<2.36m m
Tracer water	213.1	na		-15.5	U of S	
Tracer water	217.0	na		-14.22	NMT	
Rainfall	-130.9	0		-15.9	U of S	
Cluff Lake	-133.9	0		-16.15	NMT	
SL-6	-123.2	4.5		-15.6	U of S	
SL-1	-130.9	1.75		-16.2	U of S	
SL-3	-123.6	4.5		-15.5	U of S	
SL-7	-132.6	1.75		-16.5	U of S	
SL-9	-125.2	4.5		-15.9	U of S	
SL-4	-128.1	1.75		-15.8	U of S	
SL-1	-128.9	1.75		-16.2	U of S	
Lysimeter 1	-126.2	5		-14.30	NMT	
Lysimeter 2	-126.7	5		-15.76	NMT	
Lysimeter 3	-130.1	5		-15.41	NMT	
Lysimeter 5	-128.1	5		-14.55	NMT	
Lysimeter 6	-126.8	5		-15.23	NMT	
Lysimeter 7	-125.1	5		-12.91	NMT	
Lysimeter 9	-131.8	5		-14.69	NMT	
Lysimeter 10	-129.3	5		-16.18	NMT	
Lysimeter 11	-142.3	5		-13.15	NMT	
Lysimeter 13	-125.2	5		-14.87	NMT	
Lysimeter 14	-131.0	5		-14.71	NMT	
Lysimeter 15	-132.1	5		-13.54	NMT	

Sample ID	δD	depth	Cl	$\delta^{18}O$	Laboratory	pH
	‰	m	ppm	‰	Isotopes	<2.36mm
T1L1S-1B	-128.0	0.45	13.1		UBC	3.76
T1L1S-2B	-84.3	0.45	44.1	-13.04	UBC	3.75
T1L1S-3B	-69.7	0.75		-1.44	NMT	
T1L1S-4B	-63.5	0.9	30.1		UBC	3.76
T1L1S-5B	-116.3	0.8	30.1		UBC	3.73
T1L1S-6B	-105.6	0.7	22.1		UBC	3.89
T1L1S-7B	-114.2	0.45	32.1		UBC	3.80
T1L1S-8B	-110.6	0.40		-12.31	NMT	
T1L2S-6B	-95.8	1.55			UBC	
T1L2S-10B	-120.3	1.35	19.1		UBC	
T1L2S-13B	-106.7	1.5	12.1		UBC	
T1L2S-15B	-110.4	1.05	33.1		UBC	
T1L2S-16B	-104.4	1.15	19.1		UBC	
T1L2S-17B	-91.2	1.25	24.1		UBC	
T1L2S-18B	-89.3	1.35	17.1		UBC	
T1L2S-19B	-90.2	1.45	19.1		UBC	
T1L2S-20B	-81.5	1.7	20.1		UBC	
T1L2S-21B	-95.8	1.35	23.1		UBC	
T1L2S-22B	-87.7	1.5	17.1		UBC	
T1L2S-23B	-112.0	1.45	16.1		UBC	
T1L2S-24B	-104.1	1.75	16.1		UBC	
T1L2S-25B	-102.9	1.25			UBC	
T1L3S-2B	-114.5	2.65	27.4		NMT	3.80
T1L3S-3B	-96.7	2.25	29.4		NMT	3.78
T1L3S-5B	-107.2	2.1	26.4		NMT	
T1L3S-6B	-99.5	3	34.4		NMT	3.82

Sample ID	δD	depth	Cl	$\delta^{18}O$	Laboratory	pH
	‰	m	ppm	‰	Isotopes	<2.36mm
T1L3S-7B	-106.7	2.7	41.4		NMT	3.82
T1L3S-9B	-85.7	2.3	41.4		NMT	3.86
T1L3S-10B	-89.4	2.65	29.4		NMT	3.78
T1L3S-11B	-113.0	2.9	32.4		NMT	3.84
T1L3S-12B	-91.2	2.8	35.4		NMT	
T1L3S-13B	-124.2	2.95			NMT	
T1L3S-14B	-121.4	2.55			NMT	3.80
T1L4S-7B	-124.0	4.3			NMT	
T1L4S-8B	-92.2	3.2			NMT	
T1L4S-9B	-122.9	3.7			NMT	
T1L4S-10B	-111.6	4.4			NMT	
T1L4S-12A	-122.7	4.2			UBC	3.73
T2L1S-1B	-125.4	0.53	38.4		NMT	3.70
T2L1S-3B	-107.5	0.45		-8.34	NMT	
T2L1S-4B	-109.3	0.55		-8.54	NMT	
T2L1S-6B	-126.4	0.78	44.4		NMT	3.86
T2L1S-7B	-82.4	0.90		-13.81	NMT	
T2L1S-9B	-122.7	0.98	73.4		NMT	3.62
T2L1S-14B	-129.5	0.75			NMT	
T2L1S-26B	-123.0	0.93	43.4		NMT	3.87
T2L1S-35B	-107.8	0.63	37.4		NMT	3.59
T2L1S-38B	-117.4	0.95	31.4		NMT	
T2L1S-44B	-113.4	0.85	50.4		NMT	
T2L2S-7B	-111.3	1.35	53.8	-12.1	NMT	3.65
T2L2S-8B	-116.1	1.45	38.8		NMT	3.63

Sample ID	δD	depth	Cl	$\delta^{18}O$	Laboratory	pH
	‰	m	ppm	‰	Isotopes	<2.36mm
T2L2S-10B	-125.7	1.8	31.8		NMT	
T2L2S-13B	-123.4	1.15	48.8		NMT	3.84
T2L2S-14B	-105.2	1.25	36.8	-10.1	NMT	
T2L2S-15B	-122.5	1.35	39.8		NMT	3.67
T2L2S-16B	-122.9	1.45	35.8		NMT	3.86
T2L2S-17B	-126.5	1.85	44.8		NMT	3.76
T2L2S-22B	-129.0	1.8	59.1		UBC	
T2L2S-24B	-92.7	1.05	54.1		UBC	3.77
T2L2S-31B	-127.5	1.15	54.4		NMT	
T2L2S-32B	-117.3	1.25	125.4	-7.4	NMT	
T2L2S-34B	-123.9	1.45			NMT	
T2L2S-35B	-117.0	1.85			NMT	
T2L2S-46B	-120.5	1.15			NMT	
T2L2S-47B	-121.3	1.25	37.8		NMT	
T2L2S-48B	-118.4	1.35	51.8		NMT	
T2L2S-49B	-117.5	1.45	37.8		NMT	
T2L3S-1	-122.9	2.5	85.4	-10.2	NMT	
T2L3S-3	-126.3	2.9	46.8	-13.2	NMT	
T2L3S-4	-113.6	3.0			NMT	
T2L3S-5	-117.7	2.6	75.4	-9.9	NMT	3.77
T2L3S-6	-116.3	2.4			NMT	
T2L3S-7	-127.2	2.3	38.4		NMT	3.81
T2L3S-8	-84.7	2.2			NMT	
T2L3S-35B	-121.2	3	95.4		NMT	3.78
T2L3S-44	-122.5	3.2	59.1	-12.6	UBC	
T2L3S-44B	-109.5	3.2			NMT	

Sample ID	δD	depth	Cl	$\delta^{18}O$	Laboratory	pH
	‰	m	ppm	‰	Isotopes	<2.36mm
T2L4S-8B	-124.6	3.7	57.4		NMT	3.75
T2L4S-9B	-122.3	4.2	38.1	-13.6	NMT	3.70
T2L4S-10B	-130.4	4.2	34.1		NMT	3.65
T2L4S-11B	-122.8	4.0			NMT	
T2L4S-12	-131.4	4.2	22.1	-12.1	UBC	3.65
T2L4S-12B	-128.4	4.2			NMT	
T2L4S-13B	-116.5	4.5			NMT	
T3L1S-1B	-97.8	0.45	96.1		UBC	
T3L1S-2B	-115.6	0.55	44.1		UBC	
T3L1S-3	-111.2	0.45		-10.68	NMT	
T3L1S-3B	-116.3	0.65	42.1	-12.9	UBC	
T3L1S-4B	-121.9	0.75	32.1		UBC	
T3L1S-5B	-123.2	0.85	34.1	-14.4	UBC	
T3L1S-6B	-127.7	0.95	44.1		UBC	
T3L1S-7B	-100.1	0.45	60.1		UBC	
T3L1S-8B	-117.8	0.55			UBC	
T3L1S-8B	-118.2	0.55			UBC	
T3L1S-9B	-123.6	0.65			UBC	
T3L1S-10B	-106.4	0.75		-14.23	UBC	
T3L1S-11B	-122.4	0.85			UBC	
T3L1S-12B	-74.1	0.30	27.4		UBC	
T3L1S-14B	-79.3	0.65	23.4		UBC	
T3L1S-15B	-124.1	0.65			UBC	
T3L1S-20B	-127.0	0.55	34.1		NMT	
T3L1S-21B	-127.8	0.65	37.4		NMT	
T3L1S-22B	-128.7	0.75	31.4		NMT	
T3L1S-23B	-131.7	0.85	25.4		NMT	

Sample ID	δD	depth	Cl	$\delta^{18}O$	Laboratory	pH
	‰	m	ppm	‰	Isotopes	<2.36mm
T3L1S-24B	-131.4	0.95	29.4		NMT	
T3L1S-26B	-125.6	0.94	67.4	-13.0	NMT	
T3L1S-30B	-123.4	0.75	28.1		NMT	
T3L1S-31B	-123.9	0.85	36.4	-9.9	NMT	
T3L1S-32A	-123.3	0.96		-4.5	NMT	
T3L1S-32B	-124.3	0.95			UBC	
T3L1S-33	-102.8	0.45	82.1		UBC	
T3L1S-33B	-103.1	0.45	82.1		UBC	
T3L1S-34B	-114.9	0.55	80.1		UBC	
T3L1S-34B	-114.9	0.55	80.1		UBC	
T3L1S-35B	-114.9	0.65	49.1	-13.2	UBC	
T3L1S-36B	-121.3	0.75	48.1	-13.8	UBC	
T3L1S-37B	-122.1	0.85	34.1	-13.7	UBC	
T3L1S-38B	-125.3	0.95	33.1	-15.0	UBC	
T3L1S-39B	-103.4	0.45			UBC	
T3L1S-40B	-114.6	0.55	49.1	-8.4	UBC	
T3L1S-41B	-119.4	0.65			UBC	
T3L1S-42	-113.3	0.75	42.4		UBC	
T3L1S-43B	-117.4	0.85			UBC	
T3L1S-44B	-126.0	0.95			UBC	
T3L1S-51B	-83.7	0.25		-14.02	UBC	
T3L1S-52B	-116.2	1.0			UBC	
T3L1S-53B	-115.5	0.55		-13.34	NMT	
T3L1S-54B	-118.7	0.45	56.1	-13.10	UBC	
T3L1S-55B	-121.8	0.55	73.1	-14.73	UBC	
T3L1S-56B	-112.5	0.65	41.1		UBC	
T3L1S-57B	-103.7	0.75	51.1		UBC	
T3L1S-58B	-110.7	0.85	51.1		UBC	

Sample ID	δD	depth	Cl	$\delta^{18}O$	Laboratory	pH
	‰	m	ppm	‰	Isotopes	<2.36mm
T3L1S-59B	-112.2	0.95	53.1		UBC	
T3L2S-1B	-121.6	1.5	46.8		NMT	
T3L2S-2B	-121.4	1.7		-12.45	NMT	
T3L2S-3B	-126.4	1.65			NMT	
T3L2S-4B	-123.5	1.8			NMT	
T3L2S-5B	-124.8	1.05	23.8		NMT	
T3L2S-6B	-125.7	1.15	24.8		NMT	
T3L2S-7B	-125.1	1.25			NMT	
T3L2S-8B	-126.9	1.35			NMT	
T3L2S-9B	-126.5	1.45	24.8		NMT	
T3L2S-11B	-114.3	1.85	107.4	-8.5	NMT	
T3L2S-12B	-82.5	1.05			NMT	
T3L2S-13B	-110.5	1.15			NMT	
T3L2S-14B	-117.6	1.25	10.8		NMT	
T3L2S-15B	-121.6	1.35	25.4		NMT	
T3L2S-16B	-118.7	1.85	46.4		NMT	
T3L2S-21B	-123.4	1.15	42.4		NMT	
T3L2S-22B	-118.5	1.25	66.4		NMT	
T3L2S-23B	-127.6	1.35	44.4		NMT	
T3L2S-24B	-130.3	1.45			NMT	
T3L2S-25B	-130.3	1.85	31.1		NMT	
T3L2S-27B	-125.3	1.85	41.1	-12.6	NMT	
T3L2S-28B	-128.3	1.45			NMT	
T3L2S-29B	-124.6	1.35	56.4		NMT	
T3L2S-31B	-124.5	1.25	54.4		NMT	
T3L2S-36B	-121.2	1.25	43.4		NMT	

Sample ID	δD	depth	Cl	$\delta^{18}O$	Laboratory	pH
	‰	m	ppm	‰	Isotopes	<2.36mm
T3L2S-37B	-129.1	1.35			NMT	
T3L2S-38B	-126.2	1.45	61.4		NMT	
T3L2S-40B	-81.5	1.05			NMT	
T3L2S-41B	-103.1	1.15			NMT	
T3L2S-42B	-106.6	1.25			NMT	
T3L2S-44	-108.2	1.45			NMT	
T3L2S-44B	-107.4	1.45	33.4	-13.8	NMT	
T3L2S-45B	-126.5	1.85	30.4	-13.7	NMT	
					NMT	
T3L3S-10	-114.0	2.6	82.4	-13.0	NMT	
T3L3S-11	-120.0	2.4	51.4		NMT	
T3L3S-12	-129.9	2.8	35.8		NMT	
T3L3S-13	-121.2	2.88	81.4	-12.9	NMT	
T3L3S-14	-121.3	2.65	48.4		NMT	
					NMT	
T3L4S-10B	-124.0	3.8	67.4		NMT	
T3L4S-11B	-122.8	3.75			NMT	
T3L4S-14B	-121.7	4			NMT	
T3L4S-16B	-123.2	3.9	74.4		NMT	
T3L4S-17B	-119.5	4	78.4		NMT	
T3L4S-18B	-116.3	4			NMT	
T3L4S-19B	-122.8	4	107.4	-14.1	NMT	